Heterogeneity of ribosomes in vivo in mouse model

Marie Roxanne Brunchault

THÈSE

Pour obtenir le grade de

DOCTEUR DE L'UNIVERSITÉ GRENOBLE ALPES

Spécialité : Neurosciences - Neurobiologie

Arrêté ministériel : 25 mai 2016

Présentée par

Marie Roxanne BRUNCHAULT

Thèse dirigée par **Marylin VANTARD**
et co-encadrée par **Stéphane BELIN**, Inserm

préparée au sein du **Laboratoire Grenoble Institut des Neurosciences**
dans **l'École Doctorale Chimie et Sciences du Vivant**

Hétérogénéité des ribosomes in vivo dans le modèle murin

Heterogeneity of ribosomes in vivo in mouse model

Thèse soutenue publiquement le **30 novembre 2021**,
devant le jury composé de :

Madame Marylin VANTARD
DIRECTRICE DE RECHERCHE, CNRS délégation Alpes, Directrice de thèse
Monsieur Jean-Jacques DIAZ
DIRECTEUR DE RECHERCHE, INSERM délégation Auvergne-Rhône-Alpes, Rapporteur
Madame Juliette GODIN
CHARGE DE RECHERCHE HDR, INSERM délégation Grand Est, Rapporteure
Monsieur Alain BUISSON
PROFESSEUR DES UNIVERSITES, Université Grenoble Alpes, Président
Monsieur Frédéric CATEZ
CHARGE DE RECHERCHE, CNRS délégation Rhône Auvergne, Examinateur

Remerciements

Je remercie Stéphane Belin pour l'opportunité de travailler sur ce projet, pour son aide au cours de ces trois ans et pour avoir corrigé ce manuscrit. Je remercie également nos collaborateurs du CEA, Yohann Couté et Anne-Marie Hesse pour leur aide précieuse à ce projet. Je remercie spécialement Anne-Marie d'avoir pris le temps de m'expliquer les subtilités de la MS et d'avoir été très réactive concernant chaque demande que j'ai pu faire au cours de cette thèse. Je remercie également Marylin Vantard pour sa disponibilité et ses conseils pour mener à bien cette thèse.

Je remercie Juliette Godin et Jean Jacques Diaz d'avoir accepté d'évaluer ce travail. Je les remercie ainsi que Frédéric Catez et Alain Buisson d'avoir accepté de faire partie de mon jury de thèse.

Je remercie mon comité de suivi de thèse Fabienne Agasse, Frédéric Catez et Jean-Christophe Deloulme qui ont suivi l'évolution de cette thèse. Merci pour les discussions qui m'ont permis de faire évoluer ce projet. Je remercie Guy Royal, Cécile Caron, Catherine Desplanques, Christophe Rubiot et Cécile Massit pour leur présence et leur aide au cours des derniers mois et qui ont permis l'aboutissement de ce travail.

Un grand merci à Floriane Albert, maîtresse du western blot, pour son aide au cours de ma première année. Merci d'avoir également été un soutien moral. Bon vent pour la suite! Merci à Céline Delpech pour sa bonne humeur, ses bons conseils, les sessions d'écriture, les discussions dans le labo tard le soir, les fous rires. Bref merci d'avoir été là. Cette thèse n'aurait pas été la même sans 'Nickel Michel'! Merci à Eloïse Gronlier et Maëva Laquitaine pour leur bonne humeur, pour avoir égayé les sessions d'écriture à la bibliothèque et pour ces moments passés en dehors du boulot (Vive la fondue !!) Merci également à mes collègues, actuels et anciens, pour leur aide avec les manips, les discussions scientifiques et non scientifiques, les blind tests et les karaokés pour rendre plus agréables les moments passés au laboratoire.

Je remercie les membres du GIN pour leur aide. Je remercie spécialement Béatrice Blot pour son aide précieuse avec les clonages et la génération de plasmides. Je remercie également Christophe Bosc pour avoir répondu à chaque question que j'avais concernant les structures 3D et Chimera. Merci également à Sylvain, Fabien, Laure et Flore pour leur aide avec les souris.

Je remercie du fond du cœur mes amis qui m'ont soutenu : Cloé pour ces temps passées à s'encourager et à se dire qu'on y arriverait , Thibault pour m'avoir écouté et encouragé, Térence pour la motivation et l'aide sur excel et Christophe pour son soutien et sa bienveillance. Merci à la team Olivia, Sarah, Marine, Nina et Cassandra. Merci de me faire autant rire. Merci d'avoir été là. Merci pour votre soutien, votre joie de vivre, les fous rires… Merci à Mirette, Jean-Luc, Audrey et le reste de la famille pour votre présence à tout instant. Merci d'avoir été là quand j'étais au plus bas et de m'avoir aidé à remonter la pente. Merci à la team sport Vincent, Eric et Laury pour la tuerie sportive et la motivation.

Merci infiniment à mes parents et à Tim qui sont toujours derrière moi et qui me poussent à aller de l'avant. Merci pour la patience, les conseils (le sacréchien !) et merci de croire en moi. Un très grand merci à Val pour son aide indispensable au cours de ma thèse, surtout au moment de la rédaction. Merci Val et Adri d'avoir fait le déplacement pour venir me soutenir.

Je souhaite exprimer toute ma reconnaissance à Celui sans qui je ne serais pas là aujourd'hui.

Merci à tous. Je m'excuse si j'ai oublié de mentionner quelques personnes. Je vous remercie d'avoir été dans cette aventure à mes côtés. A bientôt sous d'autres horizons !

Résumé

Les protéines sont des effecteurs cellulaires qui sont impliqués dans beaucoup de processus cellulaires. Elles sont synthétisées au cours de la traduction par le complexe de traduction qui est composé de ribosomes, de facteurs de traductions, de facteurs associées au ribosome et d'ARN de transfert. Ce complexe est étudié depuis quelques années mais ce n'est que récemment que les études ont pointé vers une fonction régulatrice de ce complexe. Il a été proposé que chaque composante de ce complexe puisse adapter sa composition afin de contrôler la traduction globale ou celle d'ARN messager spécifiques. Cependant, ce concept reste à être démontré in vivo.

Mon projet principal se concentre sur une composante de ce complexe : les ribosomes. Les ribosomes sont des macro-complexes composés de quatre molécules d'ARN ribosomaux et d'environ 80 protéines ribosomales (PRs). Ce complexe forme des régions fonctionnelles tel que le tunnel de l'ARNm ou le centre de décodage. L'objectif principal était de définir la composition du ribosome en termes de PRs dans le modèle murin. En utilisant une approche protéomique avec une chromatographie liquide couplée à la spectrométrie de masse en tandem, nous avons défini la composition en protéines ribosomales des ribosomes dans différents organes murins. Nous montrons avec une quantification relative l'existence de deux groupes de PR : les PR invariables et les PR variables, incluant les paralogues RPL3 et RPL10. L'analyse structurale montre que les PR variables sont localisées dans les zones fonctionnelles du ribosomes comme le tunnel de l'ARNm ou le tunnel de sortie de la protéine néosynthétisée. Nous avons vérifié l'expression protéique de 12 PR par quantification absolue. L'étude de corrélation entre les taux d'ARNm et de protéine montre que même si la majorité de PR ont des taux corrélés, certains montrent des différences majeurs.

La deuxième étude se base sur une deuxième composante du complexe de la traduction : les facteurs associés au ribosome. Nous avons fait une analyse *in silico* les données obtenues précédemment dans l'étude protéomique pour identifier les groupes fonctionnels qui étaient enrichis dans chaque tissu. Nous nous sommes concentrés sur les sous parties du système nerveux central et des tissus musculaire. Notre analyse révèle que le ribo-intéractome de chaque tissu et même région semble montrer des spécificités fonctionnelles.

Le dernier projet s'est concentré sur le rôle fonctionnel du ribosomes au cours d'un processus pathologique : la lésion du système nerveux central. Nous avons analysé l'effet de trois PR (RPS4X/eS3, RPS14/uS11 et RPL22/eL22) sur la régénération axonale et la survie

cellulaire. Nous nous sommes également concentrés sur l'effet du niveau de 2'O méthylation sur ce processus. Seul RPL22/eL22 semble diminuer la suivie neuronale in vivo.

En conclusion, cette étude permet de mieux appréhender le concept d'hétérogénéité de ribosomes *in vivo*, en conditions physiologiques. Nous voyons également que cette hétérogénéité s'étend aussi jusqu'au facteurs associé au ribosome. Cela ouvre de nouvelles voies d'étude sur la contribution du complexe de traduction au niveau de la régulation de la traduction.

Abstract

Proteins are final cell effectors that regulate most processes occurring in cells. They are synthesised through translation of messenger RNA or mRNA by the translation complex which is composed of ribosomes, translation factors, ribosome associated factors and transfer RNAs. This translational complex has been studied for decades but only studies from the past 30 years suggested that it could have a regulatory role. It was proposed that components of the translational complex could adapt their composition to control either the global level of translation and/or the translation of specific mRNAs. However, this hypothesis remains to be clearly demonstrated at the protein level *in vivo*.

The main project was focused on one of the main components of this translational complex: the ribosome. Ribosomes are macro-complexes composed of ribosomal RNA and ribosomal proteins forming various functional regions such as the mRNA tunnel or the decoding centre. The main objective was to define the ribosome content in terms of ribosomal protein (RP) *in-vivo* across multiple mice organs, using a proteomic approach, and understand how possible variations in RP composition could affect their functions. Our results from relative quantification using liquid chromatography tandem mass spectrometry (LC-MS/MS) shows that there are two groups of ribosomal proteins: the invariable 'core' RPs and the variable RPs, including tissue-specific RP paralogues such as RPL3L and RPL10L. Structural analysis shows that variable RPs were located in functional regions of the ribosome such as the mRNA tunnel or the nascent peptide exit tunnel. We confirmed the RP profile of 12 RPs by absolute quantification. Analysis of correlation between mRNA and protein levels showed that while these levels were correlated for some RP, others showed differences.

The second project was focused on the ribosome-associated factors. Using the dataset from the main project, we did an *in silico* analysis to identify the groups of protein that were possibly interacting with the ribosome. We chose to focus on central nervous system (CNS) subparts and on muscle-type tissues from our study. Gene ontology analysis shows that the ribo-interactome also seems to be specialised.

The final project focused on the functional impact of modulating either ribosomal proteins or the level of rRNA 2'O methylations on cell survival and axonal regeneration after central nervous system injury. 3 RP were selected : RPS4X/eS3, RPS14/uS11 and RPL22/eL22.

Interestingly, preliminary results show that among the RPs, only one RP, RPL22/eL22, significantly decreases the level of survival post injury.

In conclusion, this work shed some light on the RP heterogeneity observed in the ribosomes in physiological conditions. This heterogeneity is not limited to RP as there is also a heterogeneous distribution of ribosome associated factors. This study opens new doors to study the contribution of the translation complex to translation regulation.

Abbreviations

2'OMe	2'-O methylation
4E-BP	eIF4E-binding protein
AA	amino acids
AD	Alzheimer's disease
CP	central protuberance
CTB	Cholera Toxin Subunit B
DBA	Diamond Blackfan Anaemia
DDA	data dependent acquisition
DIA	data independent acquisition ()
DC	decoding centre
eEF	eukaryotic elongation factor
eEF2K	eEF2 kinase
ERK	extracellular ligand-regulated kinase
eIF	eukaryotic initiation factor
eL	eukaryotic large ribosomal protein
eRF	eukaryotic releasing factor
eS	eukaryotic small ribosomal protein
ETS	external transcribed sequences
FBL	Fibrillarin
HD	Huntington disease
GO	gene ontology
IRES	internal ribosome entry site
i-RPS	Initiation RPS
ITS	internal transcribed sequences
LSU	large subunit
KCl	potassium chloride
MEF	mouse embryonic fibroblasts
mRNA	messenger RNA
MS	mass spectrometry
mTOR	mammalian target of rapamycin
NPET	nascent peptide exit tunnel
ORF	open reading frame
PD	Parkinson disease
PDCD4	programmed cell death 4
PIC	pre-initiation complex
PLAP	Placental Alkaline Phosphatase
p-RPS	processing RPS
PRM	Parallel Reaction Monitoring
PTC	peptidyl transferase centre
PTM	post-translational modifications
RP	ribosomal protein
RPG	ribosomal protein gene
RPL	large ribosomal protein
RPS	small ribosomal protein
rRNA	ribosomal RNA
SILAC	stable isotope labelling by amino acids in cell culture
siRNA	small interfering RNA
SRM	Selected Reaction Monitoring

shRNA	short hairpin RNA
snoRNP	small nucleolar ribonucleoproteins
SSU	small subunit
TBI	traumatic brain injury
TCS	Treacher Collins syndrome
TIF-1A	transcription initiation factor-1A
tRNA	transfer RNA
uL	universal large ribosomal protein
uS	universal small ribosomal protein
UTR	untranslated region

List of Figures

List of tables

This present paper-based thesis is divided into three sections. The introduction will set the landmarks on translation regulation while focussing on the ribosome, its heterogeneity and its implication in physio-pathology. The second part will present the results obtained through the analysis the RP distribution across different organs in the mouse model, the study of ribosome associated factors from these organs and the role of ribosomes in a pathological condition which is the CNS injury. The third section includes the discussion with the biological implication of the current results, conclusion and prospects.

Through the entire manuscript, the following nomenclature rules will be applied: DNA/mRNA symbols are italicised with first letter upper case and all the rest lower case. Proteins are not italicized and all upper case.

Introduction

1 The translation complex: focus on the ribosome

Translation is a well-orchestrated sequence of the events that leads to the synthesis of proteins. The process is controlled by the translation complex (TC). The TC is made up of 4 major components: ribosomes, transfer RNA (tRNA), translation factors and ribosome-associated factors (Archer et al., 2016; Shirokikh et al., 2017). This complex, which targets messenger RNAs (mRNAs), has a dynamic composition throughout translation.

Ribosomes are macro-complexes with a molecular weight of about 4.3 x 10^3 kDa in humans. They were first observed in 1955 and were called microsomes as they were bound to the endoplasmic reticulum membrane (Palade, 1955). They would later be called ribonucleoprotein particles of the microsome fraction and finally, ribosomes. They are made up of 2 subunits: the large ribosomal subunit (LSU) and the small subunit (SSU). The subunits are themselves composed of proteins called ribosomal proteins (RPs) and specific RNA molecules called ribosomal RNA (rRNA). This complex is recruited to an mRNA and decodes the mRNA. It has an enzymatic activity in catalysing formation of peptide bonds between amino acids and is also in charge of the quality control of the nascent polypeptide chain (Dever and Green, 2012; Brandman and Hegde, 2016; Merrick and Pavitt, 2018).

tRNAs are the second component of the TC. They are transcribed by RNA polymerase (RNA pol) III. It is a single molecule of RNA folded by Watson and Crick interactions to form a clover-leaf structure (Holley et al., 1965). It consists of 4 arms: the amino acid acceptor arm with a CCA extension which is linked to an amino acid by aminoacyl tRNA synthetase, the anticodon arm that will pair with the codon present on an mRNA, the TΨC arm which is involved in the interactions with the ribosome and the D arm that stabilises the tertiary structure of the tRNA (**Figure 1**). It also has a variable loop that is involved in the tRNA recognition by aminoacyl tRNA synthetase. tRNAs act as adaptors between mRNA and protein (Kim et al., 1974; Giegé et al., 2012).

Translation factors are RNA binding proteins that bind to mRNA or ribosomes during translation. There are 3 types: initiation factors, elongation factors and releasing factors, each involved in initiation, elongation and termination of translation respectively. In eukaryotes, there are 18 different initiation factors called eIFs, 4 elongation factors called eEFs and 2 releasing factors called eRF (Safer, 1989; Jackson et al., 2010). Each factor plays a specific role during translation that will be detailed in chapter 2.

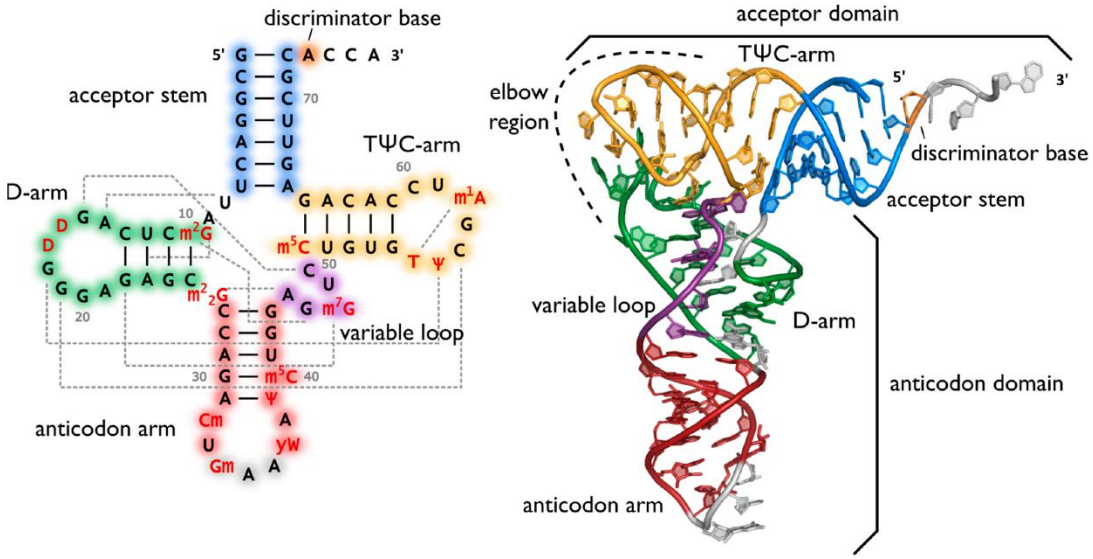

Figure 1: Structure of tRNA
Schematic representation of the primary and secondary structure of tRNA with the D, anticodon, TΨC and amino acid acceptor arms. – from (Lorenz et al., 2017)

The final components of the TC are ribosome-associated factors or RAFs. They compose the riboproteome or ribointeractome (Reschke et al., 2013; Simsek et al., 2017). There are two criteria to define RAFs. Firstly, it must interact transiently with the ribosome during translation and secondly, it must not be a translation factor. Improvements in mass spectrometry (MS) analysis have enabled the identification of several factors but new RAFs are still being discovered with progress in sensitivity of measurements and processing of MS results. To identify RAFs, ribosomes are isolated either through immunoprecipitation or by centrifugation on sucrose gradient or sucrose cushion. They are usually analysed through liquid chromatography tandem mass spectrometry (LC-MS/MS) (Belin et al., 2010; Reschke et al., 2013; Heiman et al., 2014; Rivera et al., 2015; Simsek et al., 2017; Imami et al., 2018). Some RAFs regulate translation such as Staufen1 and Sec61 (Ricci et al., 2014; Voorhees et al., 2014) or stabilise mRNA such as PABP (Imami et al., 2018). They can be chaperons that control the folding of nascent polypeptides or involved in protein quality control (Reschke et al., 2013; Simsek et al., 2017; Imami et al., 2018)

The translation complex will assemble to translate mRNA. mRNAs are produced by RNA Pol II from DNA templates. All mRNAs are composed of 5' and 3' untranslated regions (UTR) and an open reading frame (ORF) flanked by the initiation site in 5' and the termination site on the 3' side and consisting of successive codons (**Figure 2**). Codons are degenerate and

can therefore code for the same amino acids (Crick et al., 1961). Two features, that are not present on the DNA, are added to mRNA. At the 5' end, a cap is added to prevent 5'-3' exonuclease degradation. The cap is a guanine that is methylated on N7 and is linked to the first nucleotide by a 5'-5' triphosphate bond (Furuichi, 2015). The second feature is a poly-A tail added post transcriptionally through the cleavage and the polyadenylation of the 3' end by poly-A polymerase. This tail interacts with poly-A binding protein (PABP) to ensure the stability of mRNA and translation initiation (Sachs and Davis, 1989). The poly-A tail is also required for export of mRNA from the nucleus (Curinha et al., 2014) .

Figure 2: Structure of mRNA
Schematic representation of an mRNA molecule with the 5' cap, 5'UTR, 3' UTR, ORF in red and the poly-A tail. The initiation and termination site are also indicated.

All components will interact throughout the translation process. Any impairment to one of the components of the TC can lead to abortion of the translation process or synthesis of a mutated protein (Tahmasebi et al., 2018). Throughout the present work, I will focus on one of the components of the TC: the ribosome.

1.1 Structure and functional domains of the ribosome

As indicated earlier, ribosomes are the protein-producing organelle within cells and are made up of 2 subunits, the large ribosomal subunit (LSU) and the small subunit (SSU). Though they are conserved between prokaryotes and eukaryotes, analysis of their basic composition have shown that there are major differences. The prokaryotic ribosome, also called 70S ribosome, contains 54 RPs and 3 rRNAs and is about 2.3MDa. The LSU is composed of 33 RPs, the 23S rRNA and 5S rRNA while the SSU is composed of 21 RPs and the 16S rRNA (Ben-Shem et al., 2011; Jenner et al., 2012; Anger et al., 2013; Khatter et al., 2015).

The eukaryotic ribosome, also called 80S ribosome, can weigh up to 4.3MDa. There are 79 RPs in yeast and 80 RPs in higher eukaryotes. They all contain 4 rRNA molecules. In human and yeast, the SSUs are composed of 33 RPs and an 18S rRNA. There are shared similarities between yeast and human LSUs as they both contain the 5.8S and 5S rRNA (Ben-Shem et al., 2011; Jenner et al., 2012; Anger et al., 2013; Khatter et al., 2015). However, they differ slightly as the yeast LSU contains 46 RPs while the human LSU contains 47 RPs (Melnikov et al., 2012). Moreover, yeast have a 25S rRNA whereas the human ribosome contains a 28S rRNA. The additional rRNA form extensions (**Figure 3** - dotted lines on human ribosome). Both prokaryotic and eukaryotic ribosomes share a common core of 34 RP and 3 rRNA (Melnikov et al., 2012) (**Figure 3**)

Resolving the ribosomal structure proved itself to be difficult. It was dependent on technical advances notably X-ray crystallography and cryo-electron microscopy. These studies ended up with a Nobel prize in chemistry in 2009 awarded to Venkatraman Ramakrishnan, Thomas A. Steitz and Ada E. Yonath for their work on the structure and function of the bacterial ribosome. However, it was not until 2011 that the first structure of the eukaryotic ribosome was obtained at 3.0 Å resolution (Ben-Shem et al., 2011). Since then, several ribosomes have been mapped and collected on Protein Data Bank (www.rcsb.org). Most eukaryotic ribosome structures come from the yeast model. There are also structures from human and rabbit cell lines. The first murine ribosome surface image at a 3.3 Å resolution was obtained in January 2021 but the structure of the 80S ribosome could not be resolved (Kraushar et al., 2021).

For the sake of clarity, the rest of this manuscript will summarize knowledge on the eukaryotic ribosome, unless stated otherwise.

Each subunit possesses two sides: the solvent side, exposed to the cytoplasm, and the interface for interactions between the LSU and the SSU. I will first describe each feature of the large and small subunit and will end with the description of the A, P and E site which is shared by both subunits.

1.1.1 The large subunit

The large 60S subunit is composed of about 47 distinct large ribosomal proteins called eL and uL (e = eukaryotic ; u = universal ; old nomenclature: RPL) (Ban et al., 2014) (**Table 1**) and 3 rRNA molecules namely the 28S, 5S et 5.8S. The key landmarks of the LSU are, on

the solvent side: the central protuberance, L1 stalk, GTPase associated region, P stalks, sarcin-ricin loop and peptide exit tunnel. At the interface are the aminoacyl site, peptidyl site, exit site which are shared with the SSU, and peptidyl transferase centre (**Figure 4**)

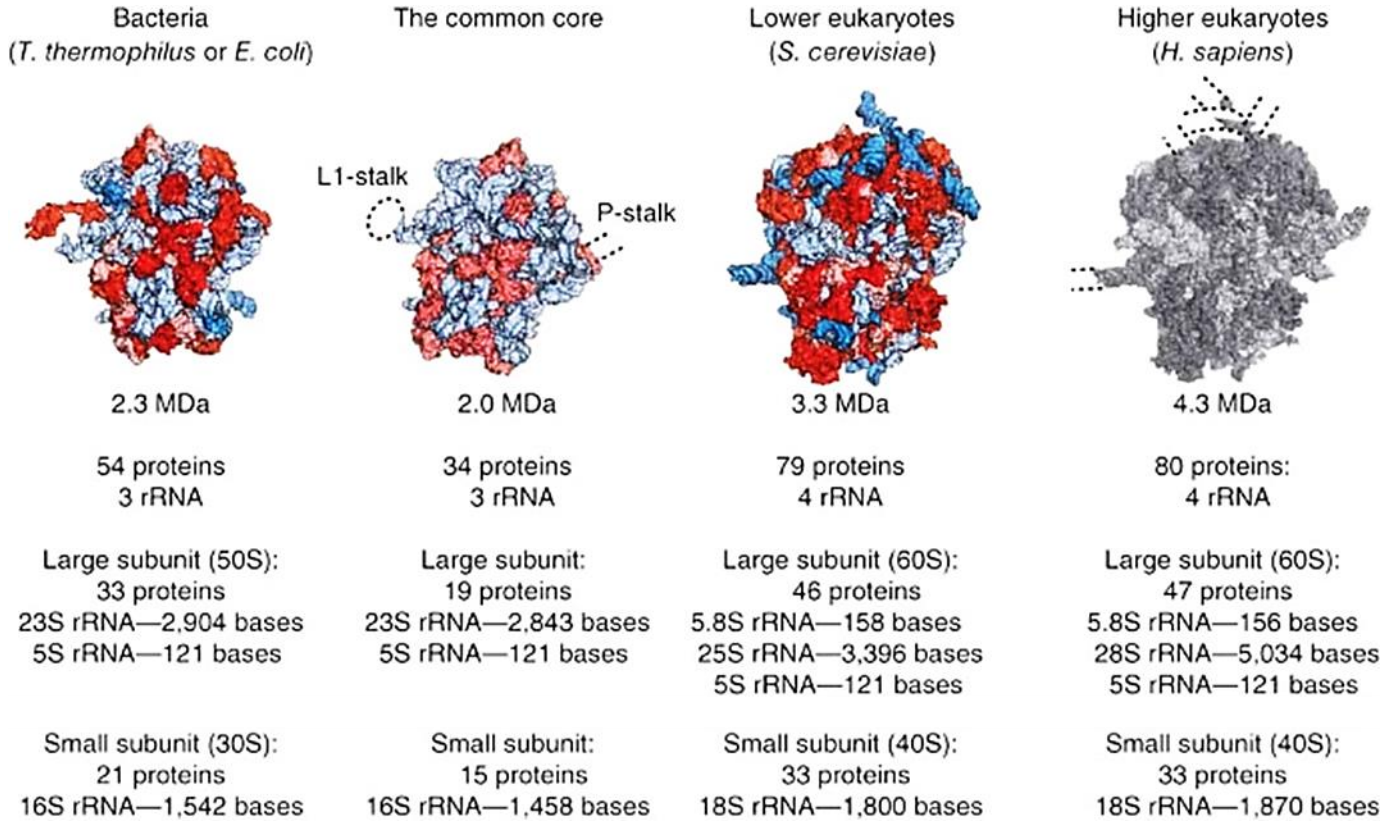

Figure 3: Comparison between the prokaryotic and eukaryotic ribosome
The 70S and 80S ribosomes share a common core. Conserved proteins are indicated in red and rRNA extension segments in blue. The common structures between the yeast and the human ribosomes are indicated in grey on the human ribosome. The dotted lines on the human ribosome show RNA extensions that are only observed in humans. – from (Melnikov et al., 2012)

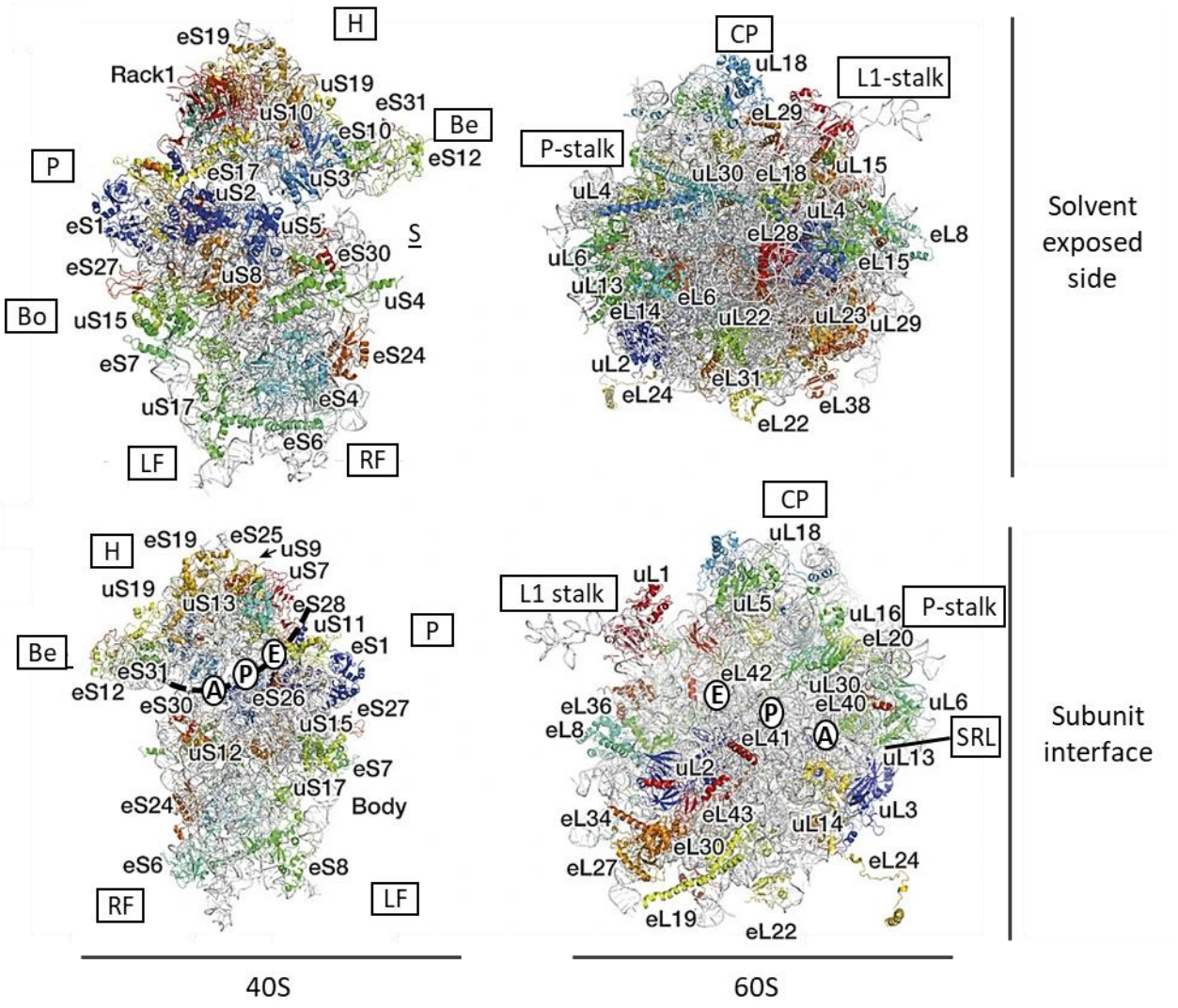

Figure 4: Reconstruction of a human ribosome based on cryo-EM data
The 60S and the 40S subunits are both shown from the solvent side and the subunit interface. The major structural components of the 60S SU are the central protuberance (CP), the P and L1 stalk, the sarcin-ricin loop (SRL) and the exit tunnel. For the 40S subunit are the head (H), beak (Be), platform (P), shoulder (S), body (Bo), left foot (LF) and right foot (RF). A-, P- and E-sites are indicated on both SU. The mRNA groove is indicated by a dotted line. – adapted from (Khatter et al., 2015) (PDB: 4ug0)

New name[#]	Taxonomic range[*]	Bacteria name	Yeast name	Human name
uL1	BAE	L1 (Δ)	L1	L10A
uL2	BAE	L2	L2	L8
uL3	BAE	L3	L3	L3
uL4	BAE	L4	L4	L4
uL5	BAE	L5	L11	L11
uL6	BAE	L6	L9	L9
eL6	E	–	L6	L6
eL8	AE	–	L8	L7A
bL9	B	L9 (Δ)	–	–
uL10	BAE	L10	P0	P0
uL11	BAE	L11 (Δ)	L12	L12
bL12	B	L7/12	–	–
uL13	BAE	L13	L16	L13A
eL13	AE	–	L13	L13
uL14	BAE	L14	L23	L23
eL14	AE	–	L14	L14
uL15	BAE	L15 (Δ)	L28	L27A
eL15	AE	–	L15	L15
uL16	BAE	L16	L10	L10
bL17	B	L17	–	–
uL18	BAE	L18	L5	L5
eL18	AE	–	L18	L18
bL19	B	L19	–	–
eL19	AE	–	L19	L19
bL20	B	L20	–	–
eL20[§]	AE	–	L20	L18A
bL21	B	L21 (Δ)	–	–
eL21	AE	–	L21	L21
uL22	BAE	L22	L17	L17
eL22	E	–	L22	L22
uL23	BAE	L23	L25	L23A
uL24	BAE	L24 (Δ)	L26	L26
eL24	AE	–	L24	L24
bL25	B	L25 (Δ)	–	–
bL27	B	L27 (Δ)	–	–
eL27	E	–	L27	L27
bL28	B	L28	–	–
eL28	E	–	–	L28
uL29	BAE	L29 (Δ)	L35	L35
eL29	E	–	L29	L29
uL30	BAE	L30 (Δ)	L7	L7
eL30	AE	–	L30	L30
bL31	B	L31 (Δ)	–	–
eL31	AE	–	L31	L31
bL32	B	L32 (Δ)	–	–
eL32	AE	–	L32	L32
bL33	B	L33 (Δ)	–	–
eL33	AE	–	L33	L35A
bL34	B	L34 (Δ)	–	–
eL34	AE	–	L34	L34
bL35	B	L35 (Δ)	–	–
bL36	B	L36 (Δ)	–	–
eL36	E	–	L36	L36
eL37	AE	–	L37	L37
eL38	AE	–	L38	L38
eL39	AE	–	L39	L39
eL40	AE	–	L40	L40
eL41	AE	–	L41	L41
eL42	AE	–	L42	L42
eL43	AE	–	L43	L43
P1/P2	AE	–	P1/P2(AB)	P1/P2 (αβ)

New name[#]	Taxonomic range[*]	Bacteria name	Yeast name	Human name
bS1	B	S1	–	–
eS1	AE	–	S1	S3A
uS2	BAE	S2	S0	SA
uS3	BAE	S3	S3	S3
uS4	BAE	S4	S9	S9
eS3	AE	–	S4	S4
uS5	BAE	S5	S2	S2
bS6	B	S6 (Δ)	–	–
eS6	AE	–	S6	S6
uS7	BAE	S7	S2	S5
eS7	E	–	S7	S7
uS8	BAE	S8	S22	S15A
eS8	AE	–	S8	S8
uS9	BAE	S9	S16	S16
uS10	BAE	S10	S20	S20
eS10	E	–	S10	S10
uS11	BAE	S11	S14	S14
uS12	BAE	S12	S23	S23
eS12	E	–	S12	S12
uS13	BAE	S13	S18	S18
uS14	BAE	S14	S29	S29
uS15	BAE	S15 (Δ)	S13	S13
bS16	B	S16	–	–
uS17	BAE	S17	S11	S11
eS17	AE	–	S17	S17
bS18	B	S18	–	–
uS19	BAE	S19	S15	S15
eS19	AE	–	S19	S19
bS20	B	S20 (Δ)	–	–
bS21	B	S21 (Δ)	–	–
bTHX	B	THX	–	–
eS21	E	–	S21	S21
eS24	AE	–	S24	S24
eS25	AE	–	S25	S25
eS26	E	–	S26	S26
eS27	AE	–	S27	S27
eS28	AE	–	S28	S28
eS30	AE	–	S30	S30
eS31	AE	–	S31	S27A
RACK1	E	–	Asc1	RACK1

[#]b: bacterial, e: eukaryotic, u: universal
[*]B: Bacteria, A: Archaea, E: Eukaryotes
Δ: gene is not essential
[§]protein LX in Archaea

Table 1: New standard nomenclature
New standard nomenclature according to (Ban et al., 2014)

1.1.1.1 The central protuberance

The central protuberance (CP) is made up of the 28S and 5S rRNAs along with RPs such as RPL11/uL5 and RPL5/uL18 amongst others. RPL11 and RPL5 are both essential for the 23S and 5S rRNAs interactions in *E.coli* (Gray et al., 1972; Chen and Ehrke, 1976; Bogdanov et al., 1995; Schuwirth et al., 2005; Korepanov et al., 2012). It was demonstrated with cryo-EM modelling that components of the CP were participating in inter-subunit bridges. It connects for example the decoding centre, with a 5S rRNA extension, to functional regions of the LSU such as the peptidyl transferase centre to allow a coordinated translation process (Rhodin et al., 2011; Liu and Fredrick, 2016) (**Figure 5**).

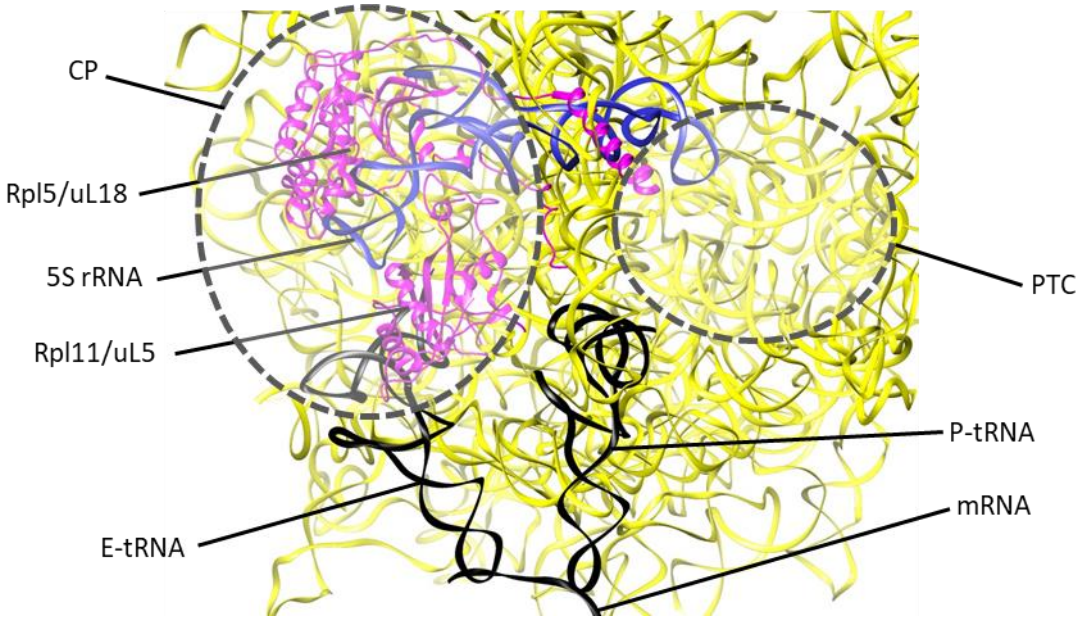

Figure 5: Structure of the central protuberance
Illustration of a human ribosome from cryo-EM (PDB: 6oli) (Li et al., 2019). Only the 5S rRNA (blue), the 28S rRNA (yellow) and the ribosomal proteins uL18 and uL5 (magenta) are shown. The 5S rRNA extends from the CP to the PTC. tRNAs in the P- and E- site are indicated along with the mRNA.

1.1.1.2 L1 stalk

The L1 stalk is a flexible structure composed of RPL10a/uL1 and helices H76, H77 and H78 from the 28S rRNA. A hinge point is situated at the RP-rRNA junction (Spahn et al., 2004a). L1 stalk is not essential to the ribosomal function as it may be absent from ribosomes in the polysome fraction (McIntosh et al., 2011). However it is required for the efficient export of the 60S subunit to the cytoplasm (Musalgaonkar et al., 2019). It is known to interact with the

deacylated tRNA in the E site to allow its exit from the ribosome, thus enabling a new elongation cycle. Fluorescence resonance energy transfer (FRET) assay revealed that the stalk can adopt an open or a closed conformation by transitioning through a hybrid 'half-closed' conformation (Chandramouli et al., 2008; Fei et al., 2008; Cornish et al., 2009; Trabuco et al., 2010). In closed conformation, the L1 stalk is positioned directly at the exit of the E-site to prevent tRNA departure from the ribosome. These conformations were also seen in mammalian ribosomes during elongation (Chandramouli et al., 2008).

1.1.1.3 GTPase associated centre

The GTPase associated centre (GAC) is the landing dock for translational GTPases (trGTPases). These trGTPases are required for GTP hydrolysis during translation (Rodnina et al., 2000; M et al., 2005). It is made up of the sarcin-ricin loop and the P-stalk.

1.1.1.3.1 Sarcin-ricin loop

The sarcin/ricin loop (SRL) is a highly conserved region of helix 95 of 25S/28S rRNA. It is a highly-organised hairpin which is held in place through Watson and Crick base pairing and electrostatic interactions (Szewczak et al., 1993). Its name originates from ribotoxin α-sarcin and ribosome-inactivating protein ricin that targets this loop (Ackerman et al., 1988; Olombrada et al., 2020). Contrary to other rRNA domains, the SRL is directly exposed to the cytoplasm and is essential for elongation (Correll et al., 1998; Yusupov et al., 2001). In bacteria, the hairpin structure is recognised by translation factors such as trGTPase EF-G via its GTP-binding domain (Yusupov et al., 2001; Mitkevich et al., 2012). Studies have shown that cleavage of SRL induces the inhibition of elongation due to defects in the recruitment of translation factors (García-Ortega et al., 2010; Grela et al., 2019).

1.1.1.3.2 P stalk

The P stalk is the eukaryotic analogue of the L7/L12 stalk in bacteria. It is composed of acidic proteins RPLP0/uL10, RPLP1/P1 and RPLP2/P2. Within the complex, RPLP0/uL10 interacts with two RP heterodimers of RPLP1/P1 and RPLP2/P2 thus forming a pentameric complex (**Figure 6A**). These proteins are acidic in nature, with an identical sequence of about

10 amino acids at the C-terminus of the proteins (**Figure 6C**). RPLP1/P1 and RPLP2/P2 have 4 α-helices at the N-terminus for dimerization. (**Figure 6B**). The high flexibility of this structure is due to the presence of a hinge region within the P proteins. In yeast, the binding of the P1/P2 dimers to RPLP0/uL10 are independent from one another. However, there are two essential requirements for the formation of the P stalk: (i) the dimer P1A-P2B and (ii) the amino acid sequence of RPLP0/uL10 from position 199 to 230 (Krokowski et al., 2006). This structure is anchored to the ribosome and held in position by RPL12/uL11 and the SRL (Egebjerg et al., 1990)

This structure is only added in the later stages of the 60S maturation and is necessary to a functional ribosome (Remacha et al., 1995; Lo et al., 2010). For its integration in the LSU, RPLP0/uL10 is phosphorylated on the N terminal (Filipek et al., 2020). The P stalk facilitates the hydrolysis of GTP to GDP (Liljas and Sanyal, 2018). Deleting RPLP0/uL10, RPLP1/P1 and RPLP2/P2 completely abrogates translation. A functional ribosome requires at least RPLP0/uL10 alongside with a 30 amino acid extension at its C-terminus corresponding to the C-terminus sequence of RPLP1/P1 and RPLP2/P2 (Remacha et al., 1995). These C-terminals are required to recruit elongation factors and for eEF2-dependent GTPase activity (Köpke et al., 1992; Bargis-Surgey et al., 1999; Vard et al., 1997)

It is interesting to point out that replacing the L7/L12 stalk by the P stalk in bacterial 50S subunit allow translation only if eukaryotic elongation factors eEF1 and 2 are added to the medium as the ribosomes are no longer able to recruit the prokaryotic equivalent EF-Tu and EF-G (Uchiumi et al., 2002a, 2002b)

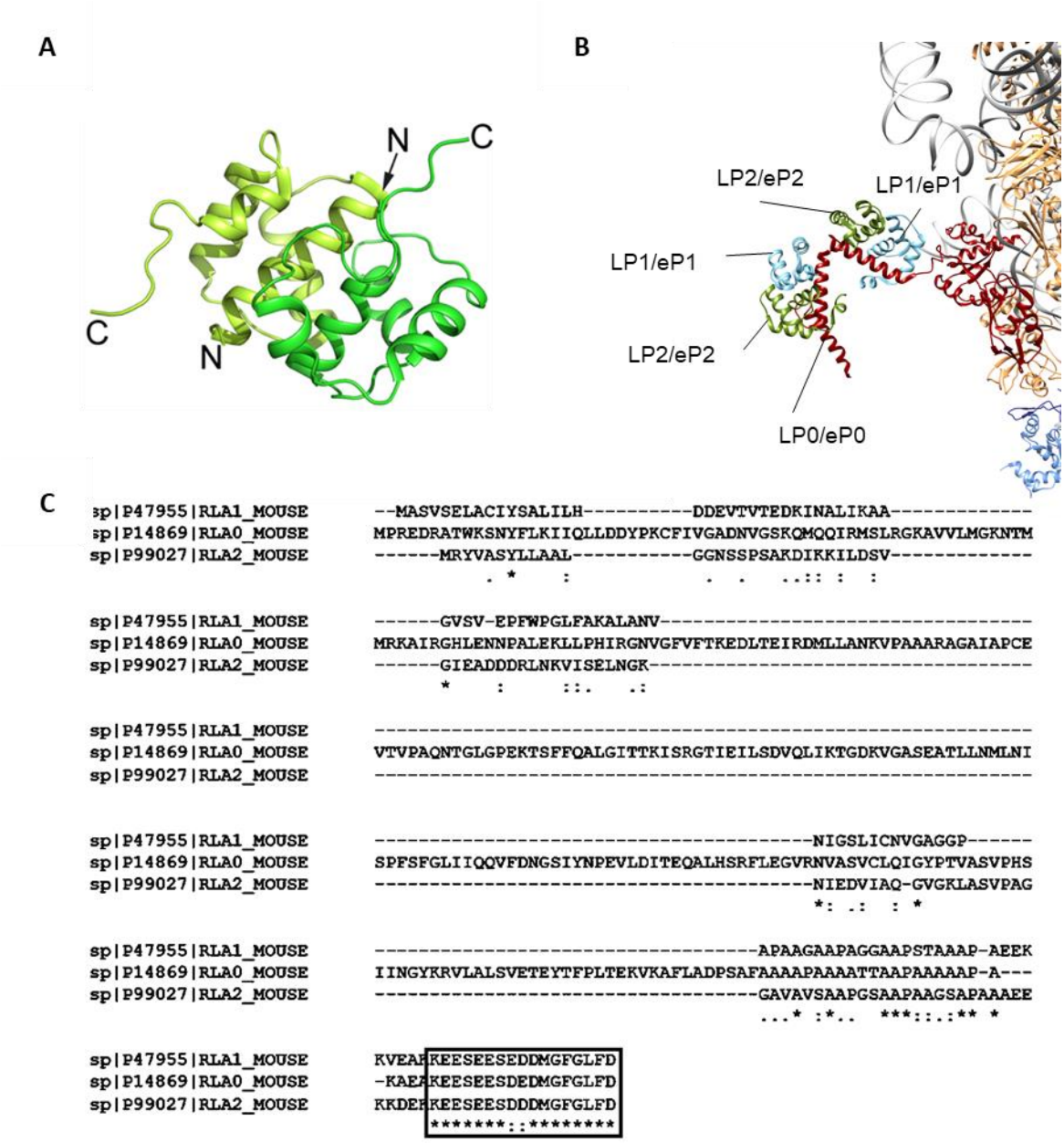

Figure 6: Primary and quaternary structure of the P stalk on a human ribosome
(A) Structure of P1/P2 dimer (PDB: 2LBF) (Liljas and Sanyal, 2018) (B) Structure of the P-stalk anchored to the ribosome by RPL12/uL11 and 28S rRNA. Structures were created on UCSF Chimera (1.15 version) PDB code: 6zme (Thoms et al., 2020) (C) Homology in murine P0, P1 and P2 sequences. CLUSTAL multiple sequence alignment by MUSCLE (3.8 version)

1.1.1.4 Nascent polypeptide exit tunnel (NPET)

This tunnel, referred by Markin as the nascent peptide 'birth canal' (Mankin, 2006), is formed by 28S rRNA, RPL4/uL4, RPL17/uL22 and RPL39/eL39 in eukaryotes (Schulze and Nierhaus, 1982; Zhang et al., 2013b). It runs from the peptidyl transferase centre, through the body, to the solvent side resulting in a tube of about 90 Å-long, 15 Å-wide (**Figure 7A**).

It is divided into 2 parts: the upper part closer to the PTC and the lower part which is connected to the solvent side. The two parts are separated by a constriction due to RPL4/uL4 and RPL22/uL22. A comparative analysis from 2019 compared 20 structures of prokaryotic and eukaryotic ribosomes. They identified two major differences between eukaryotic and prokaryotic ribosomes. Firstly, the 70S ribosomes had only one constriction due to the presence of RPL4/uL4 and RPL22/uL22 whereas the 80S ribosome had a second constriction due to the positioning of an RPL4/uL4 loop. The second difference is the shape of the tunnel which is different in eukaryotes, due to the presence of RPL39/eL39, instead of an extension of RPL23A/uL23 which is present in prokaryotes (Dao Duc et al., 2019; Guzel et al., 2020) (**Figure 7C**).

A recent study pointed out that the absence of RPL4/uL4 during ribosome maturation in the nucleolus results in a defect in the nascent polypeptide exit tunnel. (Wilson et al., 2020). On the other hand, by inserting a mutation of RPL17/uL22, Wekselman and colleagues were able to alter its spatial conformation and consequently, modify its interaction with the 28S rRNA hence changing the shape of the tunnel. Strikingly, the peptide migration within the tunnel was unaffected (Wekselman et al., 2017). Some insights on these effects could come from changes in ribosome stalling or pausing through mutations of the NPET (Takamatsu et al., 2020). Indeed, the progression of the nascent chain inside the NPET induces local conformation changes that can modulate the activity of the PTC (described later) thus influencing the stalling mechanism in ribosomes (Ramu et al., 2011; Ito and Chiba, 2013; Lu and Deutsch, 2014)

Some studies suggest that co-translational folding of the nascent peptide could take place within the NPET during elongation (Fedorov and Baldwin, 1997; Lu and Deutsch, 2005). This could imply that the NPET itself could act as a chaperone for small protein folding (Nilsson et al., 2015). It is difficult to observe this phenomenon as it occurs inside the tunnel. A recent study using optical tweezers to investigate the cotranslational folding of proteins. Optical tweezers uses the properties of light through polystyrene beads (Nobel prize of Physics 2018 –

reviewed in (Killian et al., 2018)) By attaching one bead to the N-terminal of the nascent peptide and the another on RPL4/uL4 inside the tunnel, they are able to measure the distance between the beads. They can also stretch the nascent peptide by pulling on the bead to remove any folding that could be formed. Using a small protein domain of ADR1 flanked by two tags as model, they revealed that the nascent protein could fold inside the NPET as there was on average an additional 31 amino acids upon stretching of the nascent peptides. They also show that folding occurred more easily when it was in the NPET, most likely due to electrostatic interactions (Wruck et al., 2021).

At the exit of the NPET, on the solvent side, are RPL26/uL24, RPL35/uL29 and RPL23A/uL23 (**Figure 7B**). RPL26/uL24 could be involved in the translocation of the nascent peptide to the endoplasmic reticulum. It can recruit ubiquitin-like modifier UFM1 that forms part of the ribosome-associated quality control to either induce translocation or the proteasome-mediated decay of the newly synthesised protein (Wang et al., 2020b). RPL35/uL29 acts as an adaptor for the nascent protein-associated complex involved in protein folding (Pech et al., 2010; Gamerdinger et al., 2019). Lastly, RPL23A/uL23 is known to interact with mTORC2 during translation to phosphorylate and stabilise newly synthesised Akt polypeptides (Oh et al., 2010)

1.1.1.5 Peptidyl transferase centre

The peptidyl transferase centre (PTC) is composed of 28S rRNA only and is located near to the A- and P- sites of the LSU, which will be later described. The closest ribosomal proteins, which are at least 20 Å away from the PTC are : RPL8/uL2, RPL3/uL3, RPL4/uL4, RPL10/uL16, RPL21/eL21 and RPL29/eL29 (**Figure 8**) (Klinge et al., 2011). The section of 28S rRNA composing the PTC is divided in a pseudo symmetrical ribosomal region and is thought to have emerged from the fusion of 2 RNAs molecules (Rivas and Fox, 2020). Each region is linked to either the A or the P site (Agmon et al., 2003, 2005).

This centre is rather flexible to adapt to the circulating tRNAs and the nascent peptide that exits through the NPET. Any alteration to the 28S rRNA or surrounding proteins can modify the translating properties of ribosomes. Studies have shown that point substitution mutations on RPL3/uL3 or rRNA induced changes in conformation in the centre resulting in a less accessible binding site (Bøsling et al., 2003; Pringle et al., 2004; Long et al., 2009) but no changes in the translating abilities of the ribosomes (Polacek et al., 2001)

The PTC is central to the catalytic activity of the ribosome. It catalyses two reactions: (i) the formation of the peptide bond and (ii) the release of the nascent peptide from the ribosome. This is achieved by decreasing the activation energy required to initiate these reactions. During the formation of a new peptide bond, between an amino acid and a polypeptide, there should be a nucleophilic attack between the amine group of the amino acid of the aminoacyl-tRNA of the A site and the ester bond from the peptidyl-tRNA in the P-site. This reaction is followed by the formation of an unstable tetrahedral intermediate that will rapidly dissociate. We therefore have the polypeptide chain attached to the tRNA present in the A-site on one side, and on the other, a de-aminoacylated tRNA in the P site. At the end of translation, a hydrolysis reaction will free both the newly synthesised polypeptide and the deacylated tRNA

The PTC and the NPET are interconnected. The presence of a polypeptide in the NPET can induce a nascent peptide translation arrest, that is, ribosome stalling (Seidelt et al., 2009). During the study of this mechanism, Ramu and colleagues discovered that the conformation of the PTC A-site depends on the nascent peptide sequence in the NPET. They also showed that the MGIFSIFVI peptide sequence induces stalling by preventing the insertion of aa-tRNA in the A site (Ramu et al., 2011).

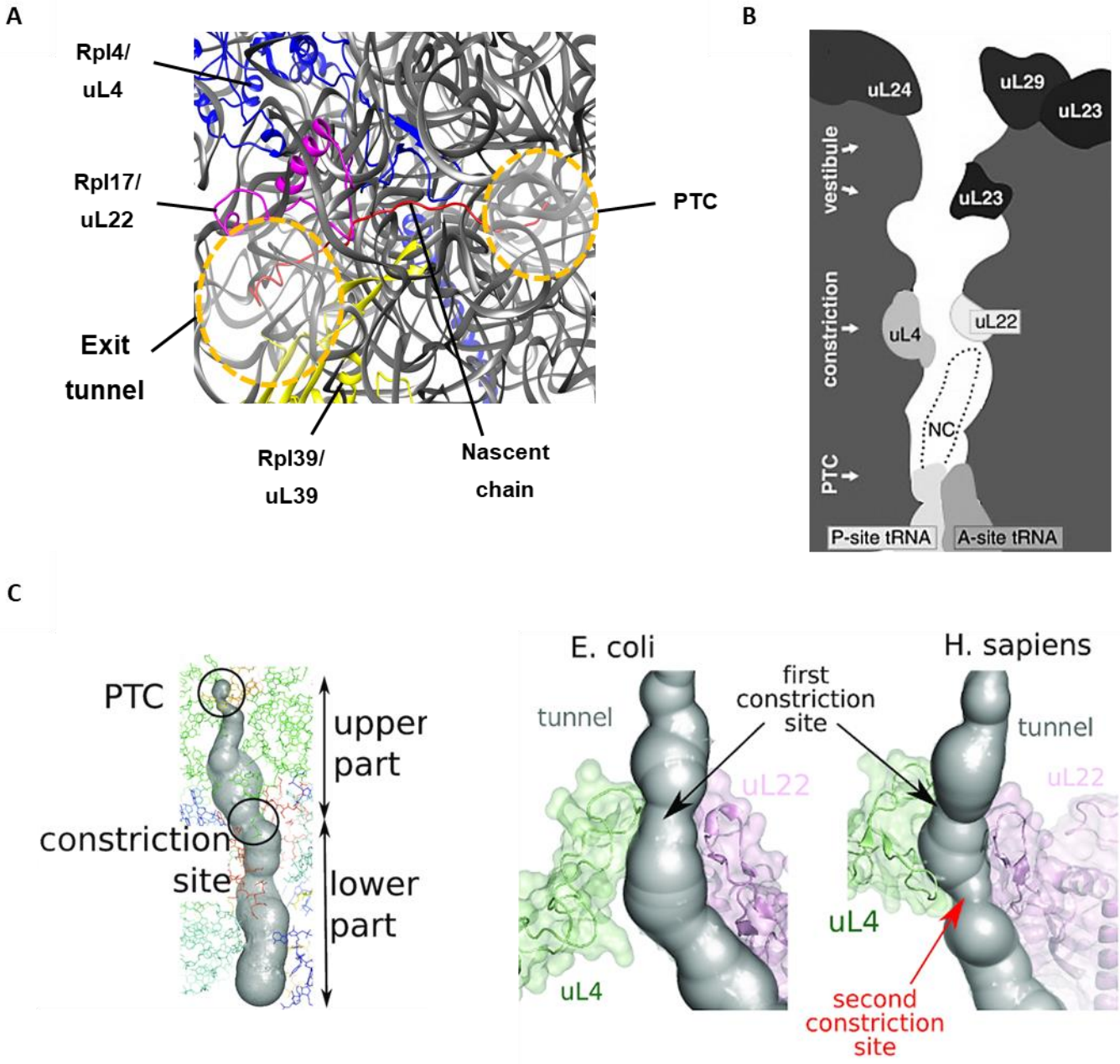

Figure 7: Representation of the NPET using cryoEM database
. (A) Transverse view of the peptide exit tunnel with respect to the PTC and the exit site on the solvent side; nascent polypeptide (red), 28S rRNA (grey), RPL4/uL4 (blue) , RPL17/uL22 (yellow) and RPL39/eL39 (magenta). The structure was created on UCSF Chimera (1.15 version) ; PDB code: 6oli (Li et al., 2019) (B) Schematic representation of the transverse view channel of RP lining the NPET (NC = nascent chain) – adapted from (Bock et al., 2018) (C) Comparison of the prokaryotic and eukaryotic NPETs – from (Dao Duc et al., 2019).

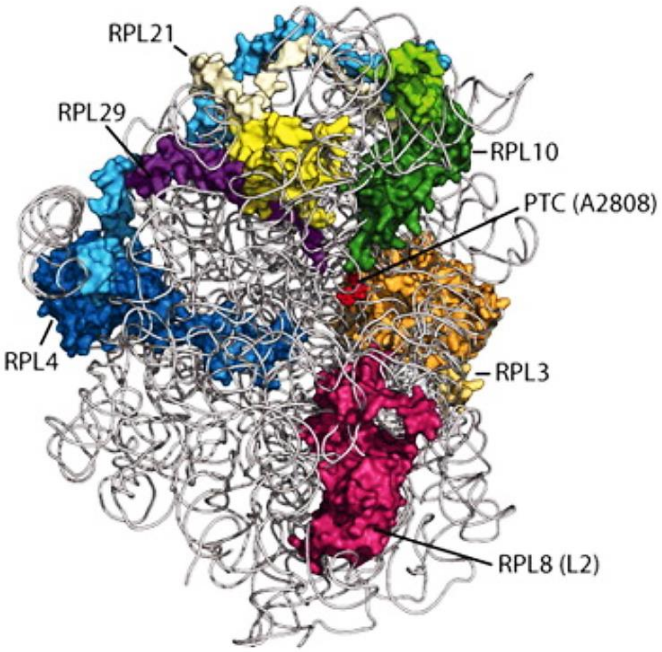

Figure 8: RP environment surrounding the PTC
Location of RPL and PTC on a 60S subunit (Klinge et al., 2011)

1.1.2 The small subunit

The eukaryotic small subunit is composed of 33 small ribosomal proteins called eS or uS (old nomenclature: RPS) (Ban et al., 2014), and an 18S ribosomal rRNA. Architecturally, it is divided in two lobes by the mRNA tunnel forming the head and the body. The mRNA enters the tunnel, in-between the head and the platform and wraps the neck of the SSU. (**Figure 4**). The head has a protrusion called the beak due to its resemblance to a bird's beak. The body is itself composed of a platform, a shoulder, a left foot and a right foot. These two regions are connected by the neck region where the mRNA tunnel is located. The SSU possesses one functional structure: the decoding centre.

- **The decoding centre**

Studies on the decoding centre, or DC, began in the 70s. At that time, it was thought that rRNA was the structural support for RPS to translate mRNAs. By the mid-70s, studies on 16S rRNA within prokaryotic ribosomes revealed a greater functional role of rRNA during

translation (Noller, 1974; Woese et al., 1975). It was only in 1978 that evidence of the direct interaction between the 16S rRNA and tRNA was obtained. (Schwartz and Ofengand, 1978). The DC is located in the A site. It is composed of 5 helices (H18, H44, H34, H24, H31) of the 18S rRNA. In eukaryotes, it is surrounded by RPS3/uS3, RPS9/uS4, RPS2/uS5, RPS15/uS19, RPS23/uS12, and RPS30/eS30 (**Figure 9**). The role of the DC during each elongation cycle is to ensure the recruitment of cognate tRNA, while eliminating near-cognate tRNAs which can differ by only one mismatch. It is therefore constantly monitoring the mRNA-tRNA interactions. When a cognate tRNA, bound to eEF1A-GTP, binds to the codon in the A site, there is a conformational change in eEF1A and the subsequent hydrolysis of GTP to GDP. eEF1a-GDP is then released so that the tRNA is can be fully inside the A site, with the amino acid close to the PTC (Gromadski and Rodnina, 2004; Khairulina et al., 2010; Poirot and Timsit, 2016; Shao et al., 2016; Timsit and Bennequin, 2019; Timsit et al., 2021)

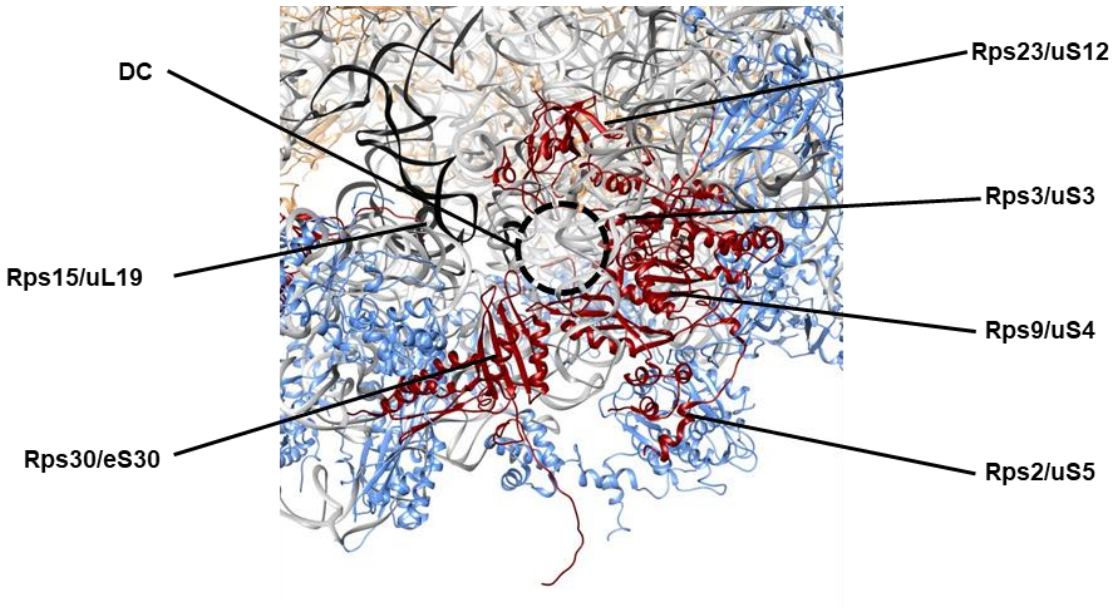

Figure 9: Environment of the Decoding Centre
Representation of the DC based on cryoEM data. The DC and the associated RPS are indicated. PDB code: 6oli. USCF Chimera (1.15 version)

When the ribosome stalls at the stop codon, the releasing factors bind and recognise the stop codon in the A-site of the ribosome by an induced-fit mechanism (Cheng et al., 2009; Jackson et al., 2012). This recognition causes a conformational change in the DC which subsequently induces the remodelling of the PTC and finally, the release of the peptide (Youngman et al., 2006, 2007).

1.1.3 The aminoacyl, peptidyl and exit sites

The aminoacyl, peptidyl and exit sites (A-, P- and E- sites respectively) are tRNA-binding sites and are found both on the SSU and the LSU. Mechanistically, the LSU accommodates a tRNA molecule while the SSU contains the mRNA being translated. The A-site runs from the DC in the small subunit to the PTC in the LSU (**Figure 10**). Binding to the A-site is mRNA-dependent and requires translation factors such as eEF1 and 2. Structurally, it is made up of RPL3/uL3 and RPs from the DC. RPL3/uL3 is located at the entrance of the A-site and is referred to as the 'gatekeeper of the A site' (Meskauskas and Dinman, 2007).

The P-site contains a tRNA molecule esterified to the nascent polypeptide. It is primarily structured by RPL5/uL18, RPL10/uL16 and RPL36A/eL42. (Fabijanski and Pellegrini, 1981) Inside the P-site, RPL5/uL18 anchors the peptidyl tRNA to the P-site (Meskauskas and Dinman, 2001) while RPL10/uL16 extends to the P-site PTC and is required for maturation of the P-site during ribosome biogenesis (Armache et al., 2010a; Sulima et al., 2014; Patchett et al., 2017) (**Figure 10**). RPL36A/eL42 on the other hand interacts with the 3'end of the peptidyl tRNA involved in the PTC reaction (Baouz et al., 2009). RPL36A/eL42 also extends to the E-site (Li et al., 2019). tRNA binding at the P-site is stronger than that of the A-site. Note that in presence of high Mg^{2+} concentrations, tRNA can interact with the P site in a mRNA-independent manner. The transfer of the mRNA-tRNA complex from the A to the P site is monitored by helix H38 of the 23S/25S/28S rRNA, also called the "A-site finger". Simultaneously RPS18/uS13 ensures the maintenance of the reading frame (Komoda et al., 2006).

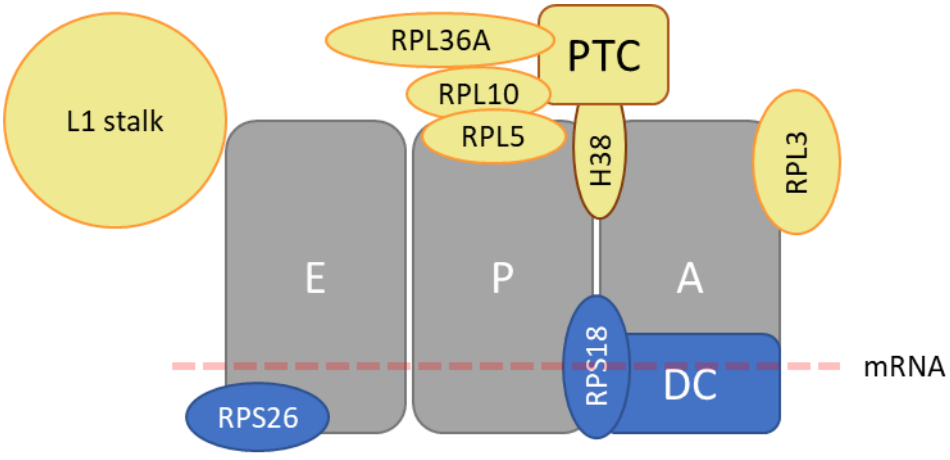

Figure 10: Schematic representation of the A, P and E- sites
The structure of the A, P and E- sites with the functional regions and the associated ribosomal proteins.

The E site is where the deacylated tRNA will move to be unloaded from the ribosome. The release of the tRNA is controlled by the L1 stalk and RPS26/eS26 ensures the maintenance of the mRNA in the E-site (Sharifulin et al., 2012).

All the functional regions have coordinated activities to ensure an optimal translational process.

1.1.4 Intersubunit bridges

The intersubunit bridges maintain the two subunits in close contact and stabilise the 80S structure. The bridges consist of RNA-RNA interactions toward the middle of the structure and RNA-protein and protein-protein interactions towards the periphery (Spahn et al., 2001, 2004a). In addition to ensuring stability, it has a degree of rotation to allow translocation and release of unbound tRNA. In eukaryotes, RPL11/uL5, RPL19/eL19, RPL24/eL24 and RPL41/eL41 interact with the SSU while the expansion segments of the 60S subunit interact with RPS3A/eS1 and RPS8/eS8 of the 40S subunit (Klinge et al., 2012; Tamm et al., 2019).

Expansion segments correspond to specific parts of rRNA. They can be mobile and are not associated with RP (Armache et al., 2010b). They are involved in translation fidelity and recruit proteins involved in peptide processing (Fujii et al., 2018). All intersubunit bridges are summarised in Figure 11. A recent study from 2018 in bacteria showed that controlling the interactions between LSU and SSU can influence the type of mRNA that are translated. For example, bacteria contain orthogonal ribosomes, a specific class of ribosomes, which target specifically orthogonal mRNAs. By engineering a link between the 16S and 23S rRNA, the tethered ribosomes or Ribo-T were able to mediate the translation of orthogonal mRNA (Orelle et al., 2015; Schmied et al., 2018). Such experiments are yet to be performed on eukaryotic ribosomes so as to monitor how differences in subunit interactions can influence their respective translatome, that is, the translated mRNA subset.

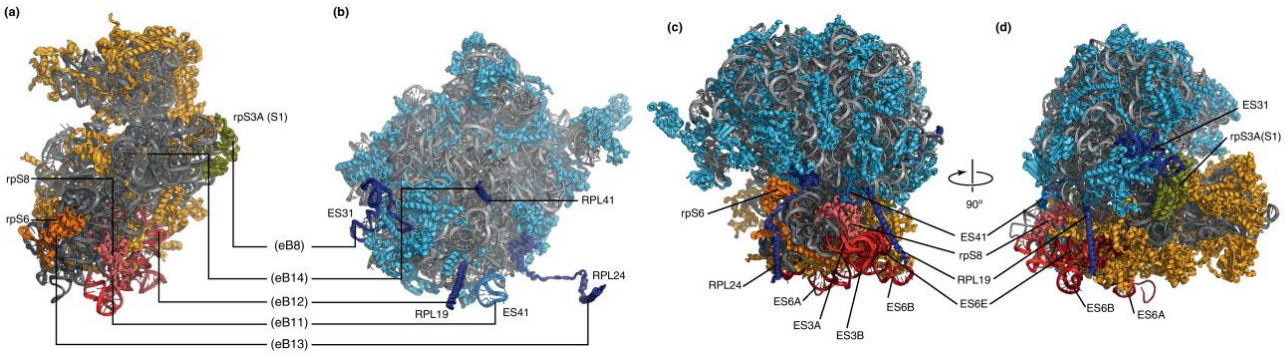

Figure 11: Intersubunit bridges of an 80S ribosome
(a, b) RP bridges (EBs) between the LSU and the SSU. (c, d) rRNA/eS) and RP bridges – from (Klinge et al., 2012)

1.1.5 Communication within the ribosome

RPs are constant monitors of the ribosome state and it is essential to coordinate translation factors recruitment, tRNA movement in the ribosome, mRNA present in the mRNA groove, among others. It was therefore suggested that there could be communications between regions of the ribosome in which RP would form a network within the ribosome and thus enable coordinated activities. This network is assimilated to neuronal circuits with synapses between proteins and/or regions of rRNA (Poirot and Timsit, 2016; Sengupta et al., 2019; Timsit and Bennequin, 2019) (**Figure 12**).

The most probable form of communication would certainly be the change in protein conformation or interactions. For example, when nascent polypeptide chains adopt specific conformations within the NPET, they induce a conformational change that signals to the PTC to stall the ribosome (Seidelt et al., 2009). However, the exact mechanism of this remodelling is yet to be deciphered. Studies are still on-going to understand how interactions between the various components influence the ribosome's ability to recognise and translate mRNAs.

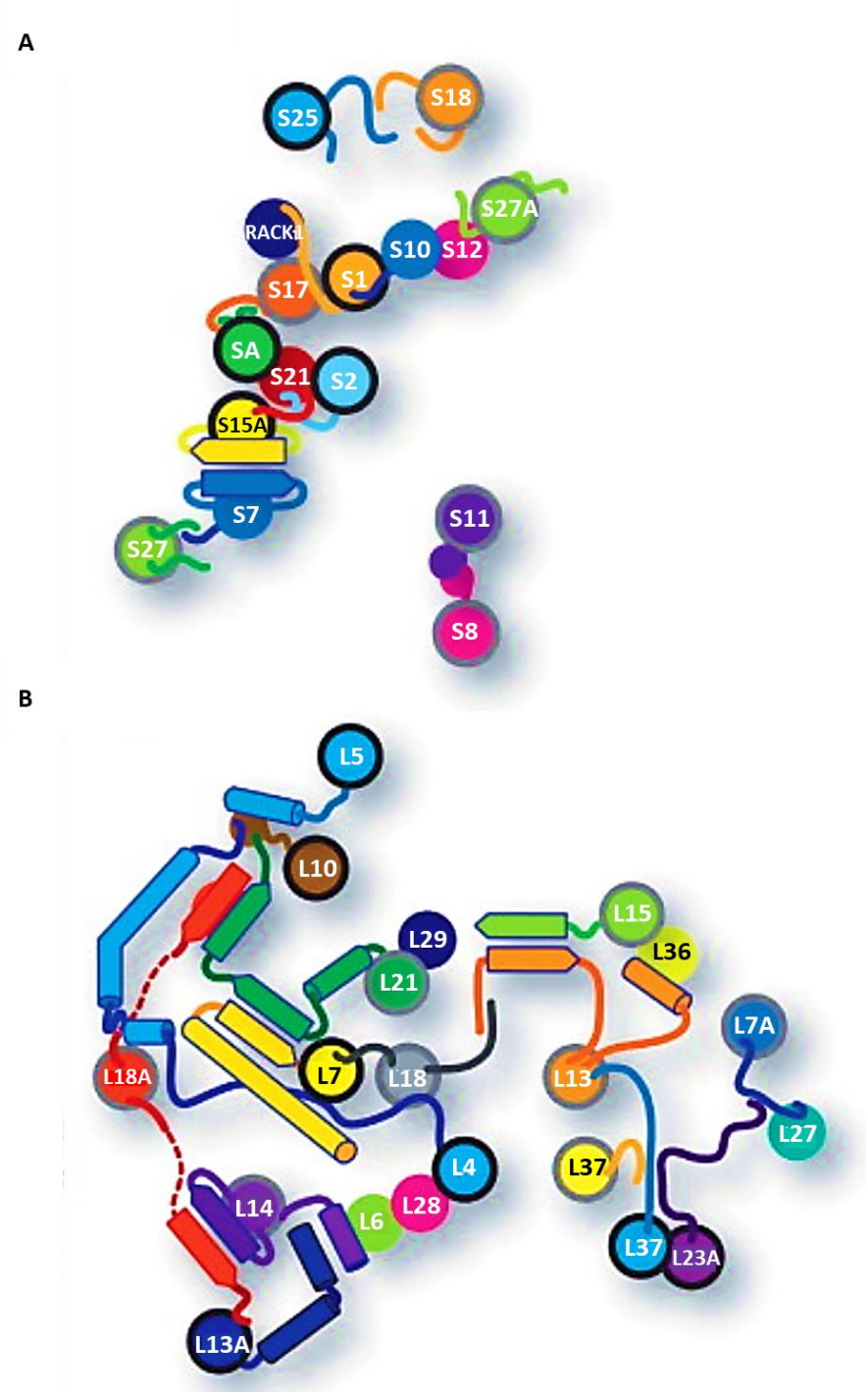

Figure 12: Schematic representation of the network in the 40S and 60S subunits
(A) Interaction between protein domains of RPS in the SSU (B) Interaction between protein domains of RPL in the LSU. Arrows indicate β-sheets while tubes indicate α-helices – adapted from (Klinge et al., 2012)

1.2 Ribosome biogenesis

Ribosome biogenesis is the process by which ribosomes are synthesised and assembled. It is a highly ordered and tightly controlled process. It is one of the most energy-consuming cellular processes. Approximately 7500 subunits are synthesised per minute in active yeast cells (Warner, 1999). Eukaryotic ribosome biogenesis has mostly been studied in yeast but there are increasing studies on the mammalian ribosome underlining the similarities but also the differences between the two eukaryotic organelles. Ribosomes consist of two components that are synthesised separately: RP and rRNA.

1.2.1 Ribosomal protein synthesis

RP-coding genes (RPG) are spread across the genome (Uechi et al., 2001). In yeast, about 150 000 RPs are produced per minute. RNA pol II transcribes RPG for the large and the small subunits. RP mRNAs are then spliced resulting in mature mRNA. The intronic regions of these mRNAs contain small nucleolar RNAs or snoRNAs. These snoRNAs are used in C/D and H/ACA snoRNPs complexes that modify rRNA (described below). Most RP mRNAs contain 5' terminal oligopyrimidine tract (5′ TOP), that is, a cytidine residue at the cap site and up to 13 consecutive pyrimidines flowing the cap. These 5'TOP are present for regulatory purposes (Levy et al., 1991). Anvi and colleagues showed that the replacement of the 5' terminus of *Rpl32* by the 5' terminus of beta-actin resulted in the abolition of translation regulation of *Rpl32* mRNA. 5'TOP regulation is cell type-specific and dependent on the cellular context (Avni et al., 1997).

These mRNAs are exported to the cytoplasm where they are translated into proteins and undergo post-translational modifications. RPs are mostly basic in nature and tend to cluster. Chaperons and transporters are therefore required to prevent the clustering of proteins and to shuttle RPs back in the nucleus, and more precisely in the nucleolus so that they can be incorporated into the pre-ribosome particle. For the latter to be possible,, RPs contain nuclear localisation signals (NLS) that are recognised by importin β-like transport receptors such as Importin β, transportin, RanBP5 and RanBP7 (Jäkel and Gürlich, 1998; Chou et al., 2010).

1.2.2 Ribosomal RNA and modifications

A ribosome contains 4 distinct rRNA molecules: 18S, 28S, 5.8S and 5S rRNAs. 18S, 28S and 5.8S rRNAs synthesis takes place in the nucleolus whereas the 5S rRNA is synthesised outside the nucleolus. Transcription initiation factor RNA (TIF) IIIA, TIF-IIIB, TIF-IIIC and RNA Pol III associate to a 5S rDNA promoter to synthesise the 5S rRNA. The 5S will then migrate to the nucleolus to be incorporated in the LSU. On the other hand, 18S, 5.8S and 28S rRNAs are encoded in by 47S rDNA located in the fibrillar centre of the nucleolus. Upstream binding factor (UBF), selectivity factor (SL)-1 and TIF-IA recruit RNA Pol I to the 47S rDNA promoter region to initiate transcription. This transcription step is the rate-determining step of ribosome biogenesis. The resulting transcript is a single precursor called the 47S pre-rRNA. It is composed of the 18S, 5.8S and 28S rRNAs, separated by internal transcribed sequences 1 and 2 (ITS1 and ITS2) and are flanked by the 5' and 3' external transcribed sequences (5'ETS and 3'ETS) (**Figure 13A**).

rRNA modifications are added co-transcriptionally and post-transcriptionally. In human, the most frequent modifications are 2'O-methylations (2'OMe) with 106 sites, followed by the pseudouridylation (Ψ), with 95 predicted sites (Krogh et al., 2016; Penzo and Montanaro, 2018). 2'OMe are methyl groups that are added on the oxygen of the C2 of the ribose. Ψ involves the isomerisation of uracil in 5-ribosyl uracil. These modifications are added through RNA-RNA interactions by 2 different small nucleolar ribonucleoproteins (snoRNP) called C/D snoRNPs, and H/ACA snoRNPs.

2'OMe are added by C/D box snoRNPs. They are composed of C/D snoRNAs that have a stem-internal loop-stem structure (**Figure 13B**). They contain a C box (5'-NUGAUGA-3') and a D motif (5'-CUGA-3') at the 5' and 3' termini respectively. They also contain a K-loop composed of C'/D' motif. This region contains the target site of 2'OMe. snoRNAs act as guides that are complementary to the regions around the target site. They associate with 15.5K, an RNA binding protein and heterodimer NOP56/NOP58 that interacts with 2'O methyltransferase Fibrillarin (FBL) and also stabilises the stem-internal loop-stem structure (**Figure 13C**) (Cahill et al., 2002; Lin et al., 2011; Watkins and Bohnsack, 2012; Höfler et al., 2021) .

Pseudouridylations are added by H/ACA box snoRNPs. H/ACA box snoRNAs generally form 2 hairpin structures. A hinge or H motif (5'-ANANNA-3') is located between the hairpin and an ACA nucleotide sequence, called ACA box, is found at the 3' end (**Figure 13D**). They are associated with NOP10, pseudouridine synthase Dyskerin, , NHP2 and GAR1

(**Figure 13E**) (Henras et al., 1998; Reichow and Varani, 2008; Koo et al., 2011). These associated proteins maintain the structure of the snoRNP. A comprehensive database of human H/ACA and C/D box snoRNAs sequences can be found at (Bouchard-Bourelle et al., 2020). Other modifications such as N^7-methylguanosine and N^6,N^6-dimethyladenosine are also present on eukaryotic rRNA (Brand et al., 1977; Alberty et al., 1978). N^7-methylguanosine are guanine methylated on the nitrogen in 7^{th} position similar to the 5' cap found on mRNA and is present in 40% of nuclear 18S pre-rRNA in yeast (Brand et al., 1977; Enroth et al., 2019). The addition of this methylation to G1575 of the 18S rRNA during late 40S maturation induce a conformational change and the formation of a ridge between the P and E sites (Létoquart et al., 2014) N^6,N^6-dimethyladenosine is through to be involved in the subunit joining in bacteria (Rife and Moore, 1998). A database of RNA modifications can be found at https://iimcb.genesilico.pl/modomics/ (Boccaletto and Bagiński, 2021)

1.2.3 rRNA processing

rRNA processing consists of a series of cleavages in the presence of RP and associated factors. There are more than 170 associated factors involved in rRNA processing. They form the nucleolar proteome (Couté et al., 2006) (**Figure 14**). The first cleavages of the 47S occur at A' and 02 sites to yield 45S pre-rRNA.

There are 2 pathways for the processing of the 45S pre-rRNA. The pathway selected will depend on the location of the first cleavage of the 45S pre-rRNA. If the first cleavage occurs on A' and 1 sites, the 5'ETS is removed and a single 41S precursor is formed (**Figure 13A, left**). Factors forming the SSU processome (RPS, U3 snoRNA and associated factors) ensure the correct cleavage of the 5'ETS (Sharma and Tollervey, 1999; Osheim et al., 2004; Ferreira-Cerca et al., 2005). This 41S pre-rRNA will be further cleaved on site 2 to form the 21S pre-rRNA, containing the 18S rRNA and ITS1, and a 32S pre-rRNA, containing both 5.8S and 18S rRNAs bound by ITS2.

- The 21S pre-rRNA is then cleaved at site E by hUTP24, a component of the SSU processome with an endonucleolytic activity. This is quickly followed by 5'-3' trimming by XRN2. Site 3 is then finally cleaved by endonuclease NOB1 to form the 18S-E rRNA (Pertschy et al., 2009; Preti et al., 2013; Wells et al., 2016). NOB1 and poly(A)-specific ribonuclease and other factors are transported along with the 18S-E rRNA to the cytoplasm for the final trimming at site 3 to form the 18S rRNA (Preti et al., 2013; Montellese et al., 2017).

- The 32S pre-rRNA is cleaved at the site 4 by endonuclease Las1 to form the 28S rRNA and an intermediate 12S pre-rRNA containing 5.8S rRNA (Gasse et al., 2015; Schillewaert et al., 2012). ITS2 on the 12S intermediate is removed by exonuclease ISG20L2 (Couté et al., 2008). Fragments of ITR2 on the 28S rRNA are removed by 5'-3' exonuclease XRN2 (Wang and Pestov, 2011). The final products are the 5.8S and 28S rRNA.

If the first cleavage by Nop52 or RNAse MRP is on site 2, the two resulting molecules are the 30S pre-rRNA (containing the 18S rRNA, 5'ETS and ITS1) and the 32S pre-rRNA (containing the 5.8S and 28S rRNA that are still connected by ITR2) (Yoshikawa et al., 2015; Goldfarb and Cech, 2017) (**Figure 13A, right**). The 5'ETS of the 30S pre-rRNA is cleaved by endonucleases on sites A0 and 1 resulting in the formation of the 21S pre-rRNA (Kent et al., 2009). The subsequent processing of the 21S and 32S pre-rRNA are identical to the first pathway.

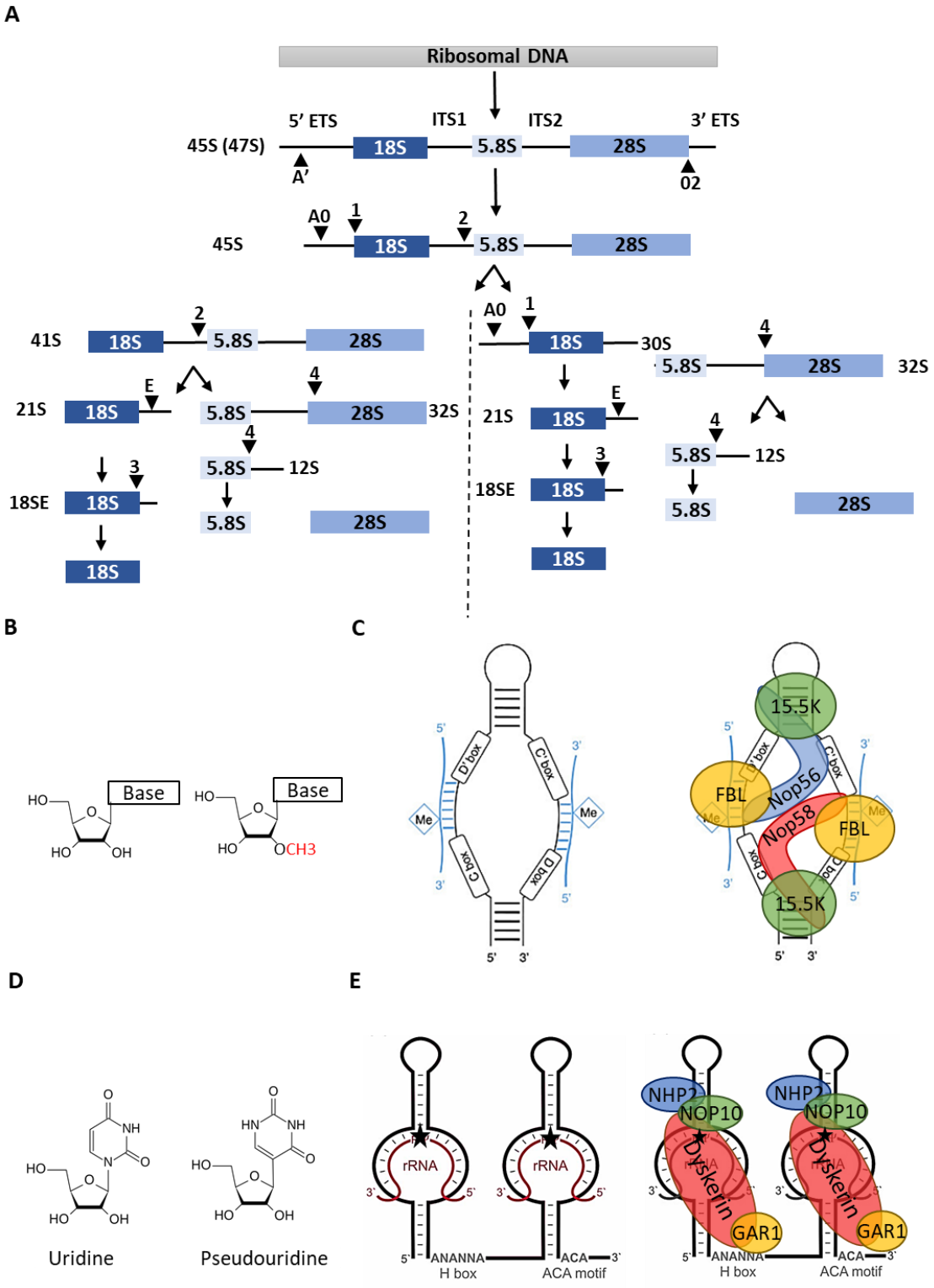

Figure 13: Synthesis, processing and modifications of rRNA

(A) Processing of the 47S rRNA to form the 18S, 5.8S and 28S rRNAs (B) 2'O methylations are added on the oxygen molecule bound to the C2. (C) C/D box snoRNP with the snoRNA and associated proteins. (D) Isomerisation of uridine in pseudouridine. (E) H/ACA box snoRNP that guides pseudouridylation. NHP2, NOP1, GAR1 and Dyskerin associate to a H/ACA snoRNA.

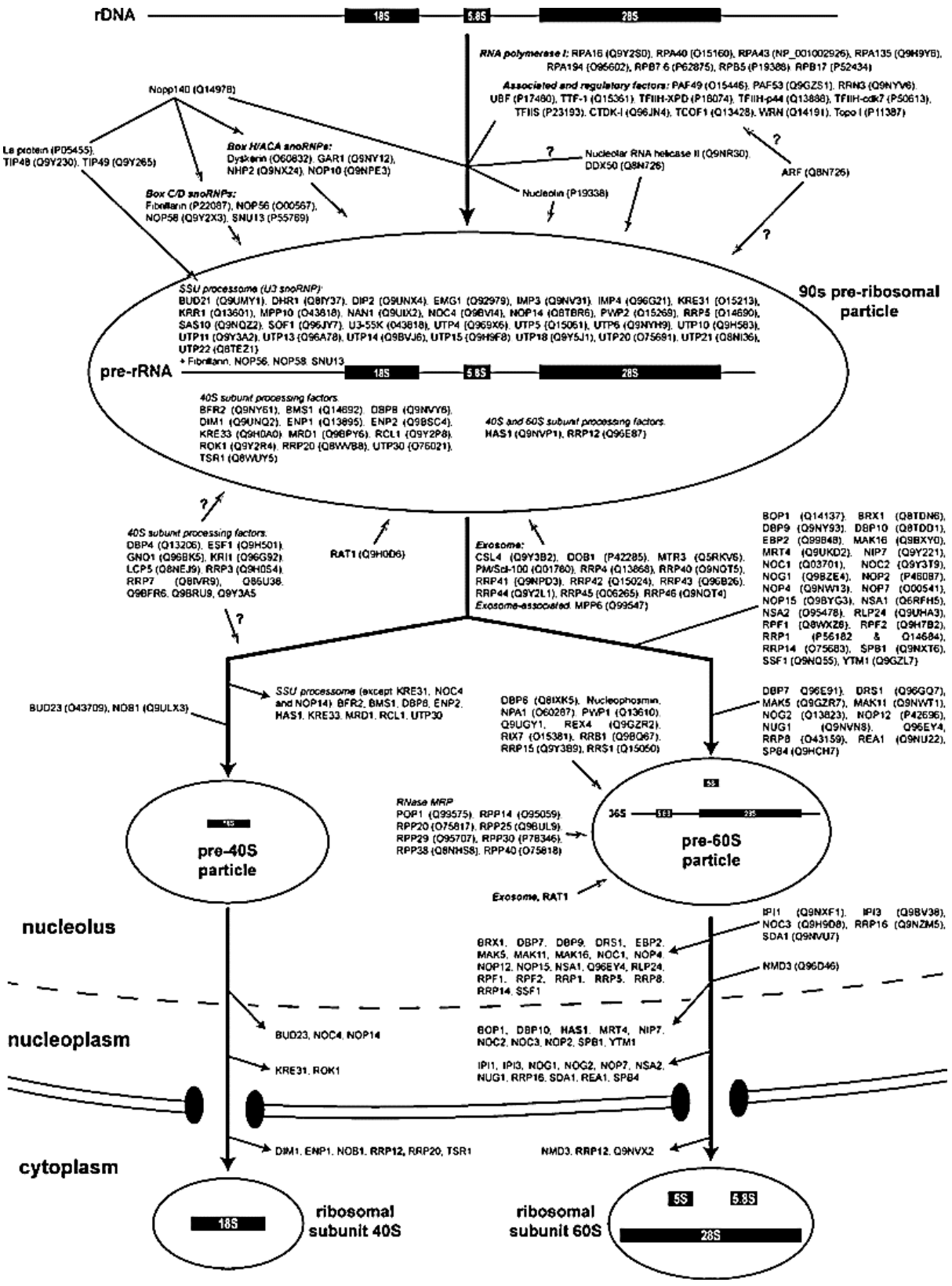

Figure 14: Associated factors involved in rRNA processing and ribosome assembly
More than 170 factors were identified by proteomic analysis. They are involved at each step of the subunits maturation – from (Couté et al., 2006)

1.2.4 Ribosome assembly and maturation

The first RPSs are recruited during the 47S rRNA synthesis. They bind to the portion of rRNA corresponding to the 18S rRNA. (Fox et al., 2019; Piazzi et al., 2019). RPS are incorporated by assembly factors which will bind to the pre-rRNA to form the 90S preribosomal particle. This process takes place in the dense fibrillar compartment of the nucleolus. The assembly of the pre-rRNA with the different RPSs induces several conformational rearrangements to facilitate recruitment of the next factors. Among the first RPS to be recruited are RPS7 and RPS24. For example, RRP7 interacts with RPS27/eS27 to be integrated into the preribosomal particle. RPS27/eS27 deletion is lethal in yeast (Baudin-Baillieu et al., 1997).

Focussing on the SSU assembly, O'Donohue and colleagues identified two functional groups of RPS during mammalian ribosome assembly in HeLa cells (**Figure 16**). Initiation RPS (i-RPS) are required in the first steps of maturation. The knockdown of one of the 16 i-RPS abrogates early ribosome maturation as it causes mild to strong accumulation of 45S and 30S pre-rRNA due to a lack of downstream pre-40S-ribosomes formation (O'Donohue et al., 2010). The accumulation of 45S and 30S pre-rRNA was also observed in yeast with RPS14/uS11 knockdown (Jakovljevic et al., 2004)

The second group is composed of processing RPS (p-RPS). p-RPS are required in the downstream cleavage process (O'Donohue et al., 2010). The knockdown of p-RPS allows partial or complete formation of the 21S and 188S-E rRNA. Upon RPSA/uS2, RPS18/uS13, RPS19/eS19 and RPS21/eS21 knockdowns in the HeLa cells, the formation of 21S pre-rRNA was observed but no subsequent processing. RPS2/uS5, RPS3/uS3, RPS17/eS17, RPS20/uS10, RPS27a/ eS31, and RPS29/uS14 depleted cells exhibited a partial processing of the 21S pre-rRNA to 18S-E rRNA but the final step leading to the 18S rRNA maturation was not observed. RPS10/eS10, RPS12/eS12, RPS19/eS19, RPS25/eS25, and RPS26/eS26 knockdown showed higher levels of 18S-E rRNA. (Flygare et al., 2007; Robledo et al., 2008; Aspesi et al., 2017),

In this study, O'Donohue and colleagues could not define a clear-cut effect with RPS30/eS30 knockdown and another study showed that *Rps30* knockout in yeast did not completely abrogate ribosome biogenesis (Ferreira-Cerca et al., 2005). These RPS are listed in **Figure 15** below. The differential results suggest that there are possibly differences between the assembly in yeast and mammalian ribosomes.

i-RPS	p-RPS
eS1/RPS3a	uS2/RPSA
eS4/RPS4	uS5/RPS2
uS7/RPS5	uS3/RPS3
eS6/RPS6	eS10/RPS10
eS7/RPS7	eS12/RPS12
eS8/RPS8	uS19/RPS15
uS4/RPS9	eS17/RPS17
uS17/RPS11	uS13/RPS18
uS15/RPS13	eS19/RPS19
uS11/RPS14	uS10/RPS20
uS9/RPS16	eS21/RPS21
uS8/RPS15a	eS25/RPS25
uS12/RPS23	eS26/RPS26
eS24/RPS24	eS31/RPS27a
eS27/RPS27	uS14/RPS29
eS28/RPS28	

Group	I			II		
Phenotype	20S not detected			20S detected		
Sub-group	a	b	c	a	b	c
rRNA species accumulating after depletion	35S/23S A0,A1,A2,D inhibited A3 delay	35S/23S/22S A1,A2,D inhibited A0 delay	35S/23S/+1-D A0,A1,A2, inhibited A3 delay; D ? can occur with delay	35S/23S/20S A0,A1,A2,A3 delay	35S/23S/22S A0,A1,A2,A3 delay	35S/23S/21S A0,A1,A2,A3 delay
RPS	RPS13 RPS14 RPS16	RPS1 RPS6 RPS8 RPS9 RPS11 RPS23 RPS24	RPS27	RPS5 RPS15 RPS30	RPS7 RPS10 RPS26 RPS28 RPS31	RPS0 RPS2 RPS3 RPS18 RPS19 RPS20

Figure 15: Classification of RPS according to their impact of their deletion on ribosome biogenesis
(Top) table with the 2 class of mammalian RPs (O'Donohue et al., 2010) (Bottom) table with the classification of RP in the yeast model (Ferreira-Cerca et al., 2005)

All these steps occur in the nucleus. At the end of nuclear maturation, the mRNA groove, decoding centre and platform are formed (Baßler and Hurt, 2019). The pre-40S precursor (18S-E pre-rRNA) is then exported to the cytoplasm. Nuclear export of the processed 40S subunits are controlled by factors such as nucleophosmin and nucleoporin (Stage-Zimmermann et al., 2000; Maggi et al., 2008). In the cytoplasm, ribosomal protein RACK1 and RPS26/eS26 are required for the final rRNA processing to the 18S rRNA (Larburu et al., 2016;

Peña et al., 2016; Plassart et al., 2021). Until complete maturation, assembly factors stay bound to the immature SSU to prevent early initiation of translation. For example, GTPase-like TSR1 and kinase RIO2 bind behind the head and the platform to block the mRNA tunnel and initiator tRNA binding site (Strunk et al., 2012). Five other factors NOB1, PNO1, DIM1, LTV1 and ENP1 are also present (Strunk et al., 2011).

For the LSU assembly, there are 3 major assembly stages (**Figure 17**). The first step occurs in the nucleolus. Similarly to RPS, RPL are added in a sequential pattern by associated factors (Gamalinda et al., 2014). In the first steps of assembly, RPL5/uL18 and RPL11/uL5 are recruited to the 5S rRNA with the help of ribosome assembly factors Rpf2 and Rrs1 to form a 5S ribonucleoprotein complex (RNP) (Zhang et al., 2007; Klinge et al., 2011; de la Cruz et al., 2015). The 5S RNP participates in the maturation of functional regions of the LSU (Micic et al., 2020). By the end of the nucleolar processing, the solvent side and the NPET are formed (Wu et al., 2016).

The second step is the formation of the intersubunit region and the central protuberance in the nucleus. RPL10/uL16 is required for nuclear maturation (Pachler et al., 2004). Arx1 is required for the remodelling and formation of the CP (Barrio-Garcia et al., 2016). Nmd3 is an adaptor protein localised near the PTC. It acts as a checkpoint during ribosome biogenesis and is required for the nuclear export of the pre-60S particle (Ma et al., 2017). Nucleophosmin interacts with RPL5/uL18 for the shuttling of the mature 60S subunit (Yu et al., 2006) Then finally, in the cytoplasm, the intersubunit region is remodelled to its final conformation and the PTC is formed (Barrio-Garcia et al., 2016; Wu et al., 2016; Ma et al., 2017; Sanghai et al., 2018). RPLP0/uL10, RPL12/uL11, RPL10/eL40, Rpl24/eL24 and RPL41/eL41 are among the last RPL incorporated in the LSU (Panse and Johnson, 2010; Ma et al., 2017)

The assembly of the 40S and 60S subunits occur concomitantly in an approximate 1-to-1 balance. Gregory and colleagues conducted experiments in which they analysed how blocking a subunit assembly could impact the other subunit's assembly or stability (Gregory et al., 2019). They used yeast strains in which different RP expressions were driven by β-galactosidase promoter. By switching from a galactose to a glucose culture medium, they stopped specific RP expression and analysed the impact on the other subunit. They selected strains with at least 80% cell viability post RP silencing. Interestingly, they did not obtain the same results when silencing the RPSs and the RPLs. Repressing RPL4/uL4, RPL5/uL18, RPL17/uL22, RPL43/eL43 or 5S RNP assembly factors Rpf2 or Rrs1 expressions induce a reduction of 60S

subunit formation and the accumulation of 40S subunit. Nuclear export of both pre-40S and pre-60S subunits were blocked. Silencing RPS2/uS7, RPS9/uS4, or assembly factor Rrp7 induced the formation of an intermediate 55S particle which seems to be rapidly degraded and a decrease in pre-40S export. RPS14/uS11, RPS20/uS10, RPS31/uS31 silencing did not induce the accumulation of 60S. These results showed that all RPs are not equal (Gregory et al., 2019; Rahman et al., 2020).

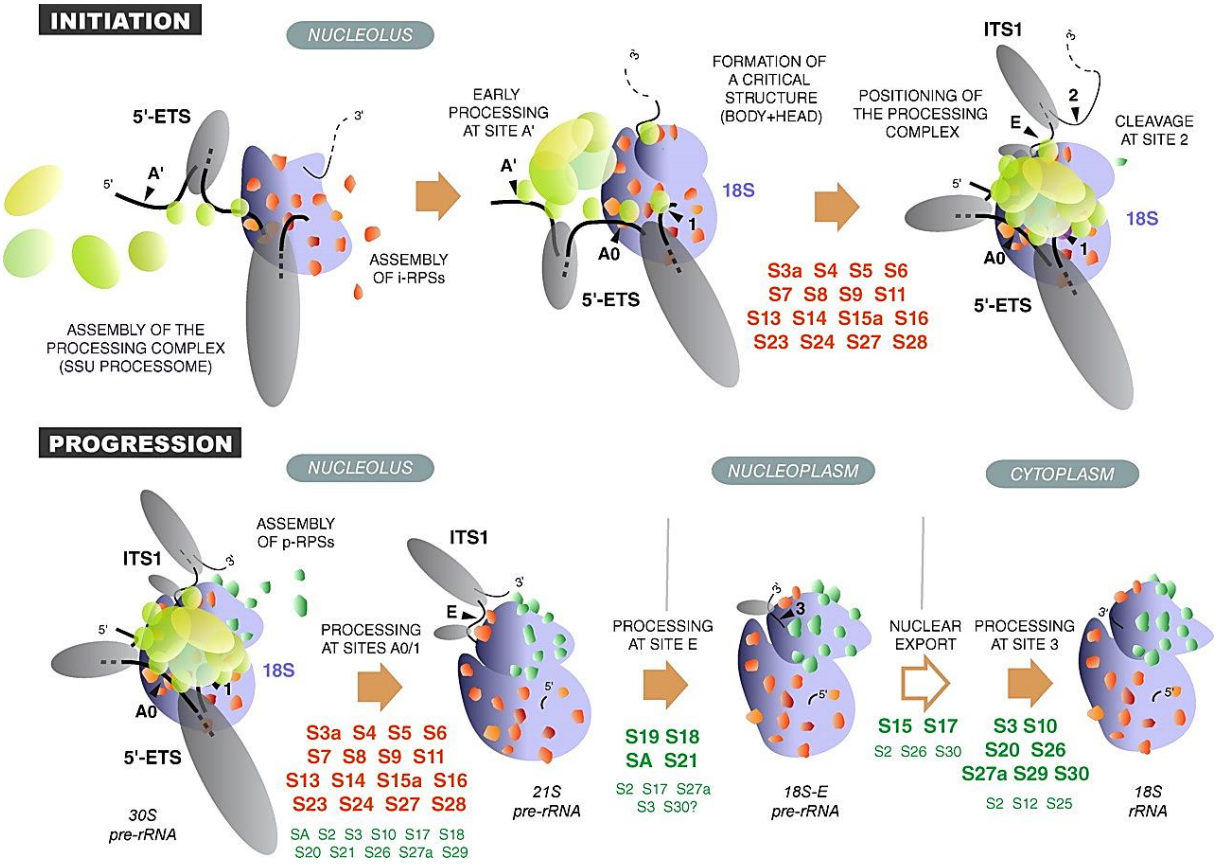

Figure 16: Proposed model for the incorporation of RPS during ribosome biogenesis in Hela cells.
– from (O'Donohue et al., 2010). The 5'ETS complex is co-transcriptionally recruited form the 90S particle, probably alongside i-RPS. i-RPS help to organise the secondary structure of the pre-rRNA while exposing internal transcribed regions for cleavage. p-RPS are then recruited to the ribosome to further participate in the folding and cleavage of the 30S pre-rRNA to 18S-E pre-rRNA. This particle is exported to the cytoplasm for the final steps of maturation. The RPS proteins required at each processing step are indicated.

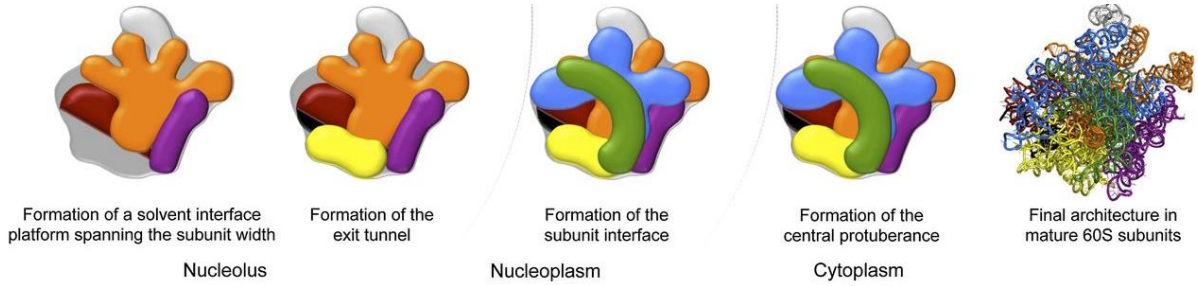

Figure 17: Maturation of the 60S preribosomal particle

RP are gradually incorporated in the pre-ribosomal particle to allow conformational modification thus forming the different active sites of the LSU – from (Gamalinda et al., 2014).

1.2.5 Regulation of ribosome biogenesis

Ribosome biogenesis is regulated by different signalling pathways themselves involved in progression in cell cycle. The 3 major signalling pathways are PI3K-AKT-mTOR, pRB-MDM2-p53 and MYC.

1.2.5.1 PI3K-AKT-mTOR signalling axis.

Target Of Rapamycin or TOR is a major regulator of ribosome biogenesis and translation and has been one of the most studied signalling pathways in eukaryotes. Mammalian TOR, mTOR, is a serine/threonine kinase that regulates spatiotemporal cell growth and cell survival (Cardenas et al., 1999; Ruoff et al., 2016; Kim and Guan, 2019). It can be found in 2 complexes: mTOR complex 1 (mTORC1) is pentameric complex composed of mTOR, DEPTOR, mLST8, Raptor, PRAS40 while mTOR complex 2 (mTORC2) is a hexametric complex with mTOR complexed to DEPTOR, mLST8, mSin1, Rictor and Protor 1/2 (Sarbassov et al., 2005; Jhanwar-Uniyal et al., 2019) (**Figure 18**). mTORC1 is sensitive to rapamycin while mTORC2 is insensitive to rapamycin (Loewith et al., 2002). Despite being a cytoplasmic protein, Tor1 can shuttle to the nucleus to target the three classes of RNA polymerases (Zhang et al., 2002; Mayer and Grummt, 2006). For example Tor1 can associate with TFIIIC to repress RNA Pol III repressor Maf1 (Kantidakis et al., 2010). Its location is regulated by nutrients level and growth factors (Li et al., 2006; Audet-Walsh et al., 2017)

mTORC1 can be activated by the PI3K/Akt pathway (Sarbassov et al., 2005) (**Figure 6**). Nutrients and growth factors bind to membrane receptors and activate phosphoinositide 3-kinase (PI3K). PI3K will act on phosphatidylinositol (4,5)-bisphosphate (PIP2) and form phosphatidylinositol (3,4,5)-trisphosphate (PIP3). PIP3 will activate protein kinase B (PKB, also called Akt). An additional phosphorylation of Akt by mTORC2 required (Sarbassov et al.,

2005). Akt will in turn phosphorylate the GTPase-activator protein complex, composed of TSC1, TSC2 and TBC1D7. Upon phosphorylation, the GTPase-activator protein complex is inhibited and cannot inactivate Rheb. Rheb is a GTPase that can activate mTORC1.

Mechanistically, mTOR regulates transcription by Pol I. In this mechanism, three factors are required for the recruitment of RNA Pol I to rDNA: transcription initiation factor IA and IB (TIF-IA and TIF-IB) and upstream binding factor (UBF). TIF-IA and UBF are both targets of mTOR. Mayer and colleagues demonstrated that rapamycin-treated cells are transcriptionally repressed through modifications in phosphorylation of specific sites of TIF-IA which reduce interactions between TIF-IA and Pol I (Claypool et al., 2004; Mayer et al., 2004). They also identified that mTORC1 is also involved in the subcellular localisation of TIF-IA. Upon treatment with rapamycin, TIF-IA was exported from the nucleus to the cytoplasm. Studies on yeast revealed that inhibition of mTOR induces the protease-dependent degradation homologue of TIF-IA, Rrn3p, thus reducing rRNA synthesis (Philippi et al., 2010). In a similar manner, UBF is regulated by phosphorylation. Phosphorylation of UBF's C-terminal by S6K1 is mTOR-dependent. Upon phosphorylation, UBF interacts with Pol I and activates rRNA synthesis (Voit and Grummt, 2001; Hannan et al., 2003)

mTOR also regulates Pol III that synthesises the 5S rRNA. It phosphorylates and inhibits Maf1, a repressor of Pol III-mediated transcription. Upon cellular stress such as nutrient depletion, mTOR induces the translocation of Maf1 from the nucleus to the cytoplasm and its degradation through the proteasome thus decreasing 5S rRNA synthesis (Kantidakis et al., 2010; Shor et al., 2010; Wang et al., 2019; Noguchi et al., 2021). mTOR also binds TFIIIC, a DNA-binding protein and a pol III initiation factor that binds to promoters of tRNA and 5S rRNA (Kantidakis et al., 2010; Graczyk et al., 2018).

Finally, mTOR controls initiation and elongation steps of translation of cytoplasmic mRNAs including RP-coding mRNAs (see chapter 2.3.1). mTOR has another leverage on RP genes transcription by modifying chromatin structure. In the yeast model, it was shown that ESA1 and RPD3, two histone H4 modifying factors, were modulated by TOR to respectively activate or repress RP gene expression through acetylation or deacetylation (Rohde and Cardenas, 2003). In 2004, Martine and colleagues determined that in the same model that Forkhead-like transcription factor FHL1, coactivator IFH1 and corepressor CRF1 were intermediates by which TOR, via protein kinase A, was regulating RP genes transcription

(Martin et al., 2004). To sum up, each component of the ribosome is largely dependent on mTOR regulation.

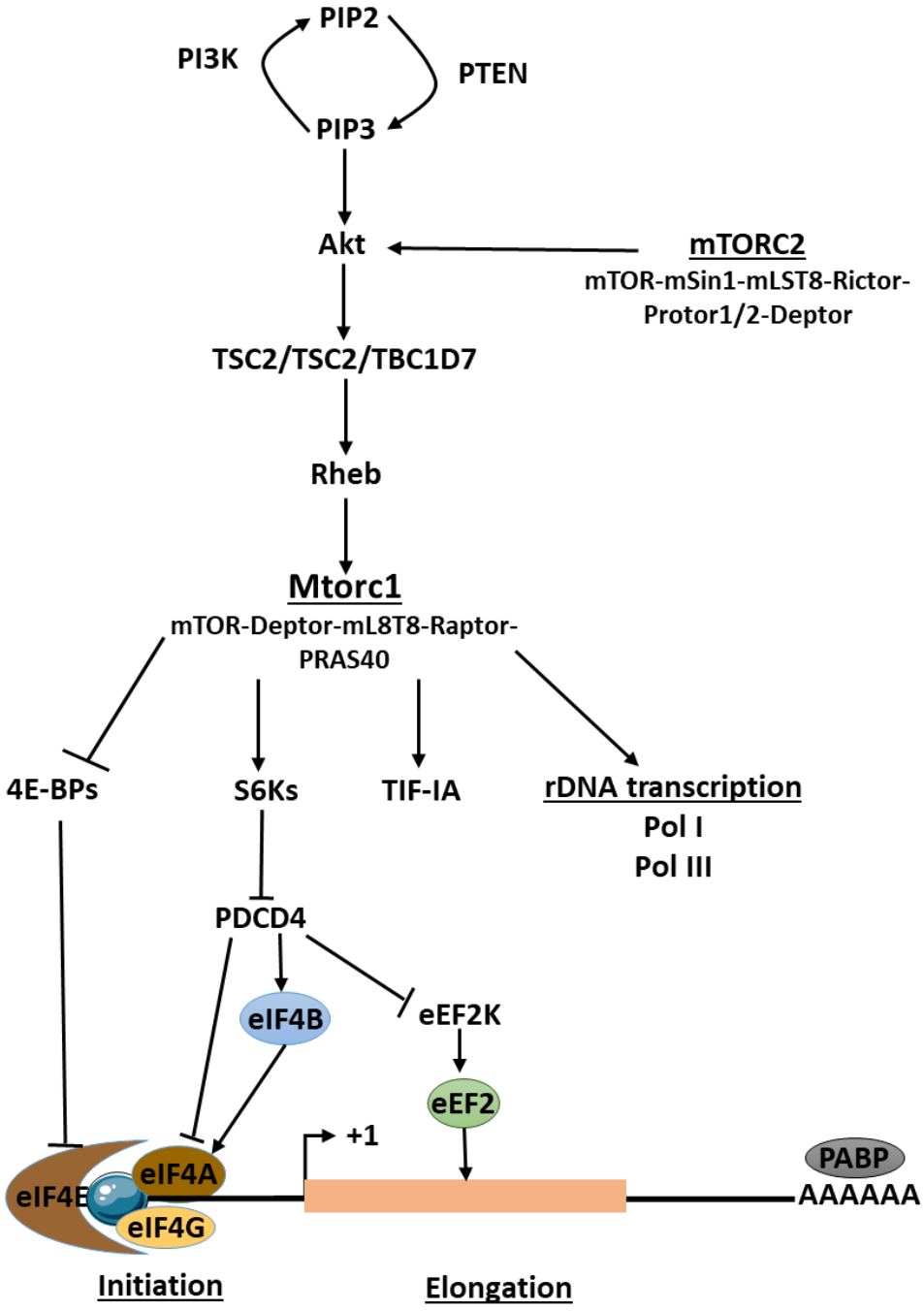

Figure 18: Control of ribosome biogenesis by mTOR pathway
mTOR affect rRNA synthesis by influencing Pol I and Pol III activity. It also affects translation of RP mRNA.

1.2.5.2 Regulation by pRB-MDM2-p53 pathway

An equilibrium between rRNA and RP components is crucial during ribosome biogenesis for progression in the cell cycle (Donati et al., 2011). Any impairment in rRNA transcription, processing or RP levels can trigger a stress signal that can lead to cell arrest. The first study that identified ribosome biogenesis as cell cycle checkpoint was published in 2000 where the abolition of the 40S subunit in liver cells, through conditional RPS6 deletion, abrogates regeneration after hepatectomy (Volarevic et al., 2000). Cells were blocked at the G1/S phase. It was later shown that this mechanism depends on p53, a tumor suppressor protein and E3 ubiquitin-protein ligase MDM2 (Pestov et al., 2001; Barna et al., 2008).

Mechanistically, there is a checkpoint during cell progression from G1 to S phase called the restriction or R point (**Figure 19**). It is controlled by retinoblastoma tumor suppressor protein or pRb which is suppressor of a set of transcription factors that regulates essential genes involved in progression into the S phase called E2F proteins. pRb is itself regulated by the Cyclin/CDK complex. Outside the G1/S checkpoint, Cyclin/CDK complex is negatively regulated by tumor suppressor protein p53 via p21 and pRb remains bound to E2F. p53 is itself regulated by oncogenic MDM2, an E3 ubiquitin ligase, which induces the inhibition of p53 and its proteasome-mediated degradation through polyubiquitination (Oliner et al., 1993; Haupt et al., 1997). The ubiquitination of p53 depends on its phosphorylation and MDM2 activity. On the other hand, p53 is more resistant to MDM2 induced degradation when it is phosphorylated in Ser15 while phosphorylation of MDM2 in serine 394 inhibits p53 association and therefore its subsequent ubiquitination and degradation (Shieh et al., 1997; Khosravi et al., 1999; Ashcroft et al., 1999; Chehab et al., 1999; Maya et al., 2001; Carr et al., 2016). Both p53 and MDM2 are regulated through an autoregulatory loop. MDM2 negatively regulates both p53 mRNA and protein by promoting their degradation while p53 promotes MDM2 transcription (Wu et al., 1993; Barak et al., 1993; Juven et al., 1993; Wu et al., 1993; Harris and Levine, 2005; Pant et al., 2013). MDM2 can also directly bind to pRB to negatively regulate its activity (Xiao et al., 1995)

MDM2 activity on p53 is optimised by MDMX which is an oncogene and a negative regulator of p53 (Finch et al., 2002; de Graaf et al., 2003; Pan and Chen, 2003; Wade et al., 2013). MDM2 is inactivated by p14ARF, a tumor suppressor protein, and will cause MDM2 to target MDMX instead of p53, thus stabilising p53 levels (Honda and Yasuda, 1999). p14ARF is positively regulated by E2F and negatively regulated by p53 (Kowalik et al., 1998; Zhu et

al., 1999) and it is located in the nucleolus. Several studies have shown that p14ARF is involved in the regulation of both synthesis and maturation of 47S rRNA precursor by interacting with transcription termination factor I (TTF-I) (Itahana et al., 2003; Sugimoto et al., 2003; Saporita et al., 2011; Lessard et al., 2012).. p14ARP can also interact with TIF-I to regulate rRNA biogenesis in a p53-independent manner (Lessard et al., 2010)

If all conditions are met at the G1/S checkpoint, pRb is inactivated by phosphorylation by the Cyclin/CDK complex and E2F is released to activate transcription and promote p14ARF, thus passing the restriction point. Under ribosomal stress, such as defects in rRNA biogenesis or starvation, RP and immature subunits accumulate in the nucleus (Gregory et al., 2019; Lessard et al., 2018). uL18/RPL5 and uL5/RPL11 bind MDM2 to stabilise p53. Other RPs such as, uL14/RPL23, uL24/RPL26, eS7/RPS7, uS11/RPS14 and eS25/RPL25 can also bind MDM2 and inhibit its E3 ubiquitin ligase activity (Meng et al., 2016; Zhou et al., 2013; Zhang et al., 2013a; Chen et al., 2007; Lohrum et al., 2003; Zhang et al., 2003, 2002; Marechal et al., 1994). p53 accumulation will induce the cell arrest program, inhibit rRNA transcription and block subunit export. p53 can also directly regulate fibrillarin levels by binding to its mRNA to repress its translation thus reducing the levels of 2'OMe (Marcel et al., 2013).

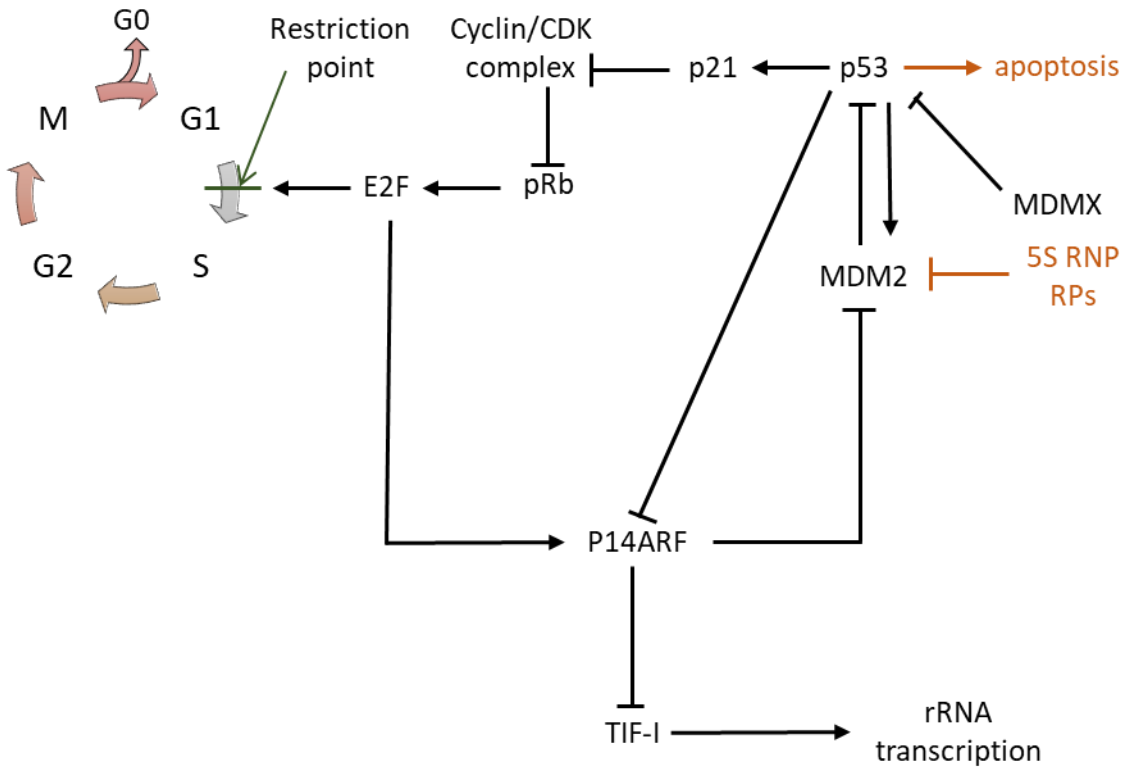

Figure 19: Regulation of ribosome biogenesis by the Rb-MDM2-p53 pathway
In black is indicated the different steps of the Rb-MDM2-p53 pathway. E2F transcription factors are released from pRB through inhibition of the Cyclin/CDK by p53 via p21 to pass the restriction point. This balance is mainly maintained by MDM2. Upon impairment of the ribosome biogenesis, the 5S RNP and other RPs can bind MDM2 to stabilise p53 and induce apoptosis (orange)

1.2.5.3 Regulation by transcription factor MYC

MYC is a pro-survival transcription factor and a major regulator of translation. It regulates ribosome biogenesis through the regulation of pol I by binding to the TATA box of rRNA genes hence promoting the expression of MYC target UBF (Poortinga et al., 2011). It also promotes the loading of SL-1 and RNA Pol I to the 47S rRNA promoter (Grandori et al., 2005). Moreover, MYC regulates pol II access to RP genes through histone acetylation by controlling the recruitment of histone acetyltransferase complex to histone H3 and H4 (Frank et al., 2001). This role of MYC is regulated by RPL5 and RPL11 which acts as a competitive inhibitor (Liao et al., 2014). Lastly, MYC regulates pol III activity via TF-IIB (Gomez-Roman et al., 2003; van Riggelen et al., 2010).

MYC also controls synthesis of other proteins essential to ribosome biogenesis such as eIF4A-I, eIF4G, the 2'O methyltransferase fibrillarin, nucleolin but also the production of snoRNAs that are necessary for the post-transcriptional modifications of rRNA (van Riggelen et al., 2010; Destefanis et al., 2020). It has been shown in a recent study using the drosophila model and human immortalised cell lines, that MYC could also regulate the synthesis of tRNA by targeting aminoacyl tRNA synthetases (Zirin et al., 2019).

In conclusion, the ribosome is a highly organised complex with a well-orchestrated sequence of events for the synthesis, 3D-organisation between RPs and rRNA to produce functional subunit that will assembled during translation.

2 Ribosome, major actor of translation

The major role of the ribosomes is to recognise the mRNA with the help of initiating factors, identify the correct reading frame and translate the mRNA into proteins. The translation process can be divided into three stages namely initiation, elongation and termination. Termination is generally followed by the ribosome recycling step.

2.1 Initiation

The first studies focussing on translation initiation started in the 70s (Nienhuis and Anderson, 1971). They wanted to understand how ribosomes were recruited and how they initiated mRNA translation. Since the 70s, the initiation step has been deeply studied and the mechanisms of canonical translation were finally elucidated (Kozak, 1987). Initiation can be divided intp two categories: cap-dependent and cap-independent. The canonical initiation is the cap-dependent initiation but there are other initiation mechanisms such as IRES-dependent initiation and non-AUG initiation. In this step, RNA-binding proteins named eukaryotic initiation factors are involved.

2.1.1 Cap-dependent initiation

There are two features that are required for cap-dependent translation: a cap on the 5' end and a polyA tail in the 3' end. To initiate translation, helicase eIF4A, cap binding eIF4E and scaffold protein eIF4G interacts to form the eIF4F complex (**Figure 20**). This complex bind to the 5' cap on the mRNA. eIF4B is required for the recruitment of ribosomes on mRNA. It optimises the ATPase and helicase activity of eIF4A (Rogers et al., 2002; Merrick and Pavitt, 2018). Scaffold initiating factors eIF4G interacts with PABP to induce mRNA circularisation. This circularisation favours not only translation initiation of polyadenylated mRNAs, but also re-initiation of translation after a translation cycle.

Meanwhile, eIF2 complexed to GTP binds an initiator tRNA thus forming the eIF2 ternary complex. The initiator tRNA is generally a tRNA bound to methionine. The ternary complex then binds a 40S subunit of a ribosome bound to eIF1, eIF1A, eIF3 and eIF5 and forms the 43S preinitiation complex (PIC). The initiator directly binds the peptidyl (P) site of the ribosome. The PIC binds an mRNA with an eIF4F complex and forms the 48S initiation complex.

Once bound to the mRNA, the complex containing the small ribosomal subunit will slide and scan the sequence until it identifies an open reading frame (ORF), that is, the correct

initiating codon: AUG. This AUG is next to a particular sequence, the Kozak sequence (A/G)CCAUGG, with a purine in -3 and a guanine in +4 (Kozak, 1987) from the initiating AUG, and with its A in +1 position. Upon codon-anticodon recognition, the 48S complex is stabilised and eIF2-GTP is hydrolysed to GDP. This hydrolysis destabilises the complex and partially dissociates eIF2 from the complex. eIF5B is then recruited to allow the fixation of the LSU. Fixation of the LSU causes the complete dissociation of eIF2 along with eIF1, eIF1A, eIF3, eIF4 and eIF5 (Unbehaun et al., 2004). At the end of initiation, a translation-competent 80S ribosome is bound to the mRNA, with the methionine-tRNA in the P-site.

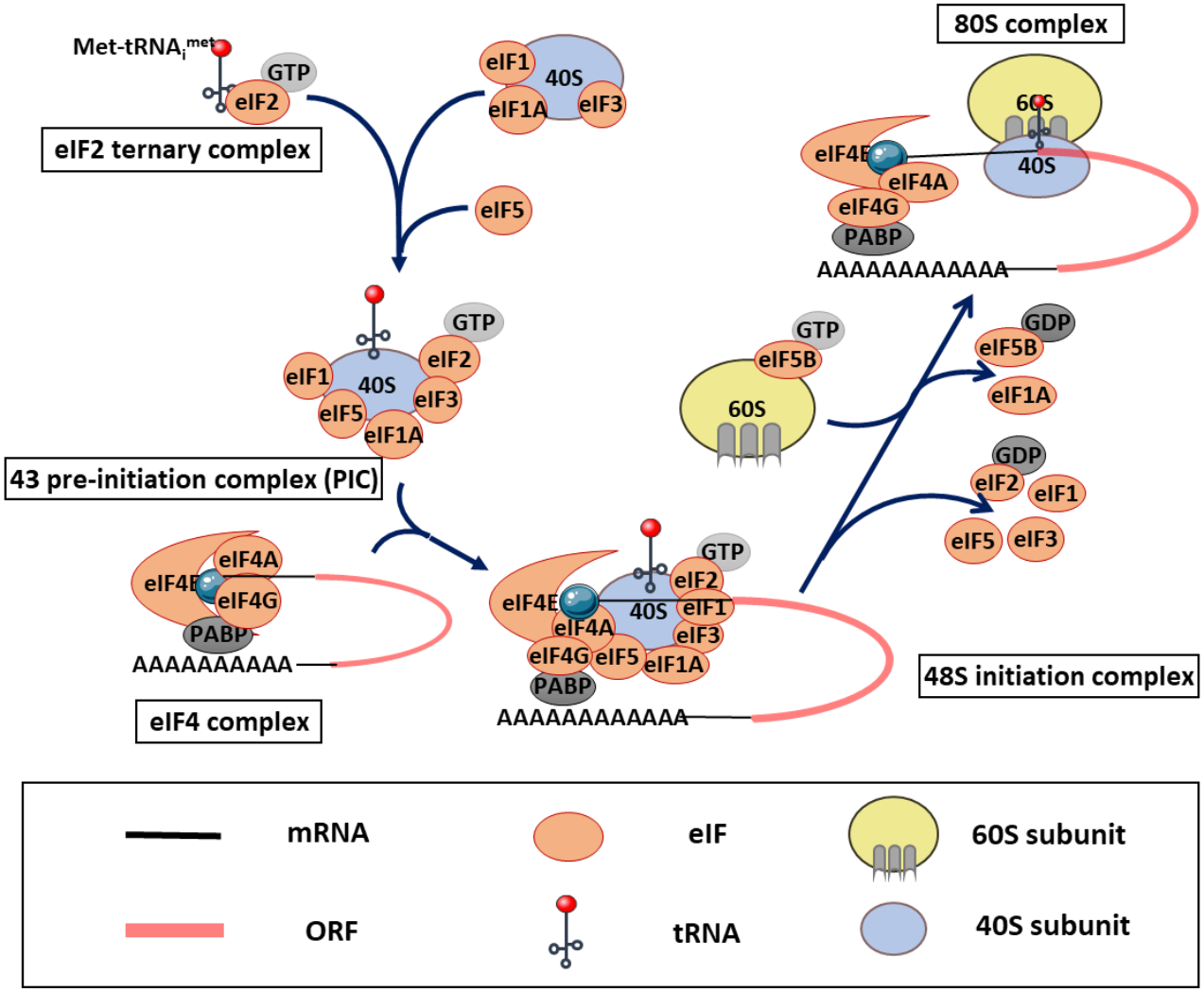

Figure 20: Cap-dependent initiation
eIF2 ternary complex, composed of eIF2-GTP- binds to the 40S subunit with associated initiation factors to form the PIC. The PIC and eIF4 complex are then recruited to an mRNA with a 5'-methylguanosine cap to form the 48S initiation complex. This complex scans the mRNA until the start codon where the 60S subunit is recruited to form the 80S ribosome.

2.1.2 Cap-independent initiation

In stress conditions, cap-dependent translation is greatly reduced (Godet et al., 2019). Alternative mechanisms were developed to allow adaptation and cell survival. This transition is induced by the mTOR-dependent sequestration of eIF4E and inhibition by phosphorylation of the eIF2 complex thus limiting its formation (Thakor and Holcik, 2012). Internal Ribosome Entry Site or IRES-dependent initiation is one of the most described mechanisms. IRES are 3D structures resulting from mRNA folding by base pairing and can be found in 5'UTR but also in the mRNA sequence (Jang et al., 1989; Leppek et al., 2018).

The first IRES were discovered in viruses, more precisely in *Picornaviridae* strain in the 80s (Jang et al., 1989; Pelletier and Sonenberg, 1988). The first structure obtained by cryo-electron microscopy was a human ribosome bound to an IRES on a viral mRNA (Spahn et al., 2004b). This was quickly followed by the resolution of the 3D structure of the IRES (Pfingsten et al., 2006; Spahn et al., 2004b). Since these findings, IRES have been identified in cellular mRNA. It is estimated that 10% of the mammalian mRNA contain IRES. The main difficulty is that there is the lack of a consensus sequence for IRES and various structures of IRES can be found. There are few databases that collect the experimentally validated IRES (Bonnal et al., 2003; Mokrejs et al., 2010; Zhao et al., 2020).

In 2019, there were 554 viral IRES-containing mRNAs, 691 in humans and 83 from other eukaryotes (Zhao et al., 2020). The latest database published is the Human IRES Atlas that gathers studies on IRES-driven translational regulation (Yang et al., 2021). These mRNAs are involved in key processes such as development, apoptosis, cell cycle, cell growth but also in tumorigenesis, viral infections or response to DNA damages. Examples of such mRNA are transcription factor *c-Myc* (Stoneley et al., 2000; Subkhankulova et al., 2001), *p53* (Candeias et al., 2006; Yang et al., 2006; Halaby et al., 2015a), insulin-like growth factor I receptor, *IGF1-R* (Giraud et al., 2001) and vascular endothelial growth factor, *VEGF* (Huez et al., 1998). These mRNAs undergo cap-dependent translation in physiological conditions and transition to an IRES-dependent translation during cell stress.

There are two types of cellular IRES. Type I cellular IRES requires a set of canonical initiation factors such as eIF4G and eIF4A and other factors called IRES Trans-Acting Factors (ITAFs) (Kwan and Thompson, 2019). ITAFs are RNA-binding proteins that facilitate or inhibit ribosome recruitment on the IRES. They have a broad range of actions running from RNA chaperon to ribosome recruitment (Stoneley and Willis, 2004; Godet et al., 2019). One

example is La Autoantigen that is recruited to ribosome binding protein 1 mRNA to promote IRES-dependent translation initiation (Gao et al., 2016). Polypyrimidine-tract-binding protein, translational control protein 80 and RNA helicase A can bind p53 to facilitate its recognition by the 40S subunit (Grover et al., 2008; Halaby et al., 2015a, 2015b). Type II cellular IRES are directly recognised by the SSU. The encephalomyocarditis virus is able to recruit the 40S subunit without eIF4G and eIF4A (Chamond et al., 2014). Variabilities in IRES structures and recruited factors suggest a high adaptability of IRES-dependent translation system.

The molecular mechanisms involved in cellular IRES are still studied but much information can be obtained from the study of viral IRES. Viral IRES can be divided in **four** groups: (i) type I viral IRES forms pseudoknots that are directly recognised by the SSU but no initiator Met-tRNA$_i^{met}$ is required (Kanamori and Nakashima, 2001; Nishiyama et al., 2003); (ii) type II viral IRES also forms a pseudoknot and requires eIF2, eIF3 and initiator Met-tRNA$_i^{met}$ (Tsukiyama-Kohara et al., 1992; Rijnbrand et al., 1997); (iii) type III viral IRES requires all canonical initiation factors and ITAFs. Translation initiation begins at the site of 40S recruitment (Pestova et al., 1996); (iv) type IV viral IRES are similar to type III but the SSU will scan the mRNA for an AUG to start translation (Sweeney et al., 2014).

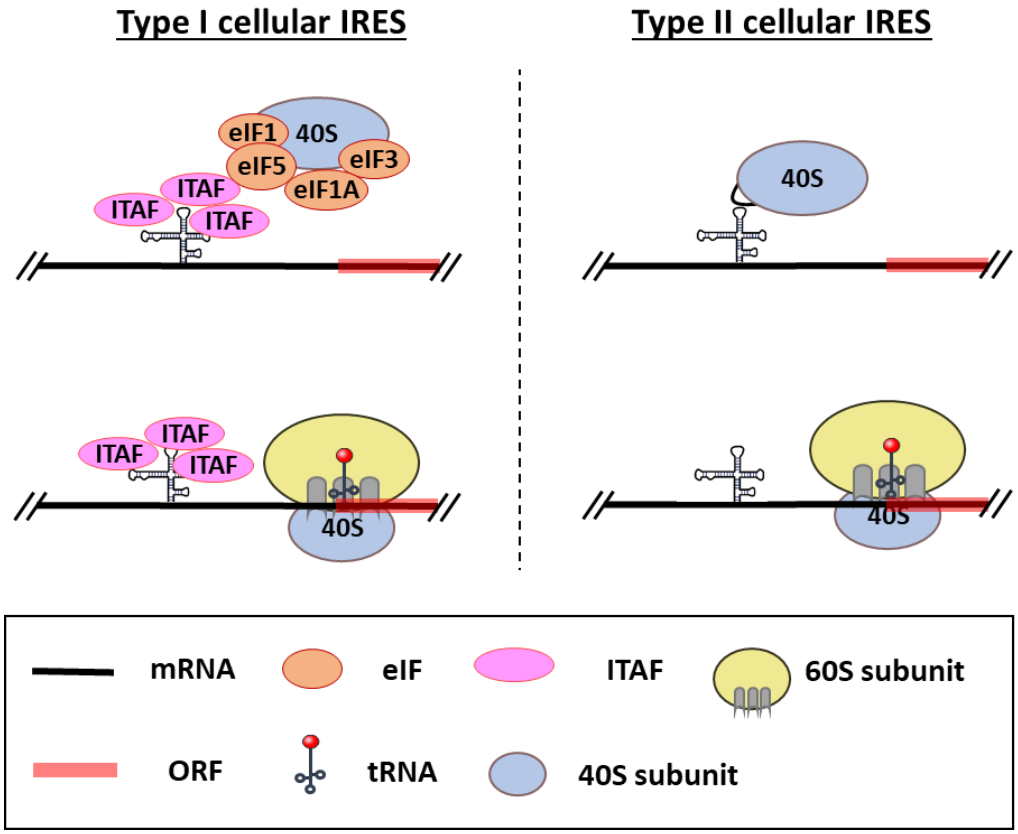

Figure 21: IRES-mediated initiation
(A) Type I cellular IRES. The 40S subunit is recruited to the mRNA indirectly through the recognition between the 18S rRNA by ITAFs located on IRES. (B) Type II cellular IRES. Direct recognition of the IRES by the SSU

2.1.3 Repeat-associated non-AUG dependent initiation

The first studies on repeat-*a*ssociated non-AUG (RAN) dependent initiation were published at the end of the 80s when Peabody and colleagues identified 7 alternative start codons (ACG, GUG, UUG, CUG, AUA, AUC, AUU) capable of initiating translation of dihydrofolate reductase (DHFR) coding mRNAs (Peabody, 1987, 1989). DHFR is essential for purine synthesis. Since this discovery, other alternative starting sites have been identified (Tikole and Sankararamakrishnan, 2006; Kochetov et al., 2013). Interestingly, non-AUG dependent initiation affects mRNAs involved in essential cell functions and in response to stress stimuli. For example, there are two isoforms of tumor-suppressor protein PTEN, PTENα and PTENβ, that are formed through the recognition of CUG and AUU respectively (Liang et al.,

2014, 2017). There can also be a RAN initiation through an IRES recognition(Schwab et al., 2004; Starck et al., 2016; Sendoel et al., 2017).

RAN initiation is promoted during cell stress (Green et al., 2017) and is associated with multiple disorders such as Huntington's disease and fragile X syndrome (Zu et al., 2011; Todd et al., 2013). Few data are available on the mechanisms involved. What is known is that Methionine-tRNA is usually the initiator tRNA (Peabody, 1989) but leucine-tRNA can also be used (Schwab et al., 2004; Starck et al., 2012). As cap-dependent initiation is inhibited by eIF2α phosphorylation, eIF2A and eIF2D can initiate translation in a GTP-independent manner (Liang et al., 2014).

2.2 Elongation

Elongation is the step where mRNA is decoded by ribosomes. tRNAs, loaded with an amino acid (aa) are recruited to the aminoacyl (A)-site. The aa incorporated in the polypeptide chain is determined by the interaction between the incoming tRNA and the codon present inside the A-site of the ribosome. Eukaryotic elongation factor 1A (eEF1A) bound to GTP is also required. The correct tRNA, also called cognate tRNA, will enter the A site with eEF1A-GTP and interact with the codon present inside the A-site. The interactions are stabilised through Watson & Crick base-pairing on +1 and +2 codon position. More tolerance is provided on the 3rd base called the wobble base. Upon match, the codon-anticodon interaction between mRNA and tRNA induces the hydrolysis of GTP to GDP and the dissociation of eEF1A from the ribosome (Crepin et al., 2014).

The proximity of both tRNAs to the A and the P sites leads to the formation of the peptide bond between the incoming aa and the nascent polypeptide. The peptide bond formation is concomitant to the polypeptide chain transfer to the tRNA present in the A-site. The whole process is catalysed by the 28S rRNA within the ribosome. The ribosome will then undergo a conformational rearrangement that leads to the translocation of tRNA from the P to the exit (E) site and from the A site to the P site. The completion of translocation requires eEF2 in the A site. The deacetylated tRNA present in the E site will exit the ribosome while the A site is ready for the next loaded tRNA. This cycle will continue until the ribosome reaches a stop codon.

During synthesis, a protein grows by 6 aa per second. In bacteria, there is one error per every 1000 to 10 000 incorporated amino acids (Allan Drummond and Wilke, 2009). The speed

is determined by many factors such as the speed for the transfer of the polypeptide chain from tRNA in the P site to the tRNA in the A site, the nature of the amino acid among others. The presence of inhibitory stem-loop structures in the mRNA, the absence of a stop codon or a poor codon-anticodon recognition (Wilson et al., 2016) can slow down and even stop the ribosome. The halt of the ribosome is called stalling or pausing. This blockage is associated with the ribosome-associated quality control that can lead to mRNA degradation (Doma and Parker, 2006), ribosome recycling (Pisareva et al., 2011; Shoemaker et al., 2010) and nascent peptide degradation (Bengtson and Joazeiro, 2010). This is schematically represented in **Figure 22 (top).**

2.3 Termination and ribosome recycling

The termination of translation is characterised by the presence of a stop codon (UAA, UAG, UGA) in the A site. Eukaryotic releasing factors eRF1 and eRF3 bind to the A site and induce, through a conformational change, the hydrolysis of the peptidyl-tRNA bond thus releasing the newly synthesised polypeptide. The post-termination ribosomal complex, composed of the 80s ribosome still bound to the mRNA, the deacylated tRNA in the P site and the releasing factors, is then recycled. The releasing factors detach from the ribosome and the ribosomal subunits dissociate. This step requires initiation factors. In a low Mg^{2+} environment, eIF3, eIF1 and eIF1A interact with the mRNA-bound 80S ribosome, with the tRNA in the P site. eIF3 induces the dissociation of the large and the small subunit while eIF1 induces the dissociation and the release of the mRNA and the tRNA (Unbehaun et al., 2004). eIF3, eIF1 and eIF1A stay fixed to the 40S subunit to prevent its reassociation with the 60S subunit (**Figure 22 botton**). In conditions of high Mg^{2+} concentration, the separation of the subunit will require the additional presence of the ATP-binding cassette transporter ABCE1.

mRNA circularisation allows proximity between the termination and the initiation sites. The 40S subunit can stay bound to the mRNA and continue the scanning process even if the eIF2 ternary complex is absent. eIF2 complex can bind to the subunit during scanning and hence allow a new translation cycle. It was also shown *in-vivo* that eIF3 could stay during elongation and termination to favour translation re-initiation. (Mohammad et al., 2017)

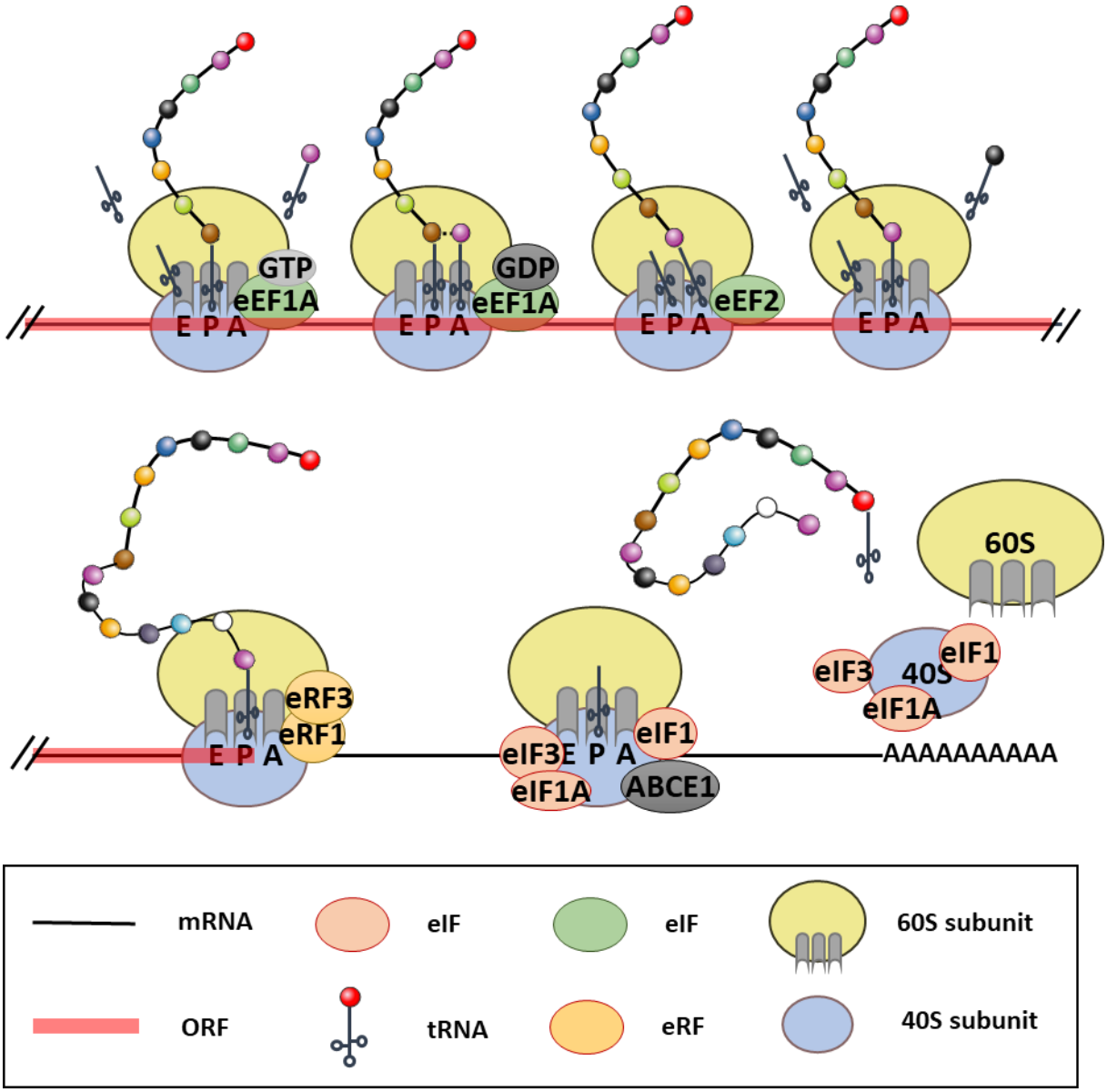

Figure 22: Elongation, termination and recycling of ribosomes
Top: An acylated aminoacyl-tRNA is recruited in the A site. As the acyl-tRNA is close to the PTC, the peptide bond is formed. Translocation occurs and the deacylated tRNA leave the ribosome through the E site while the tRNA carrying the peptide chain is inside the P site. Bottom: when the the stop codon is recognised, eRFs are recruited for the subsequent release of the peptide and dissociation of the ribosome.

2.4 Local translation: a neural specificity

For many years, we thought that translation could only take place in the cytoplasm, near the nucleus and that resulting proteins were then transported in cargos over long distances. However, the first observations of ribosomes in neurons, away from the soma, were made in

cell cultures originating from the primate spinal cord and polysomes were identified nearly 15 years later (Bodian, 1965; Steward and Levy, 1982). Moreover, in the 90s, several studies showed that mRNAs were specifically located away from the soma of neurons, within the synaptic knob, dendrites and axons (Kleiman et al., 1990; Berry and Brown, 1996; Paradies and Steward, 1997). The first studies that identified *in-vivo* local translation were published in the last 2010s (Shigeoka et al., 2016; Hafner et al., 2019).

Technical innovations in sequencing enabled the identification of more than 2000 mRNAs located in dendrites and axons of the rodent hippocampus, within RNA granules (Poon et al., 2006; Zhong et al., 2006; Taylor et al., 2009; Ohashi and Shiina, 2020). However, no addressing signal was identified. These mRNAs are transported and distributed by molecular motors to dendrites, axons and synaptic knobs. The study of ribosomal protein mRNAs localised in the axons revealed the presence of a CUIC sequence that forms a loop. Deletion of this sequence abrogates translation of these mRNAs (Shigeoka et al., 2019). Translation mainly occurs in synapses and seems to be calcium-dependent (Kim and Martin, 2015). One advantage of having localised ribosomes and mRNAs, away from the soma, is that it enables the local maintenance of protein levels and allows a rapid plasticity if there is any drastic change to these levels.

Local translation help neurons meet their requirements. During development, nerve growth factor can trigger local translation of pro-survival transcription factors that will be transported back to the nucleus through retrograde transport (Cox et al., 2008). It also allows rapid response to guidance cues. Using isolated *Xenopus* retinal growth cones, Campbell and Holt demonstrated that, when local translation is inhibited with inhibitors such as cycloheximide, Netrin-1 and semaphorin 3A no longer produce the attractive or repulsive effect respectively (Campbell and Holt, 2001). In mature neurons, local translation ensures axonal maintenance and could allow rapid response to injury (Yoon et al., 2012; Cioni et al., 2019; Shigeoka et al., 2019). During nerve injury, mTOR is locally translated to promote regeneration after axonal injury (Park et al., 2008; Terenzio et al., 2018)

2.5 Main signalling pathways regulating translation

Translation needs to be tightly regulated to prevent any disruption in synthesis that may either lead to cell death or to uncontrolled proliferation leading to oncological events. There are 2 major signalling pathways regulating translation: mTOR and MAPK.

2.5.1 mTOR pathway as a master regulator of protein synthesis

- *Translation Initiation*

4E-BPs are one of the most characterised targets of mTORC1. 4E-BPs are mRNA 5' cap-binding repressors that sequester eIF4E from the eIF4F complexes thus inhibiting initiation of eIF4E-bound mRNAs (Gingras et al., 1999). They are competitive inhibitors with scaffold protein eIF4G for the binding site on cap-binding eIF4E. There are **three** 4E-BPs: 4E-BP1, 4E-BP2 and 4E-BP3. Mechanistically, mTORC1 will phosphorylate 4E-BPs (Burnett et al., 1998; Hara et al., 2002). Further phosphorylation by CDK12 is required for the subsequent release of 4E-BPs from eIF4E thus enabling the recruitment eIF4G (Choi et al., 2019; Hay and Sonenberg, 2004) (**Figure 18**) Moreover, phosphorylation of 4E-BP1 selectively promotes 5'TOP mRNAs translation . (Levy et al., 1991; Yamashita et al., 2008; Meyuhas and Kahan, 2015).

mTORC1 can also regulate 5'TOP mRNA translation via ribosomal S6 kinase proteins (S6Ks) through raptor and GβL (Kim et al., 2003; Ruvinsky and Meyuhas, 2006). S6Ks are also serine/threonine kinases with many downstream targets. One of these targets is programmed cell death 4 (PDCD4), an inhibitor of eIF4A. p70(S6K) phosphorylates PDCD4. Upon phosphorylation, E3-ubiquitin ligase beta-TrCP ubiquitinate PDCD4 which will be degraded by the proteasomal degradation (Schmid et al., 2008). Meanwhile p90(S6K) activates eIF4B, to promote eIF4A activity by modulating its conformation (Shahbazian et al., 2006; Park et al., 2013; Andreou and Klostermeier, 2014).

- *Translation elongation*

mTORC1 regulates elongation via p70(S6K), through the phosphorylation of eukaryotic elongation factor 2 kinase (eEF2K) (Wang et al., 2001). eEF2K is a Ca^{2+}/calmodulin-dependent protein kinase that negatively regulates protein synthesis through the phosphorylation of eEF2. Hyperphosphorylation of eEF2K causes its inactivation and eEF2K cannot inhibit the activity of eEF2. Elongation can therefore proceed. It is to be noted that mTORC1-S6K-eEF2K regulation is promoted by nutrients and growth factors such as TGFβ and insulin (Das et al., 2010; Redpath et al., 1996)

- *Ribosome functioning*

mTORC1 can act indirectly, via S6K, on the ribosomal function. S6K modulates the translating ability of the ribosome by phosphorylating specific residues of RPS6/eS6 thus

affecting the selective affinity of ribosomes towards 5'TOP mRNAs involved in development, differentiation and synaptic plasticity (Ruvinsky and Meyuhas, 2006; Biever et al., 2015).

2.5.2 MAPK pathway

Mitogen-activated protein kinases, or MAPK, are serine/threonine kinases also involved in translational regulation. MAPK pathway consists of sequential phosphorylation of MAPK such as ERK, by MAPK kinase (MAPKK) such as MEK, themselves phosphorylated by MAPKK kinase RAF **(Figure 23)**. This pathway is activated by RAS which are GDP/GTP-binding molecules. Once activated, ERK activates two effectors: RSKs and MNKs.

There are **four** different isoforms of RSKs in mammals: RSK1-4. All except RSK4 exhibit a ubiquitous expression pattern across different organs. RSKs can influence multiple steps of the translation. RSKs, similarly to mTOR, are able to phosphorylate PDCD4 to alleviate its inhibition on eIF4A, eiF4B to promote translation initiation and RPS6/eS6 to modulate ribosome's translation abilities (Shahbazian et al., 2006; Roux and Topisirovic, 2018). RSKs can also promote mTOR activity via the activation of the GTPase-activator protein complex TSC1/TSC2/TBC1D7. Note that a recent study on cell lines indicated that, in nutrient-depleted conditions, the additional activity of mTORC2 could be required to enable the optimal phosphorylation of RSK by ERK (Chou et al., 2020).

MNKs are also Ser/Thr kinases that target the eIF4F complex. Upon MNK-mediated phosphorylation, eIF4E loses its affinity for the 5' cap resulting in a decrease in global mRNA translation rate (Knauf et al., 2001; Scheper et al., 2002).

Similarly to the ribosomal synthesis process, translation is also tightly controlled to ensure the adequate production of proteins when and where they are required. Signalling pathways ensure control on these processes in order to achieve homeostasis.

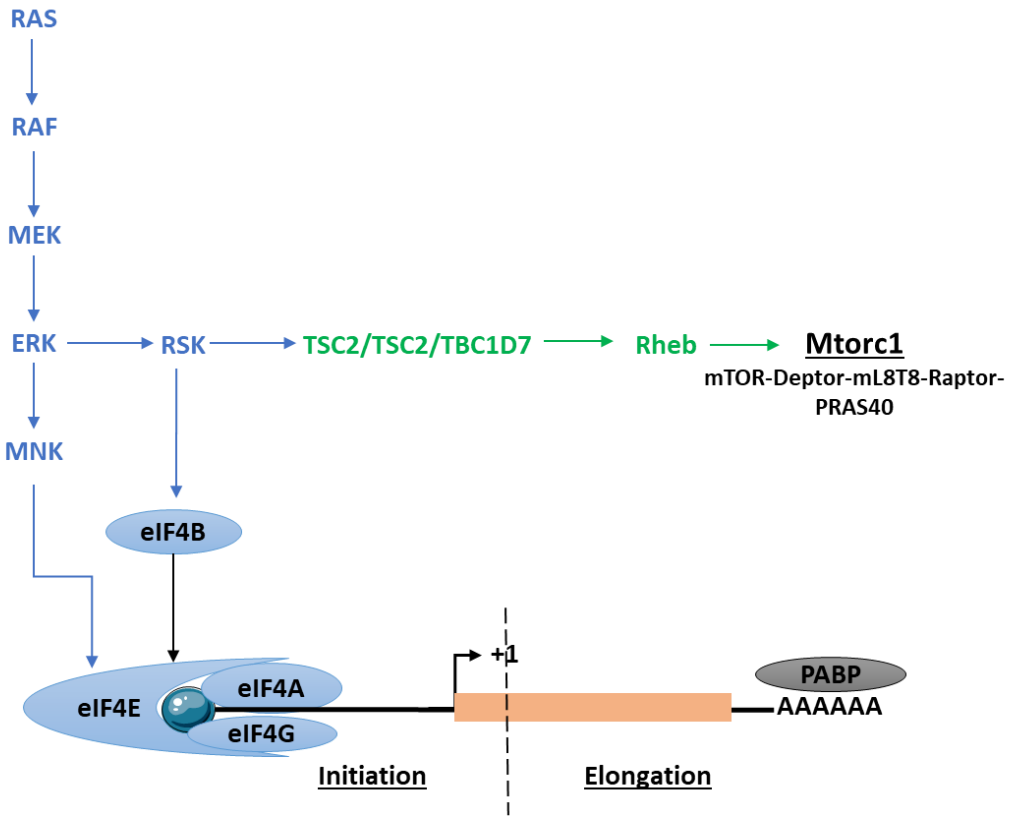

Figure 23: Regulation of translation by MAPK pathway
MAP kinases are sequentially activated to activate the final effectors RSK and MNK to regulate translation initiation.

3 Heterogeneity of ribosomes & regulation of translation

The first hypothesis about ribosome heterogeneity was suggested in the late 1950, soon after its discovery. However, it was dropped in favour of the genetic code and proposed that one ribosome was specific to one mRNA (Crick, 1958). This meant that for every new mRNA, there would be a new ribosome. Few years later, this hypothesis was disproved through bacteriophage infection of *E.coli* cultures where Brenner and colleagues discovered that bacteriophage RNA was expressed without any new ribosome synthesis (Brenner et al., 1961). They finally concluded that ribosomes were passive structures with no regulatory function that have the inherent capacity of translating mRNAs. Genuth and Barna rightly summarised history by saying that, "the field vacillated from the most extreme view of ribosome specialization to the most extreme view of ribosome homogeneity." (Genuth and Barna, 2018)

For decades, the role of ribosomes as direct regulators of translation was overlooked. They were considered as housekeeping complexes which could not discriminate between mRNAs. Since the 1980s, more and more studies contradicting this dogma were published. In the early study, RP-mutant *E.coli* cultures were generated and they identified 17 viable RP mutants (Dabbs, 1986). This study pointed out that all RP were not essential for cell survival. The following year, Gunderson *et al.* discovered that rRNA were different at each stage of the *Plasmodium berghei* life cycle (Gunderson et al., 1987). In fact, specific variants of rRNA genes seem to be expressed at specific time points during the mosquito's life cycle. In 1990, Ramagopal identified that 12 RPs were upregulated and 18 RPs were downregulated when amoeba *Dictyostelium discoideum* transitioned from a unicellular to pluricellular phase (Ramagopal, 1990).

Further studies on the Drosophila *Minute* mutants (Kongsuwan et al., 1985; Marygold et al., 2007) revealed developmental impairments, some of which were tissue specific such as cardiomyopathy or defective wing development (Marygold et al., 2005; Casad et al., 2011; Akai et al., 2018; Lee et al., 2018; Mello and Bohmann, 2020). Similar cell- and/or tissue-specific effects were seen in yeast (Komili et al., 2007; Parenteau et al., 2011), zebrafish (Amsterdam et al., 2004; Uechi et al., 2008; Lai et al., 2009), mouse (Barna et al., 2008; Barlow et al., 2010; Kondrashov et al., 2011; Perucho et al., 2014; Wilson-Edell et al., 2014) and also in human (Belin et al., 2009; Rao et al., 2012; Bolze et al., 2013; De Keersmaecker et al., 2013; Marcel et al., 2013). There are various degrees of penetrance of loss-of-function RP in each organism

(Polymenis, 2020). These findings also extend to other components of the translation complex, namely rRNA as well as RAFs, challenging the assumptions of a standardised translation machinery. In this chapter, we will consider how the translation complex and its heterogeneity can regulate translation.

There are **two** opposing theories that have been proposed explaining the tissue-specificity of mRNA translation and ribosomopathies, that is, diseases caused by the deregulation of ribosomes (**Figure 24**).

The first theory to explain the observed specificity of the ribosomal activity has been the dominating theory for decades. The theory is named abundance or concentration model which relies on the limited availability of ribosomes due to defective ribosome assembly (Lodish, 1974). According to this theory, the tissue-specificity observed in mRNA translation is explained by a limited number of available ribosomes (Ludwig et al., 2014; Kirby et al., 2015) (**Figure 24**). This would limit translation initiation in different ways, depending on the mRNA, thus accounting for the various effects. For example, in their 2014 study on Diamond Blackfan anaemia, a disease caused by altered ribosomes, Ludwig and colleagues showed that RPS19 mutation cause a drop in the level of ribosomes. They suggest that the observed drop in *Gata1* levels is due the limited number of ribosomes to recognise the highly structured 5' UTR of *Gata1* rather than a specificity of RPS19-containing ribosome to translate *Gata1* mRNA (Ludwig et al., 2014). In their 2017 review, Mills and Green suggested the broad spectrum of symptoms observed in RPL38/eL38 mutant mice would be due to a general decrease in ribosomes rather than a change in the specific translation of Hox genes by RPL38-containing ribosomes (Mills and Green, 2017)

The second theory is one in which the ribosome plays a central role in regulating translation. According to this theory, a heterogeneity in the translation complex could account for the tissue specific aspects. It could adapt to the cellular context to influence mRNA translation. Heterogeneity in the translational complex can be classified in three categories: (i) heterogeneity of RP; (ii) heterogeneity of rRNA; and (iii) heterogeneity of RAFs. **Figure 25** summarises the different origins of ribosomal heterogeneity.

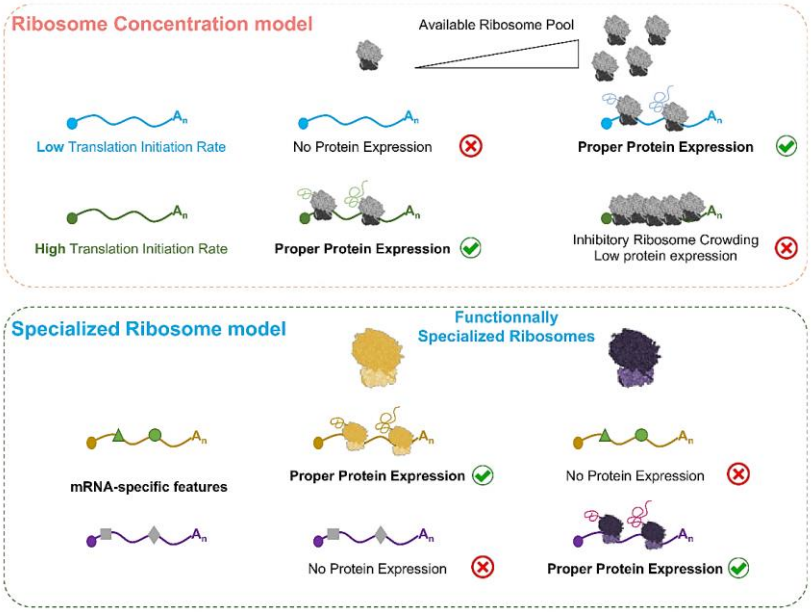

Figure 24: Illustration of the ribosome concentration model and the specialised ribosome model
In the first model, the pool of available ribosome accounts for the tissue specificity of haploinsufficient phenotype. In the second model, ribosomes can target mRNA for a specific translation – from (Gabut et al., 2020)**.**

3.1 RP heterogeneity

RPs, also called core RPs, are small proteins with a molecular weight between 10kDa and 50kDA and are mostly basic in nature. They were typically thought to be always present in ribosomes at any point in time (Uechi et al., 2001) and are regularly used as reference genes for qPCR (Thorrez et al., 2008). RPs participate in the maintenance of the architecture of the ribosome. By using knockout experiments to understand RP roles on ribosomes, studies revealed that 17 bacterial RPs and 15 yeast RPs were dispensable (Dabbs, 1986; Steffen et al., 2012). Since then, it is known that some RPs have expressed paralogs, RP stoichiometry within active ribosomes were varying and post-translational modifications in RPs seem to influence translation (**Figure 25**).

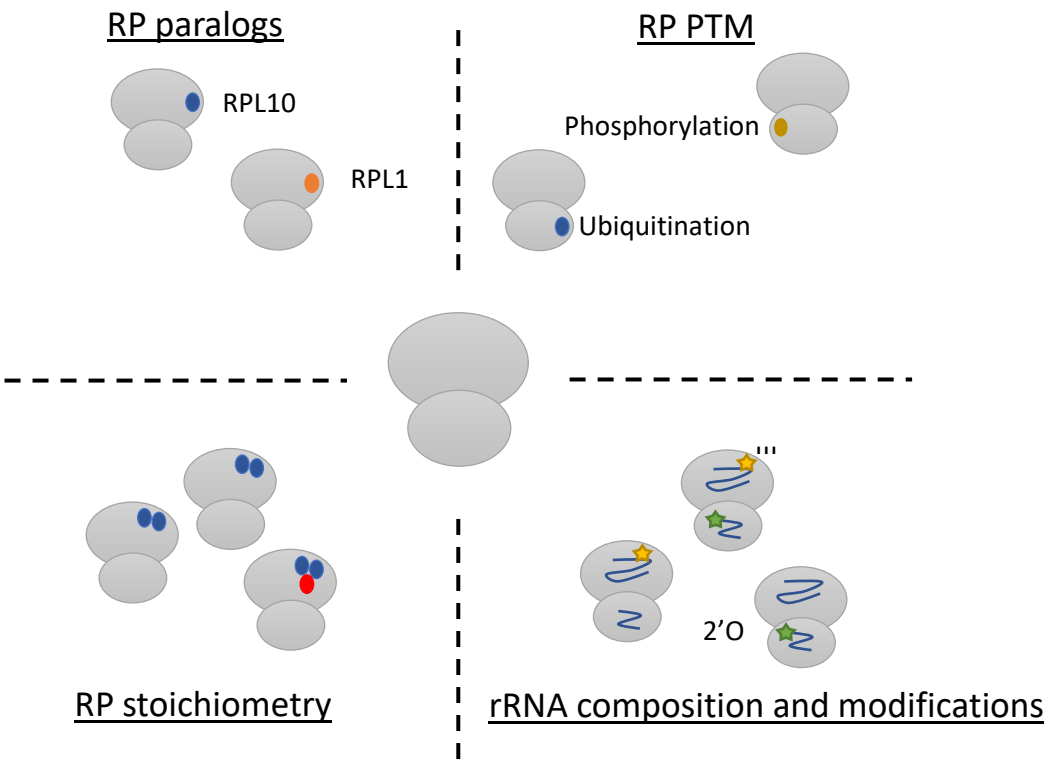

Figure 25: Summary of ribosome heterogeneity
Heterogeneity is found at different levels: RP, rRNA and RAF. There are differences of stoichiometry of RP, paralogue present and post-translational RP modifications. There are also variations on rRNA modifications and ribosome associated factors.

Insights in RP heterogeneity progressed with 2D gel analysis that enable the identification of different RP (Wada, 1986). Progress was brought afterward with transcriptomic studies then finally by proteomic analysis, more precisely in liquid chromatography coupled to tandem mass spectrometry (LC-MS/MS). It is by far the preferred technique to study ribosome composition. LC-MS/MS is a protein sequencing technique. There are possible approaches for label-free proteome-wide profiling. The bottom-up or 'shot-gun' approach involves an exhaustive analysis of the biological sample (Washburn et al., 2001). Proteins are first digested, generally with trypsin, then separated by liquid chromatography then analyses by mass spectrometry (MS). In the first MS cycle also called MS1, the precursor peptides are analysed without fragmentation. The mass (m) and retention time are analysed. In the second cycle (MS2), peptides are fragmented and analysed. Advantages of bottom-up proteomics is the wide coverage and high resolution of the technique. The second approach is the top-down proteomics in which proteins are not digested prior to analysis. It is a preferred

technique for the identification of proteoforms including PTMs and splice isoforms (Vialaret et al., 2018).

There are two different ways of monitoring the MS acquisition:

- Selected Reaction Monitoring (SRM) is ideal for discovery studies as they are sensitive, rapid and cost effective. It has a small isolation window and is adapted for the detection of small proteins. However, it is less accurate and reproducible than other methods as it does not analyse the MS2 fragments. It also does not allow a wide m/z range. (Vidova and Spacil, 2017).
- Parallel Reaction Monitoring (PRM) in which produces ions are analysed for higher resolution. We are able to follow a wider m/z range with a higher sensitivity (Peterson et al., 2012).

The sensitivity of the LC-MS/MS technique depends on the abundance and the properties of the protein in a given sample. Larger proteins are more represented as they generate more peptides than smaller proteins. For the correct identification of a protein, peptides with unique sequences must be generated which is not always possible. Moreover, only peptides present in the libraries can be detected.

3.1.1 Heterogeneity with Paralogs

In humans, most RPGs are present in single copy. Some are duplicated and either result in the same protein (e.g. eS17/RPS17) or in different isoforms or paralogs (e.g. eS4/RPS4 encoded by *Rps4x* and *Rps4y*). There are interspecies differences. In *Saccharomyces cerevisiae*, 75% of RPG are duplicated, while *Mus musculus* have a single copy of each RPG (Dharia et al., 2014; Nakao et al., 2004; Kenmochi et al., 1998). The compilation of RPG per species can be found at http://ribosome.med.miyazaki-u.ac.jp/ (Nakao et al., 2004).

Initially, paralogs were thought to have redundant roles as the growth of RP knockouts were rescued through the expression of their paralogues (Rotenberg et al., 1988). Subsequent studies revealed that they could be associated with the translation of specific sets of mRNAs and/or had a site-specific expression. For instance, in an attempt to decipher the role of duplicated genes in yeast, Komili and colleagues decided to investigate the impact of RP knockouts on budding (Komili et al., 2007). The budding site is determined by the anchoring

of *ASH1* mRNA, an mRNA specifically localised and expressed in the daughter cell during budding and required to suppress mating-type switching during cell division (Bobola et al., 1996; Gonzalez et al., 1999; Komili et al., 2007). By using a GFP reporter fused to the E3 domain of ASH1, they show that RP knockout yeast strains for one of the paralogs *Rps18b/uS13b, Rpl7a/uL30a, Rpl12b/uL11b* or *Rpl22a/eL22a* has defects in *ASH1* mRNA localisation. This underlines the essential role of specific RP in yeast. Even if there are less RP paralogs in higher eukaryotes than in lower eukaryotes, paralogs are still associated with specific location and/or functions (Gupta and Warner, 2014; Guimaraes and Zavolan, 2016). Here are listed five well-known pairs of paralogs present in higher eukaryotes.

Paralog pair	Length (amino acid)	Identity	Similarity	Gaps
Rpl3/Rpl3l	408	76%	88%	1.50%
Rpl10/Rpl10l	214	98.60%	98.60%	0%
Rpl22/Rpl22l1	128	70.30%	78.10%	4.78%
Rpl39/Rpl39l	51	94.10%	98%	0%
Rps4x/rps4l	263	92.80%	96.60%	0.40%

Table 2:Homology in protein sequence of some expressed pairs of RP paralogs in mice

3.1.1.1 RPL3/RPL3l

RPL3 and RPL3L protein sequences share 90% of similarity and 78% of identity (**Table 2**). RPL3 is located at the entrance of the A site. It is necessary for the formation of the PTC during ribosome biogenesis and ribosome activity in mature ribosomes (Schulze and Nierhaus, 1982). By inserting two substitution mutations in *RPL3* gene (G765C and C769T) in yeast, Peltz et al induced a change in the PTC that increased by four-fold the level of -1 ribosomal frameshift (Peltz et al., 1999). Its methylation on histidine 243 is associated with elongation fidelity (Al-Hadid et al., 2016; Peltz et al., 1999). By substituting histidine with an unmethylated alanine, the degree of elongation fidelity is reduced the level of stop codon readthrough increased (Al-Hadid et al., 2016)

As for *Rpl3l* mRNA, it is only detected in striated muscles including the heart and skeletal muscles (Gupta and Warner, 2014; Van Raay et al., 1996). Time course transcriptomic analysis of hypertrophic muscle revealed that *Rpl3* and *Rpl3l* were inversely regulated. During muscle hypertrophy, while overall ribosome biogenesis is decreased, RPL3/uL3 is significantly

increased and RPL3L is downregulated (Chaillou et al., 2013, 2014; Kirby et al., 2015). Functional studies on differentiating myoblasts showed that overexpression of *Rpl3l* resulted in thinner myotubes due to a decrease in myoblast fusion. While they were able to show that *Rpl3l* was acting as a negative growth regulator, they could not exclude any extra-ribosomal role of *Rpl3l* (Chaillou et al., 2016).

3.1.1.2 RPL10/RPL10L

Rpl10 gene is located on the X chromosome while *Rpl10l* gene is located on chromosome 14 in humans and chromosome 12 in mice. The protein is located near to the P and E in the ribosome. RPL10 is a tumor suppressor. Its mutation is associated with ribosome biogenesis defects and 10% of T-cell acute lymphoblastic leukaemia (De Keersmaecker et al., 2013).

Proteomic analysis using two-dimensional gel electrophoresis on different organs showed that RPL10L is testis-specific and is essential for spermatogenesis (Jiang et al., 2017; Sugihara et al., 2010). In mice, *Rpl10l*$^{-/-}$ males are sterile. Functional analysis showed that RPL10L controls ribosome biogenesis during late prophase and the prophase-metaphase transition of meiotic I division as no spermatocytes from *Rpl10l*$^{-/-}$ males were able to proceed to the second meiotic division. Sterile *Rpl10l*$^{-/-}$ males were successfully rescued with the expression of ectopic RPL10 thus showing that RPL10 can compensate for RPL10L following the X chromosome inactivation. (Jiang et al., 2017).

Rpl10l mRNA is detected by PCR in normal ovarian tissue but there is no evidence of the protein (Rohozinski et al., 2009). In fact, comparative analysis between mRNA and protein levels revealed little correlation between these levels (Komili and Silver, 2008, 2008; Schwanhäusser et al., 2011; Liu et al., 2016a). A possible reason for the absence of RPL10L could be that the ova present in ovaries have already undergone the 1st meiotic division and therefore do not require RPL10L anymore. Finally RPL10L is known to be overexpressed in both testicular and ovarian cancers (Rohozinski et al., 2009).

3.1.1.3 RPL22/RPL22L

RPL22 and RPL22L are ubiquitously expressed and are essential during development. During gastrulation, free RPL22 and RPL22L1 are localised inside the nucleus where they ensure extraribosomal functions. RPL22L1 binds several pre-mRNAs including *Smad2* pre-mRNA to repress its splicing. The mis-spliced mRNA will not be translated resulting in a decrease in protein levels of Smad2, a critical regulator of gastrulation. This decrease was observed both in zebrafish and in mouse embryos. On the other hand, RPL22 acts as an antagonist to limit Rpl22L1 repression (Zhang et al., 2017). In Drosophila melanogaster eye development, RPL22L1 shows a spatio-temporal expression pattern while RPL22 is shows no variation (Gershman et al., 2020)

Likewise, both RPL22 and RPL22L1 are essential to the hematopoietic lineage. The hematopoietic stem cells will give rise to progenitors that will migrate and colonise the thymus. The knockdown of RPL22 induces p53-dependent apoptosis of T-cell progenitors in the thymus while RPL22L1 knockdown induces p53-independent cell death of stem cells before the thymus colonisation (Anderson et al., 2007). They cannot be rescued by the other paralog as they have specific roles in space and time during hematopoietic lineage development. Mechanistically, RPL22 binds *Smad1* mRNA to repress its expression. Interestingly, in RPL22 and RPL22L1 double knockouts have a normal thymus and T-cell development (Zhang et al., 2013c). This indicates that all RP are not essential for translation (Zhang et al., 2013c).

3.1.1.4 RPL39/RPL39L

RPL39/eL39 is located inside the nascent peptide exit tunnel (Zhang et al., 2013b). *Rpl39l* mRNA is expressed in many tissues but its protein is only detected in the testis (Uechi et al., 2002; Sugihara et al., 2010; Rohozinski et al., 2009). Either *Rpl39l* mRNA is not translated, or it is expressed at levels that are undetected by the current analysis methods. RPL39L/eL39-like is present only in higher eukaryotes. qPCR analysis showed that *Rpl39l* is highly expressed in mouse embryonic stem cells and hepatocellular carcinoma tumour (Wong et al., 2014). Until now, no published studies on the influence of RPL39L/eL39-like on stemness or cell proliferation.

Considering RPL39/eL39, downregulation of its mRNA is observed in early preeclampsia, a condition of high blood pressure in pregnant women. RPL39 was knocked down by using shRNA in trophoblast cell cultures from placental samples. Flow cytometry assay showed that RPL39/eL39-silenced trophoblast cells were blocked in G1/G0 state rather than in S phase. Wound healing analysis showed that RPL39/eL39 silencing limits proliferation, migration and invasion abilities (Jie et al., 2021). Silencing RPL39/eL39 also induces the upregulation of E-cadherin, a cell adhesion molecule whose downregulation is required for the epithelial-to-mesenchymal transition and onset of migration of trophoblast cells (Francou and Anderson, 2020).

RPL39/eL39 is mutated in more than 90% of chemo-resistant breast cancer patients. It is an early biomarker of metastasis relapse. Silencing RPL39 using siRNA inhibits proliferation of breast, lung and pancreatic cancers (Dave et al., 2014; Li et al., 2014; Dave et al., 2017). RPL39 promotes the expression of inducible nitric oxide synthetase (iNOS), an enzyme involved in signalling pathways involved in angiogenesis among others (Chiarugi et al., 1998; Dave et al., 2014). In an attempt to understand the link between RPL39 and iNOS, Dave and colleagues did an *in silico* analysis on pathways that were changed in metaplastic breast cancer and downstream activator of transcription 3 (STAT3) signalling pathway was identified. The proposed mechanism is that RPL39 interacts with ubiquitin C (UBC). This heterodimer would then recruit adenosine deaminase acting on RNA 1 (ADAR1) to activate inducible nitric oxide synthase (iNOS) 2. This will induce the activation of STAT3 (Dave et al., 2014; Li et al., 2014; Dave et al., 2017). This activity of RPL39 may be extraribosomal but this still needs to be proven.

3.1.1.5 RPS4X/RPS4XL

RPS4X is X-linked. While both alleles are expressed in humans, the mouse RPS4X undergoes X-inactivation in female individuals (Ashworth et al., 1991; Zinn et al., 1991; Hamvas et al., 1992). However, not all species have an X-related RPS4. In chicken, it is located on the 4th chromosome (Zinn et al., 1994). As both *Rps4x* are expressed in humans, it was hypothesised that its haploinsufficiency could be involved in Turner Syndrome (Fisher et al., 1990; Zinn et al., 1994). Turner Syndrome results from the partial or total absence of one sex-related chromosome and patients are therefore 45, XO. However this hypothesis was disproved

by mRNA analysis of Turner Syndrome patients' fibroblasts where increased levels of *Rps4x* were identified (Geerkens et al., 1996).

In 2017, RPS4X was proposed as biomarker associated with a poor prognosis in carcinomas such in intrahepatic cholangiocarcinoma and urothelial carcinoma, a type of hepatic malignancy and bladder cancer (Tsofack et al., 2013; Paquet et al., 2015; Kuang et al., 2017). A study from 2019 in neurons show that RPS4X is locally translated *ex vivo*. Indeed by adding heavy amino acids to the medium of cultured somaless axons, Shigeoka *et al.* demonstrated that RPS4X was indeed locally translated and co-localised with ribosomes in a nucleolus-independent manner (Shigeoka et al., 2019).

RPS4XL, also known as RPS4 paralogue, is an autosomal retrogene located on the 6th chromosome. Rps4x-like mRNA was first identified as a long non-coding RNA (NCBI Reference Sequence: NR_003634.2). It was then seen in the mouse testis ribosome through proteomic analysis using two-dimensional gel electrophoresis followed by tandem mass spectrometry (Sugihara et al., 2013). This RPS4X-like is predominantly expressed in the testis, both at the mRNA and protein level, and it is present in polysomes. It is detected only on spermatogenic cells but not at the later stages of differentiation (Sugihara et al., 2013). RPS4XL has also been studied during pulmonary artery smooth muscle cells (PASMCs) proliferation. RPS4XL binds to interleukin enhancer-binding factor 3 (ILF3) and inhibits RPS6 phosphorylation to attenuate PASMCs proliferation induced by hypoxia *in vivo*. (Liu et al., 2020; Li et al., 2021).

3.1.2 Heterogeneity in RP composition and stoichiometry

For decades, the model of a ribosome with fixed composition have been accepted. Ribosomes were seen as 'simple' complexes composed of 80 ribosomal proteins and 4 rRNA. But ideas about heterogeneity in RP composition has been on the agenda for a few years. The first hypothesis on the RP stoichiometry within ribosomes started with the following question: Are RP present in one copy? The first analysis of ribosome stoichiometry was by Weber who used two-dimensional polyacrylamide gel electrophoresis and observed that there was a difference in RP stoichiometry in 50S subunits (Weber, 1972). He calculated that some RP were more copies than other RP. Four years later, Westermann and colleagues used in vivo labelling

to tag synthesised proteins with [^{3}H]lysine in hepatoma ascites cells. They then performed a two-dimensional polyacrylamide gel electrophoresis on the RP extracts. While most of RP were equimolar, RPS4/eS4 and RPS26/eS26 were less present and RPS15 and RPS19 were present in higher amounts (Westermann et al., 1976).

Ramagopal and Ennis compared *D. discoideum* amoeba at two different developmental stages. They showed, still using two-dimension electrophoresis, that 12 RP were differentially expressed at the studied stages. This suggests that RP composition can also be dynamic. As differences were both observed at the protein and mRNA levels, they proposed that the regulation of RP occurred both at the transcriptional and translational levels (Ramagopal and Ennis, 1981). One of the possible explanations for the extra copies of ribosomes could be potential extraribosomal RP (see 3.1.4 Extraribosomal roles of RPs). However, the use of ribosome purification through affinity immunoprecipitation or ultracentrifugation would eliminate this option.

Further insight on stoichiometry will be brought by progress in MS analysis. Slavov and colleagues proved that there were differences in core RPs between monosomes and polysomes in both mouse embryonic stem cells and budding yeast (Slavov et al., 2015). To do so, they analysed by MS proteins labelled with tandem mass tag from monosome and polysome fractions from embryonic stem cells. RPS4X, RPS3, RPL30 and RPL27A among others were differentially expressed. According to their study, the difference in stoichiometry was due to a difference in the number of ribosomes on each RP mRNA. This approach was interesting as it did not take in account the levels of mRNA but the ribosomal occupation of these mRNA. They did the same comparison using yeast cultured in different carbon sources: glucose or ethanol. Similarly, to what was seen with embryonic stem cells, they measured that RPL35b/uL29 was enriched in monosomes with ethanol as carbon source while RPL26a/uL24 was enriched in the polysome fraction with glucose as carbon source. By studying the occupation of RP mRNA in yeast, they came to the same conclusion that the observed stoichiometry was due to difference in ribosomal occupation (Slavov et al., 2015).

Later Shi et al. performed an absolute quantification using SRM-based MS technology on mouse embryonic stem cells. Four RPs (RPL10A/uL1, RPL38/eL38, RPS7/eS7, and RPS25/eS25) were less present in the polysome fraction (Shi et al., 2017a). Now that it was shown that RP stoichiometry varies in vitro, the question was to understand the functional implications of this difference in stoichiometry. They chose one RP, RPL10A/uL1, and

generated flagged-RPL10A/uL1. The ribosome footprint of RPL10A-containing ribosomes were preferentially translating a subset of mRNA using the IRES (Shi et al., 2017a). In the same manner, RPL38 regulates the specific translation of IRES-containing Hox mRNAs during development *in vivo* (Kondrashov et al., 2011; Xue et al., 2015). Other RP are also associated with the regulation of specific mRNA in physiological conditions such as proliferation, differentiation and cell competition (Ramagopal and Ennis, 1981; Fortier et al., 2015; Slavov et al., 2015; Guimaraes and Zavolan, 2016; Kale et al., 2018).

Interestingly, locally translated RP could also participate in variable stoichiometry. RP would be integrated into already assembled axonal ribosomes, in neurons away from the soma (Shigeoka et al., 2019). Immunofluorescence experiment on Netrin-1 treated somaless axons to promote regeneration shows a colocalization between newly synthesised RPS4x/eS4 and ribosome containing granules. They further show that the newly synthesised RP physically interacts with the ribosome. When performing knock-down experiments using morpholinos, they induced the downregulation of axonal translation without affecting ribosome biogenesis. Indeed, RPL17/uL22 and 18S rRNA levels were unchanged, which suggest a specific effect of RPS4x. They later showed in vivo, in the *Xenopus* model, that RPS4x is essential for axon branching. This major study strongly suggests that there could be a local adaptation of the ribosome composition to the surrounding signals.

Finally, it is worth noting that there are also studies that did not observe any difference in stoichiometry of RP between monosomes and polysomes. For example, Amirbeigiarab et al compared the RP composition of ribosomes from different brain regions (hippocampus, cortex, cerebellum) at 4 different time points using MS. They did not detect any RP variation across brain regions or during aging (Amirbeigiarab et al., 2019). Another analysis of a curated mRNA database did not identify any RP variation across 9 vertebrates or 33 human tissues (Kyritsis et al., 2020). Guimaraes and Zavolan also underlined that there is not variation between in RP mRNA expression across different organs thus pointing out towards an invariable stoichiometry of RP (Guimaraes and Zavolan, 2016) According to this study, differences where seemingly due to intrinsic variations rather than tissue or specie specifications.

3.1.3 Heterogeneity in post-translational modifications of RP

As with any other protein, post-translational modifications (PTM) such as phosphorylation, hydroxylation and ubiquitination can be added on RPs. Modifications can also

be removed to modulate the RP structure and eventually the ribosome structure. This phenomenon was observed during ribosome maturation where the removal of ubiquitin from RPS27A thus promoting final SSU maturation (Montellese et al., 2020). It was suggested that these modifications were the 'ribosome code', with reference to the histone code on DNA (Komili et al., 2007; Simsek and Barna, 2017). According to the 'ribosome code', modifications in RP stoichiometry or PTM on RP allows permutations that can produce specialised ribosomes (Emmott et al., 2019).

Most studies on PTMs are the phosphorylation of RPS6/eS6 involved downstream of the mTOR pathway. RPS6 is an essential RP containing 5 phosphorylation sites namely S^{235}, S^{236}, S^{240}, S^{244}, and S^{247} (Bandi et al., 1993). Phosphorylation of RPS6 is particularly important during hepatocyte regeneration. It is the only phosphorylated RP during liver regeneration (Gressner and Wool, 1974). Constitutive expression of unphosphorylatable RPS6 in mice accounts for a shrinkage of pancreatic β cells and is associated with pancreatic cancer (Ruvinsky et al., 2005; Khalaileh et al., 2013). In the presence of constitutive Akt, *Rps6*($P^{-/-}$) mice have reduced translation fidelity, increased p53 level and a higher sensitivity to DNA damages (Khalaileh et al., 2013; Wittenberg et al., 2016).

A reduction in muscle mass caused by impaired muscle growth is also observed in *Rps6*($P^{-/-}$) mice (Ruvinsky et al., 2009). RPS6 is phosphorylated in activated neurons as a response to stimuli (Knight et al., 2012). Phospho-S6 containing ribosomes translate specific sets of mRNA such as *Fos B* (branching), *Egr4* (transcription factors early growth response 4) and *Nur77* (synaptic differentiation) (Knight et al., 2012). Still, phosphorylation of RPS6 is not required for its association to polysome (Imami et al., 2018). RPS6/eS6 is not the only phosphorylated RP. During mitosis, phosphorylation of RPL12/uL11 by CDK1 is associated with translation of specific mRNA pools such as kinetochore components and mitotic spindle while global translation is unchanged (Imami et al., 2018).

RPs are also hydroxylated by ribosomal oxygenases (Chowdhury et al., 2014). RPL27A/uL15 and RPL8/uL2 are hydroxylated by MYC-induced nuclear antigen and nucleolar protein 66 respectively. These modifications are highly conserved from prokaryotes to humans (Chowdhury et al., 2014). Both RP are located near E-site and at the intersubunit side. We may speculate that hydroxylation of these RP may participate in the stability of the 80S ribosome and release of the deacylated tRNA, based on their location in the ribosome. Hydroxylation of RPs is also associated with hypoxia response. For example, in humans,

RPS23/uS12 can be hydroxylated in the nucleus by oxygenase OGFOD1, (Singleton et al., 2014). RPS23/uS12 from lower eukaryotes contains two hydroxylation sites on proline while higher eukaryotes is hydroxylated on only 1 proline (Loenarz et al., 2014). In Drosophila, inhibition of hydroxylation through knockout of ribosomal oxygenase Sudestada1, ortholog of human OGFOD1, induces unfolded protein response, autophagy and apoptosis (Katz et al., 2014). As it is located in the DC, the state of hydroxylation of RPS23/uS12 will have a direct impact on translation accuracy by influencing codon recognition by tRNA (Loenarz et al., 2014).

Likewise, RP ubiquitination also impacts ribosomal activity. For instance, RPS7/eS7 is mono-ubiquitinated during ER stress in *S. cerevisiae.* This ubiquitination induces translation of specific sets of mRNA such as *HAC1*, a transcriptional activator involved in unfolded protein response (Matsuki et al., 2020). RPS7/eS7 is polyubiquitinated in polysome. Its de-ubiquitination leads to the dissociation of the mRNA from the 40S subunit (Takehara et al., 2021). At aberrant mRNA, RPS10/eS10 and RPS20/uS10 are monoubiquitinated by E3 ubiquitin ligase ZNF598 to induce ribosome stalling and ribosome-associated quality control (Sundaramoorthy et al., 2017). If un-rescued by deubiquitinating G3BP1-family-USP10 complexes, this ubiquitination leads to lysosomal ribosomal degradation (Meyer et al., 2020).

Some proteins such as RPL40/eL40 and RPS27A/eS31 are synthesised directly fused to ubiquitin (Finley et al., 1989). Its role is to facilitate ribosome assembly by acting as chaperon during the formation of specific structures (Finley et al., 1989; Fernández-Pevida et al., 2016). Deleting *UBA52* gene that codes fusion of protein ubiquitin and RPL40/eL40 in mice and is lethal during development (Kobayashi et al., 2016). Interestingly, in yeast, ubiquitin is cleaved from RPL40/eL40 and RPS27A/eS31 during maturation of the ribosome but this is still to be proven to happen in mammalian ribosomes (Lacombe et al., 2009; Martín-Villanueva et al., 2020).

3.1.4 Extraribosomal roles of RPs

As already mentioned, some RPs have other functions besides their role in the ribosome. In 2009, Warner and McIntosh suggested three criteria to define an extraribosomal function: i) there should be an interaction between the RP and a non-ribosomal protein or nucleic acid ; ii)

this interaction should influence a cellular process ; iii) the ribosome should not be involved in this RP function (Warner and McIntosh, 2009). 40 RP have suspected extraribosomal roles. Extraribosomal RPs are usually regulators of ribosomal biogenesis or regulators of mRNA expression.

3.1.4.1 Regulator of ribosomal biogenesis

RPs act as invigilators during ribosome biogenesis. Any impairment in rRNA biogenesis, processing or unbalanced ribosomal components induce the accumulation of RPs, rRNA and immature subunits that induces nucleolar stress (Sun et al., 2010; Lessard et al., 2018; Gregory et al., 2019). For example, depleting RPS3/uS3, RPS10/eS10, RPS12/eS12, RPS15/uS19, RPS20/uS10, RPS21/eS21, RPS23/uS12, RPS29 /uS14 or RPS30/eS30 cause disruption of the nucleolar organisation while interfering with RPSA/uS2, RPS18/uS13, RPS19/eS19 and RPSS21/eS21 expression abrogate the nucleolar export of 40S preribosomes with the 21S rRNA (O'Donohue et al., 2010). In response to the nucleolar stress signals triggered by abnormal ribosome biogenesis, RPs can activate the MDM2-p53 stress response pathway. For instance, RPL5/uL18 and RPL11/uL5 are major sensors of ribosomal stress (Bursać et al., 2012). RPL5/uL18 binds to 5S-rRNA to form a ribonucleoprotein complex and then be imported inside the nucleolus to interact with RPL11/uL5 to initiate LSU assembly (Marechal et al., 1994). During ribosomal stress this ribonucleoprotein complex will competitively inhibit E3 ubiquitin ligase MDM2 subsequently causing the accumulation of p53 thus resulting in cell cycle arrest or apoptosis (Horn and Vousden, 2008; Sloan et al., 2013; Nishimura et al., 2015). During ribosomal stress RPL5/uL18 and RPL11/uL5 protect each other from proteasomal degradation, unlike other RPs, and continue to be imported into the nucleolus after nucleoli disruption (Bursać et al., 2012).

Fourteen additional RPs can also directly bind to MDM2 (**Table** 3). Other RPs influence the MDM2-p53 pathway by interacting with p53 including RPS27L (He and Sun, 2007). For now, there is a total of 25 RPs known to trigger the RP-MDM2-p53 pathway among which are RPL23/uL14, RPL26/uL24, RPS7/eS7, RPS14/uS11 and RPL25/eS25 (Marechal et al., 1994; Zhang et al., 2002; Lohrum et al., 2003; Zhang et al., 2003; Chen et al., 2007; Zhang et al., 2013a; Zhou et al., 2013; Bai et al., 2014; Liu et al., 2016b; Meng et al., 2016).

Protein	Binding to MDM2	Ablation Induces p53	L5/L11 Dependency in p53 Regulatio	Mechanism of p53 Regulation
RPL5	Yes	No	N/A	Inhibits Mdm2 E3 activity
RPL11	Yes	No	N/A	Inhibits Mdm2 E3 ligase activity; Increases p53 acetylation and transactivity
RPS3	Yes	No	N/A	Inhibits Mdm2 E3 activity
RPS15	Yes	Yes	N/A	Inhibits Mdm2 E3 activity
RPS20	Yes	Yes	N/A	Inhibits Mdm2 E3 activity
RPS25	Yes	No	N/A	Inhibits Mdm2 E3 activity
RPS27	Yes	No	N/A	Inhibits Mdm2 E3 activity
RPS27a	Yes	No	N/A	Inhibits Mdm2 E3 activity
RPL6	Yes	No	N/A	Inhibits Mdm2 E3 activity
RPL26	Yes	No	N/A	Enhances p53 translation
RPS7	Yes	Yes	L5/L11	Inhibits Mdm2 E3 activity
RPS14	Yes	Yes	L5/L11	Inhibits Mdm2 E3 activity
RPS26	Yes	Yes	L11	Inhibits Mdm2 E3 activity
RPS27L	Yes	Yes	L11	Inhibits Mdm2 E3 activity
RPL23	Yes	Yes	L5/L11	Inhibits Mdm2 E3 activity
RPL37	Yes	Yes	L11	Inhibits Mdm2 E3 activity
RPS6	No	Yes	L11	Maintains ribosomal integrity
RPS9	No	Yes	L11	Maintains ribosomal integrity
RPS19	Cell-specific	Yes	L5/L11	Maintains ribosomal integrity
RPS23	No	Yes	L11	Maintains ribosomal integrity
RPL7A	No	Yes	L11	Maintains ribosomal integrity
RPL22	No	Yes	N/A	Inhibits p53 protein synthesis
RPL24	No	Yes	L11	Maintains ribosomal integrity
RPL29	No	Yes	L11	Maintains ribosomal integrity
RPL30	No	Yes	L11	Maintains ribosomal integrity

Table 3:RPs involved in the regulation of MDM2-p53 pathway
adapted from (Liu et al., 2016b)

3.1.4.2 Regulation of mRNA expression

Few RP are known to autoregulate the mRNA. There is a feedback mechanism by which RP can regulate their own expression, through binding of their own mRNA. For instance, RPS3/uS3 (Kim et al., 2010), RPS13/uS15 (Malygin et al., 2007), RPS14/uS11 (Fewell and Woolford, 1999), RPS26/eS26 (Ivanov et al., 2005), yeast RPL2/uL2 (Presutti et al., 1991), RPL30/eS30 (Macías et al., 2008), RPS19 (Schuster et al., 2010) control their levels by inhibiting their mRNA splicing or by decreasing their mRNA half-life. RPL22/eL22 can control the expression of its paralog RPL22L1/eL22-like1 (O'Leary et al., 2013)

RPs can also regulate mRNA levels of other proteins. For example, RPL13a is an interferon-Gamma-Activated Inhibitor of translation of ceruloplasmin mRNA, a copper-carrying protein in blood. Phosphorylation of RPL13a induces its release from the LSU. Free RPL13a can bind to the 3'UTR of ceruloplasmin mRNA to regulate its expression (Mazumder et al., 2003). Similarly, during development, RPL22/eL22 and RPL22L1/eL22-like1 binds to

smad2 pre-mRNA to influence mRNA splicing (Zhang et al., 2017). While RPL22L1/eL22-like1 favours the integration of exon 9 in the mature mRNA to promote the anterior-posterior extension during gastrulation and the formation of the notochord, RPL22/eL22 induce exon 9 skipping to antagonise the effect of its paralog.

3.2 rRNA heterogeneity: composition and modifications

The human genome contains between 200 and 600 rDNA copies (Gibbons et al., 2014; Parks et al., 2018). Sequencing these regions is challenging due to the high number of repeats (Treangen and Salzberg, 2011). Early studies show that there exist different rRNA variants (Tseng et al., 2008). They observed **eleven** new 45S rRNA sequences with 25 single nucleotide variants and 76 INDELs which are short insertions or deletions (Kim et al., 2018). These variations were mostly found in the ETS and ITS regions but also in the final 28S and 18S rRNAs. No variation was detected in the 5.8S rRNA. In the 28S rRNA, most variations were located on the ES27L segment which ensures coordination between the mRNA tunnel and the peptide exit tunnel. They also observed that other variants induce the formation of enlarged stem-loop structure resulting in new interactions between RPs or other stem-loop structures (Anger et al., 2013; Kim et al., 2018). However, no experiment was performed to investigate if these modified interactions impact the ribosome functioning. This study also suggested that variants located at rRNA processing sites might affect processing efficiency (Kim et al., 2018).

All the rRNA copies are also subjected to the control by the pre-rRNA promoter regions to be expressed in cells. This was confirmed by *in silico* analysis of RNA sequencing database (Zentner et al., 2011). Study of dataset from 1000 Genome project and mouse genome from thirty-two different strains revealed that rRNA variants are conserved and stratified by ancestry, that is, there is an observed divergence between rRNA sequences across different populations (Parks et al., 2018). These rRNA variants are present in actively translating ribosomes. The variations tend to be located in important functional regions of the ribosome such as intersubunit bridges. They also exhibit a tissue-specific expression (Tseng et al., 2008; Parks et al., 2018).

In addition to rRNA variants, rRNA is modified post-transcriptionally. Considering the distribution of post transcriptional modifications, they are not distributed evenly along rRNA but mostly located in functional regions such as the PTC, the DC, the A, P and E sites or the subunit interface, suggesting that they can influence directly the ribosome's ability to translate mRNA (Decatur and Fournier, 2002). Some modifications are essential to the ribosome activity.

For instance, deletion of domain IV of 23S rRNA in yeast leads to ribosome instability and loss of the LSU (Gigova et al., 2014). Deletion of A1322 methylation in yeast and human prevents loading of the LSU on the 43S pre-initiation complex (Sharma et al., 2018). Deletion of rRNA modifications on helix 69, which acts as an intersubunit bridge and interacts with A and P site tRNAs, decreases elongation rate and a higher rate of mis-read stop codon (Liang et al., 2007). Similarly, deleting 2'OMe from the DC region impairs growth in yeast by reducing elongation rates and altering SSU production while altering pseudouridylation in the P region of rRNA, which slows down the rRNA processing rate by 60% (Liang et al., 2009). Some modifications are dispensable such as G562 methylation of the 18S rRNA in yeast whose deletion does not alter growth or translation (Yang et al., 2015). Other sites, however, are partially modified and can give rise to ribosome heterogeneity. For instance, the frequency of 2'O methylations of A100 in yeast 18S rRNA or U2345 in the 25S rRNA are respectively 68% and 76% in actively translating ribosomes (Buchhaupt et al., 2014; Taoka et al., 2016). These studies unravelled a new type of heterogeneity that can influence translation by slightly changing the stearic disposition and interactions within the ribosome.

4 Role of RP in physiology and pathology

Ribosomes have a pivotal role in maintaining protein homeostasis. Both rRNA and RP can influence ribosomal functions. In this chapter, we will focus on the role of RP in both physiological and pathological conditions.

4.1 RP during development

During development, there are huge requirements of protein synthesis to give rise to the different tissues and organs constituting an organism. RP expressions during the different phase of development are specific to match the requirements at given time and space (Uechi et al., 2006). For instance, transcriptomic analysis showed that *Rps4x* mRNA expression was modulated during the zebrafish development (Bhavsar et al., 2010) (**Figure 26A**). Rps4x is most highly expressed before gastrulation and before the formation of the zygote. This is followed by a dramatic drop at the zygote stage. Other RP show variabilities in spatial expression. In mammals, RPL38/eL38 is involved in axial skeletal patterning, that is, the establishment of somites and neural tube (Kondrashov et al., 2011). Mutation in RPL38 present in a specific mouse *Ts*/+ strain causes abnormalities including neural tube formation, deformed lumbar and thoracic vertebrae. Axial skeletal patterning involves *Hox* genes. Transcriptional analysis revealed that there was no significant difference in *Hox* transcript expression between Rpl38 mutant mice and control, indicating that the difference in phenotype originated from another process.

Polysome profiling analysis revealed RPL38 favours translation of a subset of *Hox* mRNA namely *Hoxa4*, *Hoxa5*, *Hoxa9*, *Hoxa11*, *Hoxb3*, *Hoxb13*, *Hoxc8*, *Hoxd10*. Further analysis revealed that all skeletal defects of the *Ts*/+ mouse strain was solely due to abnormal *Hox* mRNA translation caused by *Rpl38* mutation. Based on RP expression during development, it is highly suggested that there is a ribosomal signature associated with tissue and organ. However, we do not know if this difference in RP levels is maintained at adult stage.

Similarly, RPL3 is required for growth of striated muscles by regulating myotube fusion. The balance is maintained by RPL3L which limits myotube fusion (Chaillou et al., 2016). Inclusion of bi-allelic missense variants of RPL3L is associated with neonatal dilated cardiomyopathy (Ganapathi et al., 2020). However, there is no translatome analysis available to understand how translated mRNA are impacted by this change.

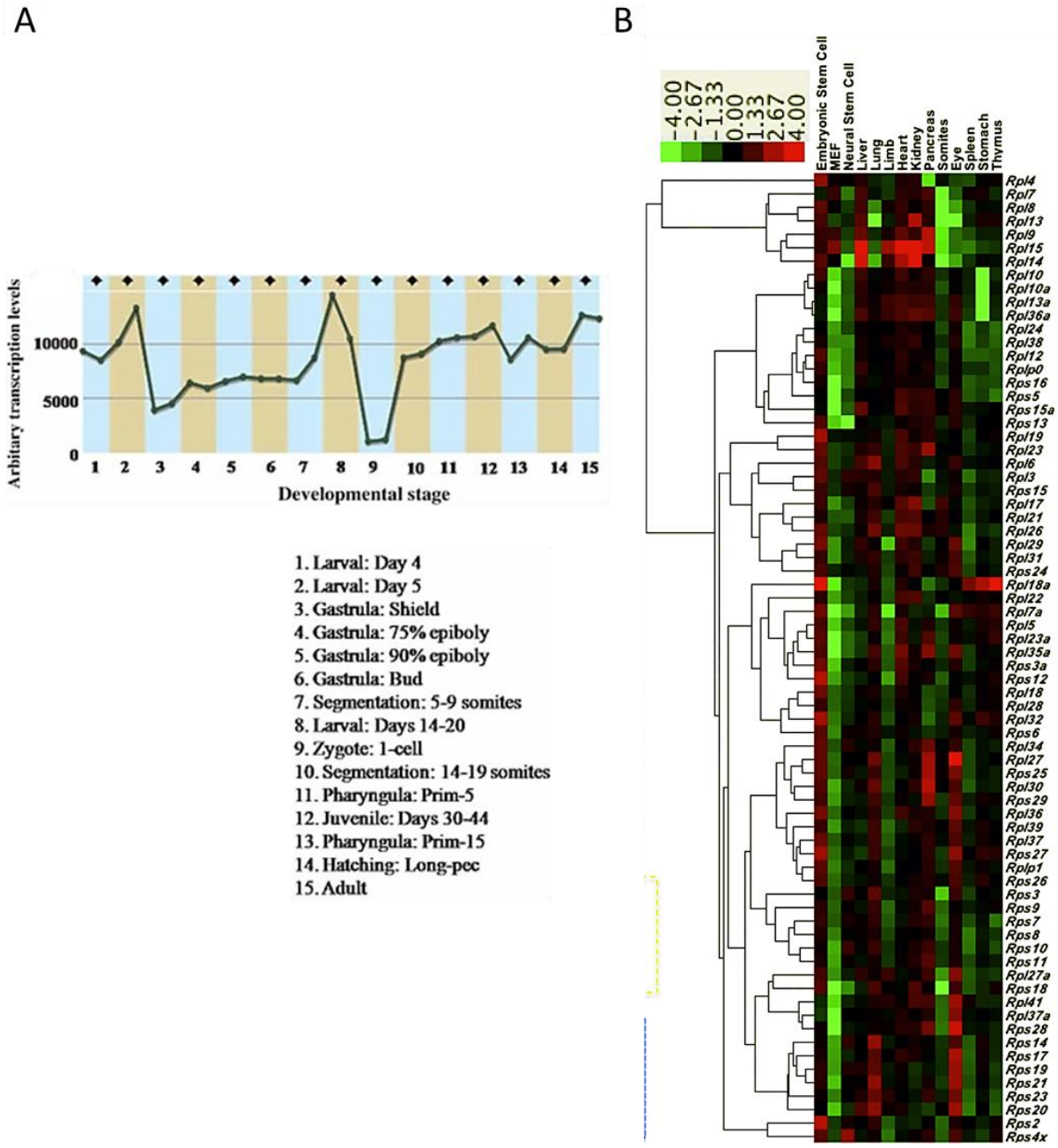

Figure 26: Spatio-temporal differences in RP expression during development
(A) transcription profile of Rps4x during zebrafish development – adapted from (Bhavsar et al., 2010) (B) RP mRNA expression across different organs during development – adapted from (Kondrashov et al., 2011)

RP levels also influence haematopoiesis. Haematopoiesis is the differentiation program that gives rise to blood cell lineage such as erythrocytes, B and T cells and monocytes. It requires a high rate of protein synthesis. GATA1 is a key lineage-determining haematopoietic transcription factor. In diseases where RP are mutated such as in Diamond Blackfan Anaemia,

GATA1 level is reduced due to a change in the 5'UTR of its mRNA (Sankaran et al., 2012; Ludwig et al., 2014; Khajuria et al., 2018). Proteomic analysis for total ribosomes using mass spectrometry revealed that only 3 RP were differentially expressed: RPS19/eS19, RPS26/eS26 and RPL5/uL18 (Khajuria et al., 2018). Some RPs are associated with specific functions. RPS14/uS14 is associated with erythroid differentiation. Conditionally inactivating RPS14/uS14 causes megakaryocyte dysplasia and loss of hematopoietic stem cell quiescence (Schneider et al., 2016). RPL22L1/eL22-like1 is required for the emergence of hematopoietic stem cells at the aorta-gonad-mesonephros while RPL22/eL22 is required for the development of T lineage progenitors within the thymus (Zhang et al., 2013c) These effects are both dependent on RPL22L1/eL22-like1 and RPL22/eL22 association with *Smad1* mRNA. RPL22/eL22 represses *smad1* translation while RPL22L1/eL22-like1 opposes this repression. Interestingly, we see that paralogs are not equivalent but have distinct roles during development.

4.2 RP and aging

Aging is a biological process that occurs in all cells, except stem cells. During its lifespan, cells are exposed to different oxidative stress causing DNA damages and undergo senescence. RP protein and rRNA levels change leading to abnormal ribosome assembly and a less efficient translation over time (Ke et al., 2017; Samir et al., 2018; Turi et al., 2019). There is an overall decrease in total ribosomes even if no net decrease in polysomes was detected (Fando et al., 1980). Cells are therefore more prone to deregulations. There are few available studies on RP and aging. Deletion of *Rpl31* and *Rpl6* are also associated with long life span (Kaeberlein et al., 2005) *Rpl10* and *Rps6* were proposed as lifespan regulators in yeast as the heterozygous deletion of each protein is associated with a 24% and 45% increased replicative lifespan respectively (Chiocchetti et al., 2007).

Single-cell transcriptomic analysis in the aging mouse brain showed the expression of 7 RPGs, including *Rps29* and *Rpl38*, were modified during aging (Ximerakis et al., 2019). A recent study comparing mouse brain tissues, namely the hypothalamus, cortex and cerebellum, at different time points (3 weeks, 4 months, 7 months and 12 months) but no difference in RP expression as detected in time or space (Amirbeigiarab et al., 2019).

4.3 Ribosomes in diseases

Any alteration to components of ribosomes may result in potentially lethal situations. There is a broad range of pathologies as RPs have different roles in space and in time. We will have a look at ribosomopathies, a group of rare diseases caused by the direct dysregulation of ribosomal components but also in cancers and neurodegenerative disorders to understand how ribosomes contribute to these diseases.

4.3.1 Ribosomopathies

Ribosomopathies are a broad group clustering several pathologies caused by defects in ribosome biogenesis. There are different categories of ribosomopathies. Pure ribosomopathies have symptoms that are directly caused by a ribosome malfunctioning whereas mixed ribosomopathies include other factors, in addition to ribosome alteration. They can be congenital or somatic. There are 19 described ribosomopathies with various mutations and penetrance (Table 4).

They are all rare diseases, that is, they affect less than 5 in 10 000 individuals (European guidelines of orphan diseases - 2018). Ribosomopathies are either caused by (i) a reduced number of functional ribosomes; (ii) a change in rDNA copy number; (iii) mutant RP resulting in ribosomes with reduced fidelity. **Figure 26** indicates the location of mutated RPs involved in ribosomopathies. The two most frequent ribosomopathies involving RP mutations are Diamond Blackfan Anaemia and 5q deletion syndrome.

4.3.1.1 Diamond Blackfan Anaemia

Diamond Blackfan Anaemia, or DBA, was the first identified ribosomopathy. It is a rare congenital hypoplasia of erythroid progenitors characterised by macrocytic anaemia with normal white blood cells and platelets. It is detected in early childhood. The symptoms of the disease are low reticulocyte count and a low percentage of red blood cell precursors in the bone marrow. They also develop skeletal and cardiac abnormalities and a higher prevalence for cancer. Genetic studies on DBA patients revealed they carry mutated RP genes. Up till now, there are 19 identified mutations. The most frequent mutations in DBA affect *Rps19, Rps26, Rpl5* and *Rpl26* genes (D'Allard and Liu, 2016; Quarello et al., 2010; Avondo et al., 2009; Uechi et al., 2008; Ulirsch et al., 2018). **Table 5** lists all the RPs that are mutated during DBA

Disease	Gene Mutated	Role in Ribosome Biogenesi	Clinical Manifestations
Diamond Blackfan anemia	**RPS19, RPS26, RPS17, RPS28, RPS29, RPS24, RPL5, RPL11, RPL35, RPL18, RPL26, RPL15, RPS27, RPL27**	**40S and 60S subunits protein**	**Macrocytic anemia, skeletal abnormalities, short stature, cardiac and genitourinary malformations, cancer predisposition**
Shwachman-Diamond syndrome	SBDS, DNAJC21, EFL1, SRP54	Assembly of 60S and 40S subunits in active 80S ribosomes	Bone marrow failure, skeletal dysplasia, cognitive impairment, and risk of developing myelodysplastic syndrome
Treacher Collins syndrome	**TCOF1, POLR1C, POLR1D, POLR1B**	**Ribosomal RNA transcription**	**Severe craniofacial defects and mental retardation**
Cartilage Hair Hypoplasia-Anauxetic dysplasia spectrum	RMRP, POP1	Ribosomal RNA processing	Short-limbed dwarfism, sparse hypoplastic hair, immunodeficiency, hypoplastic anemia, and predisposition
Dyskeratosis Congenita	DKC1, PARN, NHP2, NOP10, NPM1	Ribosomal RNA pseudouridylation and processing	Abnormal skin pigmentation, dystrophy of the nails, oral leukoplakia, bone marrow failure, and cancer
5q− syndrome	**RPS14**	**40S subunit protein**	**Macrocytic anemia and erythroid hypoplasia; may progress to AML**
Acute myeloid leukemia (AML)	NPM1	Ribosome processing	AML with normal karyotype
Pediatric acute lymphoblastic leukemia (T-ALL)	RPL5, RPL10, RPL22	60S subunit proteins	T-ALL
Relapsed CLL	RPS15, RPSA, RPS20	40S subunit proteins	Relapse after first-line treatment
Alopecia, neurologic defects, and endocrinopathy syndrome	RBM28	Ribosomal RNA processing	Alopecia, mental retardation, progressive motor deterioration, central hypogonadotropic hypogonadism and short stature, microcephaly, gynecomastia, and hypodontia
North American Indian Childhood Cirrhosis	CIRHIN, NOL11	18S rRNA processing	Transient neonatal jaundice that evolves into biliary cirrhosis requiring hepatic transplantation
Bowen-Conradi syndrome	EMG1	Ribosome assembly	Mental retardation, microcephaly, micrognathia, rocker bottom feet, and flexion contractures of the joints; causes early death
Familial colorectal cancer type X	RPS20	40S subunit protein	Hereditary colorectal cancer without mutations in mismatch repair genes
Congenital asplenia	RPSA	40S subunit protein	Absence of spleen
Aplasia cutis congenita	BMS1	Ribosomal GTPase, 18S rRNA processing	Skin defect and alopecia of the scalp
RPS23-related ribosomopathy	RPS23	40S subunit protein	Microcephaly, hearing loss, dysmorphic features, intellectual disability, and autism spectrum disorder
Leukoencephalopathy, intracranial calcifications, and cysts (LCC)	SNORD118	C/D box snoRNA U8 involved in ribosome biogenesis	Neurological disorder with leukoencephalopathy, intracranial calcifications, and cysts
Autism	RPL10	60S subunit protein	Autism spectrum disorder
Microcephaly	RPL10	60S subunit protein	Microcephaly, intellectual disability, epilepsy, and growth retardation

Table 4: List of all described ribosomopathies with their associated mutations – adapted from (Venturi and Montanaro, 2020)

Subunit	Mutated RP genes in DBA
60S	**RPL5, RPL11**, RPL15, RPL18, RPL26, RPL27, RPL31, RPL35, RPL35A
40S	RPS6, RPS7, RPS10, RPS15A, RPS17, **RPS19**, RPS24, **RPS26**, RPS27, RPS28, RPS29

Table 5: mutated RP genes in DBA
The genes indicated in bold are most frequently mutated.

The incorporation of mutated RPs results in impairment of ribosome biogenesis and assembly. For example, studies revealed that RPS19 is necessary for the processing of the pre-40S ribosomes (Léger-Silvestre et al., 2005). It is involved in the maturation of the 3' end of the 18S rRNA and the assembly of the pre-40S particle (Angelini et al., 2007; Flygare et al., 2007; Léger-Silvestre et al., 2005). Moreover, the auto-feedback loop regulating RPS19 levels is also altered in DBA. Mutated RPS19 has less affinity for the 5'UTR of its own mRNA and therefore has a lesser impact on its expression (Badhai et al., 2011; Schuster et al., 2010). In addition to ribosome biogenesis, ribosome translation capacity is also affected in DBA. Decreased levels of RPS19 correlates with the overall decreased ribosome levels in hematopoietic cells (Miyake et al., 2008; Khajuria et al., 2018). However, no change was noted in the ribosome composition. *In vivo* translatome study on DBA patients revealed that the translation of specific mRNAs with short, unstructured 5'UTR are reduced (Ludwig et al., 2014; Khajuria et al., 2018). One of these mRNAs is *Gata1* mRNA. Reducing GATA1 impairs the hematopoietic stem and progenitor cells proliferation and differentiation (Takahashi et al., 1997)

Other RP such as RPL5 and RPL11, known to bind to the 5S rRNA in the first steps of the LSU assembly, are also mutated (Zhang et al., 2007). These mutations are associated with craniofacial and heart abnormalities in DBA patients (Gazda et al., 2008; Quarello et al., 2010). This malformation is likely to be caused by defective ribosome assembly (Robledo et al., 2008; Micic et al., 2020). Similarly, Rps6 haploinsufficiency is associated with abnormal limb development. Using the mouse model for conditional Rps6 hemizygosity in limb buds of developing mice, Tiu and colleagues were able to reproduce the phenotype observed in DBA patients (Tiu et al., 2021). This phenotype is driven by p53 and a decrease in protein synthesis was detected in the developing bud. Mechanistically, p53 repressed global cap-dependent translation by increasing 4E-BP1 expression in absence of RPS6. This p53-4E-BP1-eIF4E axis seems to be shared with other ribosomopathies such as 5q- syndrome.

4.3.1.2 5q deletion Syndrome

The 5q deletion or 5q- syndrome is a mixed acquired ribosomopathy. It results from the loss of a 1.5Mb locus on the short arm of the 5th chromosome, between 5q31 and 5q32 (Boultwood et al., 2002). It is a specific form of myelodysplastic syndromes that are characterised by an ineffective haematopoiesis with peripheral cytopenia and an erythroid hypoplasia in the bone marrow. More specifically, 5q- syndrome is characterised by macrocytic anaemia with a slow progression to acute myeloid leukaemia (Heaney and Golde, 1999). It affects hematopoietic stem cells and progenitor cells.

The deletion affecting 5q directly results in haploinsufficiency of *RPS14*. Indeed, using shRNA, Ebert and colleagues showed that silencing one *RPS14* allele was sufficient to cause the decrease in erythropoiesis thus resulting in anaemia (Ebert et al., 2008). RPS14 is an i-RPS and is therefore required in the initiation of the 18S rRNA processing. Deletion of RPS14 induces the accumulation of the 30S pre-rRNA (Ferreira-Cerca et al., 2005; O'Donohue et al., 2010) This will activate the MDM2-p53 surveillance pathway and induce cell death in erythroid progenitor cells (Barlow et al., 2010; Dutt et al., 2011). In 5q deletion syndrome, other genes such as casein kinase 1A1, a regulator of β-catenin and stem cell renewal, are also affected (Cheong and Virshup, 2011; Schneider et al., 2014)

4.3.1.3 From Ribosomopathies to cancer

Patients suffering from ribosomopathies (DBA, 5q- syndrome, …) have 2.5 to 5.6 higher risk of developing cancer (Aspesi and Ellis, 2019). This is quite a paradox considering there is a hypoplasia in the bone marrow and anaemia and on the other hand, a higher probability of developing cancer. This gave to the Dameshek's riddle: "What do aplastic anemia, paroxysmal nocturnal hemoglobinuria (PNH), and hypoplastic leukemia have in common? (Dameshek, 1967).

To our knowledge, two mechanisms have been proposed. The first involves the selective loss of p53 to favour cell survival. For example, 5q- syndrome has been associated with high levels of p53 mutations and an increased risk of developing acute myeloid leukaemia (Heaney and Golde, 1999; Kulasekararaj et al., 2013; Scharenberg et al., 2017). Another way of reducing the level of p53 in cell is by reducing the number of functional ribosomes in cells. This may be a consequence of defective ribosome biogenesis such as in the Treacher Collin syndrome

(**Figure 27**). However, there is still no direct evidence that this decrease induces the loss of p53 levels or tumorigenesis (Aspesi and Ellis, 2019).

The second hypothesis rely on the alteration of the translation program by defective ribosomes termed onco-ribosomes (Sulima and De Keersmaecker, 2017). These onco-ribosomes cause abnormal translation of specific transcripts favouring tumorigenesis. For example RPL5 and RPL11 are mutated in several tumours (Sulima et al., 2017) but there are still no direct proofs that defective ribosomes in ribosomopathies can lead to tumorigenesis. We cannot exclude that tumorigenesis emerges from an extraribosomal role of RP.

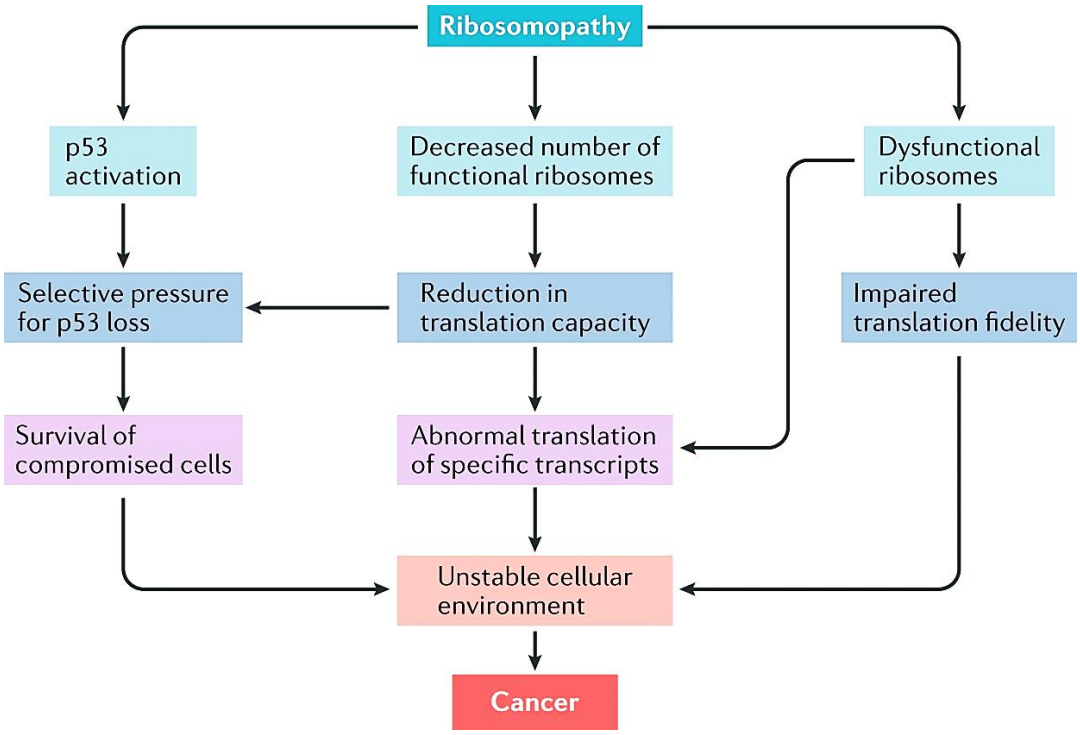

Figure 27: how ribosomopathy can favour tumorigenesis
Summary of all the possible pathway by which a ribosomopathy give rise to a tumor. from (Aspesi and Ellis, 2019).

4.3.2 Ribosomes, neurodegenerative diseases and brain injury

Neurons are sensitive cells that can adapt rapidly to changing conditions. Any chronical impairment or traumatic injury will induce a nucleolar stress which can lead to neurodegenerative disorders.

Tauopathies

Tauopathies is a class of neurodegenerative diseases caused by an altered microtubule binding protein tau expression and hyperphosphorylation that ultimately leads to neuronal loss. A well-known tauopathy is Alzheimer's disease (AD) in which hyperphosphorylated tau proteins aggregate to form neurofibrillary tangles thus causing an irreversible loss of hippocampal neurons.

One of the models used for study AD is a double transgenic mouse model of AD called APP/PS1 in which human amyloid precursor protein (APP) and presenilin 1 (PS1) are knocked in. This model shows a high level of β-amyloid production associated with cognitive impairment observed in AD. Investigations in the hippocampal proteome from young APP/PS1 mice, revealed that RPS17, RPS23, RPS26, RPS30, RPL3 and RPL19 where upregulated while RPL7a, RPL31 and RPL24 were down regulated compared to their control littermates. During aging of APP/PS1 mice, a change in RP proteome was detected. Indeed, RPL18, RPL23a, RPL27, RPL29, RPL36a,, RPL37, RPL8 and RPS4x were upregulated in APP/PS1 mice but not in the control (Elder et al., 2021). However, this study used the total hippocampal proteome. We cannot confirm that these RP were incorporated into ribosomes as there is a probability of extra-ribosomal roles. Surprisingly, *in vitro* studies using mutated tau protein and yeast or human ribosomes showed that tau protein can induce the dose-dependent sequestration of ribosomes (Banerjee et al., 2020). Further analysis revealed that mutated tau protein causes a disruption of the ribosome integrity to form tau-rRNA aggregates (Banerjee et al., 2020). The upregulation of RP expression during AD could therefore be an attempt to compensate for the loss of ribosome integrity.

During AD there is also an increase in the basal phosphorylation level of RPS6 which is known to have a direct effect on increasing tau protein levels (Pei et al., 2006; Mody et al., 2011; Caccamo et al., 2015). It is suggested that the therapeutic manipulation of ribosomal protein S6 kinase 1 (S6K1) could be a good alternative for AD treatment. Indeed, reducing RPS6 phosphorylation via the decrease of S6K1 reduced amyloid-β and tau accumulations resulting in improvement of memory deficits (Caccamo et al., 2015). However, one study from 2017 argued that RPS6 phosphorylation could rather be a feature of non-pathological neurons as only few differences were detected between their control mice and transgenic pR5 mice that express a mutated tau protein (Klingebiel et al., 2017). In frontotemporal dementia, another tauopathy where the loss of tau protein expression induces frontotemporal neuron loss,

quantitative proteomic analysis revealed that phosphorylated tau induce a down regulation in RPL23, RPLP0, RPL19 and RPS16 expressions (Evans et al., 2019). This suggests that each tauopathy can have its own RP signature.

Tau is also present inside the nucleus (Greenwood and Johnson, 1995). Nuclear tau can interact with rDNA within the nucleolus in physiological conditions (Sultan et al., 2011). They reduce rDNA transcription by inhibiting UBF recruitment to rDNA promoters (Bou Samra et al., 2017). Nuclear tau also associates with transcription termination factor-1 interacting protein 5 (TIP5), a protein involved in the chromatin remodelling complex and rDNA transcription (Anosova et al., 2015). Indeed, TIP5 recruits DNA methyltransferase to histone H3 and H4 to silence rRNA genes (Guetg et al., 2010). During AD, there is a hyperphosphorylation of nuclear tau observed. This causes a dissociation of tau from rDNA (Lu et al., 2013). This probably contributes to the synthesis of altered ribosomes.

Traumatic brain injury

An enrichment *in silico* study from 2021 focused on the gene signature in traumatic brain injury (TBI) (Ma et al., 2021). They extracted gene expression profiles blood samples before and after TBI from 29 individuals (Gill et al., 2017) and 196 gene expression profiles from brain samples (Miller et al., 2017), with 50% TBI and 50% non-TBI individuals. They identify that *Rpl27*, *Rps4x*, *Rpl23a*, *Rps15a*, and *Rpl7a* were downregulated in the brain after TBI. Transcriptomic analysis of microglia using NanoString technologies after TBI revealed that a cluster of RP was dysregulated including *Rpl34*, *Rpl32*, *Rps19*, *Rpl35*, *Rpl41*, *Rpl37a*, *Rpl36* and *Rps18* (Witcher et al., 2021). TBI triggers a cell-mediated immune response post-injury (Jassam et al., 2017) *Rpl23a* and *Rps15a* were found to correlate with the level of immune cell infiltration (Ma et al., 2021).

Results

Hypotheses and objectives

Ribosomes are macro-complexes composed of about 80 RPs and four rRNAs. They are synthesised in the nucleolus and exported to the cytoplasm where they translate mRNA. For decades, they were considered as basic components of cells but the discovery of the specificity of some ribosomes changes to influence translation questioned this assumption. All RPs are not essential to functional ribosomes as ribosomes are still able to translate when these RP are absent. Some RPs such as RPL3L or RPL10L have tissue-specific expressions and functions. It was established *in vitro* that there is a sub stoichiometric distribution of RP but data on RP composition *in vivo* are still missing

Based on available studies, we hypothesised that ribosomes are heterogeneous *in vivo.* We tested our hypothesis in the mouse model. Up till now, only one study attempted to look at the RP distribution in 3 brain tissues (hippocampus, cortex and cerebellum) at 3 different time points and no significant variations were detected (Amirbeigiarab et al., 2019). The main objectives of my PhD were to determine the stoichiometry of ribosomes in various organs and investigate how it could contribute to their functions.

We chose to compare 14 different tissues and organs by a bottom-up proteomic approach to investigate the composition of the ribosome. We used a label-free LC-MS/MS approach with a parallel reaction monitoring for the identification of proteins. We confirmed some of the RP profiles by absolute quantification. We also looked at the correlation between the protein and mRNA.

We then looked at the RAFs that were co-precipitated during ultracentrifugation to see if there was any specialisation in this component of the TC. We finished by investigating the role of ribosomes in a pathological context: the CNS injury.

1. Heterogeneity of ribosomes across organs

(Manuscript in preparation)

Ribosomal proteins signature of adult mouse organs

Marie R Brunchault[1*], Anne-Marie Hesse[2*], Julia Schaeffer[1*], Charlotte Decourt[1], Homaira Nawabi[1], Yohan Couté[2+], Stephane Belin[1+]

1- Univ. Grenoble Alpes, Inserm, U1216, Grenoble Institut Neurosciences, 38000 Grenoble, France
2- Univ. Grenoble Alpes, INSERM, CEA, UMR BioSanté U1292, CNRS, CEA, FR2048 38000, Grenoble, France

* These authors contributed equally to the work (listed by alphabetical order)
+ These authors contributed equally to the work.

Lead contact: stephane.belin@inserm.fr

Introduction

A major challenge in Biology is to understand how genes are expressed and regulated in space and time in order to control cell specificity and organism development. It is now well established that genetic expression is defined by the flow DNA-RNA-Protein. After DNA is transcribed in the nucleus, mRNAs are exported to the cytoplasm in order to be translated into proteins. Protein synthesis is a fundamental and highly energy consuming process in cellular life. It is orchestrated in a tightly ordered sequence of three steps: initiation, elongation and termination.

The ribosome is the main effector of protein synthesis. It is a large complex composed of proteins and RNAs. Even if its overall structure and function are well conserved across evolution (Petrov et al., 2014), some differences are observed among organisms. Indeed, the eukaryotic ribosome has a higher number of ribosomal proteins (r-proteins) and its ribosomal RNAs (rRNAs) are longer compared to their prokaryotic counterparts (Roberts et al., 2008). The mammalian ribosome is composed of two subunits: the large 60S subunit, formed by 46 r-proteins (RPL) and 3 rRNAs (28S, 5.8S and 5S) and the small 40S subunit, that contains 34 r-proteins (RPS) and the 18S rRNA. The ribosome decodes the information carried by mRNAs, recruiting necessary translation factors (initiation, elongation and release factors, eIF, eEF and eRF respectively) and transfer RNAs (tRNAs). Finally, the ribosome itself catalyzes the peptide bonds to form the polypeptide chain of the newly synthesized proteins.

Tremendous amount of work has focused on the regulation of the first step of the genetic flow (DNA to RNA). Thereby, detailed regulatory mechanisms for gene transcription have been thoroughly described in normal and pathological conditions. The contribution of transcription factor recruitment into promoter and enhancer regions, chromatin accessibility to the transcriptional machinery (Casamassimi and Ciccodicola, 2019; Lee and Young, 2013) and epigenetic regulations are now extensively described. In addition, the rapid development and the increasing depth of analysis of transcriptomics analyses such as RNA-sequencing accelerate the understanding of mRNA expression regulation. Besides, this is in contrast with mass spectrometry data acquisition and sensitivity. Therefore, protein expression is often extrapolated from the expression of mRNAs (Fortelny et al., 2017; Liu et al., 2016). However, i) recent comparison of transcriptomics and proteomics analyses revealed that the correlation between mRNA and protein levels is between 20% and 50% (Liu

et al., 2017; Schwanhausser et al., 2011; Vogel and Marcotte, 2012; Wang et al., 2019; Wilhelm et al., 2014) and ii) the rise of alternative protein forms that derive from the same mRNA reinforces the notion that translational control of mRNA is a major player of protein synthesis regulation (Brunet et al., 2021) (Cardon et al., 2021).

The common dogma always described the ribosome as a homogenous complex with no regulatory role, whatever the physio-pathological conditions. Recently, it emerges that the protein synthesis machinery can also actively participate in translation regulation. However, the ribosome itself appears to play a more important role in protein expression regulation than initially thought. For example, if rRNA modifications are targeted during cancer development to control IRES dependent translation (Belin et al., 2009; Erales et al., 2017; Marcel et al., 2013; Yoon et al., 2006), the rise of ribosomal proteins heterogeneity is even more important. Specific defects in ribosomal protein expression have been identified in pathologies (called ribosomopathies). For instance, mutations in 14 ribosomal proteins are linked to the Diamond Blackfan anemia and to malformations, and increase cancer predisposition (Landowski et al., 2013). The 5q- syndrome or myelodysplastic syndrome is caused by the loss of one copy for the gene coding for the ribosomal protein *Rps14* (Ebert et al., 2008).

However, even if specific variants were reported to be linked to defects in translational fidelity (Lezzerini et al., 2020; Sulima et al., 2014), the exact impact of ribosome composition in translation regulation remains unclear. More precise evidence links ribosome heterogeneity and specificity of translation. Komili and colleagues demonstrated that specific ribosomal proteins paralogues are required for localized mRNA translation in yeast (Komili et al., 2007). In mammalian development, ribosomal protein RPL38/eL38 drives specific translation of HOX genes via regulatory sequences in their 5' UTR (Kondrashov et al., 2011; Xue et al., 2015). This kind of specific ribosome composition associated with selective mRNA translation is described for the ribosomal protein of the large subunit *Rpl10a/uL1* (Shi et al., 2017), *Rpl40/eL40* (Lee et al., 2013) as well as of the small subunit *Rps25/eS25* (Shi et al., 2017). These studies pioneered the emerging concept of "specialized ribosomes". Finally, specific expression of ribosomal proteins paralogues remains the most documented event. Indeed, early transcriptomic studies revealed that ribosomal protein paralogues replace "canonical" counterparts in some organs. The ribosomal protein L3-like (RPL3l/uL3l) is only expressed in skeletal muscle for myotube formation (Chaillou et

al., 2016). Similarly, ribosomal protein L10-like (RPL10l/ul16l) is specific of the testis and absolutely required for male meiotic transition (Jiang et al., 2017).

Despite this accumulating evidence implicating ribosomal protein exchange or modification in specific physio-pathological conditions, there is still a lack of comprehensive data describing a potential ribosome heterogeneity in different cell types and tissues. Indeed, the vast majority of existing studies focused only on the mRNA expression level, while very few studies addressed the relationship between the modification in ribosome composition and its function (Amirbeigiarab et al., 2019). Available high-throughput datasets of tissue comparison are derived from transcriptomic datasets that do not necessarily reflect the stoichiometry of ribosomal proteins into cytoplasmic ribosomes implicated in protein synthesis (Guimaraes and Zavolan, 2016; Gupta and Warner, 2014).

Here, we analyzed the composition of functional cytoplasmic ribosomes across 14 different adult mouse organs. We purified ribosomes from each organ and analyzed ribosome protein composition by quantitative mass spectrometry. We show that ribosomes exhibit heterogeneity of composition not only in the case of paralogues in muscle and testis for example, but also in other organs. We have corroborated our proteomics data with available transcriptomics datasets to decipher the origin of the specialization. Altogether, our study emphasizes the specialization of the ribosome across mammalian adult organs and its potential implication in gene expression sustaining cell type specificity and function.

RESULTS

Preparation and characterization of ribosomal fraction from adult mice organs

To highlight any heterogeneity in ribosomal protein composition between various organs, we purified the ribosomal fraction from different organs of wild-type (WT) adult mice (Figure 1A). 10 types of organs were dissected out: lungs, kidneys, adrenal glands, liver, small intestine, spleen, testis, two types of muscle: heart and quadriceps femoris muscle (skeletal muscle); as well as various parts of the CNS: cortex, hippocampus, cerebellum, olfactory bulbs and retinas. We based our analysis on three independent biological replicates (N=1 mouse, except for small organs for which we pooled several animals (N=3 mice) to generate one biological replicate). After lysis, tissues were fractionated and processed for ribosome purification on a sucrose cushion as previously described (Belin et al., 2010b) (Figure 1B). We confirmed the purity of our ribosomal fractions by Western blot analysis using several subcellular fraction markers, e.g., Histone 3 (H3) for the nuclear fraction, Hsp60 for the mitochondrial fraction, and GAPDH for the cytoplasmic (post-ribosomal) fraction. With the kidney, the heart and the cerebellum as representative examples, we confirmed that the ribosomal fraction is enriched with the 40S ribosomal protein S6 (RPS6/eS6) and 60S ribosomal protein RPL22/eL22, while H3, Hsp60 and GAPDH are not present or in weak amounts in this fraction (Supplementary Figure 1A). In addition, ribosomal proteins are absent from the cytoplasmic fraction (post ribosome purification) indicating a satisfying isolation of ribosomes. The efficiency of our ribosomal purifications was also monitored by SDS-PAGE separation and Coomassie staining. For each organ, the profile of the ribosomal fraction is distinct from that of the total fraction and exhibits a strong enrichment in low- to medium-molecular weight proteins that correspond to RPs (11kDa to 47kDa in mammals (Wool et al., 1995)) (Supplementary Figure 1B).

To determine the relative content of the ribosomal fraction of the various organs, proteins were extracted, quantified and analysed by liquid-chromatography coupled to tandem mass spectrometry (Figure 1C-D). Between 587 and 2613 proteins were identified with high confidence (i.e., detection of at least one specific peptides per hit, peptide-spectrum matching false discovery rate (FDR) < 1%) in the ribosomal fraction of each organ (Table 1, Supplementary Table 1).

Fewer proteins were detected in the ribosomal fractions prepared from heart and skeletal muscle, two types of muscular tissues, possibly owing to their structure that makes them harder to homogenize. As calculated using the intensity-based absolute quantification (iBAQ, Schwanhausser et al., 2011) values, all ribosomal fractions displayed an enrichment in RPs of more than 50% for all organs, including >90% for the intestine and the spleen. Only the heart presents a lower enrichment in RPs, reaching 15% in our different purification attempts (Table 1). Altogether, these results confirmed further the efficiency of our purification procedure to enrich ribosomes from the different organs.

To analyse the reproducibility of the global workflow, we plotted the log-transformed normalized abundances of the proteins quantified in the different replicates of each organ (Supplementary Figure 2). The obtained correlation coefficients indicate a very good repeatability of our experimental design as well as high consistency between biological replicates. Next, we performed principal component analysis (PCA) on the log-transformed normalized abundances of protein hits detected in each ribosomal fraction. Strikingly, the PCA analysis revealed a strong clustering of the different biological replicates prepared for each organ across at least the first four principal components (Figure 2A). This suggests a certain level of heterogeneity at the level of ribosomal protein abundance between the ribosomal fractions of different organs. Interestingly, the ribosomal fractions from tissues of similar origin cluster together, as do muscular tissues (heart and skeletal muscle) and CNS tissues (cortex, hippocampus, cerebellum, olfactory bulb and retina), indicative of a hierarchical similarity in ribosomal fraction composition across organs. This is also shown by the correlation matrix (Pearson correlation coefficients), showing hierarchical clustering of all individual samples (Figure 2B).

Differential composition of ribosomal fractions in RPs among adult organs

Next, we focused on comparing the relative abundance of RPs in ribosomal fractions of each organ. Altogether, 32 RPs of the small subunit and 44 RPs of the large subunit were identified in all organs, as well as Rack1, 7 paralogs (RPL39L/eL39L, RPL7L1/uL30L1, RPS27L/eL27, RPL22L1/eL22L1, RPL10L/ulL6L, RPS4L/eS3L, RPL3L/uL3L) and 1 pseudogene (RPS32-ps). 76 (heart) to 85 (intestine and testis) RPs were detected in the ribosomal fraction of each organ (Table 1). Interestingly, a

few canonical RPs were not detected in some tissues, e.g., Rps15/uS19 detected in all but adrenal gland, intestine and muscle; and RPS23/uS12 detected in all but hippocampus and heart. This differential detection among organs was exacerbated with several paralogs that were not detected in the vast majority of organs, e.g., RPL3L/uL3l uniquely detected in heart and muscle, and RPL39L/eL39L and RPL10L/ul16l uniquely detected in the testis. Heterogeneity in RP distribution among ribosomal fractions was visualized by representing the relative abundance of each RP normalized by RPS2/uS5 abundance, a RP showing minimal variability across organs (Figure 3). Hierarchical clustering of sample types allowed us to visualize the proximity of different organs in terms of RP composition of the ribosomal fraction. Strikingly, the heart and muscle clustered together in a branch distinct from the rest of the organs, again probably owing to their close cellular identity as muscular tissues. The olfactory bulb and the cerebellum showed high proximity in the clustering, as did the kidney and the lung (Figure 3). Hierarchical clustering of the RPs themselves revealed that the majority of the RPs are invariable among tissues, most of them being canonical RPs (eg, RPS2/uS5, RPL22/eL22, RPL10A/uL1). Yet, very interestingly, we highlighted groups of RPs showing variability across organs: one group paralogs with unique or quasi-unique detection (e.g., RPL3L/uL3l, RPL39L/eL39L, RPL10L/ul16l); one group with variability across multiple tissues (e.g., RPS15/uS19, RPLP1/P1, RPL39/eL39); one group with variability in specific tissues (e.g., RPL10/uL16, RPS29/uS14, RPLP2/P2) (Figure 3).

Several RPs exhibit abundance variability when comparing ribosomal fraction of adult organs

We then compared the normalized abundance of each RP across ribosomal fractions of all organs (Supplementary Table 2). For each RP, we performed a statistical analysis based on ANOVA testing with post-hoc multiple comparisons and we calculated the fold-change (FC) of the maximal to the minimal value of all organs. This allowed us to highlight 58 RPs with no significant change between organs that we termed “core” (FDR-adjusted p-value > 0.01 or $\log_2$FC < 1.5) (Figure 4A and Figure 4C), among which belong for RPL7A/eL8, RPL10A/uL1, RPL12/uL11, RPS6/eS6, RPS16/uS9 and RPS24/eS24. Both large and small ribosomal proteins are represented in the core

category. We then analysed the localization of “core” and variable RPs within the quaternary structure of the ribosome using Chimera software based on PDB database (4v6x Human ribosome). We observed that “core” RPs show no significant variation among all tissues and are localized on the solvent and at the interface of the ribosome (Figure 4B). This is suggestive of an invariable, stable presence of this type of RP in the ribosomal composition independently of the cell type.

On the other hand, 27 RPs displayed significant variability (FDR-adjusted p-value < 0.01 and $\log_2$FC > 1.5) (Figure 5A and Supplementary Figure 3). In this group of variable RPs, we also found RPs whose normalized abundance is highly variable across all tissues, e.g., RPLP2/P2, RPS30/eS30 and RPS27/eS27 (Figure 5C); and RPs whose normalized abundance is significantly different in a subset of specific tissues, e.g. RPL39/eL39 not detected in the ribosomal fraction of the heart, RPS10/eS10 depleted in that of the intestine, and RPS29/uS14 depleted in that of the cerebellum (Figure 5D). The localization of the group of variable RPs appeared to be at the periphery of the quaternary structure of the ribosome. They are located on the solvent side and in critical sites such as tRNA A-site (RPL3/uL3), close to P-site (RPL10L/uL16L) or at the mRNA E- site (RPS26/eS26) (Figure 5B). Considering the variability in the RP composition of the ribosomal fraction, these observations are suggestive of a specialized function of variable, tissue-enriched or –depleted RPs in the regulation of the translational process to serve specific cell functions. This hypothesis remains to be determined.

Several paralog RPs have been shown to display tissue-specific transcript expression (Gupta and Warner, 2014b), as well as to control cell type-specific function, eg RPL10L/uL16L in the testis (Jiang et al., 2017b). Here, our mass-spectrometry-based analysis shows tissue-specificity of such paralogs at the protein level and specifically in the ribosomal fraction, such as RPL3L uniquely expressed in the heart and the muscle, and RPL10L/uL16L uniquely expressed in the testis (Supplementary Figure 4A). Very interestingly, we found that some canonical RP shows depletion specifically in the organ where its corresponding paralog is expressed. For example, RPL3/uL3 is 2-fold and 4-fold less expressed in the heart and the muscle than average of all tissues, respectively, while RPL10L/uL16L is 2-fold less expressed than average in the testis (Supplementary Figure 4A). In the ribosome conformation, it is possible that the paralog version of the RP substitutes for the canonical version in the quaternary

structure, where it may sustain a cell type-specific control of translation. For example, the paralogs RPL10L/uL16L and the canonical RPL10/uL16 differ by 3 amino acids (Supplementary Figure 4B) and their 3D conformation is nearly identical (Supplementary Figure 4C). Interestingly, we observed that RPL10L occupies the exact same place as RPL10 in the quaternary structure of the ribosome (Supplementary Figure 4D). This suggests that ribosomes cannot contain Rpl10/uL16 and RPL10L/uL16L at the same time, pointing towards a specialization of the ribosomal composition and downstream control of translation in different cell types.

We verified these results by Western blot analysis. Equal amounts of ribosomes from purified ribosomal fraction of cerebellum, cortex, liver, speel, heart and muscle were resolved in polyacrylamide gel. Strikingly, RPL3 is less present in the heart and the muscle compared to all other organs (Figure 5E), while RPS6/eS6 shows no difference between organs. This validates our previous results from the relative quantification of the ribosomal components by mass spectrometry (Figure 5E). We also looked at RPLP2/P2 and found that it is strongly decreased in the hippocampus and the retina (Figure 5E), further confirming the variability of abundance obtained in our mass-spectrometry data.

We then performed an absolute quantification to confirm the results obtained by relative quantification. We quantified two stable RPs, RPS2 and RPL34 and 10 variable RPs RPS2, RPS26, RPS30, RPL3, RPL3L, RPL10, RPL10L, RPL39, RPL39L, RPL36 and RPLP2 by using labelled peptides (Supplementary Table 2). Results confirm the stable expression of RPS2 and RPL34 across organs. We show the reduced expression of RPL10 along with specific expression of RPL10L and RPL39 in functional ribosomes in the testis (Figure 6A). The lower expression of RPLP2 in the hippocampus and the retina is also seen. We could not deduce the exact stoichiometric distribution of selected RPs across organs as peptides from the same protein exhibited differences up to a 10-fold for RPLP2 in the same organ (Figure 6B). In spite of this observation, we confirmed the variable expression of RPL3 and RPL3L in muscle type tissues. While RPS30 is indeed enriched in the testis, no enrichment was detected in the muscle. There was no drop in RPL36 level in the retina or RPS26 in the muscle/heart tissues.

Correlation to relative transcript expression of RP in adult organs

To unravel the origin of RP variation in ribosomal fractions of adult organs, we sought to analyse RP expression at the mRNA level in each organ. For this, we used published datasets of mouse and human transcriptome atlas: the transcriptomic BodyMap (Li et al., 2017), the Mouse ENCODE Consortium project (Yue et al., 2014) and the Illumina Human Body Map (GSE30611) as analysed by (Gupta and Warner, 2014b). Using available data of read per kilobase per million mapped reads (RPKM) values for each RP, we adopted the same normalization strategy as (Gupta and Warner, 2014b) and computed the RPKM normalized to the sum of RPKM of all RP of each organ times the number of RP. The relative expression of RPs among organs represented as a heatmap shows little variation at the transcript level, except for the three pair of paralogs: RPL3L/uL3L, strongly enriched in the heart and muscle, and RPL10L/uL16L and RPL39L/eL39L, strongly enriched in the testis (Supplementary Figure 5).

We compared the expression of each RP of the three transcriptomic datasets ("Mouse BodyMap", "Mouse ENCODE" and "Human Body Map") and our mass spectrometry-based analysis of ribosomal fractions. We focused on organs common to all these datasets: brain, adrenal gland, heart, kidney, liver, lung and testis. For the Mouse ENCODE dataset and our data, we extrapolated values of the brain values from the cortex. For many of the core RPs, the transcript expression does not vary across organs, e.g., RPL7A/eL8, RPL34/eL34 and RPS16/uS9 (Figure 6A). Moreover, several variable RPs show good correlation between the transcript level of all or most transcriptomic datasets. This is the case of the paralogs RPL3L, RPL10L (not reported in the Mouse ENCODE dataset), and RPS4L (not reported in the Mouse ENCODE and the Human Body Map datasets) (Figure 6B). Interestingly, the relative transcript expression of the corresponding canonical RPs correlates with the relative abundance in our mass spectrometry data. RPL3/uL3 transcript is less abundant in the heart than in the rest of the organs, while RPL10/uL16 and RPS4X/eS4 are less abundant in the testis. This is consistent with an effect of compensation of the paralog to its corresponding canonical version at the transcript level.

On the other hand, for several RPs, we observed little correlation between the relative transcript expression level and the relative abundance in the ribosomal fraction. This is the case of RPLP0/uL10 enriched in the ribosomal fraction of the testis, but invariable at the transcript level. Other examples include RPL37A/eL43 and RPS26/eS26 low in

the ribosomal fraction of the heart, but not at the transcript level (Figure 6C). From all these datasets, we observe that the relative level of transcript of an RP does not necessarily correlate with its relative abundance in the ribosomal fraction in adult organs.

DISCUSSION

With extensive characterization of the different active sites of the ribosome implicated into mRNA decoding and peptide bond formation (Khatter et al., 2015), the ribosome has always been considered as an invariable machinery that is not involved in the translation regulation and selection of mRNA to translate. Yet, this dogma has been challenged over the years by an accumulation of compelling evidence supporting the variability of ribosome composition across different cell types and in pathological and in physiological conditions (Kampen et al., 2018; Simsek et al., 2017b; Xue and Barna, 2012). Here, we performed mass spectrometry-based analysis of the ribosomal fraction to decipher the differential RP composition in 14 different organ types of adult mouse. While many RPs did not show any variability at the protein level among the ribosomal fraction of different organs, we found a substantial number of RPs that display variability in the relative abundance. Some RPs are clearly enriched or, on the other hand, depleted from specific organs (Figure 3), which supports the concept of a ribosomal protein signature of adult mouse organs (Figure 7,8).

Our proteomics data on various adult mouse organs adds to the idea of an intercellular heterogeneity in ribosomal composition. This feature may be linked to a specialized translation that ensures cell type-specific functions, which remains to be demonstrated. In addition, whether the intracellular population of ribosomes is itself heterogeneous is an important yet technically challenging question to address. At the cellular level, ribosome heterogeneity may allow the cell to respond rapidly to external stimuli by regulating gene expression through control of specific translation (Genuth and Barna, 2018).

In fact, the actual stoichiometry of the ribosome needs to be determined among these various organs. This question has been recently tackled by Barna and colleagues in mouse embryonic stem cells (Shi et al., 2017). By using selected reaction-monitoring mass spectrometry, authors gave an absolute quantification of RPs in the ribosomal fraction of cells and found a significant sub-stoichiometry of some RPs (e.g., RPL10A/uL1, RPL38/eL38, RPS25/eS25) as opposed to invariant RPs. This result supports the idea of a heterogeneous population of ribosomes within the cell to sustain various cellular functions via mRNA-specific translation (Shi et al., 2017).

The next question is then: what mechanisms are at play to control for inter-organ variation in RP ribosomal composition? In the present study, we compared our

proteomics data to transcriptomics data from available RNA-sequencing datasets in mouse and human. The transcript and protein relative expression of many RP transcripts correlate well among the different organs. This is particularly the case of paralogs RPL3L, RPL10L and RPS4L, and the respective canonical RPs RPL3, RPL10 and RPS4x that show organ-specific depletion at the transcript and at the protein level. Interestingly, this phenomenon of autoregulation has been demonstrated for the pair RPL22/RPL22L1, where RPL22 itself has been shown to repress the translation of *Rpl22l1* by binding to an hairpin structure in the mRNA (O'Leary et al., 2013). The finding that the paralog is incorporated into the ribosome, where it competes with the canonical version, adds to the hypothesis of an autonomous regulation of the ribosome composition. Importantly, several studies describe that this "RP paralog signature" confers tissue specificity through selective translation (Segev and Gerst, 2018)(Chaillou et al., 2016b).

An interesting point is to define how expression of these RPs is specifically controlled and what is the upstream regulatory mechanism. Regulation of an individual RP may occur at the transcript level under the control of one or multiple cell type-specific transcription factors. Indeed, looking at RP gene expression in human hematopoietic cell types, Guimaraes and colleagues found that some specificity of lineage-specific transcription factors to RP promoters (Guimaraes and Zavolan, 2016b). Although little difference is observed in promoter utilization in cell type-specific versus non-specific RPs, and despite the heterogeneity in promoter regulatory sequences of individual RPs, it is possible that a set of cell type-specific transcription factors orchestrate RP gene expression (Guimaraes and Zavolan, 2016b; Petibon et al., 2021). This accounts for the level of heterogeneity observed at the transcript level, where mechanisms of co-regulation of RPs remain to be determined (Kondrashov et al., 2011b).

On the other hand, our study reveals that several proteins display no or little correlation between the relative transcript expression level and the relative protein abundance. This observation brings out the hypotheses of (i) a differential post-transcriptional regulation of the protein expression among organs, and/or (ii) a differential incorporation of RP into the ribosome. This adds up to this outstanding question: how does the cell control ribosome composition? Remaining black boxes of the regulatory mechanism of ribosomal heterogeneity include: how dynamic are intracellular changes in ribosome composition; can ribosome composition be tuned in the cytoplasm (with

some recent evidence for a local remodelling brought by (Shigeoka et al., 2019b)); how does the cell integrate external stimuli, developmental or pathological programmes at the level of the ribosome composition; is ribosome heterogeneity a functional prerequisite, or conversely a cause for cellular dysfunction.

Finally, how does heterogeneity into the ribosomal protein composition impact the function of the ribosome? RP ribosomal composition is one layer of ribosome heterogeneity that confers cell type-specific function, e.g., in a developmental process or in response to the environment. This adds to other parameters that have recently emerged as critical to define ribosome heterogeneity, namely RP modification (e.g. phosphorylation, acetylation, etc.), rRNA modification (eg pseudouridylation, methylation, etc.), as well as ribosome-associated factors (Gerst, 2018)(Shi and Barna, 2015). The notion of “specialized ribosome” points towards a selective mRNA translation by a heterogenous population of ribosome that controls recruitment and translation of specific subsets of mRNA (Ferretti et al., 2017b; Segev and Gerst, 2018; Shi et al., 2017). Then, specialized translation depends on regulatory elements in the mRNA itself (e.g., internal ribosome entry sites (IRES) localized in the 5’-UTR), either through a direct ribosome-mRNA interaction, or indirectly via RNA-binding proteins.

To conclude, our present study adds up to the growing evidence that diverse cell types exhibit specific – and probably specialized – RP expression in a mammalian organism. Based on quantitative mass spectrometry data, our work brings firm evidence that this tissue-specificity occurs not only at the protein level, but also at the level of integration into functional ribosomes. Comparison with transcriptomics datasets shows that this differential RP signature does not necessarily correlate with RP mRNA level, bringing up more questions about ribosome heterogeneity regulatory mechanisms.

FIGURE LEGENDS

Figure 1: Workflow of mass spectrometry-based quantification of ribosomal fraction of adult mouse organs. (A) Different wild-type mouse organs are dissected, lysed and processed for fractionation. Each organ or pair of organs from one to three mice corresponds to one individual biological replicate. (B) After separation of the

nuclear and mitochondrial fractions, the ribosome fraction is purified on a sucrose cushion by ultracentrifugation at 250 000 x g for 2h. (C) Proteins are extracted from the ribosome fraction, loaded on a Bis-Tris's polyacrylamide gel and in-gel digested using trypsin. (D) Extracted peptides are processed for liquid chromatography coupled to tandem mass spectrometry to obtain relative quantification of protein abundance.

Figure 2: Translation complexes (TC) are specific to each tissue. (A) PCA analysis showing the clustering of biological replicates of the ribosomal fraction of each organ, for principal component 2 (PC2) versus PC1, PC3 versus PC2 and PC4 versus PC3. The cluster of CNS tissues (cortex, hippocampus, cerebellum, olfactory bulb and retina) is manually annotated in blue. The cluster of muscular tissues (heart and muscle) is manually annotated in orange. (B) Matrix of correlation of all samples (Pearson correlation coefficient).

Figure 3: Differential RP composition of the ribosomal fraction across adult mouse organs. Heatmap of the log-transformed relative abundance normalized to Rps2 for the 85 RPs detected in the ribosomal fraction of all organs, from depleted in blue to highly enriched in red. Grey boxes represent no detection of the RP in the ribosomal fraction of the corresponding organ.

Figure 4: "Core" RPs stably expressed in the ribosomal fraction of different mouse organs. (A) List of RPs of the large and of the small subunits that show no significant difference in relative abundance in the ribosomal fraction of all organs ("core" RPs) (FDR-adjusted p-value > 0.01 (ANOVA testing with post-hoc multiple comparisons) or $\log_2$FC < 1.5). (B) Visualization of molecular structure of the ribosome and localization of "core" RPs. (C) Barplot representation of the relative abundance of core RPs normalized to Rps2. The mean and standard deviation are plotted for each organ, as well as values of individual replicates.

Figure 5: Several RPs show significant variability across adult mouse organ ribosomal fractions. (A) List of RPs from the large and of the small subunits that show significant difference in relative abundance in the ribosomal fraction of all organs ("variable RPs") (FDR-adjusted p-value < 0.01 (ANOVA testing with post-hoc multiple

comparisons) and $log_2FC > 1.5$). (B) Visualization of molecular structure of the ribosome and localization of variable RPs (PDB: 4x6v). (C-D) Barplot representation of the relative abundance of variable RPs normalized to Rps2. The mean and standard deviation are plotted for each organ, as well as values of individual replicates. For ease of representation, results of the ANOVA post-hoc multiple comparison testing are represented in (D) plots only (* FDR-adjusted p-value < 0.01). *(E) Western blot analysis of the ribosomal fraction of different mouse organs showing expression of Rpl3 ("variable"), and Rpl22 and Rps6 ("core").*

Figure 6: Validation of RP profiles by absolute quantification (A) Graphs of results from absolute quantification in amol. (B) Difference in detected quantities for the same protein.

Figure 7: Comparison of the relative expression of RPs in transcriptomic-based datasets and mass spectrometry-based analysis of the ribosomal fraction among different mouse organs. (A-C) Barplot representation of the relative expression of each RP at the transcript level, with data from Mouse BodyMap (Li et al., 2017), Mouse ENCODE Consortium (Yue et al., 2014) and Illumina Human Body Map 2.0 as analyzed by (Gupta and Warner, 2014b)). The relative abundance as determined in our present study is superimposed with black dots and lines.

Figure 8: Summary of variable RPs per organs based on mass spectrometry analysis of the ribosomal fraction among different mouse organs. Relative expression of RP based on MS analysis. (Red: increased expression ; Blue : decreased expression)

Supplementary Figure 1: Validation of ribosomal fraction purification method in adult mouse organs. (A) Western blot analysis of markers of the different fractions obtained in the heart, the kidney and the retina: Histone 3 (nuclear), Hsp60 (mitochondrial and cytoplasmic), Gapdh (cytoplasmic), Rps6 and Rpl22 (ribosomal). (B) Coomassie staining of proteins of the total and ribosomal fractions of each organ loaded on a polyacrylamide gel. Protein mass (kDa) is indicated on the left as shown by the protein ladder.

Supplementary Figure 2: High consistency between biological replicates of the ribosomal fraction of each organ. Scatterplots of log-transformed protein abundance of the detected hits across replicates. The Pearson correlation coefficient is indicated on each plot.

Supplementary Figure 3: Relative abundance of variable RPs in the ribosomal fraction of each mouse organ. Barplot representation of the relative abundance of variable RPs normalized to Rps2. The mean and standard deviation are plotted for each organ, as well as values of individual replicates.

Supplementary Figure 4: Some paralogues and corresponding canonical RPs show balanced enrichment in specific organs. (A) Barplot representation of the relative abundance of Rpl3l, Rpl3, Rpl10l and Rpl10 normalized to Rps2. The mean and standard deviation are plotted for each organ, as well as values of individual replicates. For ease of representation, results of the ANOVA post-hoc multiple comparison testing are represented in (D) plots only (* FDR-adjusted p-value < 0.01). (B) Alignment of amino acid sequences of mouse Rpl10l and mouse Rpl10. (C) 3D schematic representation of the molecular structure of Rpl10l and Rpl10. (D) Visualization of the localization of Rpl10l and Rpl10 in the molecular structure of the ribosome.

Supplementary Figure 5: Relative expression of RP transcripts across adult mouse organs. Heatmap of the log-transformed relative expression for RPs detected by RNA-sequencing, from depleted in blue to highly enriched in red. Grey boxes represent no detection of the RP in the corresponding organ. Expression values from the Mouse Transcriptomic Body Map dataset (Li et al., 2017).

Table 1: Summary of the total number of total protein hits (Total), the number of RPs (RP) and the percentage of enrichment (Enrichment) for each organ.

Supplementary Table 1: List of proteins detected in the ribosomal fraction of each adult mouse organ and corresponding iBAQ values.

Supplementary Table 2: List of peptides for the absolute quantification

Supplementary Table 3: Summary of ANOVA statistical test with post-hoc multiple comparisons. Imputed minimum values are indicated in orange. Variable RPs (FDR-adjusted p-value < 0.01 and $log_2FC > 1.5$) are indicated in green.

MATERIAL AND METHODS

Tissue sampling and ribosome purification by subcellular fractionation

Wild-type (WT) C57BL/6J adult mice were used in this study, regardless of their sex, except for collection of the testis. Organs and tissues of 4 to 6 weeks-old mice were dissected and flash-frozen in liquid nitrogen. Ribosomal fraction purification was performed according to (Belin et al., 2010b). All steps were performed on ice or at 4°C. Samples were disrupted in freshly prepared buffer A (50mM Tris HCl pH 7.4, 250 mM sucrose, 250 mM KCl, 5 mM $MgCl_2$ (Sigma-Aldrich)) using a Cell Mill (RETSCH MM 400). An aliquot of the cell suspension (total fraction) was saved for SDS-PAGE. IGEPAL detergent (Sigma-Aldrich) was added to the remaining volume to a final concentration of 1%. After 20 min incubation on ice, the lysate was centrifuged at 750 x *g* to pellet nuclei (nuclear fraction) then 12 500 x *g* to pellet mitochondria (mitochondrial fraction). The supernatant (post-mitochondrial fraction) was loaded on a sucrose cushion (1.25 M sucrose, 0.25 M KCl, 5 mM $MgCl_2$, 50 mM Tris-HCl pH 7.4) and ultracentrifuged at 250 000 x *g* for 2 h (Beckman Optima TL 100 Ultracentrifuge). After ultracentrifugation, 50µl of supernatant (cytoplasmic fraction) was saved. The ribosome pellet was washed twice in ultrapure ice-cold water and resuspended either in 50µl of Laemmli buffer (ribosomal fraction) or in buffer C (tris HCl 50mM pH7.4; 5mM $MgCl_2$; 25mM KCl). 0.5µl benzonase (Sigma-Aldrich) was added to the nuclear sample and incubated for 10 min at 37°C to digest DNA.

Protein quantification

After denaturation at 95°C for 5 min, the protein concentration of all fractions was determined using Pierce BCA Protein Assay Kit (ThermoFisher Scientific).

Western blot

20µg of protein were loaded on a 12% SDS-PAGE gel and separated by electrophoresis for 4h at 230V. The proteins were then transferred on nitrocellulose membrane (Thermo Scientific) under a constant amperage of 250 mA for 3 hr. The membrane was blocked in 5% milk powder in Tris-Buffered Saline (TBS) and incubated with the following primary antibody diluted in 5% milk powder in TBS with 0.1% tween (TBS-T) overnight under agitation at 4°C: anti-RPL22 (1:2000, mouse, Santa Cruz sc-

373993), anti-RPS6 (1:5000, Rabbit, Cell Signaling 2217), anti-H3 (1:10 000, Rabbit, Cell Signaling 9715), anti-HSP60 (1:2000, mouse, Santa Cruz sc-376240), anti-GAPDH (1:5000, Mouse, Proteintech 60004-1-Ig) , anti-RPL3 (1:1000, Rabbit, Abcam ab228638), anti-RPLP2 (1:500, Rabbit, Invitrogen PA5-75863) . On the following day, membranes were washed then incubated with horseradish peroxidase-linked secondary antibodies: anti-rabbit (Proteintech SA00001-2) or anti-mouse (Millipore 12-349) diluted to 1:5000 or 1:10 000 in TBS-T. Membranes were probed with ECL substrate (100 mM Tris HCl pH 8.5, 0.5% coumaric acid (Sigma-Aldrich), 0.5% luminol (Sigma-Aldrich) and 0.15% H_2O_2 (Sigma-Aldrich)). Chemiluminescence was visualized with the ChemiDoc system (Bio-Rad).

Coomasie staining

10 µg of protein were loaded on 12% SDS-PAGE gel and separated by electrophoresis for 4h at 230V. The gel was fixed in fixing solution (50% methanol (VWR Chemicals), 10% glacial acetic acid (VWR Chemicals)) for 1hr with gentle agitation. After fixation, the gel was incubated in staining solution (0.1% Coomasie Brilliant Blue R-250 (Bio-Rad), 50% methanol, 10% glacial acetic acid) for 20 min with gentle agitation. The gel was then washed several times with destaining solution (40% methanol, 10% glacial acetic acid). Gels were imaged when the gel's background was fully distained.

Mass spectrometry-based proteomic analysis

Proteins (between 5 and 10µg) from tissue preparations were solubilized in Laemmli buffer before loading on top of a 4–12% NuPAGE gel (Life Technologies), stained with R-250 Coomassie blue (Bio-Rad) and in-gel digested using modified trypsin (sequencing grade, Promega) as previously described (Salvetti et al., 2016). The dried extracted peptides were resuspended in 5% acetonitrile and 0.1% trifluoroacetic acid and analyzed by online nanoliquid chromatography coupled to tandem mass spectrometry (LC–MS/MS) (Ultimate 3000 RSLCnano and the Q-Exactive HF, Thermo Fisher Scientific). Peptides were sampled on a 300 µm 5mm PepMap C18 precolumn (Thermo Fisher Scientific) and separated on a 75 µm 250 mm C18 column (Reprosil-Pur 120 C18-AQ, 1.9 µm, Dr. Maisch HPLC GmbH). The nano-LC method consisted of a 60 min multi-linear gradient at a flow rate of 300 nl/min, ranging from 5 to 33% acetonitrile in 0.1% formic acid. For all tissues, the spray voltage was set at 2 kV and

the heated capillary was adjusted to 270°C. Survey full-scan MS spectra (m/z = 400–1600) were acquired with a resolution of 60 000 after the accumulation of 106 ions (maximum filling time 200 ms). The 20 most intense ions were fragmented by higher-energy collisional dissociation after the accumulation of 105 ions (maximum filling time: 50 ms). MS and MS/MS data were acquired using the software Xcalibur (Thermo Scientific).

Mass spectrometry-based proteomic data processing

Data were processed automatically using Mascot Distiller software (version 2.7.1.0, Matrix Science). Peptides and proteins were identified using Mascot (version 2.6) through concomitant searches against a home-made database non-redundant in protein sequences (based on Uniprot (Mus Musculus taxonomy, July 2019 version), classical contaminants database (homemade) and their corresponding reversed databases. Trypsin/P was chosen as the enzyme and two missed cleavages were allowed. Precursor and fragment mass error tolerances were set, respectively, to 10 ppm and 25 mmu. Peptide modifications allowed during the search were: carbamidomethylation (fixed), acetyl (protein N-terminal, variable) and oxidation (variable). The Proline software (version 2.1) (Bouyssié et al., 2020) was used to merge and filter results for each tissue separately: conservation of rank 1 peptide-spectrum match (PSM) with a minimal length of 7 and a minimal score of 25. PSM score filtering is then optimized to reach a False Discovery Rate (FDR) of PSM identification below 1% by employing the target decoy approach. A minimum of one specific peptide per identified protein group was set. Proline was then used to perform MS1-based label free quantification of the peptides and protein groups from the different samples without cross-assignment activated between tissue but only between replicates. Protein iBAQ were computed from specific peptides abundances.

Ribosomal proteins were filtered out if they were not identified in the 3 replicates of at least one tissue. For each tissue and replicate, total ribosomal protein iBAQ was used to normalize iBAQ of ribosomal proteins. Statistical analysis was performed using ProStaR (Wieczorek et al., 2017) to determine differentially abundant proteins between tissues. After $\log_2$ transformation of normalized iBAQ, POV missing values were imputed with slsa method and MEC ones with 2.5-percentile value of each sample. Statistical testing was conducted using an ANOVA with a p-value cut-off allowing to

reach a FDR inferior to 1% according to the Benjamini-Hochberg procedure. Data were then manually curated. For each tissue and protein, mean and standard deviation were calculated when at least two replicates were quantified.

Quaternary structures

Crystal structures from human ribosomes were downloaded from PDB (4x6v, 6oli). All structures, except figure 5F were generated using Chimera software (Pettersen et al., 2004), version 1.15c. Labels were manually added. Figure 5F was generated using 3D Structure Viewers from PDB website.

Statistical analysis of mass spectrometry-based proteomic data

For comparison of the relative abundance of RPs among organs, RP iBAQ values in one organ was normalized to the total iBAQ values of all RPs in this organ and $\log_2$-transformed. In case of a missing value, the minimal value of each column was attributted in order to conduct statistical analysis. One-way ANOVA test with post-hoc multiple comparisons was performed. The fold-change (FC) of the maximal to the minimal value was computed for all organs. RPs were considered as “core” when the FDR-adjusted p-value was above 0.01 or when the fold-change (FC) was below 1.5 (corresponding to a ratio max to min of about 2.8). RPs were considered as “variable” when the FDR-adjusted p-value was below 0.01 and the FC was above 1.5.

Data representation and analysis

All plots were generated using R software for data representation and analysis (R Core Team, 2014). Scatterplots of protein hits were obtained by plotting the $\log_{10}$-transformed protein abundances (iBAQ) normalized to the total iBAQ of all RPs per organ, across biological replicates of each organ. To highlight biological differences in the ribosomal fraction of the different organs, principal component analysis (PCA) was performed based on the log10-transformed normalized abundances. Samples were plotted according to the first and second components, with the percentage of variation indicated for each component. To generate the heatmap of RPs, iBAQ of each RP of one organ was normalized to the iBAQ of Rps2, which shows minimal variation across samples. For each RP, the relative abundance was computed as the $\log_2$-transformation of the normalized iBAQ averaged on all organs. Barplots of the relative

expression of RPs in the ribosomal fraction of each organ were obtained from the iBAQ normalized to that of Rps2.

Analysis of transcriptomic datasets

To compare the relative expression of RP at the transcript level, we used published dataset of mouse and human transcriptomic atlas of adult organs: the Mouse Transcriptomic BodyMap (Li et al., 2017), the Mouse ENCODE Consortium project (Yue et al., 2014)) and the Illumina Human Body Map (GSE30611) as analyzed by (Gupta and Warner, 2014b) (Supplementary Table S6 of the publication). For all datasets, read per kilobase per million mapped reads (RPKM) values were retrieved. For the Mouse BodyMap, only samples from males were selected and RPKM values were averaged by organ. We selected all RPs detected in our dataset and all organs in common to the three transcriptomic datasets and our proteomic dataset, with the only apporximation of “Cortex” as “Brain” when not available. We adopted the same normalization strategy as (Gupta and Warner, 2014b) and computed the RPKM normalized to the sum of RPKM of all RP of each organ times the number of RP (RPKM * number RPs / sum(RPKM)). To generate the heatmap, we computed the $\log_2$-transformation of the normalized RPKM averaged on all considered organs. Barplots of the relative expression of RP transcripts of each organ were obtained from the normalized RPKM values averaged on all organs.

BIBLIOGRAPHY

Amirbeigiarab, S., Kiani, P., Velazquez Sanchez, A., Krisp, C., Kazantsev, A., Fester, L., Schluter, H., and Ignatova, Z. (2019). Invariable stoichiometry of ribosomal proteins in mouse brain tissues with aging. Proc Natl Acad Sci U S A 116, 22567-22572.

Belin, S., Beghin, A., Solano-Gonzalez, E., Bezin, L., Brunet-Manquat, S., Textoris, J., Prats, A.C., Mertani, H.C., Dumontet, C., and Diaz, J.J. (2009). Dysregulation of ribosome biogenesis and translational capacity is associated with tumor progression of human breast cancer cells. PLoS One 4, e7147.

Brunet, M.A., Jacques, J.F., Nassari, S., Tyzack, G.E., McGoldrick, P., Zinman, L., Jean, S., Robertson, J., Patani, R., and Roucou, X. (2021). The FUS gene is dual-coding with both proteins contributing to FUS-mediated toxicity. EMBO Rep 22, e50640.

Cardon, T., Fournier, I., and Salzet, M. (2021). Shedding Light on the Ghost Proteome. Trends Biochem Sci 46, 239-250.

Casamassimi, A., and Ciccodicola, A. (2019). Transcriptional Regulation: Molecules, Involved Mechanisms, and Misregulation. Int J Mol Sci 20.

Chaillou, T., Zhang, X., and McCarthy, J.J. (2016). Expression of Muscle-Specific Ribosomal Protein L3-Like Impairs Myotube Growth. J Cell Physiol 231, 1894-1902.

Ebert, B.L., Pretz, J., Bosco, J., Chang, C.Y., Tamayo, P., Galili, N., Raza, A., Root, D.E., Attar, E., Ellis, S.R., et al. (2008). Identification of RPS14 as a 5q- syndrome gene by RNA interference screen. Nature 451, 335-339.

Erales, J., Marchand, V., Panthu, B., Gillot, S., Belin, S., Ghayad, S.E., Garcia, M., Laforets, F., Marcel, V., Baudin-Baillieu, A., et al. (2017). Evidence for rRNA 2'-O-methylation plasticity: Control of intrinsic translational capabilities of human ribosomes. Proc Natl Acad Sci U S A 114, 12934-12939.

Fortelny, N., Overall, C.M., Pavlidis, P., and Freue, G.V.C. (2017). Can we predict protein from mRNA levels? Nature 547, E19-E20.

Guimaraes, J.C., and Zavolan, M. (2016). Patterns of ribosomal protein expression specify normal and malignant human cells. Genome Biol 17, 236.

Gupta, V., and Warner, J.R. (2014). Ribosome-omics of the human ribosome. RNA 20, 1004-1013.

Jiang, L., Li, T., Zhang, X., Zhang, B., Yu, C., Li, Y., Fan, S., Jiang, X., Khan, T., Hao, Q., et al. (2017). RPL10L Is Required for Male Meiotic Division by Compensating for RPL10 during Meiotic Sex Chromosome Inactivation in Mice. Curr Biol 27, 1498-1505 e1496.

Khatter, H., Myasnikov, A.G., Natchiar, S.K., and Klaholz, B.P. (2015). Structure of the human 80S ribosome. Nature 520, 640-645.

Komili, S., Farny, N.G., Roth, F.P., and Silver, P.A. (2007). Functional specificity among ribosomal proteins regulates gene expression. Cell 131, 557-571.

Kondrashov, N., Pusic, A., Stumpf, C.R., Shimizu, K., Hsieh, A.C., Ishijima, J., Shiroishi, T., and Barna, M. (2011). Ribosome-mediated specificity in Hox mRNA translation and vertebrate tissue patterning. Cell 145, 383-397.

Landowski, M., O'Donohue, M.F., Buros, C., Ghazvinian, R., Montel-Lehry, N., Vlachos, A., Sieff, C.A., Newburger, P.E., Niewiadomska, E., Matysiak, M., et al. (2013). Novel deletion of RPL15 identified by array-comparative genomic hybridization in Diamond-Blackfan anemia. Hum Genet 132, 1265-1274.

Lee, A.S., Burdeinick-Kerr, R., and Whelan, S.P. (2013). A ribosome-specialized translation initiation pathway is required for cap-dependent translation of vesicular stomatitis virus mRNAs. Proc Natl Acad Sci U S A 110, 324-329.

Lee, T.I., and Young, R.A. (2013). Transcriptional regulation and its misregulation in disease. Cell 152, 1237-1251.

Lezzerini, M., Penzo, M., O'Donohue, M.F., Marques Dos Santos Vieira, C., Saby, M., Elfrink, H.L., Diets, I.J., Hesse, A.M., Coute, Y., Gastou, M., et al. (2020). Ribosomal protein gene RPL9 variants can differentially impair ribosome function and cellular metabolism. Nucleic Acids Res 48, 770-787.

Liu, T.Y., Huang, H.H., Wheeler, D., Xu, Y., Wells, J.A., Song, Y.S., and Wiita, A.P. (2017). Time-Resolved Proteomics Extends Ribosome Profiling-Based Measurements of Protein Synthesis Dynamics. Cell Syst 4, 636-644 e639.

Liu, Y., Beyer, A., and Aebersold, R. (2016). On the Dependency of Cellular Protein Levels on mRNA Abundance. Cell 165, 535-550.

Marcel, V., Ghayad, S.E., Belin, S., Therizols, G., Morel, A.P., Solano-Gonzalez, E., Vendrell, J.A., Hacot, S., Mertani, H.C., Albaret, M.A., et al. (2013). p53 acts as a safeguard of translational control by regulating fibrillarin and rRNA methylation in cancer. Cancer Cell 24, 318-330.

Petrov, A.S., Bernier, C.R., Hsiao, C., Norris, A.M., Kovacs, N.A., Waterbury, C.C., Stepanov, V.G., Harvey, S.C., Fox, G.E., Wartell, R.M., et al. (2014). Evolution of the ribosome at atomic resolution. Proc Natl Acad Sci U S A 111, 10251-10256.

Roberts, E., Sethi, A., Montoya, J., Woese, C.R., and Luthey-Schulten, Z. (2008). Molecular signatures of ribosomal evolution. Proc Natl Acad Sci U S A 105, 13953-13958.

Schwanhausser, B., Busse, D., Li, N., Dittmar, G., Schuchhardt, J., Wolf, J., Chen, W., and Selbach, M. (2011). Global quantification of mammalian gene expression control. Nature 473, 337-342.

Shi, Z., Fujii, K., Kovary, K.M., Genuth, N.R., Rost, H.L., Teruel, M.N., and Barna, M. (2017). Heterogeneous Ribosomes Preferentially Translate Distinct Subpools of mRNAs Genome-wide. Mol Cell 67, 71-83 e77.

Sulima, S.O., Patchett, S., Advani, V.M., De Keersmaecker, K., Johnson, A.W., and Dinman, J.D. (2014). Bypass of the pre-60S ribosomal quality control as a pathway to oncogenesis. Proc Natl Acad Sci U S A 111, 5640-5645.

Vogel, C., and Marcotte, E.M. (2012). Insights into the regulation of protein abundance from proteomic and transcriptomic analyses. Nat Rev Genet 13, 227-232.

Wang, D., Eraslan, B., Wieland, T., Hallstrom, B., Hopf, T., Zolg, D.P., Zecha, J., Asplund, A., Li, L.H., Meng, C., et al. (2019). A deep proteome and transcriptome abundance atlas of 29 healthy human tissues. Mol Syst Biol 15, e8503.

Wilhelm, M., Schlegl, J., Hahne, H., Moghaddas Gholami, A., Lieberenz, M., Savitski, M.M., Ziegler, E., Butzmann, L., Gessulat, S., Marx, H., et al. (2014). Mass-spectrometry-based draft of the human proteome. Nature 509, 582-587.

Xue, S., Tian, S., Fujii, K., Kladwang, W., Das, R., and Barna, M. (2015). RNA regulons in Hox 5' UTRs confer ribosome specificity to gene regulation. Nature 517, 33-38.

Yoon, A., Peng, G., Brandenburger, Y., Zollo, O., Xu, W., Rego, E., and Ruggero, D. (2006). Impaired control of IRES-mediated translation in X-linked dyskeratosis congenita. Science 312, 902-906.

Figure 1

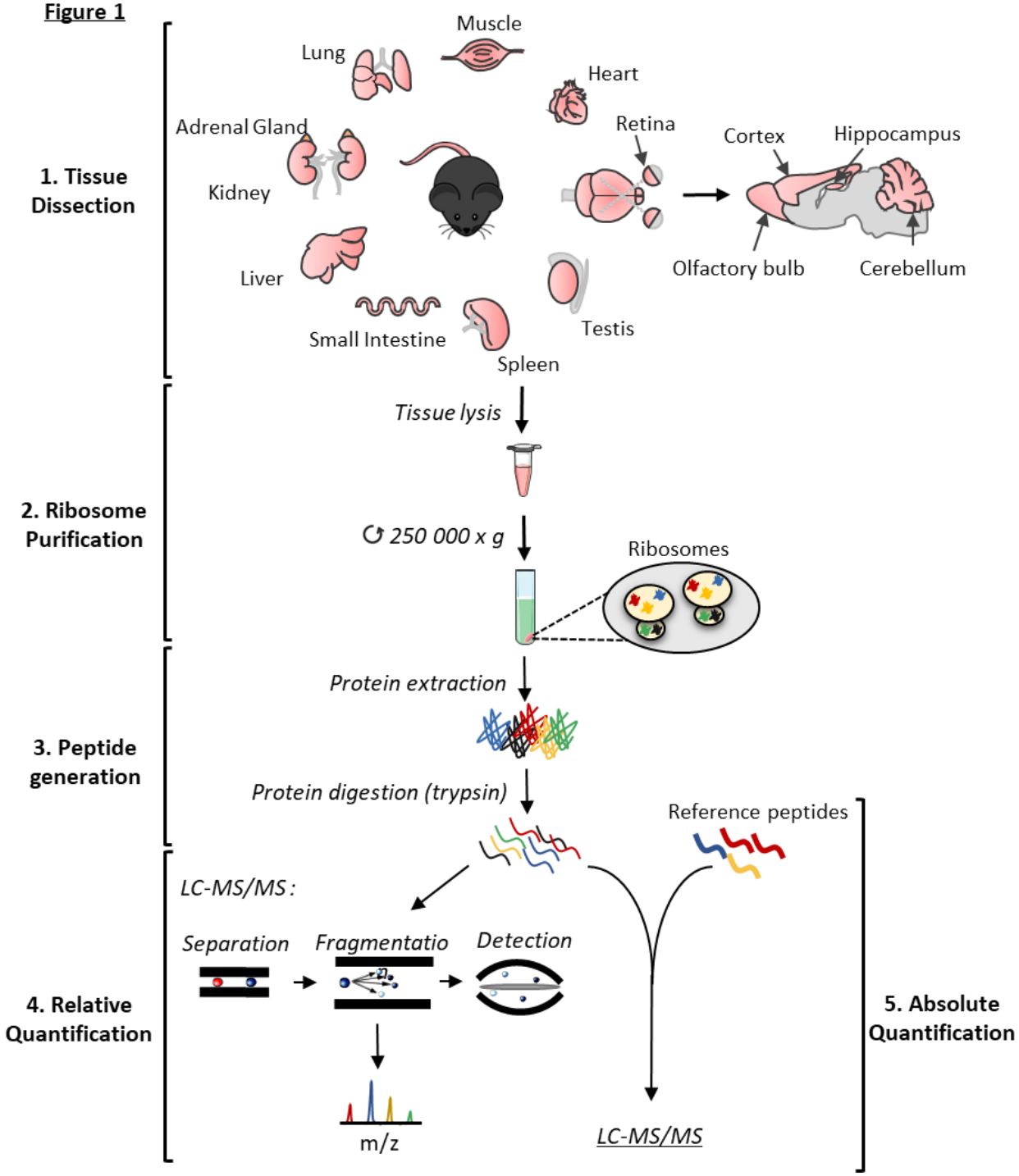
1. Tissue Dissection
Muscle
Lung
Heart
Adrenal Gland
Retina
Cortex
Hippocampus
Kidney
Olfactory bulb
Cerebellum
Liver
Testis
Small Intestine
Spleen
2. Ribosome Purification
Tissue lysis
250 000 x g
Ribosomes
3. Peptide generation
Protein extraction
Protein digestion (trypsin)
Reference peptides
4. Relative Quantification
LC-MS/MS :
Separation
Fragmentatio
Detection
m/z
LC-MS/MS
5. Absolute Quantification

Figure 2

A

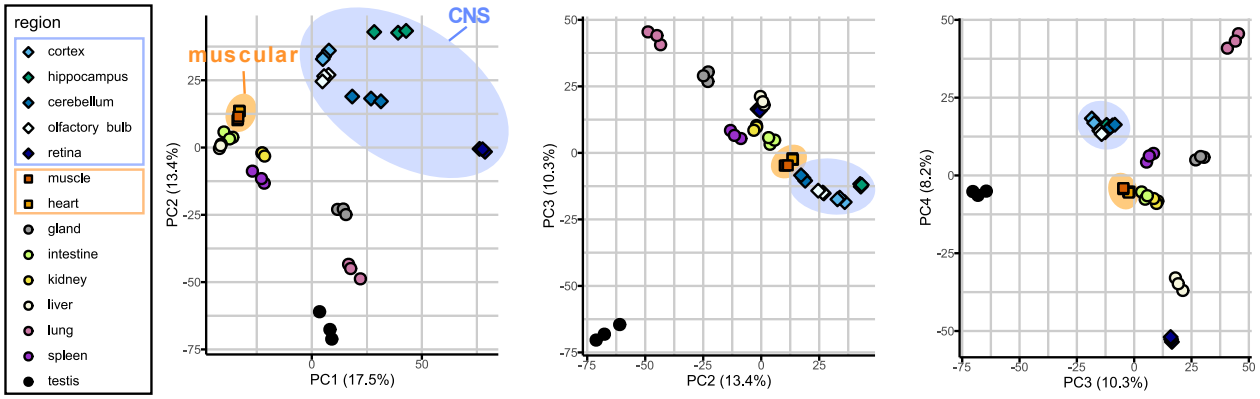
region
cortex
hippocampus
cerebellum
olfactory bulb
retina
muscle
heart
gland
intestine
kidney
liver
lung
spleen
testis
muscular
CNS
PC2 (13.4%)
PC1 (17.5%)
PC3 (10.3%)
PC2 (13.4%)
PC4 (8.2%)
PC3 (10.3%)

B

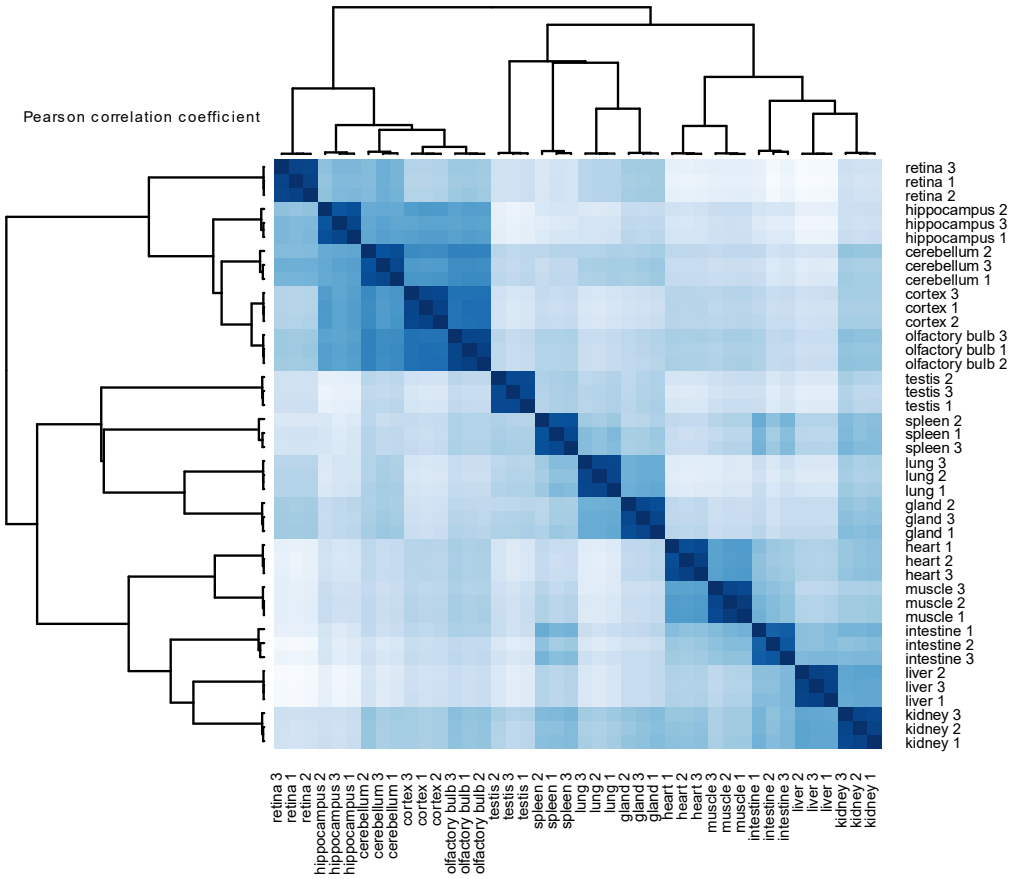
Pearson correlation coefficient
retina 3
retina 1
retina 2
hippocampus 2
hippocampus 3
hippocampus 1
cerebellum 2
cerebellum 3
cerebellum 1
cortex 3
cortex 1
cortex 2
olfactory bulb 3
olfactory bulb 1
olfactory bulb 2
testis 2
testis 3
testis 1
spleen 2
spleen 1
spleen 3
lung 3
lung 2
lung 1
gland 2
gland 3
gland 1
heart 1
heart 2
heart 3
muscle 3
muscle 2
muscle 1
intestine 1
intestine 2
intestine 3
liver 2
liver 3
liver 1
kidney 3
kidney 2
kidney 1

Figure 3

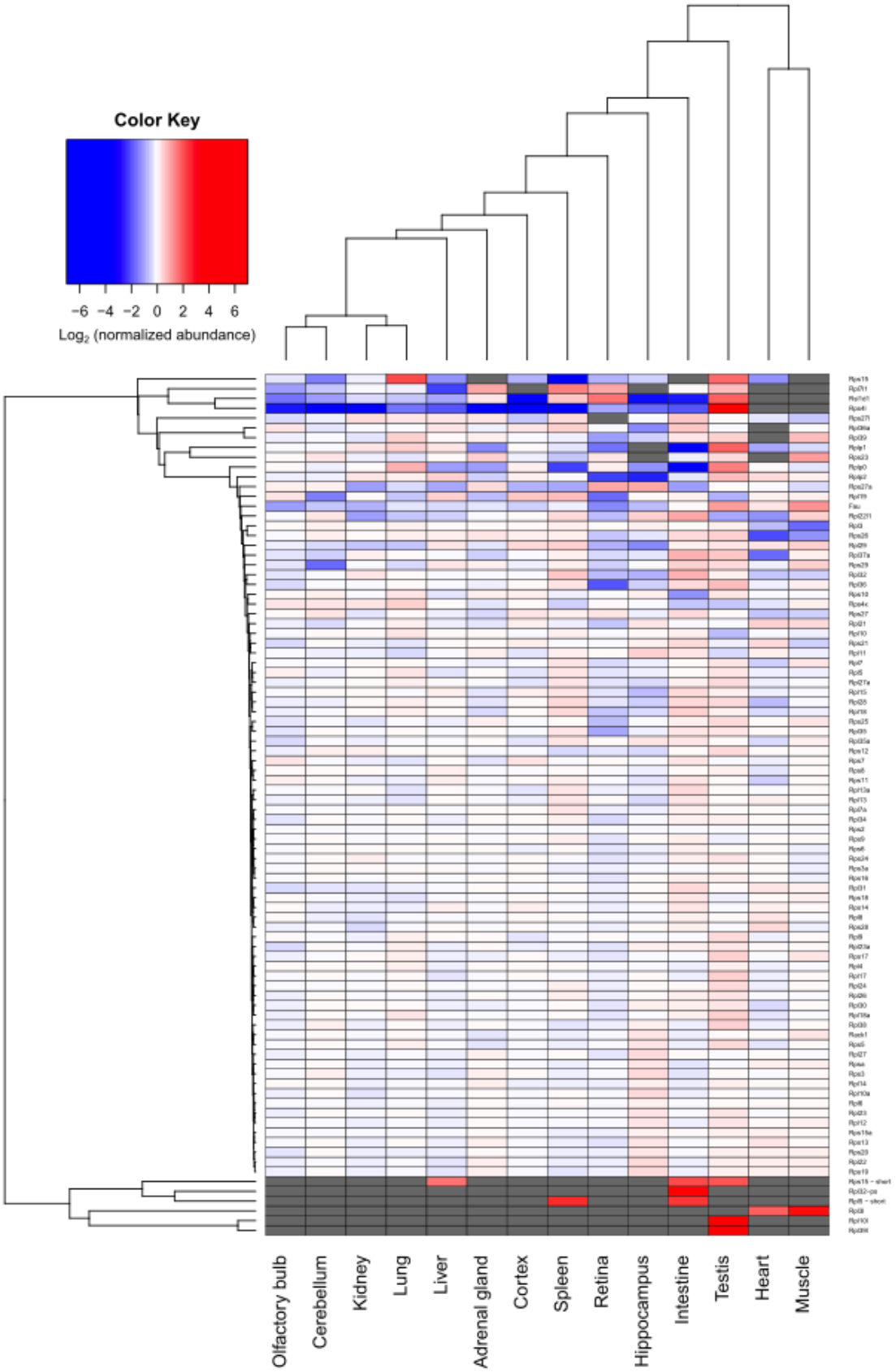
Color Key
−6 −4 −2 0 2 4 6
Log2 (normalized abundance)
Olfactory bulb
Cerebellum
Kidney
Lung
Liver
Adrenal gland
Cortex
Spleen
Retina
Hippocampus
Intestine
Testis
Heart
Muscle

Figure 4

A

RP per subunit	Ribosomal Proteins
24 RPS	S2, S3, S3a, S4x, S5, S6, S7, S8, S9, Sa, S10, S11, S12, S13, S14, S15a, S16, S17, S18, S19, S20, S21, S24, S26, S27, S27a, RACK1
32 RPL	L4, L5, L6, L7, L7a, L8, L9, L10a, L11, L12, L13, L13a, L14, L15, L17, L18, L18a, L22, L23, L23a, L24, L26, L27, L27a, L28, L30, L31, L32, L34, L35a, L37a, L38

B

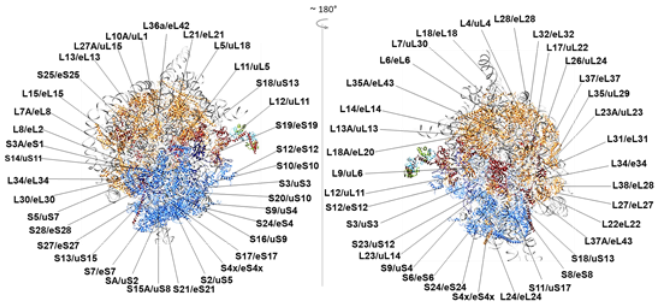

C

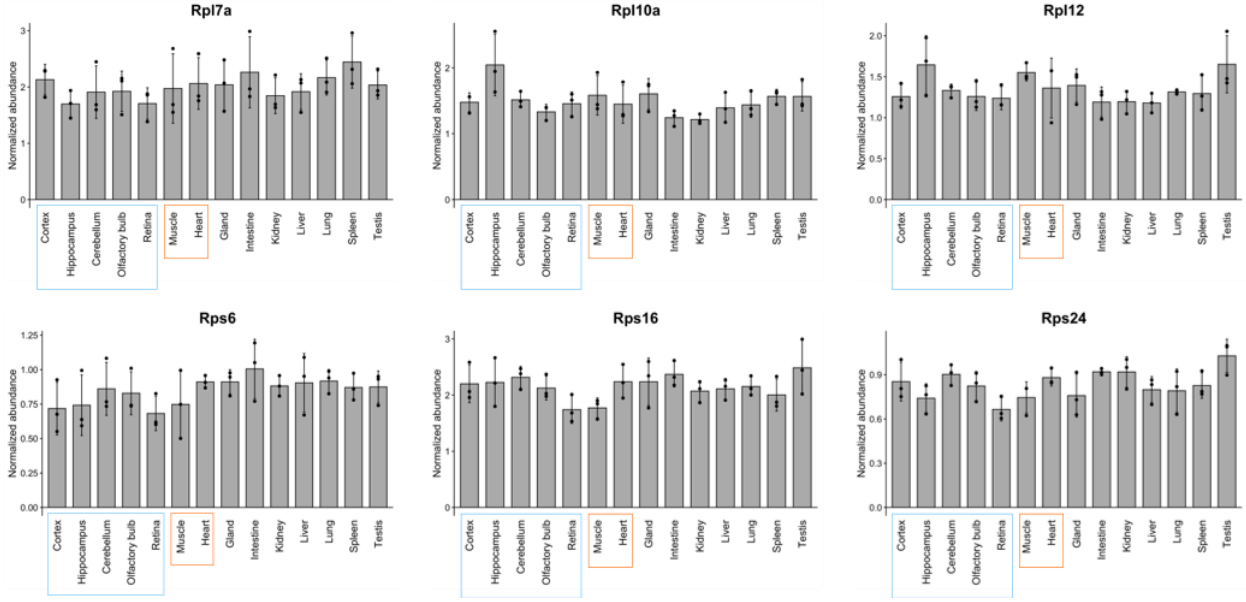

Figure 5

A

RP per subunit	Ribosomal Proteins
15 RPL	L3, L3l, L5, L7l1, L10, L10l, L22l1, L32, L36, L36a, L39, L39l, LP0, LP1, LP2
11 RPS	S4l, S4x, S10, S15, S15 - short , S23, S26, S27a, S27l, S29, S30

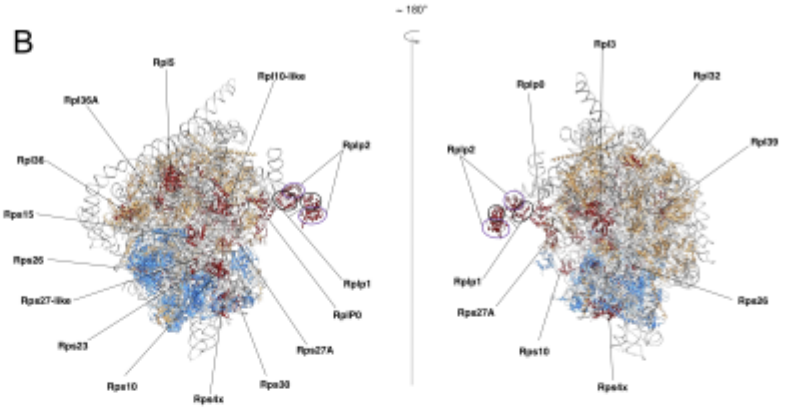

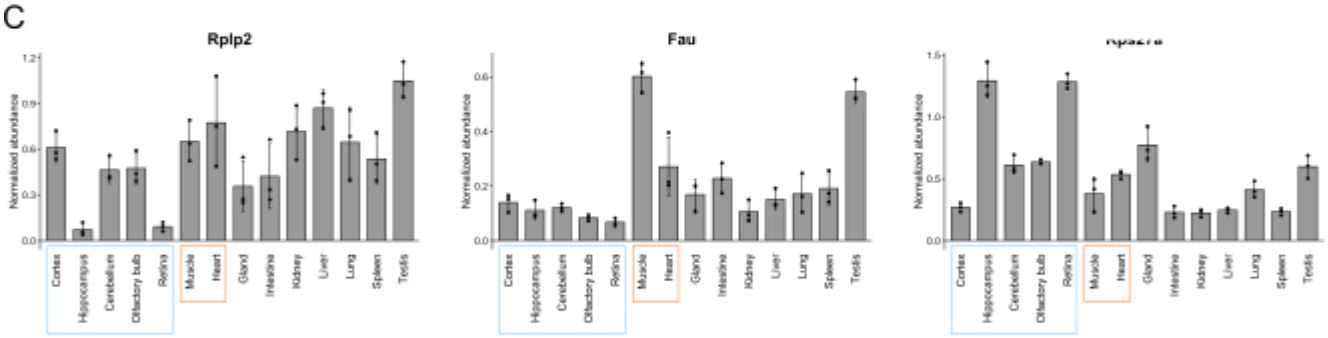

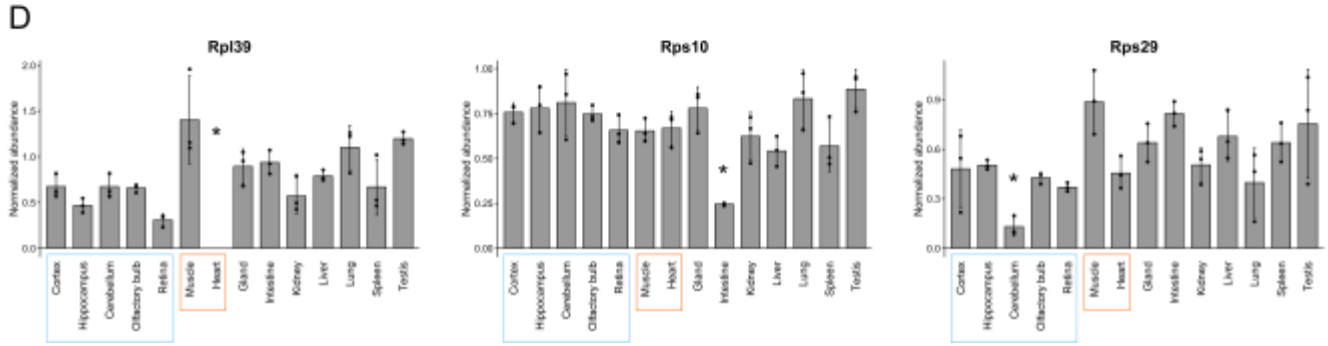

Figure 6

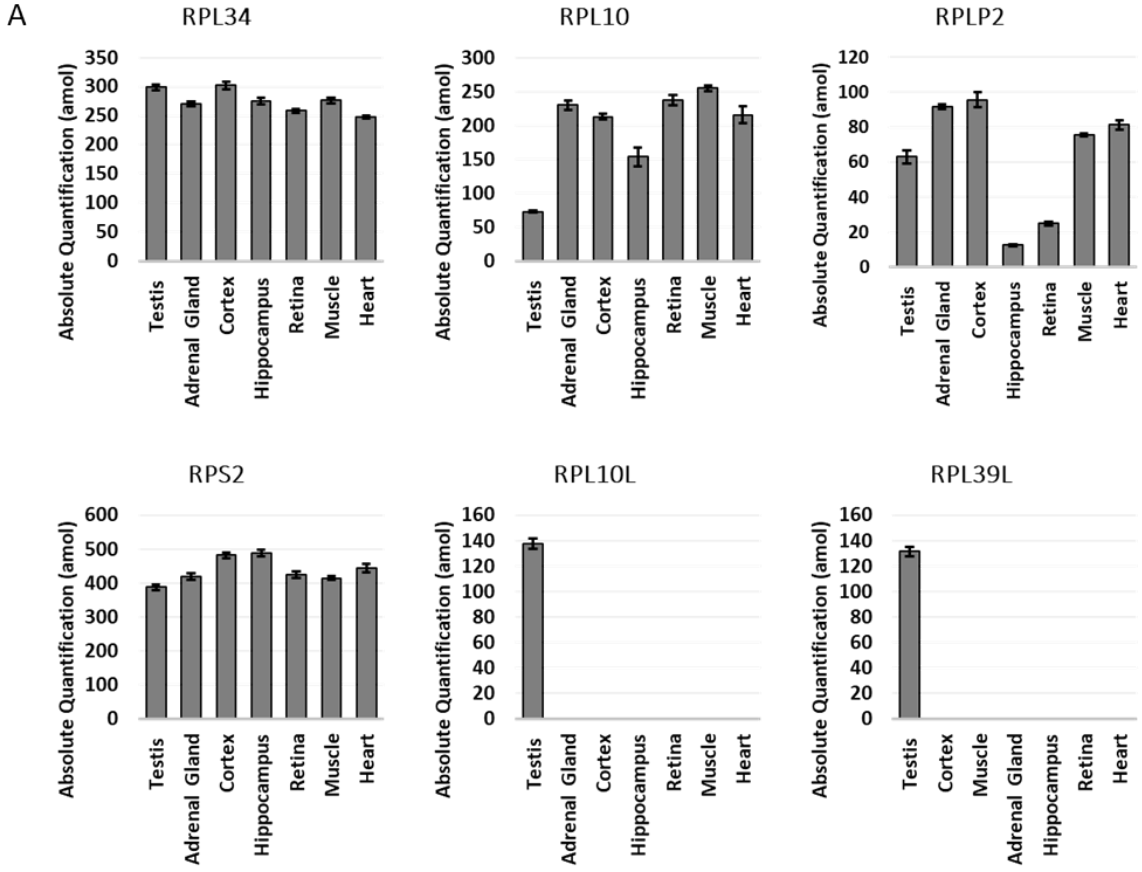
A
RPL34
RPL10
RPLP2
RPS2
RPL10L
RPL39L
Absolute Quantification (amol)
Testis
Adrenal Gland
Cortex
Hippocampus
Retina
Muscle
Heart

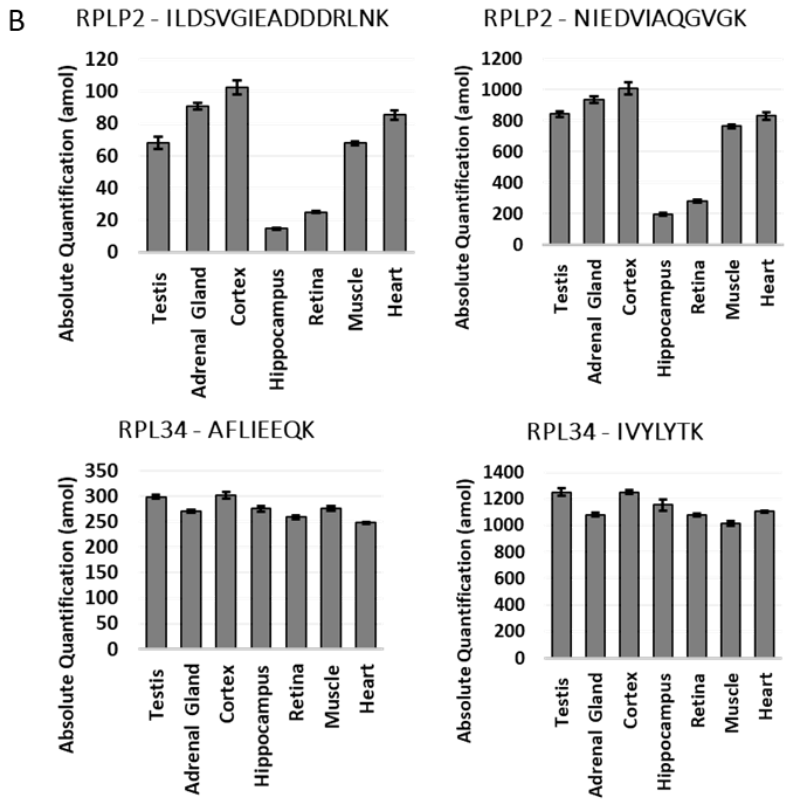
B
RPLP2 - ILDSVGIEADDDRLNK
RPLP2 - NIEDVIAQGVGK
RPL34 - AFLIEEQK
RPL34 - IVYLYTK
Absolute Quantification (amol)
Testis
Adrenal Gland
Cortex
Hippocampus
Retina
Muscle
Heart

Figure 7

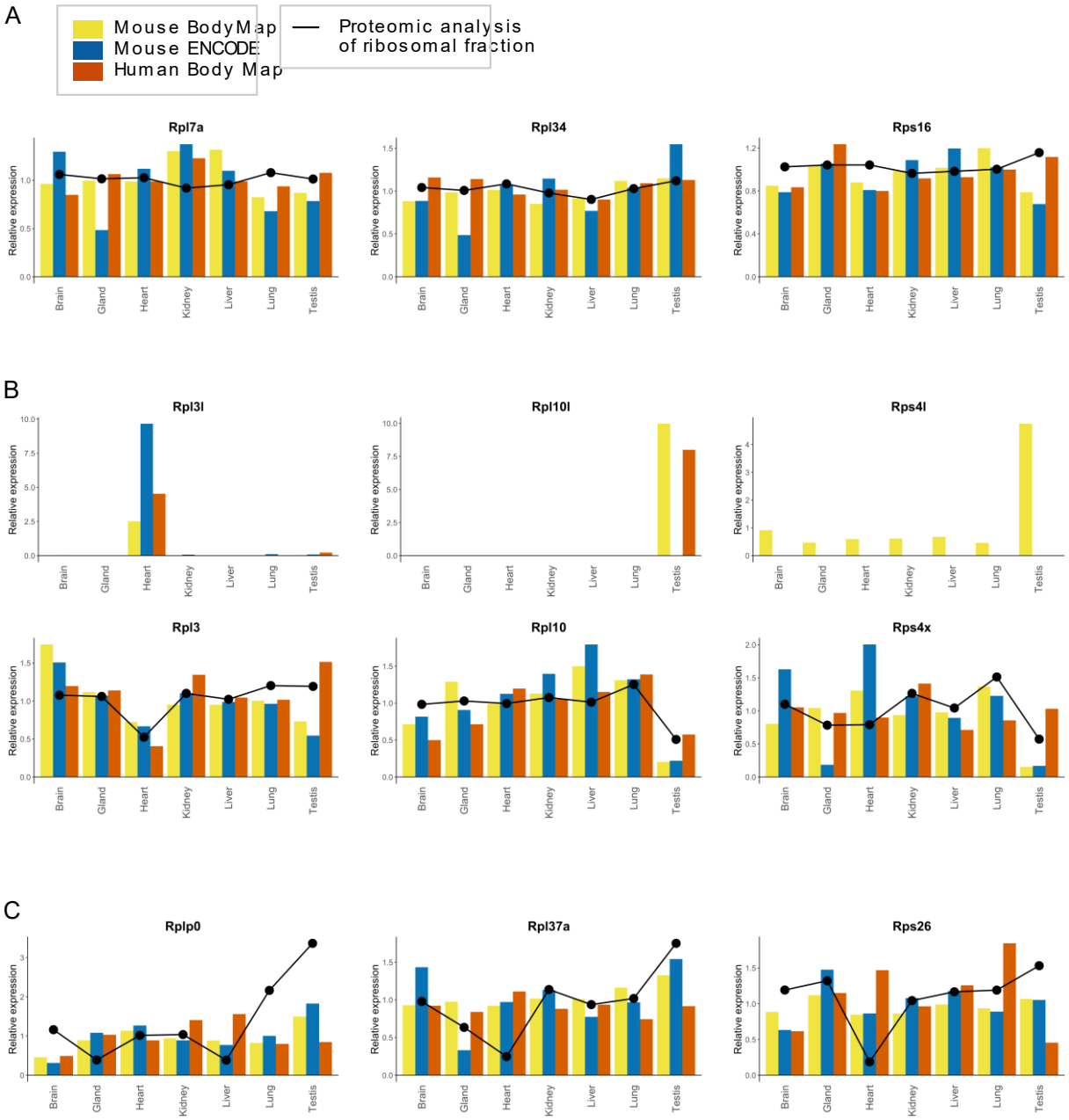
A
Mouse BodyMap
Mouse ENCODE
Human Body Map
Proteomic analysis of ribosomal fraction
Rpl7a
Rpl34
Rps16
B
Rpl3l
Rpl10l
Rps4l
Rpl3
Rpl10
Rps4x
C
Rplp0
Rpl37a
Rps26
Relative expression
Brain
Gland
Heart
Kidney
Liver
Lung
Testis

Figure 8

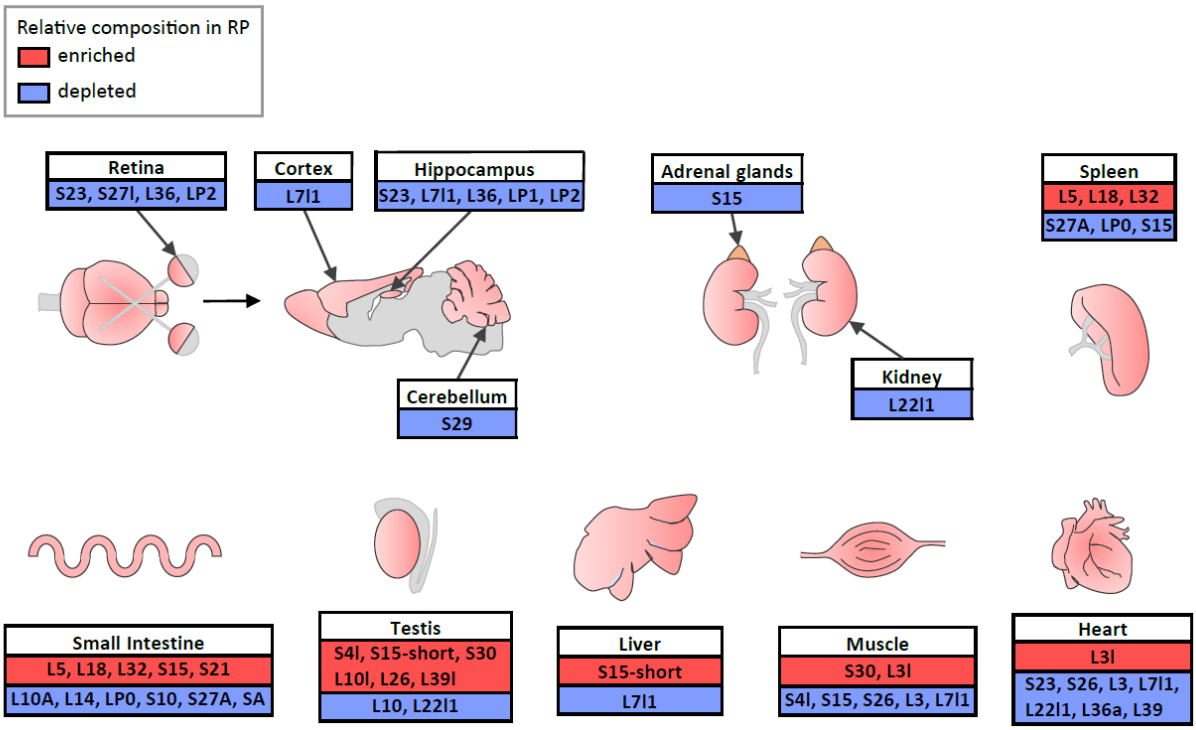
Relative composition in RP
enriched
depleted
Retina
S23, S27l, L36, LP2
Cortex
L7l1
Hippocampus
S23, L7l1, L36, LP1, LP2
Cerebellum
S29
Adrenal glands
S15
Kidney
L22l1
Spleen
L5, L18, L32
S27A, LP0, S15
Small Intestine
L5, L18, L32, S15, S21
L10A, L14, LP0, S10, S27A, SA
Testis
S4l, S15-short, S30
L10l, L26, L39l
L10, L22l1
Liver
S15-short
L7l1
Muscle
S30, L3l
S4l, S15, S26, L3, L7l1
Heart
L3l
S23, S26, L3, L7l1, L22l1, L36a, L39

Table 1

Organs	Total	RP	Enrichment (%)
Cortex	1743	80	62
Cerebellum	2141	80	73
Olfactory bulb	1750	80	75
Hippocampus	2274	77	48
Retina	2613	78	48
Muscle	587	79	70
Heart	798	76	15
Liver	1607	83	84
Intestine	1611	85	92
Adrenal gland	2132	78	66
Testis	2192	85	72
Spleen	1301	82	93
Lungs	2353	82	84
Kidney	1786	84	86

Supplementary Figure 1

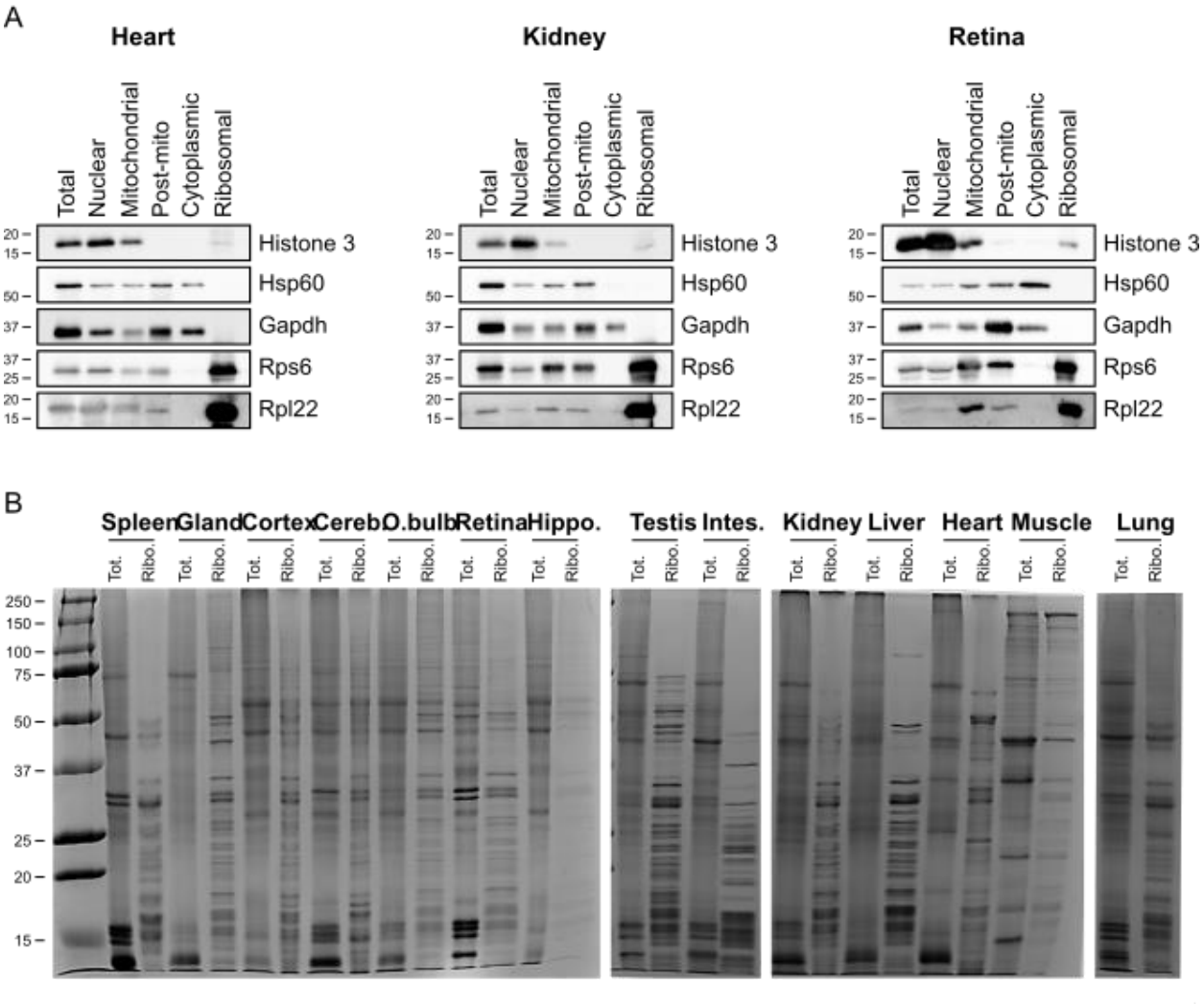

Supplementary Figure 2

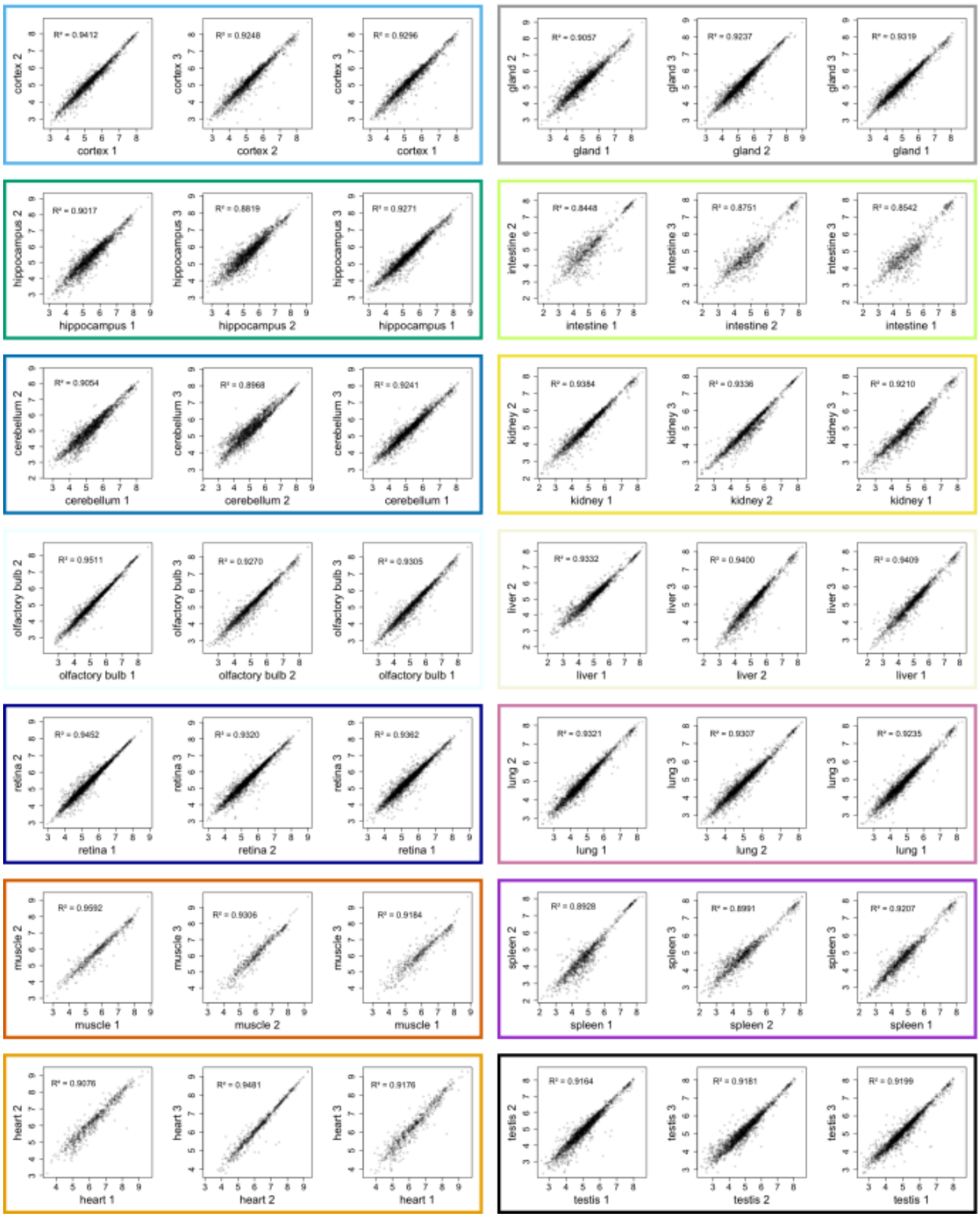

Supplementary Figure 3

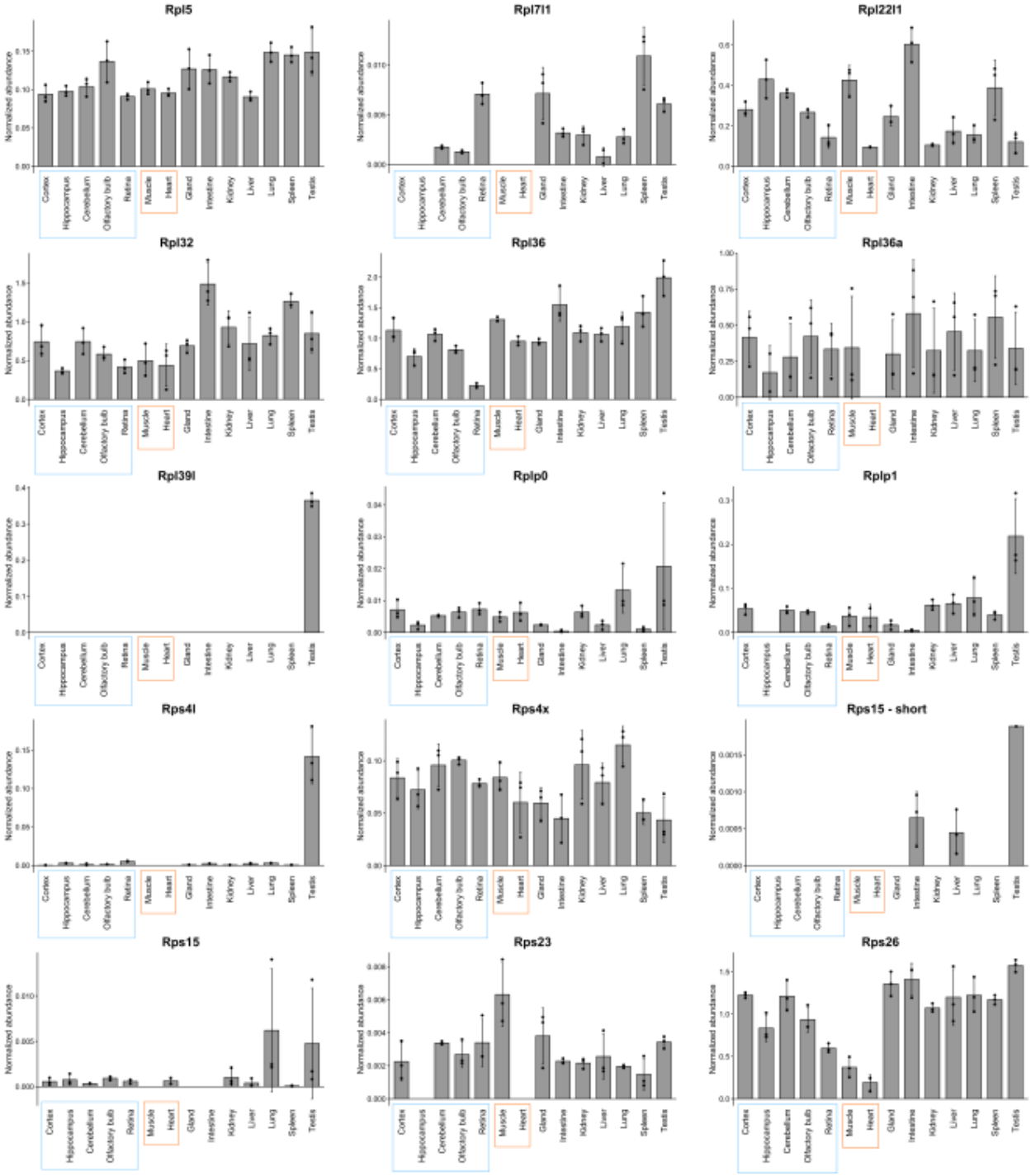

Supplementary Figure 4

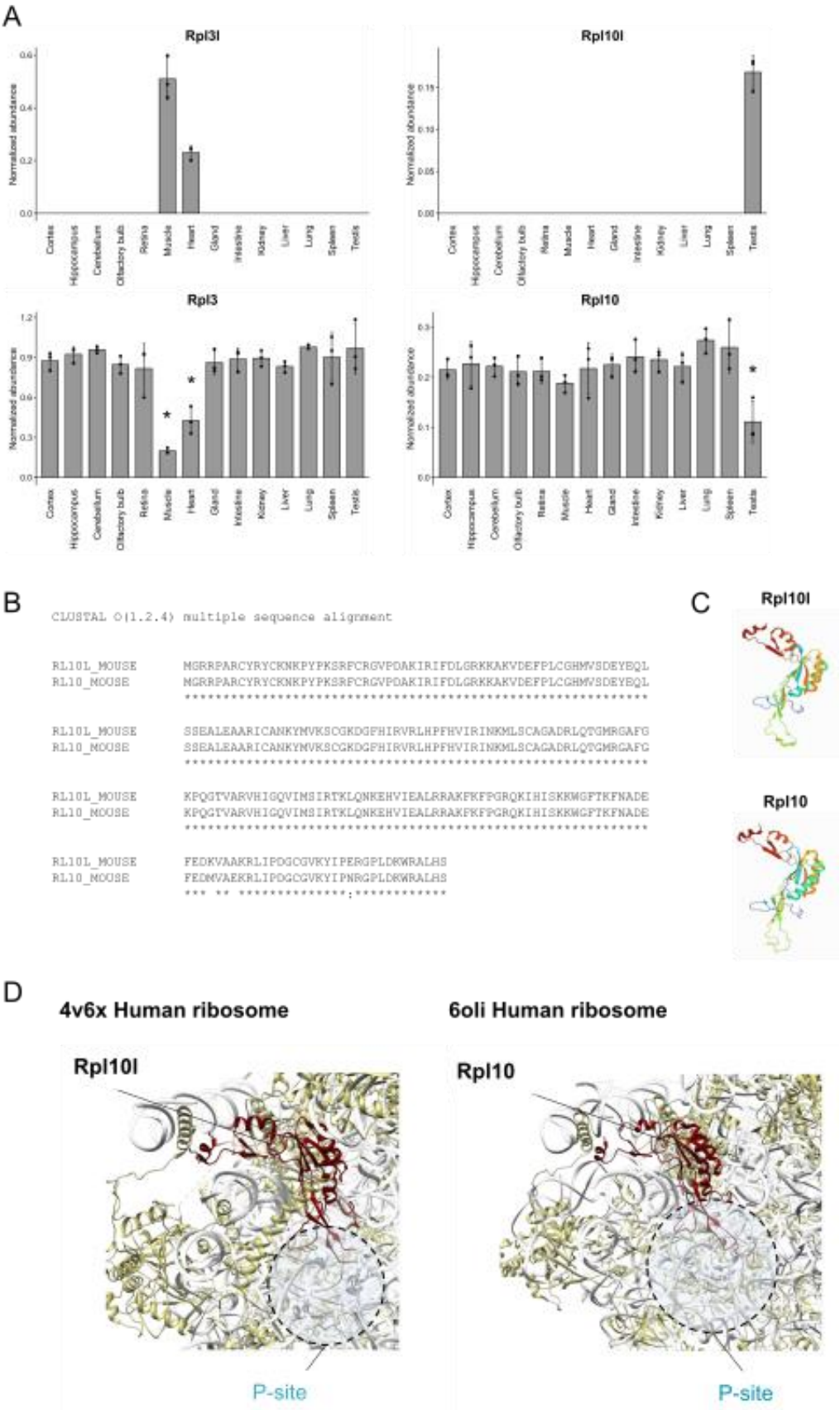

Supplementary Figure 5

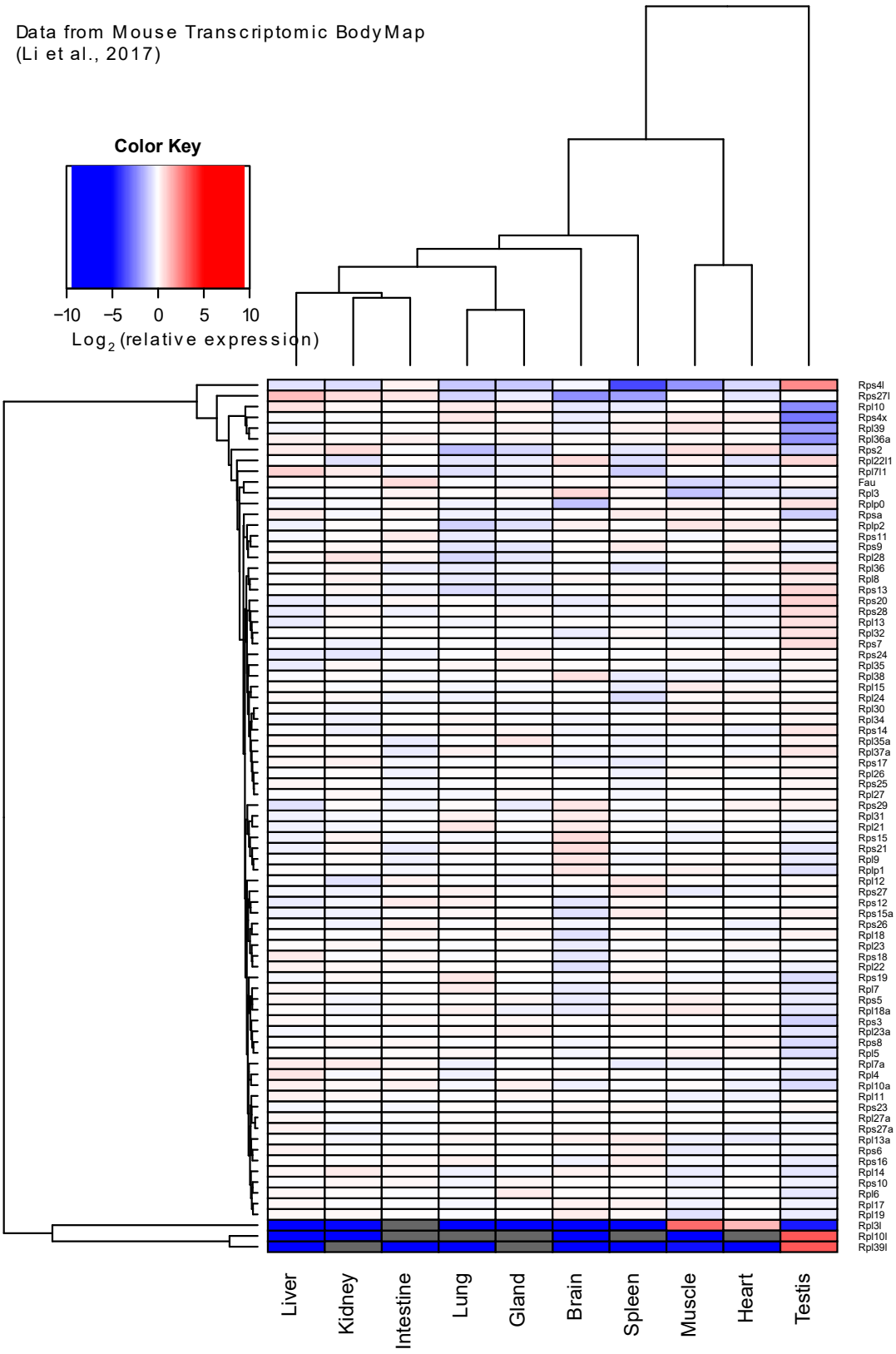

Supplementary table 1

accession	gene_nam	Spleen	Intestine	Kidney	Liver	Lung	Testis	Olfactory B	Cortex	Muscle	Cerebellur	Adrenal gl	Hippocam	Retina	Heart
sp|P62862	Fau	0.190858	0.227798	0.106412	0.151098	0.170931	0.54495	0.083318	0.139558	0.601615	0.120751	0.168701	0.110682	0.067287	0.271055
sp|P68040	Rack1	1.142903	1.181953	1.275073	1.232003	1.380288	1.435144	1.308656	1.209302	1.608987	1.320487	1.080821	1.605253	1.257766	1.345984
sp|Q6ZWV	Rpl10	0.259329	0.240733	0.23487	0.221136	0.273518	0.110891	0.210897	0.214747	0.187628	0.221556	0.224697	0.226652	0.211547	0.217219
tr|A0A3B2	Rpl10a	1.567313	1.244249	1.216199	1.3938	1.438524	1.566439	1.331102	1.478149	1.583502	1.515303	1.605266	2.044496	1.456149	1.44946
sp|P86048	Rpl10l						0.168281								
sp|Q9CXW	Rpl11	0.542657	0.6018	0.403321	0.451068	0.340554	0.321362	0.45639	0.374314	0.420756	0.392969	0.518656	0.737549	0.481134	0.53355
sp|P35979	Rpl12	1.294354	1.191722	1.195478	1.179589	1.314589	1.651861	1.259159	1.25761	1.552068	1.332559	1.394215	1.645321	1.238211	1.361499
sp|P47963	Rpl13	1.793273	1.827544	1.283308	1.442361	1.157328	1.549662	1.265292	1.286904	1.500721	1.309277	1.361141	0.986195	1.469447	1.645233
sp|P19253	Rpl13a	0.994091	1.034996	0.762892	0.811039	0.621456	0.785915	0.70177	0.595969	0.778174	0.744373	0.705424	0.663781	0.67371	0.702009
sp|Q9CR5	Rpl14	1.162657	1.089135	1.173507	1.201807	1.285547	1.577236	1.361165	1.179672	1.340995	1.335309	1.477848	1.565001	1.13052	1.413842
sp|Q9CZM	Rpl15	1.100652	1.118044	0.829733	0.952076	0.817435	0.917862	0.798201	0.926123	0.767632	0.82956	0.673897	0.446469	0.671095	0.748211
sp|Q9CPR	Rpl17	1.037189	0.892015	1.008117	0.826697	1.136958	1.558731	0.99435	1.047515	1.071874	1.131441	1.002995	1.061381	0.869517	0.91502
sp|P35980	Rpl18	2.201823	2.342125	1.635065	1.533838	1.786983	1.804128	1.298344	1.570368	1.341106	1.390581	1.11645	1.071278	0.873944	1.109092
sp|P62717	Rpl18a	0.499091	0.561369	0.459534	0.455364	0.619573	0.74701	0.422046	0.470582	0.473826	0.528731	0.464506	0.482861	0.401603	0.386898
sp|P84099	Rpl19	0.572466	0.343424	0.343091	0.462466	0.178186	0.150327	0.414654	0.523447	0.357349	0.089349	0.164355	0.34169	0.073084	0.348364
sp|O09167	Rpl21	1.079488	1.115006	1.14923	1.040211	1.359277	1.194921	1.010954	1.434332	1.709928	0.911239	0.945371	1.627444	0.688348	1.846633
sp|P67984	Rpl22	1.566499	1.669179	1.640152	1.491642	1.747143	2.109217	1.590998	1.771679	2.043048	1.702454	2.153563	2.519239	1.649123	2.115326
sp|Q9D7S	Rpl22l1	0.388355	0.604239	0.105104	0.173433	0.155664	0.120419	0.266997	0.280985	0.426784	0.361508	0.24654	0.431249	0.142663	0.094881
sp|P62830	Rpl23	0.918318	0.914018	0.86059	0.819457	0.956507	1.147794	0.844795	0.895697	0.973769	0.972914	0.950742	1.161957	0.86268	0.882682
sp|P62751	Rpl23a	1.260018	1.511947	1.157636	1.059324	1.401829	1.632722	0.918277	1.062455	1.383306	1.299447	1.35303	1.423176	0.981133	1.319964
sp|Q8BP6	Rpl24	1.482757	1.360123	1.229099	1.19881	1.346218	1.740384	1.183555	1.222655	1.388459	1.206426	1.252116	1.300792	1.126866	1.109146
sp|P61255	Rpl26	0.991203	1.07781	0.80937	0.790832	0.850261	1.102976	0.752965	0.846115	0.822583	0.934966	0.96126	0.903134	0.762839	0.836897
sp|P61358	Rpl27	3.951276	3.997156	3.318785	3.316579	3.604129	3.552556	3.263609	3.539859	3.580556	3.671389	4.28467	5.388337	3.052488	4.08024
sp|P14115	Rpl27a	1.407559	1.203321	1.137174	1.128359	1.295403	1.503317	0.975708	0.873787	1.07912	1.052185	0.989643	0.773043	0.833159	0.917634
sp|P41105	Rpl28	0.676989	0.636975	0.475806	0.515202	0.567341	0.636512	0.424031	0.479886	0.454949	0.422173	0.37684	0.304058	0.38063	0.251251
sp|P27659	Rpl3	0.901278	0.886551	0.893359	0.830237	0.976631	0.96801	0.845657	0.874112	0.198869	0.956798	0.861011	0.922733	0.815933	0.425553
sp|P62889	Rpl30	1.261383	1.357513	1.213636	1.055419	1.274627	1.55145	0.998267	1.139044	1.173382	1.178693	0.979903	1.376778	0.93154	0.845192
sp|P62900	Rpl31	1.269961	1.710131	0.957731	1.177245	1.020088	1.268842	0.887362	1.182673	1.387538	0.990329	1.251203	1.238538	1.038237	1.475391
sp|P62911	Rpl32	1.26393	1.486054	0.928499	0.718058	0.823896	0.848924	0.583579	0.742908	0.498577	0.744519	0.690223	0.364484	0.416813	0.439665
sp|Q9D1R	Rpl34	1.589362	1.61809	1.395484	1.288333	1.46848	1.599257	1.165037	1.487139	1.554689	1.501015	1.438611	1.299254	1.028342	1.547652
sp|Q6ZWV	Rpl35	1.986137	2.16733	1.489454	1.5645	1.776839	2.12043	1.33151	1.615481	1.716823	1.653112	1.643667	1.366468	0.698641	1.674502
sp|O55142	Rpl35a	1.065172	1.098461	0.762408	0.802454	0.838544	0.865091	0.612744	0.699948	0.981093	0.835956	0.897659	1.132613	0.881658	0.587422
tr|Q5M9L	Rpl36	1.425738	1.54935	1.089774	1.063797	1.189839	1.990624	0.813589	1.128074	1.306691	1.064658	0.939924	0.701403	0.223527	0.951659
sp|P83882	Rpl36a	0.555384	0.580585	0.324322	0.455683	0.324128	0.339495	0.422879	0.416261	0.344704	0.278573	0.300023	0.171758	0.334619	
sp|P61514	Rpl37a	0.411104	0.717414	0.410475	0.338157	0.367502	0.631745	0.275753	0.353245	0.427166	0.244781	0.228985	0.29449	0.261269	0.089166
sp|Q9JJI8	Rpl38	1.75831	1.977387	2.055494	1.989208	2.513742	3.40859	2.00211	2.141442	2.528166	2.58627	2.477391	2.765611	2.015857	2.089121
sp|P62892	Rpl39	0.669792	0.936959	0.571519	0.789143	1.102718	1.197393	0.658549	0.673715	1.403528	0.672526	0.893809	0.466774	0.307526	
tr|Q9CQD	Rpl39l						0.365242								
tr|E9PWZ	Rpl3l									0.509942					0.230232
sp|Q9D8E	Rpl4	1.330258	1.08246	1.245824	1.102298	1.35069	1.461681	1.233824	1.221974	1.137526	1.283845	1.269865	1.144423	1.132519	1.038365
sp|P47962	Rpl5	0.145196	0.12604	0.116606	0.090544	0.148583	0.148728	0.136672	0.093876	0.100967	0.103767	0.126962	0.097752	0.090982	0.095568
tr|Q3TKR5	Rpl5	0.004423	0.004057												
sp|P47911	Rpl6	1.454222	1.304123	1.174674	1.153182	1.280891	1.497955	1.262441	1.352053	1.485922	1.365263	1.495284	1.587561	1.363655	1.413454
sp|P14148	Rpl7	2.15558	1.843146	1.770595	1.655494	1.765933	2.094985	1.617414	1.682039	2.143375	1.615054	1.484566	1.460428	1.193657	1.095538
sp|P12970	Rpl7a	2.444325	2.262028	1.845931	1.916561	2.167599	2.035175	1.922853	2.130832	1.973451	1.909381	2.039504	1.697958	1.706393	2.062399
sp|Q9D8N	Rpl7l1	0.010905	0.003174	0.002964	0.000781	0.002767	0.006083	0.00128			0.001752	0.007137		0.007076	
sp|P62918	Rpl8	0.922563	1.050037	0.70556	0.825335	0.894503	0.930005	0.944523	0.955929	0.835661	0.797922	0.874045	0.867783	0.889344	1.147899
sp|P51410	Rpl9	0.554137	0.585265	0.49706	0.62526	0.684036	0.803014	0.609891	0.47511	0.609398	0.555945	0.605737	0.583456	0.608255	0.488708
sp|P14869	Rplp0	0.001064	0.000388	0.006394	0.002376	0.013348	0.020754	0.006391	0.007157	0.004881	0.00529	0.002394	0.002318	0.007279	0.006272
sp|P47955	Rplp1	0.039844	0.005339	0.06218	0.065415	0.078922	0.218776	0.047029	0.053974	0.037146	0.050508	0.017207		0.01416	0.03449
sp|P99027	Rplp2	0.53608	0.422336	0.716571	0.869821	0.645708	1.049447	0.474407	0.611704	0.650283	0.463733	0.356687	0.072074	0.091289	0.774339
sp|P63325	Rps10	0.569571	0.245799	0.623485	0.541762	0.833106	0.886502	0.748144	0.756832	0.653703	0.810737	0.779573	0.779718	0.657529	0.668881
sp|P62281	Rps11	1.761164	1.975082	1.295209	1.80632	1.244553	1.519737	1.655788	1.654226	1.575551	1.55504	1.369387	1.209856	1.392583	1.015748
tr|F7AEH4	Rps12	0.715967	1.018034	1.073296	1.034553	1.029589	1.370068	0.850066	0.878469	1.029834	1.118684	0.961028	0.677561	0.777409	1.009527
sp|P62301	Rps13	1.637837	1.962039	1.75263	1.755817	2.005544	1.992205	1.842405	1.866222	2.015971	2.078191	2.337792	2.44735	1.6141	2.503147
sp|P62264	Rps14	1.950067	2.557998	1.696017	2.188525	1.741272	1.848265	2.006528	2.203378	1.97134	1.702064	1.826624	1.816208	1.765649	2.265306
sp|P62843	Rps15	8.01E-05		0.001013	0.000393	0.006206	0.004762	0.000907	0.000552		0.000334		0.000758	0.00057	0.000622
tr|D3YTQ9	Rps15		0.000648		0.000447										
sp|P62245	Rps15a	1.396395	1.794566	1.518833	1.505448	1.613591	1.832504	1.493301	1.561564	1.698001	1.535171	1.798008	1.928118	1.403835	1.853383
sp|P14131	Rps16	2.002306	2.368869	2.070176	2.110621	2.152251	2.484844	2.124436	2.200003	1.771587	2.315668	2.236606	2.224866	1.741205	2.237356
sp|P63276	Rps17	0.718322	0.78789	0.847626	0.698005	0.900869	1.182056	0.663732	0.807048	0.972221	0.784438	0.722443	0.735881	0.618724	0.735821
sp|P62270	Rps18	1.403394	1.814959	1.274168	1.401733	1.168644	1.30632	1.554857	1.567391	1.668889	1.325705	1.406712	1.561933	1.304629	1.476568
sp|Q9CZX	Rps19	1.044416	1.156664	1.09965	1.060624	1.237736	1.48744	1.119971	1.25219	1.440628	1.352193	1.49185	1.793194	1.140434	1.512864
sp|P25444	Rps2	1	1	1	1	1	1	1	1	1	1	1	1	1	1
sp|P60867	Rps20	2.674521	2.884532	2.558632	2.634914	2.607522	3.275708	2.417232	2.860076	3.454276	3.058034	3.164177	3.840641	2.571418	3.294543
sp|Q9CQR	Rps21	0.803242	1.167557	0.698862	0.827193	0.662903	0.721104	0.565191	0.900245	0.502592	0.849422	0.85181	0.934202	0.782656	1.096178
sp|P62267	Rps23	0.001487	0.002273	0.00216	0.002557	0.001959	0.003434	0.002687	0.002254	0.006316	0.003377	0.003813		0.003397	
sp|P62849	Rps24	0.827206	0.920071	0.918949	0.79887	0.791252	1.028266	0.82404	0.853691	0.745703	0.902841	0.758647	0.741195	0.665138	0.880713
sp|P62852	Rps25	1.610342	1.729194	1.204121	1.336139	1.478798	2.186184	1.208507	1.519699	2.039057	1.53765	1.833267	1.432826	0.854198	1.634296
sp|P62855	Rps26	1.169468	1.411364	1.072108	1.198134	1.222373	1.573391	0.935249	1.223569	0.370334	1.211794	1.35667	0.833964	0.596849	0.191601
sp|Q6ZWL	Rps27	0.394208	0.497602	0.277503	0.29168	0.345563	0.353451	0.364071	0.429199	0.224015	0.435462	0.239167	0.285889	0.447838	0.206294
sp|P62983	Rps27a	0.233413	0.228409	0.223621	0.246084	0.410667	0.598065	0.634879	0.269777	0.37942	0.611535	0.773301	1.292534	1.284061	0.534004
sp|Q6ZWY	Rps27l	0.328073	0.416349	0.341818	0.308833	0.311836	0.243799	0.171132	0.133469	0.141921	0.2014	0.313855	0.23531		0.178364
sp|P62858	Rps28	1.10343	1.310156	0.828384	1.150459	1.10655	1.105147	1.009045	1.16458	0.978823	1.033467	1.112152	1.196334	0.949056	1.639751
sp|P62274	Rps29	0.638882	0.815008	0.50435	0.67691	0.396578	0.753543	0.426831	0.480445	0.886176	0.130034	0.638622	0.503105	0.369607	0.455073
sp|P62908	Rps3	0.212902	0.209859	0.220248	0.208125	0.223522	0.270633	0.243331	0.263953	0.283098	0.288747	0.298829	0.378753	0.25209	0.253317
sp|P97351	Rps3a	1.136856	1.272081	1.351235	1.306147	1.372443	1.410132	1.262019	1.42348	1.151647	1.399226	1.228276	1.280028	1.16482	1.373626
tr|Q3V1Z5	Rps4l	0.000594	0.002431	0.000669	0.002347	0.003017	0.141704	0.001306	0.000339		0.001019	0.000724	0.002968	0.005315	
sp|P62702	Rps4x	0.050383	0.044955	0.096167	0.079334	0.115055	0.043511	0.100499	0.083718	0.084094	0.095833	0.059583	0.072434	0.078364	0.060199
tr|D3YYM	Rps5	0.573109	0.546839	0.610543	0.612282	0.707354	0.850396	0.578166	0.625636	0.69025	0.684463	0.500202	0.774129	0.587549	0.510532
sp|P62754	Rps6	0.870653	1.005141	0.881814	0.90372	0.917237	0.873948	0.828827	0.71765	0.74773	0.860753	0.910754	0.741498	0.682011	0.910532
sp|P62082	Rps7	1.123127	1.424007	0.974382	1.237767	0.90089	1.136755	1.445651	1.502592	1.174873	1.097376	0.956818	1.126577	1.257303	0.99866
sp|P62242	Rps8	2.147787	2.033999	2.036712	2.276077	1.929247	2.260113	2.183861	1.901763	2.108726	2.062913	1.997592	1.71291	1.97535	1.518626
sp|Q6ZWN	Rps9	2.237085	2.271539	1.987709	2.062401	1.860747	1.788063	1.92511	2.197923	2.052986	2.078714	1.895433	2.166695	1.630063	2.127477
sp|P14206	Rpsa	1.42306	1.323833	1.547002	1.448388	1.691165	1.666588	1.624753	1.612328	2.001823	1.790661	1.79472	2.242895	1.662605	2.068104

Supplementary Table 2

Protein ID	Reference peptides		
Rps2	GTGIVSAPVPK*	K*	indicates heavy K (+8)
	GCcamTATLGNFAK*	R*	indicates heavy R (+10)
Rps26	DISEASVFDAYVLPK*	Ccam	indicates C modified with Carbamidomethylation
	NIVEAAAVR*	Mox	indicates M modified with Oxidation
Rpl3	HGSLGFLPR*		
	DDASK*PVHLTAFLGYK*		
	VACcamIGAWHPAR*		
Rpl10	VHIGQVIMoxSIR*		
	VHIGQVIMSIR*		
	FNADEFEDMVAEK*R*		
	FNADEFEDMoxVAEK*R*		
	FNADEFEDMVAEK*		
	FNADEFEDMoxVAEK*		
Rpl34	IVYLYTK*		
	AFLIEEQK*		
Rps30	FVNVVPTFGK*		
Rplp2	K*ILDSVGIEADDDR*LNK*		
	ILDSVGIEADDDR*LNK*		
	NIEDVIAQGVGK*		
Rpl36	YPMAVGLNK*		
	YPMoxAVGLNK*		
	EVCcamGFAPYER*		
Rpl39	QNR*PIPQWIR*		
Rpl3l	DDPSQPVHLTAFLGYK*		
	QVPVHSVFSQSEVIDVIAVTK*		
rps10l	FNADEFEDK*		
	FNADEFEDK*VAAK*		
Rpl39l	QNR*PIPQWIQMK*		
	QNR*PIPQWIQMoxK*		

2. *In silico* analysis of RAFs

Alongside with the ribosome are the ribosome-associated factors (RAFs) often identified as riboproteome or ribointeractome (Reschke et al., 2013; Simsek et al., 2017). They are defined as proteins that interact with the ribosome or the mRNA during translation or nascent protein quality control. The first study on RAFs was made in 1973 (Gilbert and Johnson, 1973). They observed that the removal of RAF by using KCl inhibited protein synthesis. Since then, studies have been using sophisticated techniques such as stable isotope labelling by amino acids in cell culture (SILAC)-based mass spectrometry approach to identify proteins associated with actively translating ribosomes. Using MEFs and human immortalized cell lines and prostate cancer cell lines, Reschke and colleagues identified between 575 and 991 proteins, depending on the cell lines. GO analysis showed that the proteins are involved in protein synthesis (e.g RAD23B involved in recruitment of elongation factors), mRNA stability (e.g; LARP4B) and post-translational modification (e.g.: SPSB2 which is present in the E3 ubiquitin-protein ligase complex) among others. Comparison of the different datasets revealed that there is an alteration of the riboproteome in cancer. This was confirmed by the analysis of riboproteomic genes across 15 types of cancers which were also modified during cancer. In 2017, Simsek et al., characterised the riboproteome from mouse embryonic stem cells (Simsek et al., 2017). They identified similar groups of protein such as post-translational modifiers such as kinase CDK1 and E3 ubiquitin-protein ligase NEDD4. Metabolism-related RAFs such as pyruvate kinase were also detected.

Studies usually use sucrose density gradient ultracentrifugation or ribosome affinity purification coupled to mass spectrometry. However, a major drawback is that there was no analysis to confirm that these proteins were true ribosome interactants. In other words, contaminants can be co-precipitated and identified but have no direct interaction with ribosomes. To circumvent this issue, Imami and colleagues proposed a way of determining true ribosome-associated proteins (Imami et al., 2018). In their study, they used a SILAC-based mass spectrometry approach to analyse mammalian polysome-associated proteins. They constructed a spectral profile based on all RPs from the polysome fraction and compared this to the profile of suspected polysome-associated proteins. They postulated that interactants should have similar profiles. Based on their analysis, they identified 145 interactants from an ~1500 initial protein set. Gene ontology analysis on the 145 proteins revealed that it is enriched in proteins associated with ribonucleoprotein complex biogenesis, mRNA stabilisation and

translation regulation. Similar approaches could be used in future studies as not all proteins identified in the process are necessarily ribosome interactants.

Year by year, more RAFs are being identified. For example, Huntingtin, which is mutated in Huntington's disease, can induce stalling of the ribosome and repress translation (Eshraghi et al., 2021). There is a change in RAFs between physiological and pathological conditions such as cancer that can have consequences on the efficiency and specificity of mRNA translation. We were interested in understanding which proteins were interacting with ribosomes in each organ.

Results & Discussion

Between 591 to 2617 proteins were identified during the MS analysis. To identify RAFs, RPs and translation factors were manually removed from each list. The resulting lists were analysed in DAVID (https://david.ncifcrf.gov/, (Huang et al., 2009) and STRING (von Mering et al., 2003) to identify the functional groups present. We realised that components from the potential RAFs list originated from the nuclear or mitochondrial complexes (**Figure 1**)

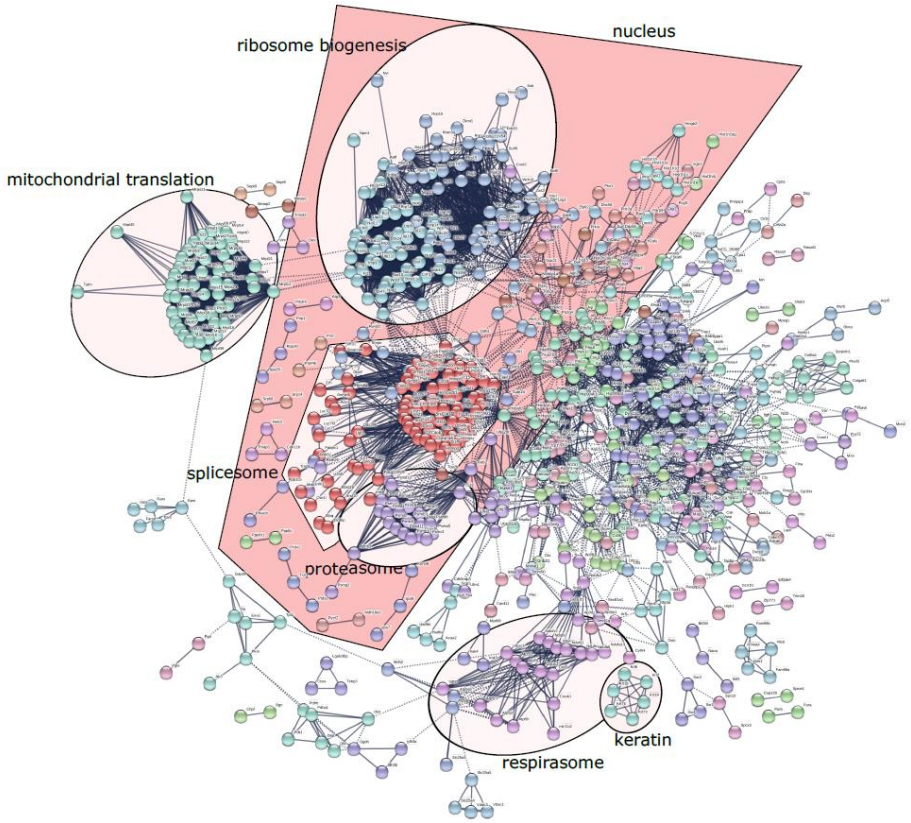

Figure 1: Example of STRING projection of RAFs from the spleen before curation

To have a clearer picture of RAFs, the lists were curated by removing any factors associated with the nucleus or mitochondria. From all the available lists, we decided to focus on the CNS subparts (Hippocampus, cortex, cerebellum, retina and olfactory bulb) and the two muscle-type tissues, muscles and heart.

RAFs from the CNS:

The curated lists from each part of the CNS were compared to identify common and specific RAFs. 612 RAFs were common to all subparts while between 88 and 602 proteins were specific to each subregion (**Figure 2**). Common components include GO terms associated with neuron projection, focal adhesion and axon (**Figure 3A**)

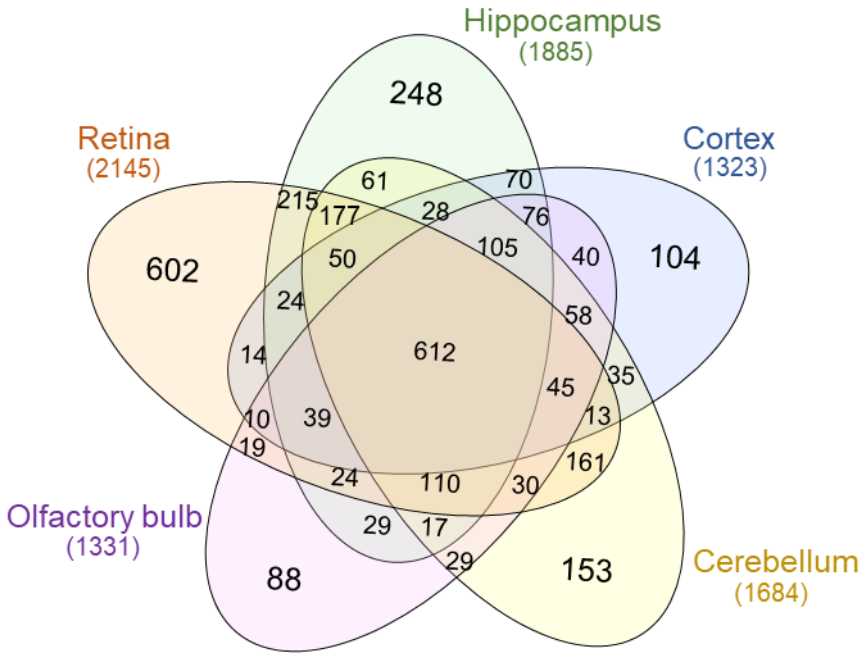

Figure 2: Venn diagram showing shared and specific RAFs across brain regions. The number of potential RAFs in each organ is indicated between brackets.

Specific RAFs from each region were analysed using DAVID. Interestingly, specific RAFs are associated with specific functions of the subpart considered. For example, the olfactory bulb contains proteins linked to neuronal projection development and the retina has proteins associated with visual perception (**Figure 3B**). The RAFs associated with each subregion probably contributes to the tissue-specialisation such as light detection.

A

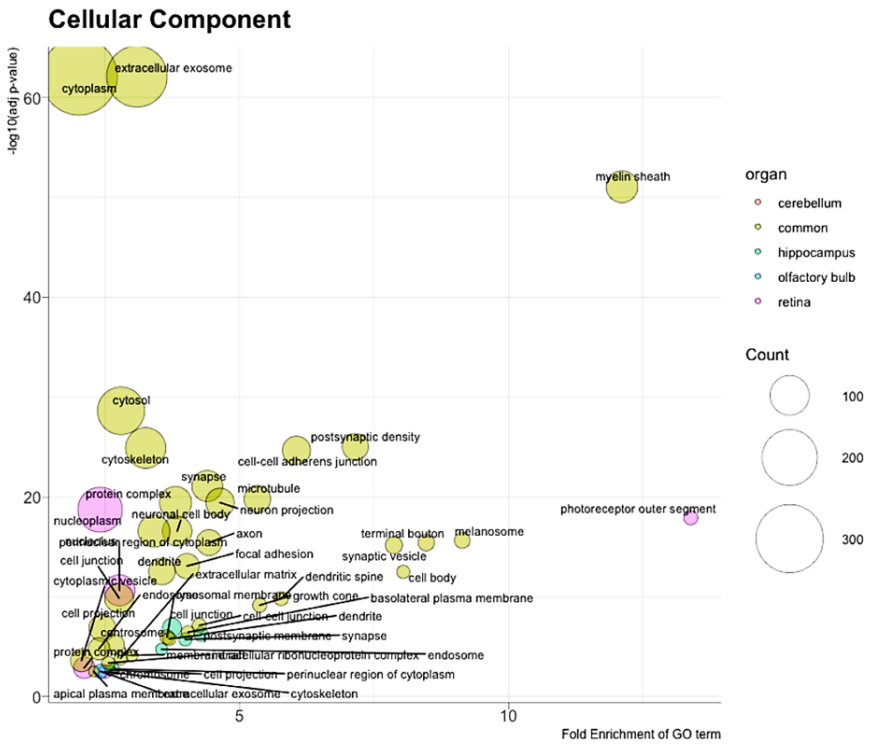

B

CNS subpart	GO biological process category	Fold enrichment	P value
Cerebellum	positive regulation of synapse maturation	37.64	0.003
	long-term synaptic potentiation	11.27	0.005
	ion transport	2.60	0.010
	regulation of translation	5.70	0.011
	cell migration	4.34	0.012
Cortex	calcium ion transport	8.02	0.003
	transport	2.11	0.005
	calcium ion transmembrane transport	10.27	0.007
	protein oligomerization	10.12	0.035
	positive regulation of peptidyl-serine phosphorylation	9.16	0.042
Hippocampus	RNA splicing	6.54	7.65E-10
	protein phosphorylation	4.03	1.52E-09
	phosphorylation	3.79	5.57E-09
	mRNA processing	4.89	7.09E-08
	nervous system development	3.52	5.31E-05
Olfactory Bulb	neuron projection development	8.91	0.002
	nervous system development	4.60	0.004
	positive regulation of neuron projection development	7.18	0.018
	negative regulation of cytoplasmic translation	82.57	0.024
	response to herbicide	61.92	0.031
Retina	visual perception	11.91	5.86E-36
	response to stimulus	5.22	9.39E-14
	covalent chromatin modification	4.14	4.62E-11
	photoreceptor cell maintenance	12.05	5.16E-11
	transcription, DNA-templated	1.92	5.95E-11

Figure 3: DAVID analysis of CNS RAFs. (A) Bubble plot showing enriched of cellular component GO terms in each region of the CNS. The size of the bubble depends on the number of identified protein composing this group. Note that the olfactory bulb is not presented as only few proteins were present (B) Table showing the GO terms enriched specifically in each brain region.

RAFs from the muscle-type tissue:

We also compared RAFs from muscles and heart. After curation, we were left with 435 and 312 RAFs for the heart and the muscle respectively. 153 were shared by both tissues (**Figure 4A**). Analysis of GO terms shows an enrichment in terms associated with glycolytic process and muscle contraction (**Figure 4B**).

A

B

Tissue	GO biological process category	Fold enrichment	P value
Heart	cardiac muscle contraction	17.41	5.233E-10
	sarcomere organization	19.61	1.223E-07
	transport	2.04	1.889E-06
	regulation of anion transport	42.21	3.443E-06
	positive regulation of organelle organization	75.97	8.808E-06
Muscle	muscle contraction	35.08	1.419E-15
	positive regulation of protein localization to Cajal body	101.21	1.098E-09
	regulation of muscle contraction	41.07	1.288E-08
	positive regulation of telomerase RNA localization to Cajal body	53.98	5.651E-08
	Positive regulation of establishment of protein localization to telomere	74.97	3.426E-07
Common	muscle contraction	24.47	2.702E-09
	glycolytic process	22.66	6.04E-06
	muscle organ development	12.95	9.618E-05
	mitochondrial electron transport, ubiquinol to cytochrome c	41.83	0.0001
	regulation of the force of heart contraction	23.64	0.0006

Figure 3: DAVID analysis of RAFs from muscle-type tissue. (A) Venn diagram showing shared and specific RAFs between the heart and the brain. The number of potential RAFs in each organ is indicated between brackets. (B) Table showing the GO terms enriched specifically in each brain region.

Surprisingly, in some organs such as the heart, muscle and retina, suspected RAFs contribute tissue functions such as contraction or photoreceptor cell maintenance. This further supports the hypothesis that the translation complex could directly contribute to regulating translation and also cell functions. Knowing that RAFs, as any other proteins, also undergo PTM modifications, it would be interesting to understand how they can modulate the functions

of the translational complex and impact tissue specialisation. We still need to confirm interactions between the ribosomes and RAFs through co-immunoprecipitation and also investigate its contribution to translation and specific functions.

3. Preliminary results on Ribosome modulation in CNS axonal regeneration

Axons from the adult mammalian central nervous system are unable to regenerate. As a consequence, any lesion will eventually lead to neuron death. This absence of regeneration is due to extrinsic factors, i.e. the inhibitory environment and intrinsic factors, i.e. the internal program in neurons that prevent regeneration (Kaplan et al., 2015). Many factors that influence regeneration have been identified such as STAT3, Myc, PTEN and Krüppel-like transcription factors (Park et al., 2008; Moore et al., 2009; Smith et al., 2009; Sun et al., 2011; Qin et al., 2013; Belin et al., 2015). The main focus was on the transcriptional regulation of regeneration but more points towards the translational regulation of regeneration. Interestingly, myc and PTEN are also involved in translation regulation by regulating ribosomes biogenesis.

Ribosomes are macro-complexes composed of about 90 ribosomal proteins and 4 rRNA molecules. Once thought to be of fixed composition, increasing amounts of evidence seems to point towards the specialisation. For example, RPL38 is known to regulate *Hox* mRNA expression during development (Kondrashov et al., 2011). Shigeoka and colleagues show that there is an on-site expression of both RPs when growth is stimulated (Shigeoka et al., 2019). We therefore hypothesised that the expression of these RPs could favour cell growth after axotomy. RPL22 was downregulated upon CNS injury (Belin et al., 2015). We were also interested in the 2'-O-methylation (2'OMe) levels. Changing the level of 2'OMe has impact on the translation abilities of ribosomes (Erales et al., 2017). 2'OMe affect IRES mediated translation (Erales et al., 2017; Yi et al., 2021). IRES mediated translation is favoured during cell stress (Spriggs et al., 2008).

We used the model of the retinal ganglion cells (RGCs) and the optic nerve to investigate the role of ribosomal proteins and 2'OMe in axon regeneration and neuronal survival of CNS neurons. RGCs form the innermost layer of the retina and are the only cells projecting through the optic nerve to the brain. By crushing the optic nerve, we impact a specific cell population. We can therefore analyse the effect of candidate molecules on regeneration and cell survival.

Material and method

Mice

Wild-type (WT) adult (6 week-to 10-week-old) mice were used in this study, regardless of sex. All the in vivo experiments were performed in accordance with our ethics protocol approved by the institution, local ethics committee and the French and European guidelines (APAFIS#9145-201612161701775v3 and APAFIS#26565-2020061613307385v3).

Intravitreal injection

4-week-old mice were anesthetised and intravitreally injected with AAV2-RPS4X-flag, AAV2-RPS14-flag, AAV2-RPL22-flag, AAV2-fibrillarin-flag or AAV2-fibrillarinK265A-flag (diluted in PBS, titers: 1.0-1.5 x 10^{12}). To do so, the external edge of the eye was clamped using a mini bulldog serrefines clamp (FST) to display the conjunctiva. 1µl of AAV2-RPx-flag or CTB-555 (1mg/mL) was injected into the vitreous cavity using a glass micropipette connected to a Hamilton syringe (Park et al., 2008; Schaeffer et al., 2020). One day before sacrifice, 1µl of CTB-555 (Cholera toxin subunit B, Alexa Fluor 555-conjugated, ThermoFisher Scientific; 1mg/mL) was injected into the vitreous cavity using the same procedure.

Optic nerve injury

6-week-old mice were anesthetized with intraperitoneal injection of ketamine (60–100 mg/kg) and xylazine (5–10 mg/kg). A mini bulldog serrefines clamp was placed to display the conjunctiva. The conjunctiva was incised lateral to the cornea. The refractor bulbi muscles were gently separated and the optic nerve was crushed with forceps (Drumont #5 FST) at 1mm from the eyeball during 5 seconds (Park et al., 2008; Schaeffer et al., 2020)

Intracardial perfusion

At 8 weeks, mice were anesthetized as described above, then intracardially perfused with ice-cold PBS for 3min and with ice-cold 4% formaldehyde in PBS for 3min. Eye and optic nerves were dissected out and samples were post-fixed overnight at 4°C in 4% formaldehyde.

Optic nerve clarification

Optic nerve clarification was performed as described (Dodt et al., 2007; Schaeffer et al., 2020). After intracardial perfusion and post-fixation of the eyes, optic nerves were dissected and dehydrated in ethanol. Optic nerves were incubated for 2hours in hexane, then transparized in benzyl benzoate/benzyl alcohol (2:1) (Sigma-Aldrich). Optic nerves were imaged using a spinning disk confocal microscope (Andor Dragonfly).

Imaging of axon regeneration

Imaging of optic nerve was performed as described before using a spinning disk confocal microscope (Andor Dragonfly) (Schaeffer et al., 2020). Z stacks were acquired every 2µm to scan the entire width of the cleared optic nerves. Here, a custom stitching module in MetaMorph to stitch images with 10% overlap was used. Maximum z projection of stacks was generated using ImageJ to visualize and quantify axon regeneration.

Axon Regeneration Quantification

Quantification was performed as described previously (Schaeffer et al., 2020). On a maximum z projection image (16-bit image), the injury site was manually defined with a straight line as the site where CTB labelling drops in intensity in the optic nerve. The fluorescence intensity profile was measured at specific distances from the injury site (e.g.,200, 500, 750, 1000, 1500, 2000, 2500, and 3000µm) along a central line manually drawn orthogonally to the optic nerve. The background measurement was made by measuring the intensity profile in a region with no regeneration. the integrated fluorescence intensity was calculated at each distance using R software and normalize to the optic nerve width at each distance. This integrated intensity was then normalised to the maximal intensity value of all distances in the regenerating region to account for variations between optic nerves. Finally, the normalised integrated intensity of background is removed from the normalized integrated intensity at each distance.

Immunofluorescence and imaging

Samples were post-fixed in 4% formaldehyde (Sigma) overnight at 4°C. The next day, they were washed 3 times in PBS 1X and blocked for 1h with 3% BSA, 0.1% PBS-Triton. They were then incubated with the following primary antibodies diluted in the blocking solution, overnight at 4°C: anti-flag (1:100, mouse, Sigma), anti-RBPMS (1:100, guinea pig, Millipore). This was followed by incubation with Alexa-fluor conjugated (anti-guinea pig, Jackson; anti-Mouse, Invitrogen) antibodies according to standard protocol (dilution 1:200). Slides were mounted with Fluoromount-G (ThermoFisher Scientific). Retina was imaged under an epifluorescence microscope Nikon Ti Eclipse.

Results and discussion

To understand the role of each RP or 2'OMe on regeneration, we establish a workflow (**Figure 1**). Each candidate is cloned in a plasmid and tested in vitro for expression and integration in cytoplasmic ribosomes. The adeno-associated virus 2 (AAV2) construct containing the validated RP construct was then produced and tested by injection in the intravitreal cavity of 4-week-old mice. AAV2 has a specificity for RGCs. The threshold for a correct viral efficacy was set at 95% of infection (**Figure 2B**). The optic nerve was crushed 2 weeks later. Axon regeneration and RGC survival was measured 2 weeks post-crush.

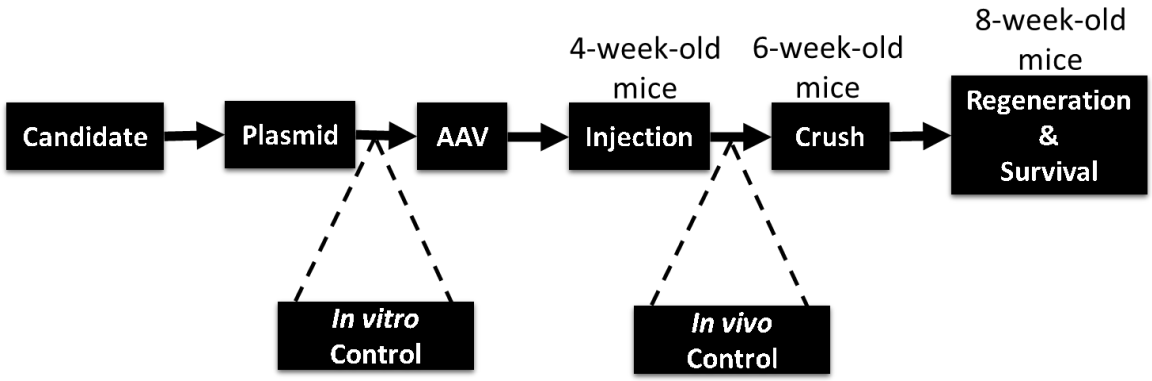

Figure 1: Workflow to test the influence of modulating RP or 2'OMe on regeneration and cell survival

Influence of single RPs modulation on axonal regeneration and cell survival

We followed the workflow described above. After ensuring that the constructs were correctly expressed, we measured RGC survival between control which was PLAP and in conditions were an RP is overexpressed. Quantification revealed that RGC survival was not affected upon RPS4X or RPS14 overexpression (**Figure 2B, 2C**). No difference was detected between the 2 conditions and their control. On the other hand, overexpressing RPL22 caused a significant decrease in RGC cell survival (**Figure 2B**). Preliminary results obtained by dual luciferase assay revealed that this mechanism could be linked to an increase in p53 levels upon increase in RPL22 levels (data not shown).

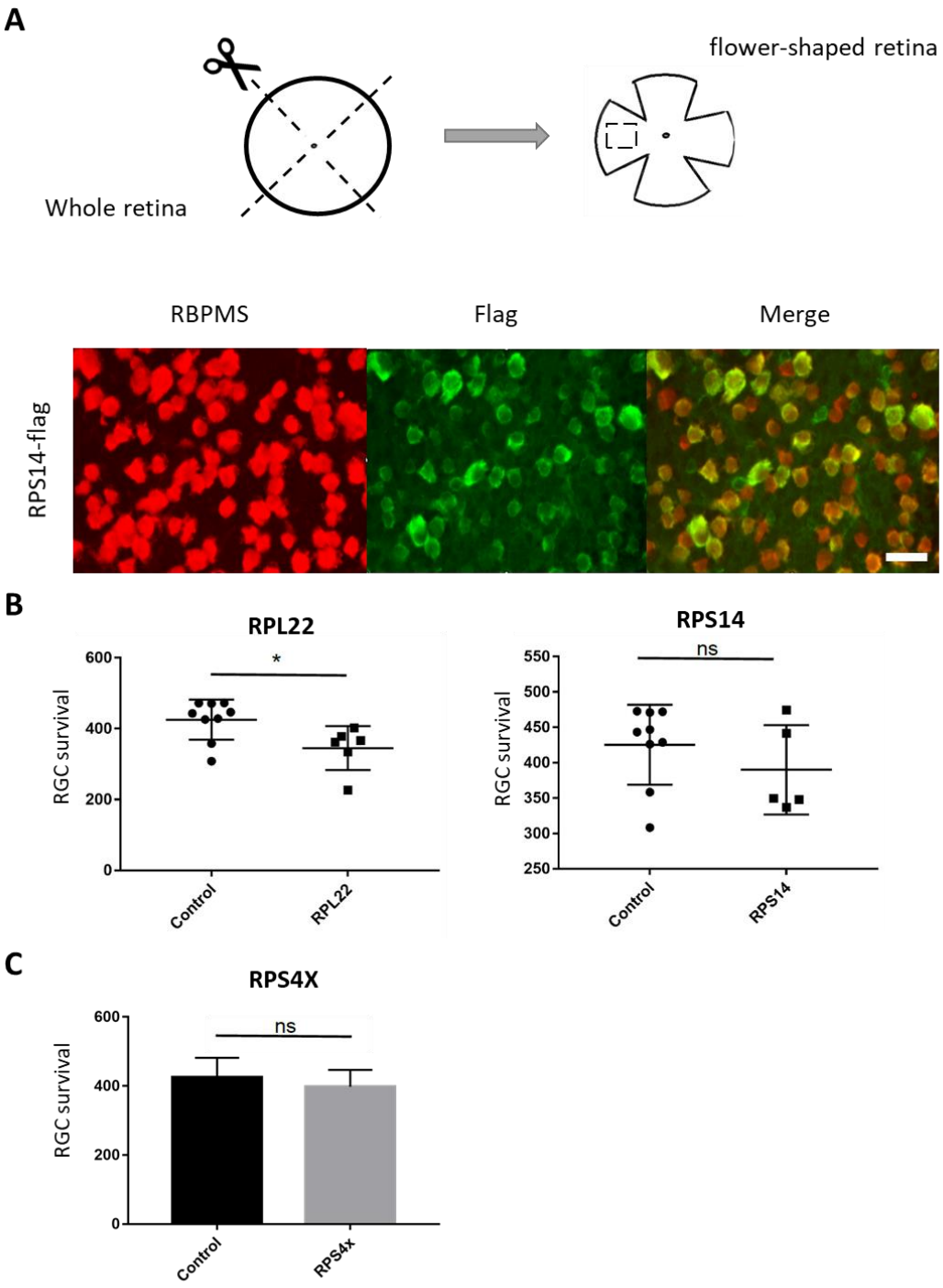

Figure 2: Influence of RP on RGCs survival. (A) the cup-shaped retina is cut open for observation under microscope. 95% infection rate of the RPS14 construct. RBPMS (red) is an RGC marker. Flagged RP (green) is expressed in RGCs. Scale bar = 50µm. (C and D) Plot and bar chart showing Quantification of RGC survival as measured by RBPMS staining 14 days post injury (Student test, *p<0.5, control: n=8 ; RP : n=5, Error bars indicate SEM)

We also investigated axonal regeneration. We use CTB conjugated with Alexa 555 to stain the axons (**Figure 3A**). RPS4X and RPS14 seem to slightly promote axonal regeneration but this increase was not significant. It is possible that each RP, on their own, cannot significantly change the translation program to produce short or long-distance regeneration. Testing the collective modulation of RPs by overexpressing RPS4X, RPS14, RPL22 could collectively induce sufficient changes in the translatome to influence regeneration.

Influence of fibrillarin overexpression on axonal regeneration and cell survival

Similarly, to analyse the effects of 2'O methylations on regeneration, we overexpressed AAV2-Fibrillarin-flag (Fib), or an inactive mutant AAV2-FibrillarinK265A-flag (K265A). AAV2-PLAP was used as control. The AAV was injected in 4-week-old mice. 2 weeks after infection, the optic nerve was crushed. Axons are then allowed to regenerate for 2 weeks. Before sacrificing the mice, CTB-555 was injected intravitreally to stain axons. Quantification of RGCs showed that there was no significant difference in RGC survival upon increase of 2'OMe. Surprisingly, we got contradicting results when overexpressing fibrillarin on regeneration. In our first experiment, more regenerating axons were observed in the Fib condition compared to PLAP. This effect was lost in the K265 condition. The second experiment had an unexpected outcome. In fact, all the previously observed effects were abrogated. The only difference noted between the two experiments was the difference in AAV2-fibrillarin-flag virus titers as it was more concentrated in the second experiment. However, up till now, there has been no published data on a dose-dependent effect of fibrillarin. Further experiment will be required to confirm a dose dependent effect of 2'OMe that could influence cellular functions.

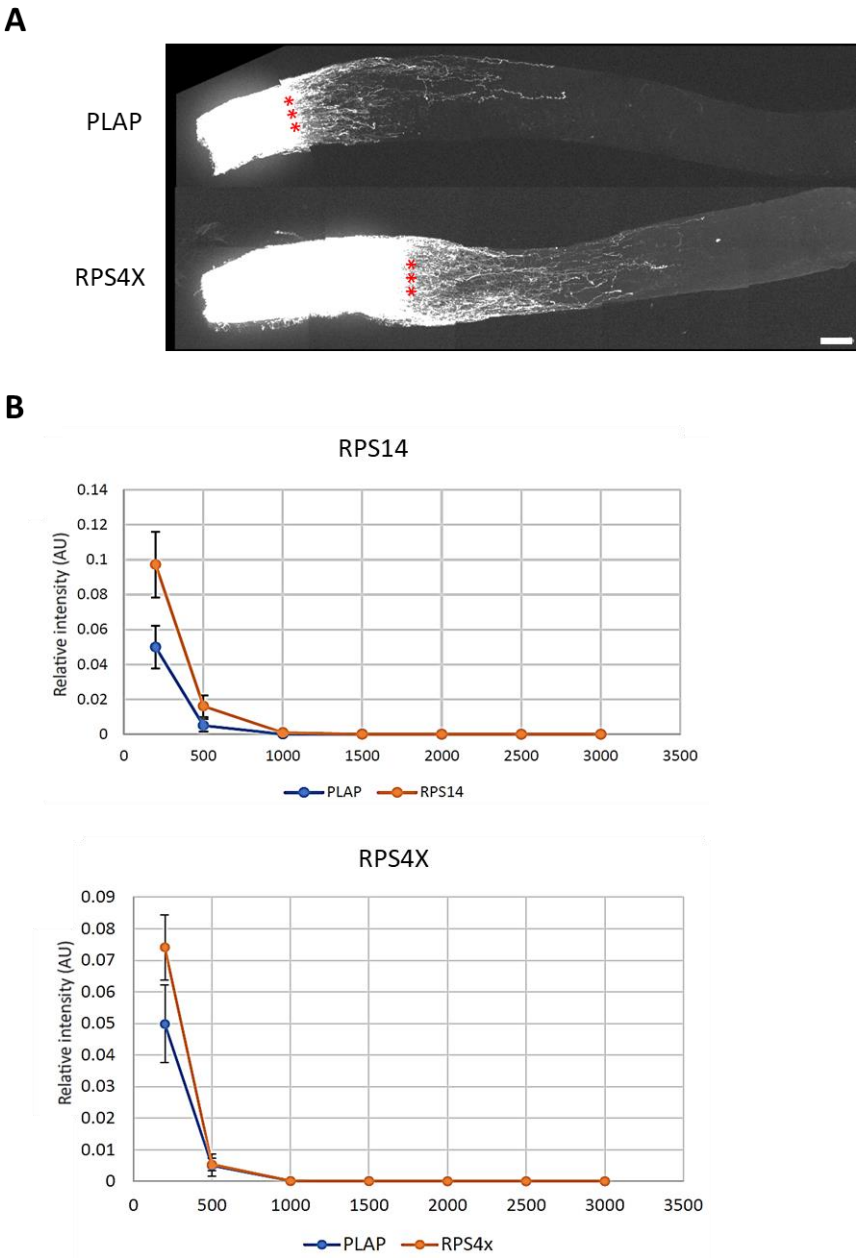

Figure 3: Influence of RP on axon regeneration. (A) Representative confocal images of the optic nerve sections from WT mice (infected with AAV2-PLAP or AAV2-RPS4X. Axons are labelled with CTB. Red stars indicate the crush site. Scale bar, 100 μm. (B) Quantification of axon regeneration (integrated intensity). Data expressed as mean for each condition. (Student test, *p<0.5, control : n=8 ; RP : n=5, Error bars indicate SEM)

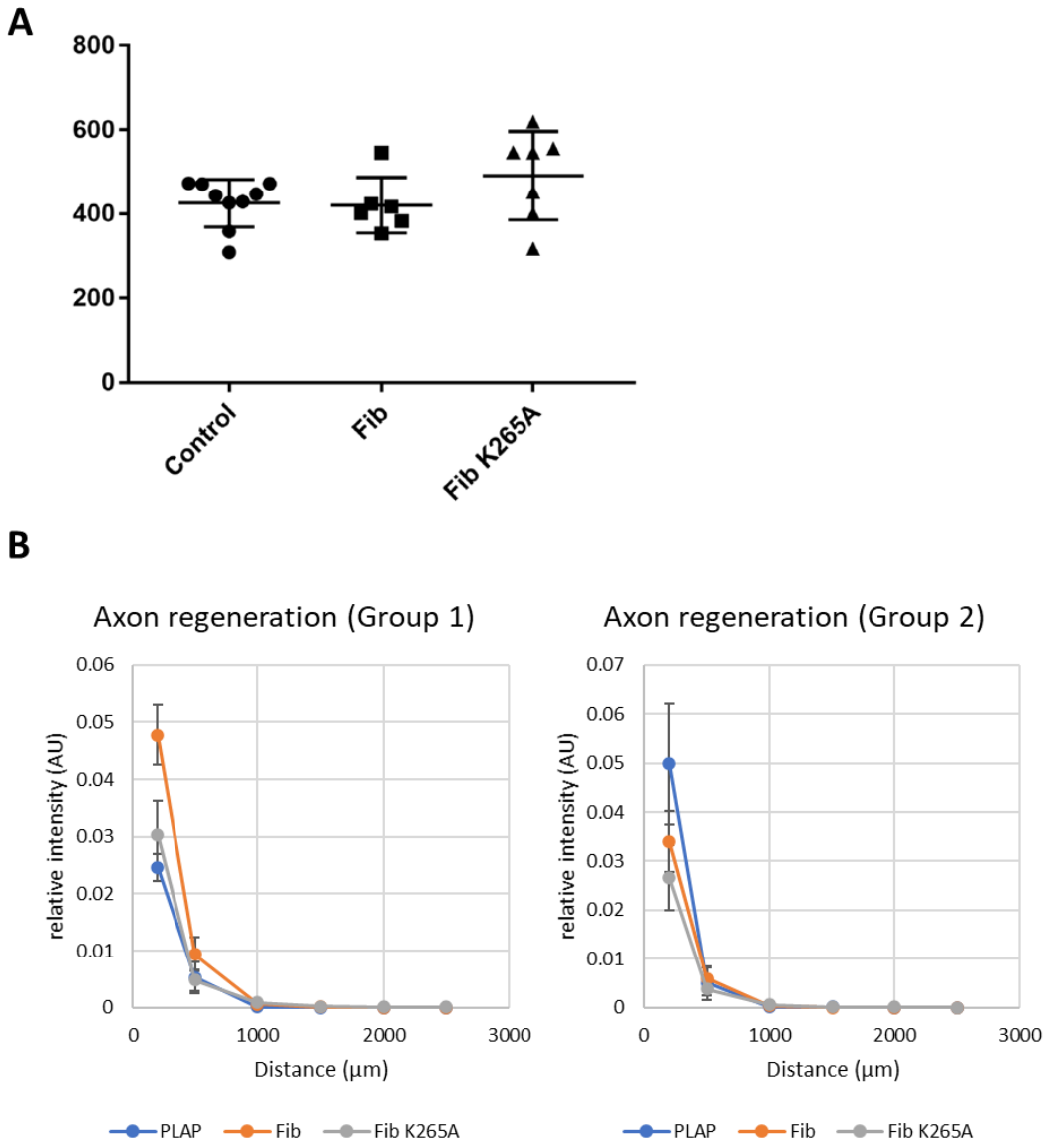

Figure 4: Influence of increasing 2'OMe on RGCs survival and axonal regeneration. (A) Quantification of RGC survival as measured by RBPMS staining 14 days post injury (ANOVA test, control: n=9; Fibrillarin: n=6; K265A: n=7, Error bars indicate SEM) (B) Quantification of axon regeneration (integrated intensity). Data expressed as mean for each condition. (ANOVA test, Groupe 1: control: n=5; Fibrillarin: n=5; K265A: n=6; Group 2: control: n=9; Fibrillarin: n=6; K265A: n=7, Error bars indicate SEM)

Discussion & Conclusion

Ribosomal heterogeneity in physiological conditions.

The ribosome is a 4.3 MDa complex composed of about 80 RP. Most RP are located on the solvent side while very few are located at the subunit interface. Even nowadays, studies still question if ribosomes, and more precisely RP are differentially expressed (Amirbeigiarab et al., 2019; Kyritsis et al., 2020). There were reasonable doubts remaining as most studies used transcriptomic analysis or were made *in vitro* (Slavov et al., 2015; Shi et al., 2017). There was a need of a clearer picture of the composition of ribosomes *in vivo*.

By comparing the ribosomes of 14 different tissues and organs, we identified stable and variable RP. We verified 2 stable and 10 variable RPs by absolute quantification. We confirmed the enrichment of RPL3L, RPL10L, RPL39L, depletion of RPL3, RPL10, variations of RPLP2, RPS30. However, no variation was detected with RPS26, RPS2. We also verified the correlation by comparing our proteomic data with available transcriptomic data. While some RP showed a good level of correlation between protein and transcript level (e.g. RPS3, RPL7A, RPL34), other showed less correlation (e.g. RPLP0, RPS26)

- **What are the structural implications of stable and variable RPs?**

We showed that nearly 75% of RP do not show any variation. They are localised mostly on the solvent side, probably constituting the basic structure of the ribosomes and have a role in stabilising the ribosomal architecture. These RP probably contribute to the basic translating functions of the ribosomes such as mRNA recognition, scanning and protein quality control. Examples of the stable RPs are RACK1, RPL10A and RPS14. RACK1 regulates translation by recruiting protein kinase C which is known to prevent initiation factor eIF6 from binding to the ribosome (Grosso et al., 2008). However our results cannot eliminate the probability of a preferential distribution of these proteins among monosomes or polysomes as all ribosomes were collectively analysed (Slavov et al., 2015).

The remaining 25% of RPs showed variations supporting the idea that there is a sub-stoichiometric distribution of RP within ribosomes (Slavov et al., 2015; Shi et al., 2017). Only one RP from our study, RPL10, shared the same depletion with the study from Shi and colleagues on mouse embryonic stem cells. No significant variations were detected with

RPL10A, RPL11, RPL38, RPL40, RPS7 and RPS25 underlining the difference between the stem cells and the mature organs (Shi et al., 2017). However, in their 2017 study, Shi and colleagues used only 1 peptide for RPL38, RPL40 and RPS7, 3 of the 6 RP showing variations. Based on our observations, a major difficulty in absolute quantification is that peptides from the same protein did not necessarily give same quantitative results due to difficulties in solubilising the peptides in the solvents or peptide stability issues. Therefore, it would be safe to take critical with results based on a single peptide. A better but costly solution is to use labelled proteins instead of labelled peptides. RPL38, that are required at specific steps during mice development (Kondrashov et al., 2011), showed no variation in adult mice suggesting that there is a regulation in space and time.

Most of these variable RP are only present in eukaryotes. Here, we show that RPL10L, RPL3L, RPL39L and RPS4L have tissue-specific variations(Rohozinski et al., 2009; Sugihara et al., 2010; Chaillou et al., 2013; Sugihara et al., 2013). We also show that these RPs are integrated into functional ribosomes *in vivo*. Some paralogs show a tissue-specific balance between pairs such as RPL10/RPL10L and RPL3/RPL3L. We confirm that RPS4L is mostly expressed in the testis (Sugihara et al., 2013). These paralogs share a high homology between the sequences and therefore have only slight differences in the primary to the quaternary structures. They are thought to occupy the same position in the ribosome even if this is only verified for RPL10 and RPL10L.

When focussing on the location of the variable RP, they are located at near the A site (RPS23/uS12, RPS27A/eS31, RPS30/eS30, RPL3/eL3, RPL3L/eL3-like), at the P-site (RPS27A/eS31, RPL10/uL16, RPL10L/uL16-like) or near the E site (RPL36/eL36, RPL36A/aL42). The location of these RP implies that they can have a direct effect on translation and impact the interaction between tRNA and mRNA. The presence of one RP creates conformational changes that can bring the tRNA closer to the PTC thus speeding up the polymerisation of amino acids. It also influences the accommodation of tRNA in the A-site or recognition of mRNA such as RPS26-depleted ribosomes in the recognition of stress-response pathway mRNA (Ferretti et al., 2017) . The position of RPL3/eL3 or RPL3L/eL3-like at the entrance for instance can modify the interaction of the tRNA with the decoding centre. During the decoding process, stronger interaction between tRNA and mRNA due to a specific RP environment can leave less options for the womble base recognition thus ensuring a higher fidelity in translation and a lower error rate.

To go further, it would be interesting to understand how modulating the RPs close to the A, P and E sites affect tRNA transit in the ribosome. For example, RPL3/eL3 and RPL3L/eL3-like are both located at the entry of the A site and could therefore influence translation or mRNA recognition. An in vitro single-molecule assay has recently been described to follow eukaryotic cap-dependent translation initiation kinetics (Wang et al., 2020a). This technology is based on the translation of Firefly mRNA with 3xFlag in 5'. The initiation kinetics is determined based of the time taken for the flag to emerge from the ribosome and be recognised by flag antibodies.

Other variable RPs are located on the P-stalk (RPLP0uL10, RPLP1/P1 and RPLP2/P2) and at the exit of the NPET (RPL39/eL39, RPL39L/eL39-like). The consequences of having variable RPs on the P-stalk include a change in stress response. During cell stress, RPLP0/uL10 and the C-termini of RPLP1/P1 and RPLP2/P2 interact and activate GCN2, a kinase that will phosphorylate eIF2α (Wek, 2018; Inglis et al., 2019). The absence of the P-stalk will affect the cell's ability to respond to cellular stress. Similarly, changes in the shape of the NPET affect the ribosome-associated protein quality control, peptide exit and ultimately, the elongation cycle via interactions between the NPET and the PTC.

Finally, RPs have multiple interactions with other RP within each subunit, and in intersubunit bridges such as RPL5/uL18 from the central protuberance and RPS23/uS12. Therefore, any difference in RP composition will impact the neighbouring RPs. There is a cooperative conformational change to increase stability, translocation and tRNA release from the E site (Ning et al., 2014). A quick way of knowing which RPs are impacted is by using a three dimensional reconstruction model from cryo EM. Any molecule within 10 Å from the RP will be impacted by changes affecting the RP. The most accurate technique would be to generate cryo EM models to understand exactly how the structure is changed by the presence or absence of variable RP.

In our study, we highlighted a sub stoichiometric distribution of RPs across organs. The MS data were reprocessed to identify possible change in phosphorylation levels on RPs. It is important to note that the process of ribosomes purification was not optimised for the measurement of phosphorylated proteins. Yet, some RPS are specifically phosphorylated in one or two organs but not observed in others. Further experiments, optimised for the study of phosphorylated proteins are required to confirm these results. It would be interesting to

investigate if other PTMs such as methylations or ubiquitylation differ across the different tissues.

- **<u>What are the functional implications of the ribosome specialisation with respect to the TC?</u>**

A previous study concluded that there were no variations in RP composition across different parts of the brain (Amirbeigiarab et al., 2019). Our results contradict this conclusion by suggesting that there could be a ribosomal signature for some region of the central nervous system (retina, hippocampus, cortex and cerebellum). The signatures are summarised in the figure below.

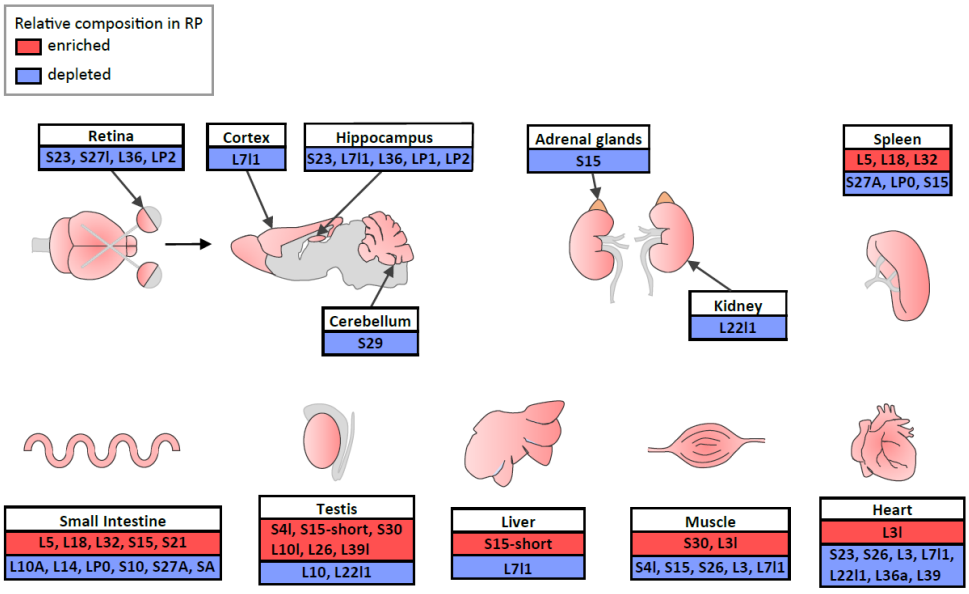

Summary of RP signature per organ. (From Brunchault et al., in preparation)

In literature, most RP signatures are not associated with any specific brain functions except for RPLP2/P2 which is suggested to be associated with synaptic plasticity and cognition in hippocampal cells (Tiwari et al., 2021). It would be interesting to see how the different signatures of ribosomes affect the translatome in the different brain regions. More importantly, the RP signature is also associated with regional differences in RAFs. With variations in RP and RAFs, it is very likely that rRNA 2'OMe levels are also different.

Till now, only few roles of variable RP have been identified. For instance, in the kidney, RPL22L1/eL22-like1 expression is associated with tumour progression in kidney renal clear cell carcinoma (Xiang et al., 2020). RPS15, RPL32 and RPLP0 are often used as reference when comparing the spleen with other organs (Hobbs et al., 1993; Peters et al., 2007; Wu et al., 2017; Kaur et al., 2018) but our results show that RPL32 enriched while RPS15 and RPLP0 are less expressed in the spleen and should not be used as reference.

Most of the variable RP in the intestine are already associated with a function. We validate RNA seq analysis by showing that RPS15 is highly expressed in intestinal cells thus partially confirming the intestinal RP signature (Mallik and Zhao, 2019). Low levels of RPL10A in the intestine is correlated with a decrease peripheral blood graft rejection in intestinal transplant patients (Andreev et al., 2011; Li et al., 2015) while alteration of RPS10 is often observed in colorectal carcinogenesis (Frigerio et al., 1995) It is suggested that mutations in RPSA is associated with the formation of idiopathic intestinal varices (Kerkhofs et al., 2020)

We identified low levels of RPS4L in muscles. Its expression is thought to be hypoxia-regulated and associated with proliferation of Hypoxic Pulmonary Artery Smooth Muscle Cells (Liu et al., 2020). To summarise, we have some insight on the contribution of RP to pathogenic events such as DBA, but analysis will be required to understand how the variable RP affects mRNA specificity, elongation rate and potentially error rate to match cell functions in physio-pathological conditions.

For example, we already know that the overexpressing RPL3L/eL3-like in muscle cell cultures decreases myoblast fusion (Chaillou et al., 2016). Sequencing and comparing the translatome of RPL3L/eL3-like with RPL3/eL3 overexpressing culture would give some understanding on the difference in translated mRNA subsets. These mRNA would probably be related to cell surface protein interaction, cell adhesion and myotube formation. Elongation rate can be used to monitor tRNA transit in the ribosome. RPL3/eL3 being at the entry of the A-site could probably affect translation initiation.

Lastly, a change RP can affect the riboproteome or ribointeractome, i.e. the factors interacting with the ribosome which will change furthermore the activity of the ribosomal complex (Reschke et al., 2013; Simsek et al., 2017)

How can insights on ribosome diversity *in vivo*, in physiological conditions be relevant in pathology?

The knowledge gained through the study of heterogeneity of ribosomes set the ground for the study of their dysregulation. Our preliminary results from the RP influence on regeneration and cell survival also pointed out that changing the expression of a single RP is probably not sufficient to change the translatome. This hypothesis can be supported by the fact that multiple RPs mutations are required to trigger the development of ribosomopathies. This is not limited to RP. We also investigate modulating rRNA 2'O methylations, by overexpressing fibrillarin and an inactive form K265A fibrillarin. Increase in 2'O methylations did promote short distance regeneration, but this regenerative effect seems to be lost upon high expression of fibrillarin. This suggests that there could be a balance that is required to promote regeneration.

Knowing the structure of a ribosome based on its composition can also help in drug development in the future. If we hypothesise that a ribosome with a specific RPs composition will, in theory, have a specific structure, we could use drug design to develop molecules that can decipher between different ribosomes and could target specific subsets of ribosomes.

- ## Hypothesis on the origins of ribosome heterogeneity & conclusion

There are different hypotheses to explain ribosome heterogeneity. If we look at the ribosome biogenesis, we know that the integration of RPs is driven by associated factors. If ribosome heterogeneity arises at this level, it implies firstly that there can be a difference at the RP transcription or translational. Yet, many organs had RP transcripts but showed no evidence that these mRNA were effectively translated into proteins. There could therefore be a selective translation of specific RP such as RPL39L and RPL3L. These RPs still need to be incorporated into the ribosome. For paralogs, there are 2 possibilities: either one of the paralogs is randomly integrated during assembly or a specific associated factor will bring the specific paralog to the pre-ribosomal particle. The first hypothesis is supported by our results was mRNA transcript mostly correlates with the levels of protein. There would therefore be a specific transcriptional program to determine the composition of the ribosomes. The second hypothesis would mean that there is a specific associated factor program that will lead to the production of specialised

ribosomes. Unfortunately, most studies focussed on the essential/non-essential nature of these factors on the production of pre-RNA intermediates rather than on specific functions of each factor. To distinguish between the two hypotheses, an interesting experiment would be to immunoprecipitated RP from nuclear fractions. Nuclear RP are RP that are integrated in the ribosome during biogenesis. If paralogs are randomly integrated to the ribosome, they both should be bound to the same assembly factors. Otherwise, different sets of assembly factors should be identified.

In the brain, we find that each region has a specific RP signature. In neurons, the composition of the ribosome can possibly be modulated through local translation and integration of locally synthesised RP (Shigeoka et al., 2019). This is an interesting mechanism for a rapid adaptation of the ribosome to the protein requirement of the cell at a given time. More studies are required to understand how a different RP composition affects neuronal transmission or plasticity.

This study opens the path for the study of RPs sub stoichiometric distribution *in vivo*, in the mouse model. However, there are some limits that remain to be cleared. We cannot rule out the presence of late 60S particles originating from the nuclei. Indeed, even if most ribosomes originate from the cytoplasm, minor nuclei rupture was observed during the purification of ribosomes. Secondly, our results were obtained on heterogeneous cell populations composing an organ or part of the organ. Yet the specialisation is observed at the level of RP but also at the level of RAFs.

Bibliography

Ackerman, E.J., Saxena, S.K., and Ulbrich, N. (1988). Alpha-sarcin causes a specific cut in 28 S rRNA when microinjected into Xenopus oocytes. J. Biol. Chem. *263*, 17076–17083.

Agmon, I., Auerbach, T., Baram, D., Bartels, H., Bashan, A., Berisio, R., Fucini, P., Hansen, H.A.S., Harms, J., Kessler, M., et al. (2003). On peptide bond formation, translocation, nascent protein progression and the regulatory properties of ribosomes. Derived on 20 October 2002 at the 28th FEBS Meeting in Istanbul. Eur. J. Biochem. *270*, 2543–2556.

Agmon, I., Bashan, A., Zarivach, R., and Yonath, A. (2005). Symmetry at the active site of the ribosome: structural and functional implications. Biol. Chem. *386*, 833–844.

Akai, N., Igaki, T., and Ohsawa, S. (2018). Wingless signaling regulates winner/loser status in Minute cell competition. Genes Cells Devoted Mol. Cell. Mech. *23*, 234–240.

Alberty, H., Raba, M., and Gross, H.J. (1978). Isolation from rat liver and sequence of a RNA fragment containing 32 nucleotides from position 5 to 36 from the 3' end of ribosomal 18S RNA. Nucleic Acids Res. *5*, 425–434.

Al-Hadid, Q., Roy, K., Chanfreau, G., and Clarke, S.G. (2016). Methylation of yeast ribosomal protein Rpl3 promotes translational elongation fidelity. RNA N. Y. N *22*, 489–498.

Allan Drummond, D., and Wilke, C.O. (2009). The evolutionary consequences of erroneous protein synthesis. Nat. Rev. Genet. *10*, 715–724.

Amirbeigiarab, S., Kiani, P., Velazquez Sanchez, A., Krisp, C., Kazantsev, A., Fester, L., Schlüter, H., and Ignatova, Z. (2019). Invariable stoichiometry of ribosomal proteins in mouse brain tissues with aging. Proc. Natl. Acad. Sci. U. S. A. *116*, 22567–22572.

Amsterdam, A., Sadler, K.C., Lai, K., Farrington, S., Bronson, R.T., Lees, J.A., and Hopkins, N. (2004). Many ribosomal protein genes are cancer genes in zebrafish. PLoS Biol. *2*, E139.

Anderson, S.J., Lauritsen, J.P.H., Hartman, M.G., Foushee, A.M.D., Lefebvre, J.M., Shinton, S.A., Gerhardt, B., Hardy, R.R., Oravecz, T., and Wiest, D.L. (2007). Ablation of ribosomal protein L22 selectively impairs alphabeta T cell development by activation of a p53-dependent checkpoint. Immunity *26*, 759–772.

Andreev, V.P., Tryphonopoulos, P., Blomberg, B.B., Tsinoremas, N., Weppler, D., Neuman, D.-R., Volsky, A., Nishida, S., Tekin, A., Selvaggi, G., et al. (2011). Peripheral blood gene expression analysis in intestinal transplantation: a feasibility study for detecting novel candidate biomarkers of graft rejection. Transplantation *92*, 1385–1391.

Andreou, A.Z., and Klostermeier, D. (2014). eIF4B and eIF4G jointly stimulate eIF4A ATPase and unwinding activities by modulation of the eIF4A conformational cycle. J. Mol. Biol. *426*, 51–61.

Angelini, M., Cannata, S., Mercaldo, V., Gibello, L., Santoro, C., Dianzani, I., and Loreni, F. (2007). Missense mutations associated with Diamond-Blackfan anemia affect the assembly of ribosomal protein S19 into the ribosome. Hum. Mol. Genet. *16*, 1720–1727.

Anger, A.M., Armache, J.-P., Berninghausen, O., Habeck, M., Subklewe, M., Wilson, D.N., and Beckmann, R. (2013). Structures of the human and Drosophila 80S ribosome. Nature *497*, 80–85.

Anosova, I., Melnik, S., Tripsianes, K., Kateb, F., Grummt, I., and Sattler, M. (2015). A novel RNA binding surface of the TAM domain of TIP5/BAZ2A mediates epigenetic regulation of rRNA genes. Nucleic Acids Res. *43*, 5208–5220.

Archer, S.K., Shirokikh, N.E., Beilharz, T.H., and Preiss, T. (2016). Dynamics of ribosome scanning and recycling revealed by translation complex profiling. Nature *535*, 570–574.

Armache, J.-P., Jarasch, A., Anger, A.M., Villa, E., Becker, T., Bhushan, S., Jossinet, F., Habeck, M., Dindar, G., Franckenberg, S., et al. (2010a). Localization of eukaryote-specific ribosomal proteins in a 5.5-Å cryo-EM map of the 80S eukaryotic ribosome. Proc. Natl. Acad. Sci. *107*, 19754–19759.

Armache, J.-P., Jarasch, A., Anger, A.M., Villa, E., Becker, T., Bhushan, S., Jossinet, F., Habeck, M., Dindar, G., Franckenberg, S., et al. (2010b). Cryo-EM structure and rRNA model of a translating eukaryotic 80S ribosome at 5.5-A resolution. Proc. Natl. Acad. Sci. U. S. A. *107*, 19748–19753.

Ashcroft, M., Kubbutat, M.H., and Vousden, K.H. (1999). Regulation of p53 function and stability by phosphorylation. Mol. Cell. Biol. *19*, 1751–1758.

Ashworth, A., Rastan, S., Lovell-Badge, R., and Kay, G. (1991). X-chromosome inactivation may explain the difference in viability of XO humans and mice. Nature *351*, 406–408.

Aspesi, A., and Ellis, S.R. (2019). Rare ribosomopathies: insights into mechanisms of cancer. Nat. Rev. Cancer *19*, 228–238.

Aspesi, A., Monteleone, V., Betti, M., Actis, C., Morleo, G., Sculco, M., Guarrera, S., Wlodarski, M.W., Ramenghi, U., Santoro, C., et al. (2017). Lymphoblastoid cell lines from Diamond Blackfan anaemia patients exhibit a full ribosomal stress phenotype that is rescued by gene therapy. Sci. Rep. *7*, 12010.

Audet-Walsh, É., Dufour, C.R., Yee, T., Zouanat, F.Z., Yan, M., Kalloghlian, G., Vernier, M., Caron, M., Bourque, G., Scarlata, E., et al. (2017). Nuclear mTOR acts as a transcriptional integrator of the androgen signaling pathway in prostate cancer. Genes Dev. *31*, 1228–1242.

Avni, D., Biberman, Y., and Meyuhas, O. (1997). The 5' terminal oligopyrimidine tract confers translational control on TOP mRNAs in a cell type- and sequence context-dependent manner. Nucleic Acids Res. *25*, 995–1001.

Avondo, F., Roncaglia, P., Crescenzio, N., Krmac, H., Garelli, E., Armiraglio, M., Castagnoli, C., Campagnoli, M.F., Ramenghi, U., Gustincich, S., et al. (2009). Fibroblasts from patients with Diamond-Blackfan anaemia show abnormal expression of genes involved in protein synthesis, amino acid metabolism and cancer. BMC Genomics *10*, 442.

Badhai, J., Schuster, J., Gidlöf, O., and Dahl, N. (2011). 5'UTR variants of ribosomal protein S19 transcript determine translational efficiency: implications for Diamond-Blackfan anemia and tissue variability. PloS One *6*, e17672.

Bai, D., Zhang, J., Xiao, W., and Zheng, X. (2014). Regulation of the HDM2-p53 pathway by ribosomal protein L6 in response to ribosomal stress. Nucleic Acids Res. *42*, 1799–1811.

Ban, N., Beckmann, R., Cate, J.H., Dinman, J.D., Dragon, F., Ellis, S.R., Lafontaine, D.L., Lindahl, L., Liljas, A., Lipton, J.M., et al. (2014). A new system for naming ribosomal proteins. Curr. Opin. Struct. Biol. *24*, 165–169.

Bandi, H.R., Ferrari, S., Krieg, J., Meyer, H.E., and Thomas, G. (1993). Identification of 40 S ribosomal protein S6 phosphorylation sites in Swiss mouse 3T3 fibroblasts stimulated with serum. J. Biol. Chem. *268*, 4530–4533.

Banerjee, S., Ferdosh, S., Ghosh, A.N., and Barat, C. (2020). Tau protein- induced sequestration of the eukaryotic ribosome: Implications in neurodegenerative disease. Sci. Rep. *10*, 5225.

Baouz, S., Woisard, A., Sinapah, S., Le Caer, J.-P., Argentini, M., Bulygin, K., Aguié, G., and Hountondji, C. (2009). The human large subunit ribosomal protein L36A-like contacts the CCA end of P-site bound tRNA. Biochimie *91*, 1420–1425.

Barak, Y., Juven, T., Haffner, R., and Oren, M. (1993). mdm2 expression is induced by wild type p53 activity. EMBO J. *12*, 461–468.

Bargis-Surgey, P., Lavergne, J.P., Gonzalo, P., Vard, C., Filhol-Cochet, O., and Reboud, J.P. (1999). Interaction of elongation factor eEF-2 with ribosomal P proteins. Eur. J. Biochem. *262*, 606–611.

Barlow, J.L., Drynan, L.F., Hewett, D.R., Holmes, L.R., Lorenzo-Abalde, S., Lane, A.L., Jolin, H.E., Pannell, R., Middleton, A.J., Wong, S.H., et al. (2010). A p53-dependent mechanism underlies macrocytic anemia in a mouse model of human 5q- syndrome. Nat. Med. *16*, 59–66.

Barna, M., Pusic, A., Zollo, O., Costa, M., Kondrashov, N., Rego, E., Rao, P.H., and Ruggero, D. (2008). Suppression of Myc oncogenic activity by ribosomal protein haploinsufficiency. Nature *456*, 971–975.

Barrio-Garcia, C., Thoms, M., Flemming, D., Kater, L., Berninghausen, O., Baßler, J., Beckmann, R., and Hurt, E. (2016). Architecture of the Rix1-Rea1 checkpoint machinery during pre-60S-ribosome remodeling. Nat. Struct. Mol. Biol. *23*, 37–44.

Baßler, J., and Hurt, E. (2019). Eukaryotic Ribosome Assembly. Annu. Rev. Biochem. *88*, 281–306.

Baudin-Baillieu, A., Tollervey, D., Cullin, C., and Lacroute, F. (1997). Functional analysis of Rrp7p, an essential yeast protein involved in pre-rRNA processing and ribosome assembly. Mol. Cell. Biol. *17*, 5023–5032.

Belin, S., Beghin, A., Solano-Gonzàlez, E., Bezin, L., Brunet-Manquat, S., Textoris, J., Prats, A.-C., Mertani, H.C., Dumontet, C., and Diaz, J.-J. (2009). Dysregulation of ribosome biogenesis and translational capacity is associated with tumor progression of human breast cancer cells. PloS One *4*, e7147.

Belin, S., Hacot, S., Daudignon, L., Therizols, G., Pourpe, S., Mertani, H.C., Rosa-Calatrava, M., and Diaz, J.-J. (2010). Purification of ribosomes from human cell lines. Curr. Protoc. Cell Biol. *Chapter 3*, Unit 3.40.

Belin, S., Nawabi, H., Wang, C., Tang, S., Latremoliere, A., Warren, P., Schorle, H., Uncu, C., Woolf, C.J., He, Z., et al. (2015). Injury-induced decline of intrinsic regenerative ability revealed by quantitative proteomics. Neuron *86*, 1000–1014.

Ben-Shem, A., Loubresse, N.G. de, Melnikov, S., Jenner, L., Yusupova, G., and Yusupov, M. (2011). The Structure of the Eukaryotic Ribosome at 3.0 Å Resolution. Science *334*, 1524–1529.

Berry, F.B., and Brown, I.R. (1996). CaM I mRNA is localized to apical dendrites during postnatal development of neurons in the rat brain. J. Neurosci. Res. *43*, 565–575.

Bhavsar, R.B., Makley, L.N., and Tsonis, P.A. (2010). The other lives of ribosomal proteins. Hum. Genomics *4*, 327–344.

Biever, A., Valjent, E., and Puighermanal, E. (2015). Ribosomal Protein S6 Phosphorylation in the Nervous System: From Regulation to Function. Front. Mol. Neurosci. *8*.

Bobola, N., Jansen, R.P., Shin, T.H., and Nasmyth, K. (1996). Asymmetric accumulation of Ash1p in postanaphase nuclei depends on a myosin and restricts yeast mating-type switching to mother cells. Cell *84*, 699–709.

Boccaletto, P., and Bagiński, B. (2021). MODOMICS: An Operational Guide to the Use of the RNA Modification Pathways Database. Methods Mol. Biol. Clifton NJ *2284*, 481–505.

Bock, L.V., Kolář, M.H., and Grubmüller, H. (2018). Molecular simulations of the ribosome and associated translation factors. Curr. Opin. Struct. Biol. *49*, 27–35.

Bodian, D. (1965). A SUGGESTIVE RELATIONSHIP OF NERVE CELL RNA WITH SPECIFIC SYNAPTIC SITES. Proc. Natl. Acad. Sci. U. S. A. *53*, 418–425.

Bogdanov, A.A., Dontsova, O.A., Dokudovskaya, S.S., and Lavrik, I.N. (1995). Structure and function of 5S rRNA in the ribosome. Biochem. Cell Biol. Biochim. Biol. Cell. *73*, 869–876.

Bolze, A., Mahlaoui, N., Byun, M., Turner, B., Trede, N., Ellis, S.R., Abhyankar, A., Itan, Y., Patin, E., Brebner, S., et al. (2013). Ribosomal protein SA haploinsufficiency in humans with isolated congenital asplenia. Science *340*, 976–978.

Bonnal, S., Boutonnet, C., Prado-Lourenço, L., and Vagner, S. (2003). IRESdb: the Internal Ribosome Entry Site database. Nucleic Acids Res. *31*, 427–428.

Bøsling, J., Poulsen, S.M., Vester, B., and Long, K.S. (2003). Resistance to the peptidyl transferase inhibitor tiamulin caused by mutation of ribosomal protein l3. Antimicrob. Agents Chemother. *47*, 2892–2896.

Bou Samra, E., Buhagiar-Labarchède, G., Machon, C., Guitton, J., Onclercq-Delic, R., Green, M.R., Alibert, O., Gazin, C., Veaute, X., and Amor-Guéret, M. (2017). A role for Tau protein in maintaining ribosomal DNA stability and cytidine deaminase-deficient cell survival. Nat. Commun. *8*, 693.

Bouchard-Bourelle, P., Desjardins-Henri, C., Mathurin-St-Pierre, D., Deschamps-Francoeur, G., Fafard-Couture, É., Garant, J.-M., Elela, S.A., and Scott, M.S. (2020). snoDB: an interactive database of human snoRNA sequences, abundance and interactions. Nucleic Acids Res. *48*, D220–D225.

Boultwood, J., Fidler, C., Strickson, A.J., Watkins, F., Gama, S., Kearney, L., Tosi, S., Kasprzyk, A., Cheng, J.-F., Jaju, R.J., et al. (2002). Narrowing and genomic annotation of the commonly deleted region of the 5q- syndrome. Blood *99*, 4638–4641.

Brand, R.C., Klootwijk, J., Van Steenbergen, T.J., De Kok, A.J., and Planta, R.J. (1977). Secondary methylation of yeast ribosomal precursor RNA. Eur. J. Biochem. *75*, 311–318.

Brandman, O., and Hegde, R.S. (2016). Ribosome-associated protein quality control. Nat. Struct. Mol. Biol. *23*, 7–15.

Buchhaupt, M., Sharma, S., Kellner, S., Oswald, S., Paetzold, M., Peifer, C., Watzinger, P., Schrader, J., Helm, M., and Entian, K.-D. (2014). Partial methylation at Am100 in 18S rRNA of baker's yeast reveals ribosome heterogeneity on the level of eukaryotic rRNA modification. PloS One *9*, e89640.

Burnett, P.E., Barrow, R.K., Cohen, N.A., Snyder, S.H., and Sabatini, D.M. (1998). RAFT1 phosphorylation of the translational regulators p70 S6 kinase and 4E-BP1. Proc. Natl. Acad. Sci. U. S. A. *95*, 1432–1437.

Bursać, S., Brdovčak, M.C., Pfannkuchen, M., Orsolić, I., Golomb, L., Zhu, Y., Katz, C., Daftuar, L., Grabušić, K., Vukelić, I., et al. (2012). Mutual protection of ribosomal proteins L5 and L11 from degradation is essential for p53 activation upon ribosomal biogenesis stress. Proc. Natl. Acad. Sci. U. S. A. *109*, 20467–20472.

Caccamo, A., Branca, C., Talboom, J.S., Shaw, D.M., Turner, D., Ma, L., Messina, A., Huang, Z., Wu, J., and Oddo, S. (2015). Reducing Ribosomal Protein S6 Kinase 1 Expression Improves Spatial

Memory and Synaptic Plasticity in a Mouse Model of Alzheimer's Disease. J. Neurosci. Off. J. Soc. Neurosci. *35*, 14042–14056.

Cahill, N.M., Friend, K., Speckmann, W., Li, Z.-H., Terns, R.M., Terns, M.P., and Steitz, J.A. (2002). Site-specific cross-linking analyses reveal an asymmetric protein distribution for a box C/D snoRNP. EMBO J. *21*, 3816–3828.

Campbell, D.S., and Holt, C.E. (2001). Chemotropic Responses of Retinal Growth Cones Mediated by Rapid Local Protein Synthesis and Degradation. Neuron *32*, 1013–1026.

Candeias, M.M., Powell, D.J., Roubalova, E., Apcher, S., Bourougaa, K., Vojtesek, B., Bruzzoni-Giovanelli, H., and Fåhraeus, R. (2006). Expression of p53 and p53/47 are controlled by alternative mechanisms of messenger RNA translation initiation. Oncogene *25*, 6936–6947.

Cardenas, M.E., Cutler, N.S., Lorenz, M.C., Di Como, C.J., and Heitman, J. (1999). The TOR signaling cascade regulates gene expression in response to nutrients. Genes Dev. *13*, 3271–3279.

Carr, M.I., Roderick, J.E., Zhang, H., Woda, B.A., Kelliher, M.A., and Jones, S.N. (2016). Phosphorylation of the Mdm2 oncoprotein by the c-Abl tyrosine kinase regulates p53 tumor suppression and the radiosensitivity of mice. Proc. Natl. Acad. Sci. U. S. A. *113*, 15024–15029.

Casad, M.E., Abraham, D., Kim, I.-M., Frangakis, S., Dong, B., Lin, N., Wolf, M.J., and Rockman, H.A. (2011). Cardiomyopathy is associated with ribosomal protein gene haplo-insufficiency in Drosophila melanogaster. Genetics *189*, 861–870.

Chaillou, T., Lee, J.D., England, J.H., Esser, K.A., and McCarthy, J.J. (2013). Time course of gene expression during mouse skeletal muscle hypertrophy. J. Appl. Physiol. Bethesda Md 1985 *115*, 1065–1074.

Chaillou, T., Kirby, T.J., and McCarthy, J.J. (2014). Ribosome biogenesis: emerging evidence for a central role in the regulation of skeletal muscle mass. J. Cell. Physiol. *229*, 1584–1594.

Chaillou, T., Zhang, X., and McCarthy, J.J. (2016). Expression of Muscle-Specific Ribosomal Protein L3-Like Impairs Myotube Growth. J. Cell. Physiol. *231*, 1894–1902.

Chamond, N., Deforges, J., Ulryck, N., and Sargueil, B. (2014). 40S recruitment in the absence of eIF4G/4A by EMCV IRES refines the model for translation initiation on the archetype of Type II IRESs. Nucleic Acids Res. *42*, 10373–10384.

Chandramouli, P., Topf, M., Ménétret, J.-F., Eswar, N., Cannone, J.J., Gutell, R.R., Sali, A., and Akey, C.W. (2008). Structure of the Mammalian 80S Ribosome at 8.7 Å Resolution. Structure *16*, 535–548.

Chehab, N.H., Malikzay, A., Stavridi, E.S., and Halazonetis, T.D. (1999). Phosphorylation of Ser-20 mediates stabilization of human p53 in response to DNA damage. Proc. Natl. Acad. Sci. U. S. A. *96*, 13777–13782.

Chen, R., and Ehrke, G. (1976). The primary structure of the 5 S RNA binding protein L5 of Escherichia coli ribosomes. FEBS Lett. *69*, 240–245.

Chen, D., Zhang, Z., Li, M., Wang, W., Li, Y., Rayburn, E.R., Hill, D.L., Wang, H., and Zhang, R. (2007). Ribosomal protein S7 as a novel modulator of p53-MDM2 interaction: binding to MDM2, stabilization of p53 protein, and activation of p53 function. Oncogene *26*, 5029–5037.

Cheng, Z., Saito, K., Pisarev, A.V., Wada, M., Pisareva, V.P., Pestova, T.V., Gajda, M., Round, A., Kong, C., Lim, M., et al. (2009). Structural insights into eRF3 and stop codon recognition by eRF1. Genes Dev. *23*, 1106–1118.

Cheong, J.K., and Virshup, D.M. (2011). Casein kinase 1: Complexity in the family. Int. J. Biochem. Cell Biol. *43*, 465–469.

Chiarugi, V., Magnelli, L., and Gallo, O. (1998). Cox-2, iNOS and p53 as play-makers of tumor angiogenesis (review). Int. J. Mol. Med. *2*, 715–719.

Chiocchetti, A., Zhou, J., Zhu, H., Karl, T., Haubenreisser, O., Rinnerthaler, M., Heeren, G., Oender, K., Bauer, J., Hintner, H., et al. (2007). Ribosomal proteins Rpl10 and Rps6 are potent regulators of yeast replicative life span. Exp. Gerontol. *42*, 275–286.

Choi, S.H., Martinez, T.F., Kim, S., Donaldson, C., Shokhirev, M.N., Saghatelian, A., and Jones, K.A. (2019). CDK12 phosphorylates 4E-BP1 to enable mTORC1-dependent translation and mitotic genome stability. Genes Dev. *33*, 418–435.

Chou, C.-W., Tai, L.-R., Kirby, R., Lee, I.-F., and Lin, A. (2010). Importin β3 mediates the nuclear import of human ribosomal protein L7 through its interaction with the multifaceted basic clusters of L7. FEBS Lett. *584*, 4151–4156.

Chou, P.-C., Rajput, S., Zhao, X., Patel, C., Albaciete, D., Oh, W.J., Daguplo, H.Q., Patel, N., Su, B., Werlen, G., et al. (2020). mTORC2 Is Involved in the Induction of RSK Phosphorylation by Serum or Nutrient Starvation. Cells *9*, 1567.

Chowdhury, R., Sekirnik, R., Brissett, N.C., Krojer, T., Ho, C.-H., Ng, S.S., Clifton, I.J., Ge, W., Kershaw, N.J., Fox, G.C., et al. (2014). Ribosomal oxygenases are structurally conserved from prokaryotes to humans. Nature *510*, 422–426.

Cioni, J.-M., Lin, J.Q., Holtermann, A.V., Koppers, M., Jakobs, M.A.H., Azizi, A., Turner-Bridger, B., Shigeoka, T., Franze, K., Harris, W.A., et al. (2019). Late Endosomes Act as mRNA Translation Platforms and Sustain Mitochondria in Axons. Cell *176*, 56-72.e15.

Claypool, J.A., French, S.L., Johzuka, K., Eliason, K., Vu, L., Dodd, J.A., Beyer, A.L., and Nomura, M. (2004). Tor pathway regulates Rrn3p-dependent recruitment of yeast RNA polymerase I to the promoter but does not participate in alteration of the number of active genes. Mol. Biol. Cell *15*, 946–956.

Cornish, P.V., Ermolenko, D.N., Staple, D.W., Hoang, L., Hickerson, R.P., Noller, H.F., and Ha, T. (2009). Following movement of the L1 stalk between three functional states in single ribosomes. Proc. Natl. Acad. Sci. U. S. A. *106*, 2571–2576.

Correll, C.C., Munishkin, A., Chan, Y.-L., Ren, Z., Wool, I.G., and Steitz, T.A. (1998). Crystal structure of the ribosomal RNA domain essential for binding elongation factors. Proc. Natl. Acad. Sci. *95*, 13436–13441.

Couté, Y., Burgess, J.A., Diaz, J.-J., Chichester, C., Lisacek, F., Greco, A., and Sanchez, J.-C. (2006). Deciphering the human nucleolar proteome. Mass Spectrom. Rev. *25*, 215–234.

Couté, Y., Kindbeiter, K., Belin, S., Dieckmann, R., Duret, L., Bezin, L., Sanchez, J.-C., and Diaz, J.-J. (2008). ISG20L2, a novel vertebrate nucleolar exoribonuclease involved in ribosome biogenesis. Mol. Cell. Proteomics MCP *7*, 546–559.

Cox, L.J., Hengst, U., Gurskaya, N.G., Lukyanov, K.A., and Jaffrey, S.R. (2008). Intra-axonal translation and retrograde trafficking of CREB promotes neuronal survival. Nat. Cell Biol. *10*, 149–159.

Crepin, T., Shalak, V.F., Yaremchuk, A.D., Vlasenko, D.O., McCarthy, A., Negrutskii, B.S., Tukalo, M.A., and El'skaya, A.V. (2014). Mammalian translation elongation factor eEF1A2: X-ray structure and new features of GDP/GTP exchange mechanism in higher eukaryotes. Nucleic Acids Res. *42*, 12939–12948.

Crick, F.H., Barnett, L., Brenner, S., and Watts-Tobin, R.J. (1961). General nature of the genetic code for proteins. Nature *192*, 1227–1232.

de la Cruz, J., Karbstein, K., and Woolford, J.L. (2015). Functions of Ribosomal Proteins in Assembly of Eukaryotic Ribosomes In Vivo. Annu. Rev. Biochem. *84*, 93–129.

Curinha, A., Braz, S.O., Pereira-Castro, I., Cruz, A., and Moreira, A. (2014). Implications of polyadenylation in health and disease. Nucleus *5*, 508–519.

Dabbs, E.R. (1986). Mutant Studies on the Prokaryotic Ribosome. In Structure, Function, and Genetics of Ribosomes, B. Hardesty, and G. Kramer, eds. (New York, NY: Springer), pp. 733–748.

D'Allard, D.L., and Liu, J.M. (2016). Toward RNA Repair of Diamond Blackfan Anemia Hematopoietic Stem Cells. Hum. Gene Ther. *27*, 792–801.

Dameshek, W. (1967). Riddle: what do aplastic anemia, paroxysmal nocturnal hemoglobinuria (PNH) and "hypoplastic" leukemia have in common? Blood *30*, 251–254.

Dao Duc, K., Batra, S.S., Bhattacharya, N., Cate, J.H.D., and Song, Y.S. (2019). Differences in the path to exit the ribosome across the three domains of life. Nucleic Acids Res. *47*, 4198–4210.

Das, F., Ghosh-Choudhury, N., Kasinath, B.S., and Choudhury, G.G. (2010). TGFβ enforces activation of eukaryotic elongation factor-2 (eEF2) via inactivation of eEF2 kinase by p90 ribosomal S6 kinase (p90Rsk) to induce mesangial cell hypertrophy. FEBS Lett. *584*, 4268–4272.

Dave, B., Granados-Principal, S., Zhu, R., Benz, S., Rabizadeh, S., Soon-Shiong, P., Yu, K.-D., Shao, Z., Li, X., Gilcrease, M., et al. (2014). Targeting RPL39 and MLF2 reduces tumor initiation and metastasis in breast cancer by inhibiting nitric oxide synthase signaling. Proc. Natl. Acad. Sci. U. S. A. *111*, 8838–8843.

Dave, B., Gonzalez, D.D., Liu, Z.-B., Li, X., Wong, H., Granados, S., Ezzedine, N.E., Sieglaff, D.H., Ensor, J.E., Miller, K.D., et al. (2017). Role of RPL39 in Metaplastic Breast Cancer. J. Natl. Cancer Inst. *109*.

De Keersmaecker, K., Atak, Z.K., Li, N., Vicente, C., Patchett, S., Girardi, T., Gianfelici, V., Geerdens, E., Clappier, E., Porcu, M., et al. (2013). Exome sequencing identifies mutation in CNOT3 and ribosomal genes RPL5 and RPL10 in T-cell acute lymphoblastic leukemia. Nat. Genet. *45*, 186–190.

Decatur, W.A., and Fournier, M.J. (2002). rRNA modifications and ribosome function. Trends Biochem. Sci. *27*, 344–351.

Destefanis, F., Manara, V., and Bellosta, P. (2020). Myc as a Regulator of Ribosome Biogenesis and Cell Competition: A Link to Cancer. Int. J. Mol. Sci. *21*, 4037.

Dever, T.E., and Green, R. (2012). The elongation, termination, and recycling phases of translation in eukaryotes. Cold Spring Harb. Perspect. Biol. *4*, a013706.

Dharia, A.P., Obla, A., Gajdosik, M.D., Simon, A., and Nelson, C.E. (2014). Tempo and Mode of Gene Duplication in Mammalian Ribosomal Protein Evolution. PLOS ONE *9*, e111721.

Doma, M.K., and Parker, R. (2006). Endonucleolytic cleavage of eukaryotic mRNAs with stalls in translation elongation. Nature *440*, 561–564.

Donati, G., Bertoni, S., Brighenti, E., Vici, M., Treré, D., Volarevic, S., Montanaro, L., and Derenzini, M. (2011). The balance between rRNA and ribosomal protein synthesis up- and downregulates the tumour suppressor p53 in mammalian cells. Oncogene *30*, 3274–3288.

Dutt, S., Narla, A., Lin, K., Mullally, A., Abayasekara, N., Megerdichian, C., Wilson, F.H., Currie, T., Khanna-Gupta, A., Berliner, N., et al. (2011). Haploinsufficiency for ribosomal protein genes causes selective activation of p53 in human erythroid progenitor cells. Blood *117*, 2567–2576.

Ebert, B.L., Pretz, J., Bosco, J., Chang, C.Y., Tamayo, P., Galili, N., Raza, A., Root, D.E., Attar, E., Ellis, S.R., et al. (2008). Identification of RPS14 as a 5q- syndrome gene by RNA interference screen. Nature *451*, 335–339.

Egebjerg, J., Douthwaite, S.R., Liljas, A., and Garrett, R.A. (1990). Characterization of the binding sites of protein L11 and the L10.(L12)4 pentameric complex in the GTPase domain of 23 S ribosomal RNA from Escherichia coli. J. Mol. Biol. *213*, 275–288.

Elder, M.K., Erdjument-Bromage, H., Oliveira, M.M., Mamcarz, M., Neubert, T.A., and Klann, E. (2021). Age-dependent shift in the de novo proteome accompanies pathogenesis in an Alzheimer's disease mouse model. Commun. Biol. *4*, 823.

Emmott, E., Jovanovic, M., and Slavov, N. (2019). Ribosome Stoichiometry: From Form to Function. Trends Biochem. Sci. *44*, 95–109.

Enroth, C., Poulsen, L.D., Iversen, S., Kirpekar, F., Albrechtsen, A., and Vinther, J. (2019). Detection of internal N7-methylguanosine (m7G) RNA modifications by mutational profiling sequencing. Nucleic Acids Res. *47*, e126.

Erales, J., Marchand, V., Panthu, B., Gillot, S., Belin, S., Ghayad, S.E., Garcia, M., Laforêts, F., Marcel, V., Baudin-Baillieu, A., et al. (2017). Evidence for rRNA 2'-O-methylation plasticity: Control of intrinsic translational capabilities of human ribosomes. Proc. Natl. Acad. Sci. U. S. A. *114*, 12934–12939.

Eshraghi, M., Karunadharma, P.P., Blin, J., Shahani, N., Ricci, E.P., Michel, A., Urban, N.T., Galli, N., Sharma, M., Ramírez-Jarquín, U.N., et al. (2021). Mutant Huntingtin stalls ribosomes and represses protein synthesis in a cellular model of Huntington disease. Nat. Commun. *12*, 1461.

Evans, H.T., Benetatos, J., van Roijen, M., Bodea, L.-G., and Götz, J. (2019). Decreased synthesis of ribosomal proteins in tauopathy revealed by non-canonical amino acid labelling. EMBO J. *38*, e101174.

Fabijanski, S., and Pellegrini, M. (1981). Identification of proteins at the peptidyl-tRNA binding site of rat liver ribosomes. Mol. Gen. Genet. MGG *184*, 551–556.

Fando, J.L., Salinas, M., and Wasterlain, C.G. (1980). Age-dependent changes in brain protein synthesis in the rat. Neurochem. Res. *5*, 373–383.

Fedorov, A.N., and Baldwin, T.O. (1997). Cotranslational protein folding. J. Biol. Chem. *272*, 32715–32718.

Fei, J., Kosuri, P., MacDougall, D.D., and Gonzalez, R.L. (2008). Coupling of ribosomal L1 stalk and tRNA dynamics during translation elongation. Mol. Cell *30*, 348–359.

Fernández-Pevida, A., Martín-Villanueva, S., Murat, G., Lacombe, T., Kressler, D., and de la Cruz, J. (2016). The eukaryote-specific N-terminal extension of ribosomal protein S31 contributes to the assembly and function of 40S ribosomal subunits. Nucleic Acids Res. *44*, 7777–7791.

Ferreira-Cerca, S., Pöll, G., Gleizes, P.-E., Tschochner, H., and Milkereit, P. (2005). Roles of Eukaryotic Ribosomal Proteins in Maturation and Transport of Pre-18S rRNA and Ribosome Function. Mol. Cell *20*, 263–275.

Ferretti, M.B., Ghalei, H., Ward, E.A., Potts, E.L., and Karbstein, K. (2017). Rps26 directs mRNA-specific translation by recognition of Kozak sequence elements. Nat. Struct. Mol. Biol. *24*, 700–707.

Fewell, S.W., and Woolford, J.L. (1999). Ribosomal protein S14 of Saccharomyces cerevisiae regulates its expression by binding to RPS14B pre-mRNA and to 18S rRNA. Mol. Cell. Biol. *19*, 826–834.

Filipek, K., Michalec-Wawiórka, B., Boguszewska, A., Kmiecik, S., and Tchórzewski, M. (2020). Phosphorylation of the N-terminal domain of ribosomal P-stalk protein uL10 governs its association with the ribosome. FEBS Lett. *594*, 3002–3019.

Finch, R.A., Donoviel, D.B., Potter, D., Shi, M., Fan, A., Freed, D.D., Wang, C.-Y., Zambrowicz, B.P., Ramirez-Solis, R., Sands, A.T., et al. (2002). mdmx is a negative regulator of p53 activity in vivo. Cancer Res. *62*, 3221–3225.

Finley, D., Bartel, B., and Varshavsky, A. (1989). The tails of ubiquitin precursors are ribosomal proteins whose fusion to ubiquitin facilitates ribosome biogenesis. Nature *338*, 394–401.

Fisher, E.M., Beer-Romero, P., Brown, L.G., Ridley, A., McNeil, J.A., Lawrence, J.B., Willard, H.F., Bieber, F.R., and Page, D.C. (1990). Homologous ribosomal protein genes on the human X and Y chromosomes: escape from X inactivation and possible implications for Turner syndrome. Cell *63*, 1205–1218.

Flygare, J., Aspesi, A., Bailey, J.C., Miyake, K., Caffrey, J.M., Karlsson, S., and Ellis, S.R. (2007). Human RPS19, the gene mutated in Diamond-Blackfan anemia, encodes a ribosomal protein required for the maturation of 40S ribosomal subunits. Blood *109*, 980–986.

Fortier, S., MacRae, T., Bilodeau, M., Sargeant, T., and Sauvageau, G. (2015). Haploinsufficiency screen highlights two distinct groups of ribosomal protein genes essential for embryonic stem cell fate. Proc. Natl. Acad. Sci. U. S. A. *112*, 2127–2132.

Fox, J.M., Rashford, R.L., and Lindahl, L. (2019). Co-Assembly of 40S and 60S Ribosomal Proteins in Early Steps of Eukaryotic Ribosome Assembly. Int. J. Mol. Sci. *20*, 2806.

Francou, A., and Anderson, K.V. (2020). The Epithelial-to-Mesenchymal Transition (EMT) in Development and Cancer. Annu. Rev. Cancer Biol. *4*, 197–220.

Frank, S.R., Schroeder, M., Fernandez, P., Taubert, S., and Amati, B. (2001). Binding of c-Myc to chromatin mediates mitogen-induced acetylation of histone H4 and gene activation. Genes Dev. *15*, 2069–2082.

Frigerio, J.M., Dagorn, J.C., and Iovanna, J.L. (1995). Cloning, sequencing and expression of the L5, L21, L27a, L28, S5, S9, S10 and S29 human ribosomal protein mRNAs. Biochim. Biophys. Acta *1262*, 64–68.

Fujii, K., Susanto, T.T., Saurabh, S., and Barna, M. (2018). Decoding the Function of Expansion Segments in Ribosomes. Mol. Cell *72*, 1013-1020.e6.

Furuichi, Y. (2015). Discovery of m(7)G-cap in eukaryotic mRNAs. Proc. Jpn. Acad. Ser. B Phys. Biol. Sci. *91*, 394–409.

Gabut, M., Bourdelais, F., and Durand, S. (2020). Ribosome and Translational Control in Stem Cells. Cells *9*, E497.

Gamalinda, M., Ohmayer, U., Jakovljevic, J., Kumcuoglu, B., Woolford, J., Mbom, B., Lin, L., and Woolford, J.L. (2014). A hierarchical model for assembly of eukaryotic 60S ribosomal subunit domains. Genes Dev. *28*, 198–210.

Gamerdinger, M., Kobayashi, K., Wallisch, A., Kreft, S.G., Sailer, C., Schlömer, R., Sachs, N., Jomaa, A., Stengel, F., Ban, N., et al. (2019). Early Scanning of Nascent Polypeptides inside the Ribosomal Tunnel by NAC. Mol. Cell *75*, 996-1006.e8.

Ganapathi, M., Argyriou, L., Martínez-Azorín, F., Morlot, S., Yigit, G., Lee, T.M., Auber, B., von Gise, A., Petrey, D.S., Thiele, H., et al. (2020). Bi-allelic missense disease-causing variants in RPL3L associate neonatal dilated cardiomyopathy with muscle-specific ribosome biogenesis. Hum. Genet. *139*, 1443–1454.

Gao, W., Li, Q., Zhu, R., and Jin, J. (2016). La Autoantigen Induces Ribosome Binding Protein 1 (RRBP1) Expression through Internal Ribosome Entry Site (IRES)-Mediated Translation during Cellular Stress Condition. Int. J. Mol. Sci. *17*, E1174.

García-Ortega, L., Alvarez-García, E., Gavilanes, J.G., Martínez-del-Pozo, A., and Joseph, S. (2010). Cleavage of the sarcin-ricin loop of 23S rRNA differentially affects EF-G and EF-Tu binding. Nucleic Acids Res. *38*, 4108–4119.

Gasse, L., Flemming, D., and Hurt, E. (2015). Coordinated Ribosomal ITS2 RNA Processing by the Las1 Complex Integrating Endonuclease, Polynucleotide Kinase, and Exonuclease Activities. Mol. Cell *60*, 808–815.

Gazda, H.T., Sheen, M.R., Vlachos, A., Choesmel, V., O'Donohue, M.-F., Schneider, H., Darras, N., Hasman, C., Sieff, C.A., Newburger, P.E., et al. (2008). Ribosomal protein L5 and L11 mutations are associated with cleft palate and abnormal thumbs in Diamond-Blackfan anemia patients. Am. J. Hum. Genet. *83*, 769–780.

Geerkens, C., Just, W., Held, K.R., and Vogel, W. (1996). Ullrich-Turner syndrome is not caused by haploinsufficiency of RPS4X. Hum. Genet. *97*, 39–44.

Gershman, B.W., Pritchard, C.E., Chaney, K.P., and Ware, V.C. (2020). Tissue-specific expression of ribosomal protein paralogue eRpL22-like in Drosophila melanogaster eye development. Dev. Dyn. Off. Publ. Am. Assoc. Anat. *249*, 1147–1165.

Gibbons, J.G., Branco, A.T., Yu, S., and Lemos, B. (2014). Ribosomal DNA copy number is coupled with gene expression variation and mitochondrial abundance in humans. Nat. Commun. *5*, 4850.

Giegé, R., Jühling, F., Pütz, J., Stadler, P., Sauter, C., and Florentz, C. (2012). Structure of transfer RNAs: similarity and variability. Wiley Interdiscip. Rev. RNA *3*, 37–61.

Gigova, A., Duggimpudi, S., Pollex, T., Schaefer, M., and Koš, M. (2014). A cluster of methylations in the domain IV of 25S rRNA is required for ribosome stability. RNA N. Y. N *20*, 1632–1644.

Gilbert, B.E., and Johnson, T.C. (1973). Mouse brain ribosomal subunits: role of ribosome-associated factors on aminoacyl-tRNA binding and polypeptide synthesis. Brain Res. *63*, 313–322.

Gill, J., Cashion, A., Osier, N., Arcurio, L., Motamedi, V., Dell, K.C., Carr, W., Kim, H.-S., Yun, S., Walker, P., et al. (2017). Moderate blast exposure alters gene expression and levels of amyloid precursor protein. Neurol. Genet. *3*, e186.

Gingras, A.-C., Gygi, S.P., Raught, B., Polakiewicz, R.D., Abraham, R.T., Hoekstra, M.F., Aebersold, R., and Sonenberg, N. (1999). Regulation of 4E-BP1 phosphorylation: a novel two-step mechanism. Genes Dev. *13*, 1422–1437.

Giraud, S., Greco, A., Brink, M., Diaz, J.J., and Delafontaine, P. (2001). Translation initiation of the insulin-like growth factor I receptor mRNA is mediated by an internal ribosome entry site. J. Biol. Chem. *276*, 5668–5675.

Godet, A.-C., David, F., Hantelys, F., Tatin, F., Lacazette, E., Garmy-Susini, B., and Prats, A.-C. (2019). IRES Trans-Acting Factors, Key Actors of the Stress Response. Int. J. Mol. Sci. *20*.

Goldfarb, K.C., and Cech, T.R. (2017). Targeted CRISPR disruption reveals a role for RNase MRP RNA in human preribosomal RNA processing. Genes Dev. *31*, 59–71.

Gomez-Roman, N., Grandori, C., Eisenman, R.N., and White, R.J. (2003). Direct activation of RNA polymerase III transcription by c-Myc. Nature *421*, 290–294.

Gonzalez, I., Buonomo, S.B., Nasmyth, K., and von Ahsen, U. (1999). ASH1 mRNA localization in yeast involves multiple secondary structural elements and Ash1 protein translation. Curr. Biol. CB *9*, 337–340.

de Graaf, P., Little, N.A., Ramos, Y.F.M., Meulmeester, E., Letteboer, S.J.F., and Jochemsen, A.G. (2003). Hdmx protein stability is regulated by the ubiquitin ligase activity of Mdm2. J. Biol. Chem. *278*, 38315–38324.

Graczyk, D., Cieśla, M., and Boguta, M. (2018). Regulation of tRNA synthesis by the general transcription factors of RNA polymerase III - TFIIIB and TFIIIC, and by the MAF1 protein. Biochim. Biophys. Acta Gene Regul. Mech. *1861*, 320–329.

Grandori, C., Gomez-Roman, N., Felton-Edkins, Z.A., Ngouenet, C., Galloway, D.A., Eisenman, R.N., and White, R.J. (2005). c-Myc binds to human ribosomal DNA and stimulates transcription of rRNA genes by RNA polymerase I. Nat. Cell Biol. *7*, 311–318.

Gray, P.N., Garrett, R.A., Stoffler, G., and Monier, R. (1972). An attempt at the identification of the proteins involved in the incorporation of 5-S RNA during 50-S ribosomal subunit assembly. Eur. J. Biochem. *28*, 412–421.

Green, K.M., Glineburg, M.R., Kearse, M.G., Flores, B.N., Linsalata, A.E., Fedak, S.J., Goldstrohm, A.C., Barmada, S.J., and Todd, P.K. (2017). RAN translation at C9orf72-associated repeat expansions is selectively enhanced by the integrated stress response. Nat. Commun. *8*, 2005.

Greenwood, J.A., and Johnson, G.V. (1995). Localization and in situ phosphorylation state of nuclear tau. Exp. Cell Res. *220*, 332–337.

Gregory, B., Rahman, N., Bommakanti, A., Shamsuzzaman, M., Thapa, M., Lescure, A., Zengel, J.M., and Lindahl, L. (2019). The small and large ribosomal subunits depend on each other for stability and accumulation. Life Sci. Alliance *2*, e201800150.

Grela, P., Szajwaj, M., Horbowicz-Drożdżal, P., and Tchórzewski, M. (2019). How Ricin Damages the Ribosome. Toxins *11*.

Gressner, A.M., and Wool, I.G. (1974). The phosphorylation of liver ribosomal proteins in vivo. Evidence that only a single small subunit protein (S6) is phosphorylated. J. Biol. Chem. *249*, 6917–6925.

Gromadski, K.B., and Rodnina, M.V. (2004). Kinetic Determinants of High-Fidelity tRNA Discrimination on the Ribosome. Mol. Cell *13*, 191–200.

Grosso, S., Volta, V., Sala, L.A., Vietri, M., Marchisio, P.C., Ron, D., and Biffo, S. (2008). PKCbetaII modulates translation independently from mTOR and through RACK1. Biochem. J. *415*, 77–85.

Grover, R., Ray, P.S., and Das, S. (2008). Polypyrimidine tract binding protein regulates IRES-mediated translation of p53 isoforms. Cell Cycle Georget. Tex *7*, 2189–2198.

Guetg, C., Lienemann, P., Sirri, V., Grummt, I., Hernandez-Verdun, D., Hottiger, M.O., Fussenegger, M., and Santoro, R. (2010). The NoRC complex mediates the heterochromatin formation and stability of silent rRNA genes and centromeric repeats. EMBO J. *29*, 2135–2146.

Guimaraes, J.C., and Zavolan, M. (2016). Patterns of ribosomal protein expression specify normal and malignant human cells. Genome Biol. *17*, 236.

Gunderson, J.H., Sogin, M.L., Wollett, G., Hollingdale, M., de la Cruz, V.F., Waters, A.P., and McCutchan, T.F. (1987). Structurally distinct, stage-specific ribosomes occur in Plasmodium. Science *238*, 933–937.

Gupta, V., and Warner, J.R. (2014). Ribosome-omics of the human ribosome. RNA *20*, 1004–1013.

Guzel, P., Yildirim, H.Z., Yuce, M., and Kurkcuoglu, O. (2020). Exploring Allosteric Signaling in the Exit Tunnel of the Bacterial Ribosome by Molecular Dynamics Simulations and Residue Network Model. Front. Mol. Biosci. *7*.

Hafner, A.-S., Donlin-Asp, P.G., Leitch, B., Herzog, E., and Schuman, E.M. (2019). Local protein synthesis is a ubiquitous feature of neuronal pre- and postsynaptic compartments. Science *364*.

Halaby, M.-J., Harris, B.R.E., Miskimins, W.K., Cleary, M.P., and Yang, D.-Q. (2015a). Deregulation of Internal Ribosome Entry Site-Mediated p53 Translation in Cancer Cells with Defective p53 Response to DNA Damage. Mol. Cell. Biol. *35*, 4006–4017.

Halaby, M.-J., Li, Y., Harris, B.R., Jiang, S., Miskimins, W.K., Cleary, M.P., and Yang, D.-Q. (2015b). Translational Control Protein 80 Stimulates IRES-Mediated Translation of p53 mRNA in Response to DNA Damage. BioMed Res. Int. *2015*, 708158.

Hamvas, R.M., Zinn, A., Keer, J.T., Fisher, E.M., Beer-Romero, P., Brown, S.D., and Page, D.C. (1992). Rps4 maps near the inactivation center on the mouse X chromosome. Genomics *12*, 363–367.

Hannan, K.M., Brandenburger, Y., Jenkins, A., Sharkey, K., Cavanaugh, A., Rothblum, L., Moss, T., Poortinga, G., McArthur, G.A., Pearson, R.B., et al. (2003). mTOR-dependent regulation of ribosomal gene transcription requires S6K1 and is mediated by phosphorylation of the carboxy-terminal activation domain of the nucleolar transcription factor UBF. Mol. Cell. Biol. *23*, 8862–8877.

Hara, K., Maruki, Y., Long, X., Yoshino, K., Oshiro, N., Hidayat, S., Tokunaga, C., Avruch, J., and Yonezawa, K. (2002). Raptor, a binding partner of target of rapamycin (TOR), mediates TOR action. Cell *110*, 177–189.

Harris, S.L., and Levine, A.J. (2005). The p53 pathway: positive and negative feedback loops. Oncogene *24*, 2899–2908.

Haupt, Y., Maya, R., Kazaz, A., and Oren, M. (1997). Mdm2 promotes the rapid degradation of p53. Nature *387*, 296–299.

Hay, N., and Sonenberg, N. (2004). Upstream and downstream of mTOR. Genes Dev. *18*, 1926–1945.

He, H., and Sun, Y. (2007). Ribosomal protein S27L is a direct p53 target that regulates apoptosis. Oncogene *26*, 2707–2716.

Heaney, M.L., and Golde, D.W. (1999). Myelodysplasia. N. Engl. J. Med. *340*, 1649–1660.

Heiman, M., Kulicke, R., Fenster, R.J., Greengard, P., and Heintz, N. (2014). Cell type-specific mRNA purification by translating ribosome affinity purification (TRAP). Nat. Protoc. *9*, 1282–1291.

Henras, A., Henry, Y., Bousquet-Antonelli, C., Noaillac-Depeyre, J., Gélugne, J.-P., and Caizergues-Ferrer, M. (1998). Nhp2p and Nop10p are essential for the function of H/ACA snoRNPs. EMBO J. *17*, 7078–7090.

Hobbs, M.V., Weigle, W.O., Noonan, D.J., Torbett, B.E., McEvilly, R.J., Koch, R.J., Cardenas, G.J., and Ernst, D.N. (1993). Patterns of cytokine gene expression by CD4+ T cells from young and old mice. J. Immunol. *150*, 3602–3614.

Höfler, S., Lukat, P., Blankenfeldt, W., and Carlomagno, T. (2021). High-resolution structure of eukaryotic Fibrillarin interacting with Nop56 amino-terminal domain. RNA N. Y. N *27*, 496–512.

Holley, R.W., Apgar, J., Everett, G.A., Madison, J.T., Marquisee, M., Merrill, S.H., Penswick, J.R., and Zamir, A. (1965). STRUCTURE OF A RIBONUCLEIC ACID. Science *147*, 1462–1465.

Honda, R., and Yasuda, H. (1999). Association of p19(ARF) with Mdm2 inhibits ubiquitin ligase activity of Mdm2 for tumor suppressor p53. EMBO J. *18*, 22–27.

Horn, H.F., and Vousden, K.H. (2008). Cooperation between the ribosomal proteins L5 and L11 in the p53 pathway. Oncogene *27*, 5774–5784.

Huang, D.W., Sherman, B.T., and Lempicki, R.A. (2009). Systematic and integrative analysis of large gene lists using DAVID bioinformatics resources. Nat. Protoc. *4*, 44–57.

Huez, I., Créancier, L., Audigier, S., Gensac, M.C., Prats, A.C., and Prats, H. (1998). Two independent internal ribosome entry sites are involved in translation initiation of vascular endothelial growth factor mRNA. Mol. Cell. Biol. *18*, 6178–6190.

Imami, K., Milek, M., Bogdanow, B., Yasuda, T., Kastelic, N., Zauber, H., Ishihama, Y., Landthaler, M., and Selbach, M. (2018). Phosphorylation of the Ribosomal Protein RPL12/uL11 Affects Translation during Mitosis. Mol. Cell *72*, 84-98.e9.

Inglis, A.J., Masson, G.R., Shao, S., Perisic, O., McLaughlin, S.H., Hegde, R.S., and Williams, R.L. (2019). Activation of GCN2 by the ribosomal P-stalk. Proc. Natl. Acad. Sci. U. S. A. *116*, 4946–4954.

Itahana, K., Bhat, K.P., Jin, A., Itahana, Y., Hawke, D., Kobayashi, R., and Zhang, Y. (2003). Tumor suppressor ARF degrades B23, a nucleolar protein involved in ribosome biogenesis and cell proliferation. Mol. Cell *12*, 1151–1164.

Ito, K., and Chiba, S. (2013). Arrest Peptides: Cis-Acting Modulators of Translation. Annu. Rev. Biochem. *82*, 171–202.

Ivanov, A.V., Malygin, A.A., and Karpova, G.G. (2005). Human ribosomal protein S26 suppresses the splicing of its pre-mRNA. Biochim. Biophys. Acta *1727*, 134–140.

Jackson, R.J., Hellen, C.U.T., and Pestova, T.V. (2010). The mechanism of eukaryotic translation initiation and principles of its regulation. Nat. Rev. Mol. Cell Biol. *11*, 113–127.

Jackson, R.J., Hellen, C.U.T., and Pestova, T.V. (2012). Termination and post-termination events in eukaryotic translation. Adv. Protein Chem. Struct. Biol. *86*, 45–93.

Jäkel, S., and Gürlich, D. (1998). Importin β, transportin, RanBP5 and RanBP7 mediate nuclear import of ribosomal proteins in mammalian cells. EMBO J. *17*, 4491–4502.

Jakovljevic, J., de Mayolo, P.A., Miles, T.D., Nguyen, T.M.-L., Léger-Silvestre, I., Gas, N., and Woolford, J.L. (2004). The Carboxy-Terminal Extension of Yeast Ribosomal Protein S14 Is Necessary for Maturation of 43S Preribosomes. Mol. Cell *14*, 331–342.

Jang, S.K., Davies, M.V., Kaufman, R.J., and Wimmer, E. (1989). Initiation of protein synthesis by internal entry of ribosomes into the 5' nontranslated region of encephalomyocarditis virus RNA in vivo. J. Virol. *63*, 1651–1660.

Jassam, Y.N., Izzy, S., Whalen, M., McGavern, D.B., and El Khoury, J. (2017). Neuroimmunology of Traumatic Brain Injury: Time for a Paradigm Shift. Neuron *95*, 1246–1265.

Jenner, L., Melnikov, S., Garreau de Loubresse, N., Ben-Shem, A., Iskakova, M., Urzhumtsev, A., Meskauskas, A., Dinman, J., Yusupova, G., and Yusupov, M. (2012). Crystal structure of the 80S yeast ribosome. Curr. Opin. Struct. Biol. *22*, 759–767.

Jhanwar-Uniyal, M., Wainwright, J.V., Mohan, A.L., Tobias, M.E., Murali, R., Gandhi, C.D., and Schmidt, M.H. (2019). Diverse signaling mechanisms of mTOR complexes: mTORC1 and mTORC2 in forming a formidable relationship. Adv. Biol. Regul. *72*, 51–62.

Jiang, L., Li, T., Zhang, X., Zhang, B., Yu, C., Li, Y., Fan, S., Jiang, X., Khan, T., Hao, Q., et al. (2017). RPL10L Is Required for Male Meiotic Division by Compensating for RPL10 during Meiotic Sex Chromosome Inactivation in Mice. Curr. Biol. CB *27*, 1498-1505.e6.

Jie, Q., Sun, F., Li, Q., Zhu, J., Wei, Y., Yang, H., Long, P., Wang, Z., Yang, X., Li, D., et al. (2021). Downregulated ribosomal protein L39 inhibits trophoblast cell migration and invasion by targeting E-cadherin in the placenta of patients with preeclampsia. FASEB J. *35*, e21322.

Juven, T., Barak, Y., Zauberman, A., George, D.L., and Oren, M. (1993). Wild type p53 can mediate sequence-specific transactivation of an internal promoter within the mdm2 gene. Oncogene *8*, 3411–3416.

Kaeberlein, M., Powers, R.W., Steffen, K.K., Westman, E.A., Hu, D., Dang, N., Kerr, E.O., Kirkland, K.T., Fields, S., and Kennedy, B.K. (2005). Regulation of yeast replicative life span by TOR and Sch9 in response to nutrients. Science *310*, 1193–1196.

Kale, A., Ji, Z., Kiparaki, M., Blanco, J., Rimesso, G., Flibotte, S., and Baker, N.E. (2018). Ribosomal Protein S12e Has a Distinct Function in Cell Competition. Dev. Cell *44*, 42-55.e4.

Kanamori, Y., and Nakashima, N. (2001). A tertiary structure model of the internal ribosome entry site (IRES) for methionine-independent initiation of translation. RNA N. Y. N *7*, 266–274.

Kantidakis, T., Ramsbottom, B.A., Birch, J.L., Dowding, S.N., and White, R.J. (2010). mTOR associates with TFIIIC, is found at tRNA and 5S rRNA genes, and targets their repressor Maf1. Proc. Natl. Acad. Sci. U. S. A. *107*, 11823–11828.

Kaplan, A., Ong Tone, S., and Fournier, A.E. (2015). Extrinsic and intrinsic regulation of axon regeneration at a crossroads. Front. Mol. Neurosci. *8*, 27.

Katz, M.J., Acevedo, J.M., Loenarz, C., Galagovsky, D., Liu-Yi, P., Pérez-Pepe, M., Thalhammer, A., Sekirnik, R., Ge, W., Melani, M., et al. (2014). Sudestada1, a Drosophila ribosomal prolyl-hydroxylase required for mRNA translation, cell homeostasis, and organ growth. Proc. Natl. Acad. Sci. U. S. A. *111*, 4025–4030.

Kaur, R., Sodhi, M., Sharma, A., Sharma, V.L., Verma, P., Swami, S.K., Kumari, P., and Mukesh, M. (2018). Selection of suitable reference genes for normalization of quantitative RT-PCR (RT-qPCR) expression data across twelve tissues of riverine buffaloes (Bubalus bubalis). PloS One *13*, e0191558.

Ke, Z., Mallik, P., Johnson, A.B., Luna, F., Nevo, E., Zhang, Z.D., Gladyshev, V.N., Seluanov, A., and Gorbunova, V. (2017). Translation fidelity coevolves with longevity. Aging Cell *16*, 988–993.

Kenmochi, N., Kawaguchi, T., Rozen, S., Davis, E., Goodman, N., Hudson, T.J., Tanaka, T., and Page, D.C. (1998). A Map of 75 Human Ribosomal Protein Genes. Genome Res. *8*, 509–523.

Kent, T., Lapik, Y.R., and Pestov, D.G. (2009). The 5' external transcribed spacer in mouse ribosomal RNA contains two cleavage sites. RNA N. Y. N *15*, 14–20.

Kerkhofs, C., Stevens, S.J.C., Faust, S.N., Rae, W., Williams, A.P., Wurm, P., Østern, R., Fockens, P., Würfel, C., Laass, M., et al. (2020). Mutations in RPSA and NKX2-3 link development of the spleen and intestinal vasculature. Hum. Mutat. *41*, 196–202.

Khairulina, J., Graifer, D., Bulygin, K., Ven'yaminova, A., Frolova, L., and Karpova, G. (2010). Eukaryote-specific motif of ribosomal protein S15 neighbors A site codon during elongation and termination of translation. Biochimie *92*, 820–825.

Khajuria, R.K., Munschauer, M., Ulirsch, J.C., Fiorini, C., Ludwig, L.S., McFarland, S.K., Abdulhay, N.J., Specht, H., Keshishian, H., Mani, D.R., et al. (2018). Ribosome Levels Selectively Regulate Translation and Lineage Commitment in Human Hematopoiesis. Cell *173*, 90-103.e19.

Khalaileh, A., Dreazen, A., Khatib, A., Apel, R., Swisa, A., Kidess-Bassir, N., Maitra, A., Meyuhas, O., Dor, Y., and Zamir, G. (2013). Phosphorylation of ribosomal protein S6 attenuates DNA damage and tumor suppression during development of pancreatic cancer. Cancer Res. *73*, 1811–1820.

Khatter, H., Myasnikov, A.G., Natchiar, S.K., and Klaholz, B.P. (2015). Structure of the human 80S ribosome. Nature *520*, 640–645.

Khosravi, R., Maya, R., Gottlieb, T., Oren, M., Shiloh, Y., and Shkedy, D. (1999). Rapid ATM-dependent phosphorylation of MDM2 precedes p53 accumulation in response to DNA damage. Proc. Natl. Acad. Sci. U. S. A. *96*, 14973–14977.

Killian, J.L., Ye, F., and Wang, M.D. (2018). Optical Tweezers: A Force to Be Reckoned With. Cell *175*, 1445–1448.

Kim, J., and Guan, K.-L. (2019). mTOR as a central hub of nutrient signalling and cell growth. Nat. Cell Biol. *21*, 63–71.

Kim, S., and Martin, K.C. (2015). Neuron-wide RNA transport combines with netrin-mediated local translation to spatially regulate the synaptic proteome. ELife *4*.

Kim, D.-H., Sarbassov, D.D., Ali, S.M., Latek, R.R., Guntur, K.V.P., Erdjument-Bromage, H., Tempst, P., and Sabatini, D.M. (2003). GbetaL, a positive regulator of the rapamycin-sensitive

pathway required for the nutrient-sensitive interaction between raptor and mTOR. Mol. Cell *11*, 895–904.

Kim, H.D., Kim, T.-S., Joo, Y.J., Shin, H.-S., Kim, S.-H., Jang, C.-Y., Lee, C.E., and Kim, J. (2010). RpS3 translation is repressed by interaction with its own mRNA. J. Cell. Biochem. *110*, 294–303.

Kim, J.-H., Dilthey, A.T., Nagaraja, R., Lee, H.-S., Koren, S., Dudekula, D., Wood Iii, W.H., Piao, Y., Ogurtsov, A.Y., Utani, K., et al. (2018). Variation in human chromosome 21 ribosomal RNA genes characterized by TAR cloning and long-read sequencing. Nucleic Acids Res. *46*, 6712–6725.

Kim, S.H., Suddath, F.L., Quigley, G.J., McPherson, A., Sussman, J.L., Wang, A.H., Seeman, N.C., and Rich, A. (1974). Three-dimensional tertiary structure of yeast phenylalanine transfer RNA. Science *185*, 435–440.

Kirby, T.J., Lee, J.D., England, J.H., Chaillou, T., Esser, K.A., and McCarthy, J.J. (2015). Blunted hypertrophic response in aged skeletal muscle is associated with decreased ribosome biogenesis. J. Appl. Physiol. Bethesda Md 1985 *119*, 321–327.

Kleiman, R., Banker, G., and Steward, O. (1990). Differential subcellular localization of particular mRNAs in hippocampal neurons in culture. Neuron *5*, 821–830.

Klinge, S., Voigts-Hoffmann, F., Leibundgut, M., Arpagaus, S., and Ban, N. (2011). Crystal Structure of the Eukaryotic 60S Ribosomal Subunit in Complex with Initiation Factor 6. Science *334*, 941–948.

Klinge, S., Voigts-Hoffmann, F., Leibundgut, M., and Ban, N. (2012). Atomic structures of the eukaryotic ribosome. Trends Biochem. Sci. *37*, 189–198.

Klingebiel, M., Dinekov, M., and Köhler, C. (2017). Analysis of ribosomal protein S6 baseline phosphorylation and effect of tau pathology in the murine brain and human hippocampus. Brain Res. *1659*, 121–135.

Knauf, U., Tschopp, C., and Gram, H. (2001). Negative regulation of protein translation by mitogen-activated protein kinase-interacting kinases 1 and 2. Mol. Cell. Biol. *21*, 5500–5511.

Knight, Z.A., Tan, K., Birsoy, K., Schmidt, S., Garrison, J.L., Wysocki, R.W., Emiliano, A., Ekstrand, M.I., and Friedman, J.M. (2012). Molecular profiling of activated neurons by phosphorylated ribosome capture. Cell *151*, 1126–1137.

Kobayashi, M., Oshima, S., Maeyashiki, C., Nibe, Y., Otsubo, K., Matsuzawa, Y., Nemoto, Y., Nagaishi, T., Okamoto, R., Tsuchiya, K., et al. (2016). The ubiquitin hybrid gene UBA52 regulates ubiquitination of ribosome and sustains embryonic development. Sci. Rep. *6*, 36780.

Kochetov, A.V., Prayaga, P.D., Volkova, O.A., and Sankararamakrishnan, R. (2013). Hidden coding potential of eukaryotic genomes: nonAUG started ORFs. J. Biomol. Struct. Dyn. *31*, 103–114.

Komili, S., and Silver, P.A. (2008). Coupling and coordination in gene expression processes: a systems biology view. Nat. Rev. Genet. *9*, 38–48.

Komili, S., Farny, N.G., Roth, F.P., and Silver, P.A. (2007). Functional Specificity among Ribosomal Proteins Regulates Gene Expression. Cell *131*, 557–571.

Komoda, T., Sato, N.S., Phelps, S.S., Namba, N., Joseph, S., and Suzuki, T. (2006). The A-site Finger in 23 S rRNA Acts as a Functional Attenuator for Translocation *. J. Biol. Chem. *281*, 32303–32309.

Kondrashov, N., Pusic, A., Stumpf, C.R., Shimizu, K., Hsieh, A.C., Ishijima, J., Shiroishi, T., and Barna, M. (2011). Ribosome-mediated specificity in Hox mRNA translation and vertebrate tissue patterning. Cell *145*, 383–397.

Kongsuwan, K., Yu, Q., Vincent, A., Frisardi, M.C., Rosbash, M., Lengyel, J.A., and Merriam, J. (1985). A Drosophila Minute gene encodes a ribosomal protein. Nature *317*, 555–558.

Koo, B.-K., Park, C.-J., Fernandez, C.F., Chim, N., Ding, Y., Chanfreau, G., and Feigon, J. (2011). Structure of H/ACA RNP protein Nhp2p reveals cis/trans isomerization of a conserved proline at the RNA and Nop10 binding interface. J. Mol. Biol. *411*, 927–942.

Köpke, A.K., Leggatt, P.A., and Matheson, A.T. (1992). Structure function relationships in the ribosomal stalk proteins of archaebacteria. J. Biol. Chem. *267*, 1382–1390.

Korepanov, A.P., Korobeinikova, A.V., Shestakov, S.A., Garber, M.B., and Gongadze, G.M. (2012). Protein L5 is crucial for in vivo assembly of the bacterial 50S ribosomal subunit central protuberance. Nucleic Acids Res. *40*, 9153–9159.

Kowalik, T.F., DeGregori, J., Leone, G., Jakoi, L., and Nevins, J.R. (1998). E2F1-specific induction of apoptosis and p53 accumulation, which is blocked by Mdm2. Cell Growth Differ. Mol. Biol. J. Am. Assoc. Cancer Res. *9*, 113–118.

Kozak, M. (1987). An analysis of 5'-noncoding sequences from 699 vertebrate messenger RNAs. Nucleic Acids Res. *15*, 8125–8148.

Kraushar, M.L., Krupp, F., Harnett, D., Turko, P., Ambrozkiewicz, M.C., Sprink, T., Imami, K., Günnigmann, M., Zinnall, U., Vieira-Vieira, C.H., et al. (2021). Protein Synthesis in the Developing Neocortex at Near-Atomic Resolution Reveals Ebp1-Mediated Neuronal Proteostasis at the 60S Tunnel Exit. Mol. Cell *81*, 304-322.e16.

Krogh, N., Jansson, M.D., Häfner, S.J., Tehler, D., Birkedal, U., Christensen-Dalsgaard, M., Lund, A.H., and Nielsen, H. (2016). Profiling of 2'-O-Me in human rRNA reveals a subset of fractionally modified positions and provides evidence for ribosome heterogeneity. Nucleic Acids Res. *44*, 7884–7895.

Krokowski, D., Boguszewska, A., Abramczyk, D., Liljas, A., Tchórzewski, M., and Grankowski, N. (2006). Yeast ribosomal P0 protein has two separate binding sites for P1/P2 proteins. Mol. Microbiol. *60*, 386–400.

Kuang, J., Li, Q.-Y., Fan, F., Shen, N.-J., Zhan, Y.-J., Tang, Z.-H., and Yu, W.-L. (2017). Overexpression of the X-linked ribosomal protein S4 predicts poor prognosis in patients with intrahepatic cholangiocarcinoma. Oncol. Lett. *14*, 41–46.

Kulasekararaj, A.G., Smith, A.E., Mian, S.A., Mohamedali, A.M., Krishnamurthy, P., Lea, N.C., Gäken, J., Pennaneach, C., Ireland, R., Czepulkowski, B., et al. (2013). TP53 mutations in myelodysplastic syndrome are strongly correlated with aberrations of chromosome 5, and correlate with adverse prognosis. Br. J. Haematol. *160*, 660–672.

Kwan, T., and Thompson, S.R. (2019). Noncanonical Translation Initiation in Eukaryotes. Cold Spring Harb. Perspect. Biol. *11*.

Kyritsis, K.A., Ouzounis, C.A., Angelis, L., and Vizirianakis, I.S. (2020). Sequence variation, common tissue expression patterns and learning models: a genome-wide survey of vertebrate ribosomal proteins. NAR Genomics Bioinforma. *2*, lqaa088.

Lacombe, T., García-Gómez, J.J., de la Cruz, J., Roser, D., Hurt, E., Linder, P., and Kressler, D. (2009). Linear ubiquitin fusion to Rps31 and its subsequent cleavage are required for the efficient production and functional integrity of 40S ribosomal subunits. Mol. Microbiol. *72*, 69–84.

Lai, K., Amsterdam, A., Farrington, S., Bronson, R.T., Hopkins, N., and Lees, J.A. (2009). Many ribosomal protein mutations are associated with growth impairment and tumor predisposition in zebrafish. Dev. Dyn. Off. Publ. Am. Assoc. Anat. *238*, 76–85.

Larburu, N., Montellese, C., O'Donohue, M.-F., Kutay, U., Gleizes, P.-E., and Plisson-Chastang, C. (2016). Structure of a human pre-40S particle points to a role for RACK1 in the final steps of 18S rRNA processing. Nucleic Acids Res. *44*, 8465–8478.

Lee, C.-H., Kiparaki, M., Blanco, J., Folgado, V., Ji, Z., Kumar, A., Rimesso, G., and Baker, N.E. (2018). A Regulatory Response to Ribosomal Protein Mutations Controls Translation, Growth, and Cell Competition. Dev. Cell *46*, 456-469.e4.

Léger-Silvestre, I., Caffrey, J.M., Dawaliby, R., Alvarez-Arias, D.A., Gas, N., Bertolone, S.J., Gleizes, P.-E., and Ellis, S.R. (2005). Specific Role for Yeast Homologs of the Diamond Blackfan Anemia-associated Rps19 Protein in Ribosome Synthesis. J. Biol. Chem. *280*, 38177–38185.

Leppek, K., Das, R., and Barna, M. (2018). Functional 5' UTR mRNA structures in eukaryotic translation regulation and how to find them. Nat. Rev. Mol. Cell Biol. *19*, 158–174.

Lessard, F., Morin, F., Ivanchuk, S., Langlois, F., Stefanovsky, V., Rutka, J., and Moss, T. (2010). The ARF tumor suppressor controls ribosome biogenesis by regulating the RNA polymerase I transcription factor TTF-I. Mol. Cell *38*, 539–550.

Lessard, F., Stefanovsky, V., Tremblay, M.G., and Moss, T. (2012). The cellular abundance of the essential transcription termination factor TTF-I regulates ribosome biogenesis and is determined by MDM2 ubiquitinylation. Nucleic Acids Res. *40*, 5357–5367.

Lessard, F., Igelmann, S., Trahan, C., Huot, G., Saint-Germain, E., Mignacca, L., Del Toro, N., Lopes-Paciencia, S., Le Calvé, B., Montero, M., et al. (2018). Senescence-associated ribosome biogenesis defects contributes to cell cycle arrest through the Rb pathway. Nat. Cell Biol. *20*, 789–799.

Létoquart, J., Huvelle, E., Wacheul, L., Bourgeois, G., Zorbas, C., Graille, M., Heurgué-Hamard, V., and Lafontaine, D.L.J. (2014). Structural and functional studies of Bud23–Trm112 reveal 18S rRNA N7-G1575 methylation occurs on late 40S precursor ribosomes. Proc. Natl. Acad. Sci. *111*, E5518–E5526.

Levy, S., Avni, D., Hariharan, N., Perry, R.P., and Meyuhas, O. (1991). Oligopyrimidine tract at the 5' end of mammalian ribosomal protein mRNAs is required for their translational control. Proc. Natl. Acad. Sci. U. S. A. *88*, 3319–3323.

Li, C., Chen, D., Luo, M., Ge, M., and Zhu, J. (2014). Knockdown of ribosomal protein L39 by RNA interference inhibits the growth of human pancreatic cancer cells in vitro and in vivo. Biotechnol. J. *9*, 652–663.

Li, H., Tsang, C.K., Watkins, M., Bertram, P.G., and Zheng, X.F.S. (2006). Nutrient regulates Tor1 nuclear localization and association with rDNA promoter. Nature *442*, 1058–1061.

Li, W., Ward, F.R., McClure, K.F., Chang, S.T.-L., Montabana, E., Liras, S., Dullea, R.G., and Cate, J.H.D. (2019). Structural basis for selective stalling of human ribosome nascent chain complexes by a drug-like molecule. Nat. Struct. Mol. Biol. *26*, 501–509.

Li, X., Qiao, J., Yang, N., Mi, H., Chu, P., Xia, Y., Yao, H., Liu, Y., Qi, K., Yan, Z., et al. (2015). Identification of Suitable Reference Genes for Normalization of Real-Time Quantitative Polymerase Chain Reaction in an Intestinal Graft-Versus-Host Disease Mouse Model. Transplant. Proc. *47*, 2017–2025.

Li, Y., Zhang, J., Sun, H., Chen, Y., Li, W., Yu, X., Zhao, X., Zhang, L., Yang, J., Xin, W., et al. (2021). lnc-Rps4l-encoded peptide RPS4XL regulates RPS6 phosphorylation and inhibits the proliferation of PASMCs caused by hypoxia. Mol. Ther. J. Am. Soc. Gene Ther. *29*, 1411–1424.

Liang, H., He, S., Yang, J., Jia, X., Wang, P., Chen, X., Zhang, Z., Zou, X., McNutt, M.A., Shen, W.H., et al. (2014). PTENα, a PTEN isoform translated through alternative initiation, regulates mitochondrial function and energy metabolism. Cell Metab. *19*, 836–848.

Liang, H., Chen, X., Yin, Q., Ruan, D., Zhao, X., Zhang, C., McNutt, M.A., and Yin, Y. (2017). PTENβ is an alternatively translated isoform of PTEN that regulates rDNA transcription. Nat. Commun. *8*, 14771.

Liang, X., Liu, Q., and Fournier, M.J. (2007). rRNA modifications in an intersubunit bridge of the ribosome strongly affect both ribosome biogenesis and activity. Mol. Cell *28*, 965–977.

Liang, X.-H., Liu, Q., and Fournier, M.J. (2009). Loss of rRNA modifications in the decoding center of the ribosome impairs translation and strongly delays pre-rRNA processing. RNA N. Y. N *15*, 1716–1728.

Liao, J.-M., Zhou, X., Gatignol, A., and Lu, H. (2014). Ribosomal proteins L5 and L11 co-operatively inactivate c-Myc via RNA-induced silencing complex. Oncogene *33*, 4916–4923.

Liljas, A., and Sanyal, S. (2018). The enigmatic ribosomal stalk. Q. Rev. Biophys. *51*, e12.

Lin, J., Lai, S., Jia, R., Xu, A., Zhang, L., Lu, J., and Ye, K. (2011). Structural basis for site-specific ribose methylation by box C/D RNA protein complexes. Nature *469*, 559–563.

Liu, Q., and Fredrick, K. (2016). Intersubunit Bridges of the Bacterial Ribosome. J. Mol. Biol. *428*, 2146–2164.

Liu, Y., Beyer, A., and Aebersold, R. (2016a). On the Dependency of Cellular Protein Levels on mRNA Abundance. Cell *165*, 535–550.

Liu, Y., Deisenroth, C., and Zhang, Y. (2016b). RP-MDM2-p53 Pathway: Linking Ribosomal Biogenesis and Tumor Surveillance. Trends Cancer *2*, 191–204.

Liu, Y., Zhang, H., Li, Y., Yan, L., Du, W., Wang, S., Zheng, X., Zhang, M., Zhang, J., Qi, J., et al. (2020). Long Noncoding RNA Rps4l Mediates the Proliferation of Hypoxic Pulmonary Artery Smooth Muscle Cells. Hypertens. Dallas Tex 1979 *76*, 1124–1133.

Lo, K.-Y., Li, Z., Bussiere, C., Bresson, S., Marcotte, E.M., and Johnson, A.W. (2010). Defining the pathway of cytoplasmic maturation of the 60S ribosomal subunit. Mol. Cell *39*, 196–208.

Lodish, H.F. (1974). Model for the regulation of mRNA translation applied to haemoglobin synthesis. Nature *251*, 385–388.

Loenarz, C., Sekirnik, R., Thalhammer, A., Ge, W., Spivakovsky, E., Mackeen, M.M., McDonough, M.A., Cockman, M.E., Kessler, B.M., Ratcliffe, P.J., et al. (2014). Hydroxylation of the eukaryotic ribosomal decoding center affects translational accuracy. Proc. Natl. Acad. Sci. *111*, 4019–4024.

Loewith, R., Jacinto, E., Wullschleger, S., Lorberg, A., Crespo, J.L., Bonenfant, D., Oppliger, W., Jenoe, P., and Hall, M.N. (2002). Two TOR complexes, only one of which is rapamycin sensitive, have distinct roles in cell growth control. Mol. Cell *10*, 457–468.

Lohrum, M.A.E., Ludwig, R.L., Kubbutat, M.H.G., Hanlon, M., and Vousden, K.H. (2003). Regulation of HDM2 activity by the ribosomal protein L11. Cancer Cell *3*, 577–587.

Long, K.S., Poehlsgaard, J., Hansen, L.H., Hobbie, S.N., Böttger, E.C., and Vester, B. (2009). Single 23S rRNA mutations at the ribosomal peptidyl transferase centre confer resistance to valnemulin and other antibiotics in Mycobacterium smegmatis by perturbation of the drug binding pocket. Mol. Microbiol. *71*, 1218–1227.

Lorenz, C., Lünse, C.E., and Mörl, M. (2017). tRNA Modifications: Impact on Structure and Thermal Adaptation. Biomolecules *7*, 35.

Lu, J., and Deutsch, C. (2005). Folding zones inside the ribosomal exit tunnel. Nat. Struct. Mol. Biol. *12*, 1123–1129.

Lu, J., and Deutsch, C. (2014). Regional Discrimination and Propagation of Local Rearrangements along the Ribosomal Exit Tunnel. J. Mol. Biol. *426*, 4061–4073.

Lu, J., Miao, J., Su, T., Liu, Y., and He, R. (2013). Formaldehyde induces hyperphosphorylation and polymerization of Tau protein both in vitro and in vivo. Biochim. Biophys. Acta *1830*, 4102–4116.

Ludwig, L.S., Gazda, H.T., Eng, J.C., Eichhorn, S.W., Thiru, P., Ghazvinian, R., George, T.I., Gotlib, J.R., Beggs, A.H., Sieff, C.A., et al. (2014). Altered translation of GATA1 in Diamond-Blackfan anemia. Nat. Med. *20*, 748–753.

M, D., U, K., F, S., N, F., Jm, H., Ag, T., H, S., Mv, R., and Mc, W. (2005). Structural basis for the function of the ribosomal L7/12 stalk in factor binding and GTPase activation. Cell *121*.

Ma, C., Wu, S., Li, N., Chen, Y., Yan, K., Li, Z., Zheng, L., Lei, J., Woolford, J.L., and Gao, N. (2017). Structural snapshot of cytoplasmic pre-60S ribosomal particles bound by Nmd3, Lsg1, Tif6 and Reh1. Nat. Struct. Mol. Biol. *24*, 214–220.

Ma, Y., Liu, Y., Ruan, X., Liu, X., Zheng, J., Teng, H., Shao, L., Yang, C., Wang, D., and Xue, Y. (2021). Gene Expression Signature of Traumatic Brain Injury. Front. Genet. *12*, 646436.

Macías, S., Bragulat, M., Tardiff, D.F., and Vilardell, J. (2008). L30 binds the nascent RPL30 transcript to repress U2 snRNP recruitment. Mol. Cell *30*, 732–742.

Maggi, L.B., Kuchenruether, M., Dadey, D.Y.A., Schwope, R.M., Grisendi, S., Townsend, R.R., Pandolfi, P.P., and Weber, J.D. (2008). Nucleophosmin serves as a rate-limiting nuclear export chaperone for the Mammalian ribosome. Mol. Cell. Biol. *28*, 7050–7065.

Mallik, S., and Zhao, Z. (2019). Multi-Objective Optimized Fuzzy Clustering for Detecting Cell Clusters from Single-Cell Expression Profiles. Genes *10*, 611.

Malygin, A.A., Parakhnevitch, N.M., Ivanov, A.V., Eperon, I.C., and Karpova, G.G. (2007). Human ribosomal protein S13 regulates expression of its own gene at the splicing step by a feedback mechanism. Nucleic Acids Res. *35*, 6414–6423.

Mankin, A.S. (2006). Nascent peptide in the 'birth canal' of the ribosome. Trends Biochem. Sci. *31*, 11–13.

Marcel, V., Ghayad, S.E., Belin, S., Therizols, G., Morel, A.-P., Solano-Gonzàlez, E., Vendrell, J.A., Hacot, S., Mertani, H.C., Albaret, M.A., et al. (2013). p53 acts as a safeguard of translational control by regulating fibrillarin and rRNA methylation in cancer. Cancer Cell *24*, 318–330.

Marechal, V., Elenbaas, B., Piette, J., Nicolas, J.C., and Levine, A.J. (1994). The ribosomal L5 protein is associated with mdm-2 and mdm-2-p53 complexes. Mol. Cell. Biol. *14*, 7414–7420.

Martin, D.E., Soulard, A., and Hall, M.N. (2004). TOR regulates ribosomal protein gene expression via PKA and the Forkhead transcription factor FHL1. Cell *119*, 969–979.

Martín-Villanueva, S., Fernández-Pevida, A., Fernández-Fernández, J., Kressler, D., and de la Cruz, J. (2020). Ubiquitin release from eL40 is required for cytoplasmic maturation and function of 60S ribosomal subunits in Saccharomyces cerevisiae. FEBS J. *287*, 345–360.

Marygold, S.J., Coelho, C.M.A., and Leevers, S.J. (2005). Genetic analysis of RpL38 and RpL5, two minute genes located in the centric heterochromatin of chromosome 2 of Drosophila melanogaster. Genetics *169*, 683–695.

Marygold, S.J., Roote, J., Reuter, G., Lambertsson, A., Ashburner, M., Millburn, G.H., Harrison, P.M., Yu, Z., Kenmochi, N., Kaufman, T.C., et al. (2007). The ribosomal protein genes and Minute loci of Drosophila melanogaster. Genome Biol. *8*, R216.

Matsuki, Y., Matsuo, Y., Nakano, Y., Iwasaki, S., Yoko, H., Udagawa, T., Li, S., Saeki, Y., Yoshihisa, T., Tanaka, K., et al. (2020). Ribosomal protein S7 ubiquitination during ER stress in yeast is associated with selective mRNA translation and stress outcome. Sci. Rep. *10*, 19669.

Maya, R., Balass, M., Kim, S.T., Shkedy, D., Leal, J.F., Shifman, O., Moas, M., Buschmann, T., Ronai, Z., Shiloh, Y., et al. (2001). ATM-dependent phosphorylation of Mdm2 on serine 395: role in p53 activation by DNA damage. Genes Dev. *15*, 1067–1077.

Mayer, C., and Grummt, I. (2006). Ribosome biogenesis and cell growth: mTOR coordinates transcription by all three classes of nuclear RNA polymerases. Oncogene *25*, 6384–6391.

Mayer, C., Zhao, J., Yuan, X., and Grummt, I. (2004). mTOR-dependent activation of the transcription factor TIF-IA links rRNA synthesis to nutrient availability. Genes Dev. *18*, 423–434.

Mazumder, B., Sampath, P., Seshadri, V., Maitra, R.K., DiCorleto, P.E., and Fox, P.L. (2003). Regulated release of L13a from the 60S ribosomal subunit as a mechanism of transcript-specific translational control. Cell *115*, 187–198.

McIntosh, K.B., Bhattacharya, A., Willis, I.M., and Warner, J.R. (2011). Eukaryotic Cells Producing Ribosomes Deficient in Rpl1 Are Hypersensitive to Defects in the Ubiquitin-Proteasome System. PLoS ONE *6*.

Mello, S., and Bohmann, D. (2020). Counting the Minutes. ELife *9*, e53348.

Melnikov, S., Ben-Shem, A., Loubresse, N.G. de, Jenner, L., Yusupova, G., and Yusupov, M. (2012). One core, two shells: bacterial and eukaryotic ribosomes. Nat. Struct. Mol. Biol. *19*, 560–567.

Meng, X., Tackmann, N.R., Liu, S., Yang, J., Dong, J., Wu, C., Cox, A.D., and Zhang, Y. (2016). RPL23 Links Oncogenic RAS Signaling to p53-Mediated Tumor Suppression. Cancer Res. *76*, 5030–5039.

von Mering, C., Huynen, M., Jaeggi, D., Schmidt, S., Bork, P., and Snel, B. (2003). STRING: a database of predicted functional associations between proteins. Nucleic Acids Res. *31*, 258–261.

Merrick, W.C., and Pavitt, G.D. (2018). Protein Synthesis Initiation in Eukaryotic Cells. Cold Spring Harb. Perspect. Biol. *10*.

Meskauskas, A., and Dinman, J.D. (2001). Ribosomal protein L5 helps anchor peptidyl-tRNA to the P-site in Saccharomyces cerevisiae. RNA N. Y. N *7*, 1084–1096.

Meskauskas, A., and Dinman, J.D. (2007). Ribosomal protein L3: gatekeeper to the A site. Mol. Cell *25*, 877–888.

Meyer, C., Garzia, A., Morozov, P., Molina, H., and Tuschl, T. (2020). The G3BP1-Family-USP10 Deubiquitinase Complex Rescues Ubiquitinated 40S Subunits of Ribosomes Stalled in Translation from Lysosomal Degradation. Mol. Cell *77*, 1193-1205.e5.

Meyuhas, O., and Kahan, T. (2015). The race to decipher the top secrets of TOP mRNAs. Biochim. Biophys. Acta *1849*, 801–811.

Micic, J., Li, Y., Wu, S., Wilson, D., Tutuncuoglu, B., Gao, N., and Woolford, J.L. (2020). Coupling of 5S RNP rotation with maturation of functional centers during large ribosomal subunit assembly. Nat. Commun. *11*, 3751.

Miller, J.A., Guillozet-Bongaarts, A., Gibbons, L.E., Postupna, N., Renz, A., Beller, A.E., Sunkin, S.M., Ng, L., Rose, S.E., Smith, K.A., et al. (2017). Neuropathological and transcriptomic characteristics of the aged brain. ELife *6*, e31126.

Mills, E.W., and Green, R. (2017). Ribosomopathies: There's strength in numbers. Science *358*.

Mitkevich, V.A., Shyp, V., Petrushanko, I.Y., Soosaar, A., Atkinson, G.C., Tenson, T., Makarov, A.A., and Hauryliuk, V. (2012). GTPases IF2 and EF-G bind GDP and the SRL RNA in a mutually exclusive manner. Sci. Rep. *2*, 843.

Miyake, K., Utsugisawa, T., Flygare, J., Kiefer, T., Hamaguchi, I., Richter, J., and Karlsson, S. (2008). Ribosomal protein S19 deficiency leads to reduced proliferation and increased apoptosis but does not affect terminal erythroid differentiation in a cell line model of Diamond-Blackfan anemia. Stem Cells Dayt. Ohio *26*, 323–329.

Mody, N., Agouni, A., McIlroy, G.D., Platt, B., and Delibegovic, M. (2011). Susceptibility to diet-induced obesity and glucose intolerance in the APP (SWE)/PSEN1 (A246E) mouse model of Alzheimer's disease is associated with increased brain levels of protein tyrosine phosphatase 1B (PTP1B) and retinol-binding protein 4 (RBP4), and basal phosphorylation of S6 ribosomal protein. Diabetologia *54*, 2143–2151.

Mohammad, M.P., Munzarová Pondelícková, V., Zeman, J., Gunišová, S., and Valášek, L.S. (2017). In vivo evidence that eIF3 stays bound to ribosomes elongating and terminating on short upstream ORFs to promote reinitiation. Nucleic Acids Res. *45*, 2658–2674.

Mokrejs, M., Masek, T., Vopálensky, V., Hlubucek, P., Delbos, P., and Pospísek, M. (2010). IRESite--a tool for the examination of viral and cellular internal ribosome entry sites. Nucleic Acids Res. *38*, D131-136.

Montellese, C., Montel-Lehry, N., Henras, A.K., Kutay, U., Gleizes, P.-E., and O'Donohue, M.-F. (2017). Poly(A)-specific ribonuclease is a nuclear ribosome biogenesis factor involved in human 18S rRNA maturation. Nucleic Acids Res. *45*, 6822–6836.

Montellese, C., van den Heuvel, J., Ashiono, C., Dörner, K., Melnik, A., Jonas, S., Zemp, I., Picotti, P., Gillet, L.C., and Kutay, U. (2020). USP16 counteracts mono-ubiquitination of RPS27a and promotes maturation of the 40S ribosomal subunit. ELife *9*, e54435.

Moore, D.L., Blackmore, M.G., Hu, Y., Kaestner, K.H., Bixby, J.L., Lemmon, V.P., and Goldberg, J.L. (2009). KLF family members regulate intrinsic axon regeneration ability. Science *326*, 298–301.

Musalgaonkar, S., Black, J.J., and Johnson, A.W. (2019). The L1 stalk is required for efficient export of nascent large ribosomal subunits in yeast. RNA N. Y. N *25*, 1549–1560.

Nakao, A., Yoshihama, M., and Kenmochi, N. (2004). RPG: the Ribosomal Protein Gene database. Nucleic Acids Res. *32*, D168-170.

Nienhuis, A.W., and Anderson, W.F. (1971). Isolation and translation of hemoglobin messenger RNA from thalassemia, sickle cell anemia, and normal human reticulocytes. J. Clin. Invest. *50*, 2458–2460.

Nilsson, O.B., Hedman, R., Marino, J., Wickles, S., Bischoff, L., Johansson, M., Müller-Lucks, A., Trovato, F., Puglisi, J.D., O'Brien, E.P., et al. (2015). Cotranslational Protein Folding inside the Ribosome Exit Tunnel. Cell Rep. *12*, 1533–1540.

Ning, W., Fei, J., and Gonzalez, R.L. (2014). The ribosome uses cooperative conformational changes to maximize and regulate the efficiency of translation. Proc. Natl. Acad. Sci. U. S. A. *111*, 12073–12078.

Nishimura, K., Kumazawa, T., Kuroda, T., Katagiri, N., Tsuchiya, M., Goto, N., Furumai, R., Murayama, A., Yanagisawa, J., and Kimura, K. (2015). Perturbation of ribosome biogenesis drives cells into senescence through 5S RNP-mediated p53 activation. Cell Rep. *10*, 1310–1323.

Nishiyama, T., Yamamoto, H., Shibuya, N., Hatakeyama, Y., Hachimori, A., Uchiumi, T., and Nakashima, N. (2003). Structural elements in the internal ribosome entry site of Plautia stali intestine virus responsible for binding with ribosomes. Nucleic Acids Res. *31*, 2434–2442.

Noguchi, C., Wang, L., Shetty, M., Mell, J.C., Sell, C., and Noguchi, E. (2021). Maf1 limits RNA polymerase III-directed transcription to preserve genomic integrity and extend lifespan. Cell Cycle Georget. Tex *20*, 247–255.

Noller, H.F. (1974). Topography of 16S RNA in 30S ribosomal subunits. Nucleotide sequences and location of sites of reaction with kethoxal. Biochemistry *13*, 4694–4703.

O'Donohue, M.-F., Choesmel, V., Faubladier, M., Fichant, G., and Gleizes, P.-E. (2010). Functional dichotomy of ribosomal proteins during the synthesis of mammalian 40S ribosomal subunits. J. Cell Biol. *190*, 853–866.

Oh, W.J., Wu, C., Kim, S.J., Facchinetti, V., Julien, L.-A., Finlan, M., Roux, P.P., Su, B., and Jacinto, E. (2010). mTORC2 can associate with ribosomes to promote cotranslational phosphorylation and stability of nascent Akt polypeptide. EMBO J. *29*, 3939–3951.

Ohashi, R., and Shiina, N. (2020). Cataloguing and Selection of mRNAs Localized to Dendrites in Neurons and Regulated by RNA-Binding Proteins in RNA Granules. Biomolecules *10*.

O'Leary, M.N., Schreiber, K.H., Zhang, Y., Duc, A.-C.E., Rao, S., Hale, J.S., Academia, E.C., Shah, S.R., Morton, J.F., Holstein, C.A., et al. (2013). The ribosomal protein Rpl22 controls ribosome composition by directly repressing expression of its own paralog, Rpl22l1. PLoS Genet. *9*, e1003708.

Oliner, J.D., Pietenpol, J.A., Thiagalingam, S., Gyuris, J., Kinzler, K.W., and Vogelstein, B. (1993). Oncoprotein MDM2 conceals the activation domain of tumour suppressor p53. Nature *362*, 857–860.

Olombrada, M., Peña, C., Rodríguez-Galán, O., Klingauf-Nerurkar, P., Portugal-Calisto, D., Oborská-Oplová, M., Altvater, M., Gavilanes, J.G., Martínez-del-Pozo, Á., de la Cruz, J., et al. (2020). The ribotoxin α-sarcin can cleave the sarcin/ricin loop on late 60S pre-ribosomes. Nucleic Acids Res. *48*, 6210–6222.

Orelle, C., Carlson, E.D., Szal, T., Florin, T., Jewett, M.C., and Mankin, A.S. (2015). Protein synthesis by ribosomes with tethered subunits. Nature *524*, 119–124.

Osheim, Y.N., French, S.L., Keck, K.M., Champion, E.A., Spasov, K., Dragon, F., Baserga, S.J., and Beyer, A.L. (2004). Pre-18S ribosomal RNA is structurally compacted into the SSU processome prior to being cleaved from nascent transcripts in Saccharomyces cerevisiae. Mol. Cell *16*, 943–954.

Pachler, K., Karl, T., Kolmann, K., Mehlmer, N., Eder, M., Loeffler, M., Oender, K., Hochleitner, E.O., Lottspeich, F., Bresgen, N., et al. (2004). Functional interaction in establishment of ribosomal integrity between small subunit protein rpS6 and translational regulator rpL10/Grc5p. FEMS Yeast Res. *5*, 271–280.

Palade, G.E. (1955). A small particulate component of the cytoplasm. J. Biophys. Biochem. Cytol. *1*, 59–68.

Pan, Y., and Chen, J. (2003). MDM2 promotes ubiquitination and degradation of MDMX. Mol. Cell. Biol. *23*, 5113–5121.

Panse, V.G., and Johnson, A.W. (2010). Maturation of eukaryotic ribosomes: acquisition of functionality. Trends Biochem. Sci. *35*, 260–266.

Pant, V., Xiong, S., Jackson, J.G., Post, S.M., Abbas, H.A., Quintás-Cardama, A., Hamir, A.N., and Lozano, G. (2013). The p53-Mdm2 feedback loop protects against DNA damage by inhibiting p53 activity but is dispensable for p53 stability, development, and longevity. Genes Dev. *27*, 1857–1867.

Paquet, É.R., Hovington, H., Brisson, H., Lacombe, C., Larue, H., Têtu, B., Lacombe, L., Fradet, Y., and Lebel, M. (2015). Low level of the X-linked ribosomal protein S4 in human urothelial carcinomas is associated with a poor prognosis. Biomark. Med. *9*, 187–197.

Paradies, M.A., and Steward, O. (1997). Multiple subcellular mRNA distribution patterns in neurons: a nonisotopic in situ hybridization analysis. J. Neurobiol. *33*, 473–493.

Parenteau, J., Durand, M., Morin, G., Gagnon, J., Lucier, J.-F., Wellinger, R.J., Chabot, B., and Elela, S.A. (2011). Introns within ribosomal protein genes regulate the production and function of yeast ribosomes. Cell *147*, 320–331.

Park, E.-H., Walker, S.E., Zhou, F., Lee, J.M., Rajagopal, V., Lorsch, J.R., and Hinnebusch, A.G. (2013). Yeast eukaryotic initiation factor 4B (eIF4B) enhances complex assembly between eIF4A and eIF4G in vivo. J. Biol. Chem. *288*, 2340–2354.

Park, K.K., Liu, K., Hu, Y., Smith, P.D., Wang, C., Cai, B., Xu, B., Connolly, L., Kramvis, I., Sahin, M., et al. (2008). Promoting axon regeneration in the adult CNS by modulation of the PTEN/mTOR pathway. Science *322*, 963–966.

Parks, M.M., Kurylo, C.M., Dass, R.A., Bojmar, L., Lyden, D., Vincent, C.T., and Blanchard, S.C. (2018). Variant ribosomal RNA alleles are conserved and exhibit tissue-specific expression. Sci. Adv. *4*, eaao0665.

Patchett, S., Musalgaonkar, S., Malyutin, A.G., and Johnson, A.W. (2017). The T-cell leukemia related rpl10-R98S mutant traps the 60S export adapter Nmd3 in the ribosomal P site in yeast. PLOS Genet. *13*, e1006894.

Peabody, D.S. (1987). Translation initiation at an ACG triplet in mammalian cells. J. Biol. Chem. *262*, 11847–11851.

Peabody, D.S. (1989). Translation initiation at non-AUG triplets in mammalian cells. J. Biol. Chem. *264*, 5031–5035.

Pech, M., Spreter, T., Beckmann, R., and Beatrix, B. (2010). Dual binding mode of the nascent polypeptide-associated complex reveals a novel universal adapter site on the ribosome. J. Biol. Chem. *285*, 19679–19687.

Pei, J.-J., An, W.-L., Zhou, X.-W., Nishimura, T., Norberg, J., Benedikz, E., Götz, J., and Winblad, B. (2006). P70 S6 kinase mediates tau phosphorylation and synthesis. FEBS Lett. *580*, 107–114.

Pelletier, J., and Sonenberg, N. (1988). Internal initiation of translation of eukaryotic mRNA directed by a sequence derived from poliovirus RNA. Nature *334*, 320–325.

Peltz, S.W., Hammell, A.B., Cui, Y., Yasenchak, J., Puljanowski, L., and Dinman, J.D. (1999). Ribosomal protein L3 mutants alter translational fidelity and promote rapid loss of the yeast killer virus. Mol. Cell. Biol. *19*, 384–391.

Peña, C., Schütz, S., Fischer, U., Chang, Y., and Panse, V.G. (2016). Prefabrication of a ribosomal protein subcomplex essential for eukaryotic ribosome formation. ELife *5*, e21755.

Penzo, M., and Montanaro, L. (2018). Turning Uridines around: Role of rRNA Pseudouridylation in Ribosome Biogenesis and Ribosomal Function. Biomolecules *8*, E38.

Pertschy, B., Schneider, C., Gnädig, M., Schäfer, T., Tollervey, D., and Hurt, E. (2009). RNA helicase Prp43 and its co-factor Pfa1 promote 20 to 18 S rRNA processing catalyzed by the endonuclease Nob1. J. Biol. Chem. *284*, 35079–35091.

Perucho, L., Artero-Castro, A., Guerrero, S., Ramón y Cajal, S., LLeonart, M.E., and Wang, Z.-Q. (2014). RPLP1, a crucial ribosomal protein for embryonic development of the nervous system. PloS One *9*, e99956.

Pestov, D.G., Strezoska, Z., and Lau, L.F. (2001). Evidence of p53-dependent cross-talk between ribosome biogenesis and the cell cycle: effects of nucleolar protein Bop1 on G(1)/S transition. Mol. Cell. Biol. *21*, 4246–4255.

Pestova, T.V., Hellen, C.U., and Shatsky, I.N. (1996). Canonical eukaryotic initiation factors determine initiation of translation by internal ribosomal entry. Mol. Cell. Biol. *16*, 6859–6869.

Peters, I.R., Peeters, D., Helps, C.R., and Day, M.J. (2007). Development and application of multiple internal reference (housekeeper) gene assays for accurate normalisation of canine gene expression studies. Vet. Immunol. Immunopathol. *117*, 55–66.

Peterson, A.C., Russell, J.D., Bailey, D.J., Westphall, M.S., and Coon, J.J. (2012). Parallel reaction monitoring for high resolution and high mass accuracy quantitative, targeted proteomics. Mol. Cell. Proteomics MCP *11*, 1475–1488.

Pfingsten, J.S., Costantino, D.A., and Kieft, J.S. (2006). Structural basis for ribosome recruitment and manipulation by a viral IRES RNA. Science *314*, 1450–1454.

Philippi, A., Steinbauer, R., Reiter, A., Fath, S., Leger-Silvestre, I., Milkereit, P., Griesenbeck, J., and Tschochner, H. (2010). TOR-dependent reduction in the expression level of Rrn3p lowers the activity of the yeast RNA Pol I machinery, but does not account for the strong inhibition of rRNA production. Nucleic Acids Res. *38*, 5315–5326.

Piazzi, M., Bavelloni, A., Gallo, A., Faenza, I., and Blalock, W.L. (2019). Signal Transduction in Ribosome Biogenesis: A Recipe to Avoid Disaster. Int. J. Mol. Sci. *20*, 2718.

Pisareva, V.P., Skabkin, M.A., Hellen, C.U.T., Pestova, T.V., and Pisarev, A.V. (2011). Dissociation by Pelota, Hbs1 and ABCE1 of mammalian vacant 80S ribosomes and stalled elongation complexes. EMBO J. *30*, 1804–1817.

Plassart, L., Shayan, R., Montellese, C., Rinaldi, D., Larburu, N., Pichereaux, C., Froment, C., Lebaron, S., O'Donohue, M.-F., Kutay, U., et al. (2021). The final step of 40S ribosomal subunit maturation is controlled by a dual key lock. ELife *10*, e61254.

Poirot, O., and Timsit, Y. (2016). Neuron-Like Networks Between Ribosomal Proteins Within the Ribosome. Sci. Rep. *6*, 26485.

Polacek, N., Gaynor, M., Yassin, A., and Mankin, A.S. (2001). Ribosomal peptidyl transferase can withstand mutations at the putative catalytic nucleotide. Nature *411*, 498–501.

Polymenis, M. (2020). Ribosomal proteins: mutant phenotypes by the numbers and associated gene expression changes. Open Biol. *10*, 200114.

Poon, M.M., Choi, S.-H., Jamieson, C.A.M., Geschwind, D.H., and Martin, K.C. (2006). Identification of process-localized mRNAs from cultured rodent hippocampal neurons. J. Neurosci. Off. J. Soc. Neurosci. *26*, 13390–13399.

Poortinga, G., Wall, M., Sanij, E., Siwicki, K., Ellul, J., Brown, D., Holloway, T.P., Hannan, R.D., and McArthur, G.A. (2011). c-MYC coordinately regulates ribosomal gene chromatin remodeling and Pol I availability during granulocyte differentiation. Nucleic Acids Res. *39*, 3267–3281.

Presutti, C., Ciafré, S.A., and Bozzoni, I. (1991). The ribosomal protein L2 in S. cerevisiae controls the level of accumulation of its own mRNA. EMBO J. *10*, 2215–2221.

Preti, M., O'Donohue, M.-F., Montel-Lehry, N., Bortolin-Cavaillé, M.-L., Choesmel, V., and Gleizes, P.-E. (2013). Gradual processing of the ITS1 from the nucleolus to the cytoplasm during synthesis of the human 18S rRNA. Nucleic Acids Res. *41*, 4709–4723.

Pringle, M., Poehlsgaard, J., Vester, B., and Long, K.S. (2004). Mutations in ribosomal protein L3 and 23S ribosomal RNA at the peptidyl transferase centre are associated with reduced susceptibility to tiamulin in Brachyspira spp. isolates. Mol. Microbiol. *54*, 1295–1306.

Qin, S., Zou, Y., and Zhang, C.-L. (2013). Cross-talk between KLF4 and STAT3 regulates axon regeneration. Nat. Commun. *4*, 2633.

Quarello, P., Garelli, E., Carando, A., Brusco, A., Calabrese, R., Dufour, C., Longoni, D., Misuraca, A., Vinti, L., Aspesi, A., et al. (2010). Diamond-Blackfan anemia: genotype-phenotype correlations in Italian patients with RPL5 and RPL11 mutations. Haematologica *95*, 206–213.

Rahman, N., Shamsuzzaman, M., and Lindahl, L. (2020). Interaction between the assembly of the ribosomal subunits: Disruption of 40S ribosomal assembly causes accumulation of extra-ribosomal 60S ribosomal protein uL18/L5. PloS One *15*, e0222479.

Ramagopal, S. (1990). Induction of cell-specific ribosomal proteins in aggregation-competent nonmorphogenetic Dictyostelium discoideum. Biochem. Cell Biol. Biochim. Biol. Cell. *68*, 1281–1287.

Ramagopal, S., and Ennis, H.L. (1981). Regulation of synthesis of cell-specific ribosomal proteins during differentiation of Dictyostelium discoideum. Proc. Natl. Acad. Sci. U. S. A. *78*, 3083–3087.

Ramu, H., Vázquez-Laslop, N., Klepacki, D., Dai, Q., Piccirilli, J., Micura, R., and Mankin, A.S. (2011). Nascent peptide in the ribosome exit tunnel affects functional properties of the A-site of the peptidyl transferase center. Mol. Cell *41*, 321–330.

Rao, S., Lee, S.-Y., Gutierrez, A., Perrigoue, J., Thapa, R.J., Tu, Z., Jeffers, J.R., Rhodes, M., Anderson, S., Oravecz, T., et al. (2012). Inactivation of ribosomal protein L22 promotes transformation by induction of the stemness factor, Lin28B. Blood *120*, 3764–3773.

Redpath, N.T., Foulstone, E.J., and Proud, C.G. (1996). Regulation of translation elongation factor-2 by insulin via a rapamycin-sensitive signalling pathway. EMBO J. *15*, 2291–2297.

Reichow, S.L., and Varani, G. (2008). Nop10 is a conserved H/ACA snoRNP molecular adaptor. Biochemistry *47*, 6148–6156.

Remacha, M., Jimenez-Diaz, A., Santos, C., Briones, E., Zambrano, R., Rodriguez Gabriel, M.A., Guarinos, E., and Ballesta, J.P. (1995). Proteins P1, P2, and P0, components of the eukaryotic ribosome stalk. New structural and functional aspects. Biochem. Cell Biol. Biochim. Biol. Cell. *73*, 959–968.

Reschke, M., Clohessy, J.G., Seitzer, N., Goldstein, D.P., Breitkopf, S.B., Schmolze, D.B., Ala, U., Asara, J.M., Beck, A.H., and Pandolfi, P.P. (2013). Characterization and Analysis of the Composition and Dynamics of the Mammalian Riboproteome. Cell Rep. *4*, 1276–1287.

Rhodin, M.H.J., Rakauskaitė, R., and Dinman, J.D. (2011). The central core region of yeast ribosomal protein L11 is important for subunit joining and translational fidelity. Mol. Genet. Genomics *285*, 505–516.

Ricci, E.P., Kucukural, A., Cenik, C., Mercier, B.C., Singh, G., Heyer, E.E., Ashar-Patel, A., Peng, L., and Moore, M.J. (2014). Staufen1 senses overall transcript secondary structure to regulate translation. Nat. Struct. Mol. Biol. *21*, 26–35.

Rife, J.P., and Moore, P.B. (1998). The structure of a methylated tetraloop in 16S ribosomal RNA. Struct. Lond. Engl. 1993 *6*, 747–756.

van Riggelen, J., Yetil, A., and Felsher, D.W. (2010). MYC as a regulator of ribosome biogenesis and protein synthesis. Nat. Rev. Cancer *10*, 301–309.

Rijnbrand, R., van der Straaten, T., van Rijn, P.A., Spaan, W.J., and Bredenbeek, P.J. (1997). Internal entry of ribosomes is directed by the 5' noncoding region of classical swine fever virus and is dependent on the presence of an RNA pseudoknot upstream of the initiation codon. J. Virol. *71*, 451–457.

Rivas, M., and Fox, G.E. (2020). Further Characterization of the Pseudo-Symmetrical Ribosomal Region. Life *10*, 201.

Rivera, M.C., Maguire, B., and Lake, J.A. (2015). Isolation of ribosomes and polysomes. Cold Spring Harb. Protoc. *2015*, 293–299.

Robledo, S., Idol, R.A., Crimmins, D.L., Ladenson, J.H., Mason, P.J., and Bessler, M. (2008). The role of human ribosomal proteins in the maturation of rRNA and ribosome production. RNA *14*, 1918–1929.

Rodnina, M.V., Stark, H., Savelsbergh, A., Wieden, H.J., Mohr, D., Matassova, N.B., Peske, F., Daviter, T., Gualerzi, C.O., and Wintermeyer, W. (2000). GTPases mechanisms and functions of translation factors on the ribosome. Biol. Chem. *381*, 377–387.

Rogers, G.W., Komar, A.A., and Merrick, W.C. (2002). eIF4A: the godfather of the DEAD box helicases. Prog. Nucleic Acid Res. Mol. Biol. *72*, 307–331.

Rohde, J.R., and Cardenas, M.E. (2003). The tor pathway regulates gene expression by linking nutrient sensing to histone acetylation. Mol. Cell. Biol. *23*, 629–635.

Rohozinski, J., Anderson, M.L., Broaddus, R.E., Edwards, C.L., and Bishop, C.E. (2009). Spermatogenesis associated retrogenes are expressed in the human ovary and ovarian cancers. PloS One *4*, e5064.

Rotenberg, M.O., Moritz, M., and Woolford, J.L. (1988). Depletion of Saccharomyces cerevisiae ribosomal protein L16 causes a decrease in 60S ribosomal subunits and formation of half-mer polyribosomes. Genes Dev. *2*, 160–172.

Roux, P.P., and Topisirovic, I. (2018). Signaling Pathways Involved in the Regulation of mRNA Translation. Mol. Cell. Biol. *38*.

Ruoff, R., Katsara, O., and Kolupaeva, V. (2016). Cell type-specific control of protein synthesis and proliferation by FGF-dependent signaling to the translation repressor 4E-BP. Proc. Natl. Acad. Sci. *113*, 7545–7550.

Ruvinsky, I., and Meyuhas, O. (2006). Ribosomal protein S6 phosphorylation: from protein synthesis to cell size. Trends Biochem. Sci. *31*, 342–348.

Ruvinsky, I., Sharon, N., Lerer, T., Cohen, H., Stolovich-Rain, M., Nir, T., Dor, Y., Zisman, P., and Meyuhas, O. (2005). Ribosomal protein S6 phosphorylation is a determinant of cell size and glucose homeostasis. Genes Dev. *19*, 2199–2211.

Ruvinsky, I., Katz, M., Dreazen, A., Gielchinsky, Y., Saada, A., Freedman, N., Mishani, E., Zimmerman, G., Kasir, J., and Meyuhas, O. (2009). Mice deficient in ribosomal protein S6 phosphorylation suffer from muscle weakness that reflects a growth defect and energy deficit. PloS One *4*, e5618.

Sachs, A.B., and Davis, R.W. (1989). The poly(A) binding protein is required for poly(A) shortening and 60S ribosomal subunit-dependent translation initiation. Cell *58*, 857–867.

Safer, B. (1989). Nomenclature of initiation, elongation and termination factors for translation in eukaryotes. Eur. J. Biochem. *186*, 1–3.

Samir, P., Browne, C.M., Rahul, null, Sun, M., Shen, B., Li, W., Frank, J., and Link, A.J. (2018). Identification of Changing Ribosome Protein Compositions using Mass Spectrometry. Proteomics *18*, e1800217.

Sanghai, Z.A., Miller, L., Molloy, K.R., Barandun, J., Hunziker, M., Chaker-Margot, M., Wang, J., Chait, B.T., and Klinge, S. (2018). Modular assembly of the nucleolar pre-60S ribosomal subunit. Nature *556*, 126–129.

Sankaran, V.G., Ghazvinian, R., Do, R., Thiru, P., Vergilio, J.-A., Beggs, A.H., Sieff, C.A., Orkin, S.H., Nathan, D.G., Lander, E.S., et al. (2012). Exome sequencing identifies GATA1 mutations resulting in Diamond-Blackfan anemia. J. Clin. Invest. *122*, 2439–2443.

Saporita, A.J., Chang, H.-C., Winkeler, C.L., Apicelli, A.J., Kladney, R.D., Wang, J., Townsend, R.R., Michel, L.S., and Weber, J.D. (2011). RNA helicase DDX5 is a p53-independent target of ARF that participates in ribosome biogenesis. Cancer Res. *71*, 6708–6717.

Sarbassov, D.D., Guertin, D.A., Ali, S.M., and Sabatini, D.M. (2005). Phosphorylation and regulation of Akt/PKB by the rictor-mTOR complex. Science *307*, 1098–1101.

Schaeffer, J., Delpech, C., Albert, F., Belin, S., and Nawabi, H. (2020). Adult Mouse Retina Explants: From ex vivo to in vivo Model of Central Nervous System Injuries. Front. Mol. Neurosci. *13*, 599948.

Scharenberg, C., Giai, V., Pellagatti, A., Saft, L., Dimitriou, M., Jansson, M., Jädersten, M., Grandien, A., Douagi, I., Neuberg, D.S., et al. (2017). Progression in patients with low- and intermediate-1-risk del(5q) myelodysplastic syndromes is predicted by a limited subset of mutations. Haematologica *102*, 498–508.

Scheper, G.C., van Kollenburg, B., Hu, J., Luo, Y., Goss, D.J., and Proud, C.G. (2002). Phosphorylation of eukaryotic initiation factor 4E markedly reduces its affinity for capped mRNA. J. Biol. Chem. *277*, 3303–3309.

Schillewaert, S., Wacheul, L., Lhomme, F., and Lafontaine, D.L.J. (2012). The evolutionarily conserved protein Las1 is required for pre-rRNA processing at both ends of ITS2. Mol. Cell. Biol. *32*, 430–444.

Schmid, T., Jansen, A.P., Baker, A.R., Hegamyer, G., Hagan, J.P., and Colburn, N.H. (2008). Translation inhibitor Pdcd4 is targeted for degradation during tumor promotion. Cancer Res. *68*, 1254–1260.

Schmied, W.H., Tnimov, Z., Uttamapinant, C., Rae, C.D., Fried, S.D., and Chin, J.W. (2018). Controlling orthogonal ribosome subunit interactions enables evolution of new function. Nature *564*, 444–448.

Schneider, R.K., Ademà, V., Heckl, D., Järås, M., Mallo, M., Lord, A.M., Chu, L.P., McConkey, M.E., Kramann, R., Mullally, A., et al. (2014). Role of casein kinase 1A1 in the biology and targeted therapy of del(5q) MDS. Cancer Cell *26*, 509–520.

Schneider, R.K., Schenone, M., Ferreira, M.V., Kramann, R., Joyce, C.E., Hartigan, C., Beier, F., Brümmendorf, T.H., Germing, U., Platzbecker, U., et al. (2016). Rps14 haploinsufficiency causes a block in erythroid differentiation mediated by S100A8 and S100A9. Nat. Med. *22*, 288–297.

Schulze, H., and Nierhaus, K.H. (1982). Minimal set of ribosomal components for reconstitution of the peptidyltransferase activity. EMBO J. *1*, 609–613.

Schuster, J., Fröjmark, A.-S., Nilsson, P., Badhai, J., Virtanen, A., and Dahl, N. (2010). Ribosomal protein S19 binds to its own mRNA with reduced affinity in Diamond-Blackfan anemia. Blood Cells. Mol. Dis. *45*, 23–28.

Schuwirth, B.S., Borovinskaya, M.A., Hau, C.W., Zhang, W., Vila-Sanjurjo, A., Holton, J.M., and Cate, J.H.D. (2005). Structures of the bacterial ribosome at 3.5 A resolution. Science *310*, 827–834.

Schwab, S.R., Shugart, J.A., Horng, T., Malarkannan, S., and Shastri, N. (2004). Unanticipated antigens: translation initiation at CUG with leucine. PLoS Biol. *2*, e366.

Schwanhäusser, B., Busse, D., Li, N., Dittmar, G., Schuchhardt, J., Wolf, J., Chen, W., and Selbach, M. (2011). Global quantification of mammalian gene expression control. Nature *473*, 337–342.

Schwartz, I., and Ofengand, J. (1978). Photochemical cross-linking of unmodified acetylvalyl-tRNA to 16S RNA at the ribosomal P site. Biochemistry *17*, 2524–2530.

Seidelt, B., Innis, C.A., Wilson, D.N., Gartmann, M., Armache, J.-P., Villa, E., Trabuco, L.G., Becker, T., Mielke, T., Schulten, K., et al. (2009). Structural Insight into Nascent Polypeptide Chain–Mediated Translational Stalling. Science *326*, 1412–1415.

Sendoel, A., Dunn, J.G., Rodriguez, E.H., Naik, S., Gomez, N.C., Hurwitz, B., Levorse, J., Dill, B.D., Schramek, D., Molina, H., et al. (2017). Translation from unconventional 5' start sites drives tumour initiation. Nature *541*, 494–499.

Sengupta, A., Rice, G.M., and Weeks, K.M. (2019). Single-molecule correlated chemical probing reveals large-scale structural communication in the ribosome and the mechanism of the antibiotic spectinomycin in living cells. PLoS Biol. *17*, e3000393.

Shahbazian, D., Roux, P.P., Mieulet, V., Cohen, M.S., Raught, B., Taunton, J., Hershey, J.W.B., Blenis, J., Pende, M., and Sonenberg, N. (2006). The mTOR/PI3K and MAPK pathways converge on eIF4B to control its phosphorylation and activity. EMBO J. *25*, 2781–2791.

Shao, S., Murray, J., Brown, A., Taunton, J., Ramakrishnan, V., and Hegde, R.S. (2016). Decoding Mammalian Ribosome-mRNA States by Translational GTPase Complexes. Cell *167*, 1229-1240.e15.

Sharifulin, D., Khairulina, Y., Ivanov, A., Meschaninova, M., Ven'yaminova, A., Graifer, D., and Karpova, G. (2012). A central fragment of ribosomal protein S26 containing the eukaryote-specific motif YxxPKxYxK is a key component of the ribosomal binding site of mRNA region 5' of the E site codon. Nucleic Acids Res. *40*, 3056–3065.

Sharma, K., and Tollervey, D. (1999). Base pairing between U3 small nucleolar RNA and the 5' end of 18S rRNA is required for pre-rRNA processing. Mol. Cell. Biol. *19*, 6012–6019.

Sharma, S., Hartmann, J.D., Watzinger, P., Klepper, A., Peifer, C., Kötter, P., Lafontaine, D.L.J., and Entian, K.-D. (2018). A single N1-methyladenosine on the large ribosomal subunit rRNA impacts locally its structure and the translation of key metabolic enzymes. Sci. Rep. *8*, 11904.

Shi, Z., Fujii, K., Kovary, K.M., Genuth, N.R., Röst, H.L., Teruel, M.N., and Barna, M. (2017). Heterogeneous Ribosomes Preferentially Translate Distinct Subpools of mRNAs Genome-wide. Mol. Cell *67*, 71-83.e7.

Shieh, S.Y., Ikeda, M., Taya, Y., and Prives, C. (1997). DNA damage-induced phosphorylation of p53 alleviates inhibition by MDM2. Cell *91*, 325–334.

Shigeoka, T., Jung, H., Jung, J., Turner-Bridger, B., Ohk, J., Lin, J.Q., Amieux, P.S., and Holt, C.E. (2016). Dynamic Axonal Translation in Developing and Mature Visual Circuits. Cell *166*, 181–192.

Shigeoka, T., Koppers, M., Wong, H.H.-W., Lin, J.Q., Cagnetta, R., Dwivedy, A., de Freitas Nascimento, J., van Tartwijk, F.W., Ströhl, F., Cioni, J.-M., et al. (2019). On-Site Ribosome Remodeling by Locally Synthesized Ribosomal Proteins in Axons. Cell Rep. *29*, 3605-3619.e10.

Shirokikh, N.E., Archer, S.K., Beilharz, T.H., Powell, D., and Preiss, T. (2017). Translation complex profile sequencing to study the in vivo dynamics of mRNA-ribosome interactions during translation initiation, elongation and termination. Nat. Protoc. *12*, 697–731.

Shoemaker, C.J., Eyler, D.E., and Green, R. (2010). Dom34:Hbs1 promotes subunit dissociation and peptidyl-tRNA drop-off to initiate no-go decay. Science *330*, 369–372.

Shor, B., Wu, J., Shakey, Q., Toral-Barza, L., Shi, C., Follettie, M., and Yu, K. (2010). Requirement of the mTOR kinase for the regulation of Maf1 phosphorylation and control of RNA polymerase III-dependent transcription in cancer cells. J. Biol. Chem. *285*, 15380–15392.

Simsek, D., and Barna, M. (2017). An emerging role for the ribosome as a nexus for post-translational modifications. Curr. Opin. Cell Biol. *45*, 92–101.

Simsek, D., Tiu, G.C., Flynn, R.A., Byeon, G.W., Leppek, K., Xu, A.F., Chang, H.Y., and Barna, M. (2017). The Mammalian Ribo-interactome Reveals Ribosome Functional Diversity and Heterogeneity. Cell *169*, 1051-1065.e18.

Singleton, R.S., Liu-Yi, P., Formenti, F., Ge, W., Sekirnik, R., Fischer, R., Adam, J., Pollard, P.J., Wolf, A., Thalhammer, A., et al. (2014). OGFOD1 catalyzes prolyl hydroxylation of RPS23 and is involved in translation control and stress granule formation. Proc. Natl. Acad. Sci. U. S. A. *111*, 4031–4036.

Slavov, N., Semrau, S., Airoldi, E., Budnik, B., and van Oudenaarden, A. (2015). Differential Stoichiometry among Core Ribosomal Proteins. Cell Rep. *13*, 865–873.

Sloan, K.E., Bohnsack, M.T., and Watkins, N.J. (2013). The 5S RNP Couples p53 Homeostasis to Ribosome Biogenesis and Nucleolar Stress. Cell Rep. *5*, 237–247.

Smith, P.D., Sun, F., Park, K.K., Cai, B., Wang, C., Kuwako, K., Martinez-Carrasco, I., Connolly, L., and He, Z. (2009). SOCS3 deletion promotes optic nerve regeneration in vivo. Neuron *64*, 617–623.

Spahn, C.M., Beckmann, R., Eswar, N., Penczek, P.A., Sali, A., Blobel, G., and Frank, J. (2001). Structure of the 80S ribosome from Saccharomyces cerevisiae--tRNA-ribosome and subunit-subunit interactions. Cell *107*, 373–386.

Spahn, C.M., Gomez-Lorenzo, M.G., Grassucci, R.A., Jørgensen, R., Andersen, G.R., Beckmann, R., Penczek, P.A., Ballesta, J.P., and Frank, J. (2004a). Domain movements of elongation factor eEF2 and the eukaryotic 80S ribosome facilitate tRNA translocation. EMBO J. *23*, 1008–1019.

Spahn, C.M.T., Jan, E., Mulder, A., Grassucci, R.A., Sarnow, P., and Frank, J. (2004b). Cryo-EM visualization of a viral internal ribosome entry site bound to human ribosomes: the IRES functions as an RNA-based translation factor. Cell *118*, 465–475.

Spriggs, K.A., Stoneley, M., Bushell, M., and Willis, A.E. (2008). Re-programming of translation following cell stress allows IRES-mediated translation to predominate. Biol. Cell *100*, 27–38.

Stage-Zimmermann, T., Schmidt, U., and Silver, P.A. (2000). Factors affecting nuclear export of the 60S ribosomal subunit in vivo. Mol. Biol. Cell *11*, 3777–3789.

Starck, S.R., Jiang, V., Pavon-Eternod, M., Prasad, S., McCarthy, B., Pan, T., and Shastri, N. (2012). Leucine-tRNA initiates at CUG start codons for protein synthesis and presentation by MHC class I. Science *336*, 1719–1723.

Starck, S.R., Tsai, J.C., Chen, K., Shodiya, M., Wang, L., Yahiro, K., Martins-Green, M., Shastri, N., and Walter, P. (2016). Translation from the 5' untranslated region shapes the integrated stress response. Science *351*, aad3867.

Steffen, K.K., McCormick, M.A., Pham, K.M., MacKay, V.L., Delaney, J.R., Murakami, C.J., Kaeberlein, M., and Kennedy, B.K. (2012). Ribosome deficiency protects against ER stress in Saccharomyces cerevisiae. Genetics *191*, 107–118.

Steward, O., and Levy, W.B. (1982). Preferential localization of polyribosomes under the base of dendritic spines in granule cells of the dentate gyrus. J. Neurosci. Off. J. Soc. Neurosci. *2*, 284–291.

Stoneley, M., and Willis, A.E. (2004). Cellular internal ribosome entry segments: structures, trans-acting factors and regulation of gene expression. Oncogene *23*, 3200–3207.

Stoneley, M., Chappell, S.A., Jopling, C.L., Dickens, M., MacFarlane, M., and Willis, A.E. (2000). c-Myc protein synthesis is initiated from the internal ribosome entry segment during apoptosis. Mol. Cell. Biol. *20*, 1162–1169.

Strunk, B.S., Loucks, C.R., Su, M., Vashisth, H., Cheng, S., Schilling, J., Brooks, C.L., Karbstein, K., and Skiniotis, G. (2011). Ribosome assembly factors prevent premature translation initiation by 40S assembly intermediates. Science *333*, 1449–1453.

Strunk, B.S., Novak, M.N., Young, C.L., and Karbstein, K. (2012). A translation-like cycle is a quality control checkpoint for maturing 40S ribosome subunits. Cell *150*, 111–121.

Subkhankulova, T., Mitchell, S.A., and Willis, A.E. (2001). Internal ribosome entry segment-mediated initiation of c-Myc protein synthesis following genotoxic stress. Biochem. J. *359*, 183–192.

Sugihara, Y., Honda, H., Iida, T., Morinaga, T., Hino, S., Okajima, T., Matsuda, T., and Nadano, D. (2010). Proteomic analysis of rodent ribosomes revealed heterogeneity including ribosomal proteins L10-like, L22-like 1, and L39-like. J. Proteome Res. *9*, 1351–1366.

Sugihara, Y., Sadohara, E., Yonezawa, K., Kugo, M., Oshima, K., Matsuda, T., and Nadano, D. (2013). Identification and expression of an autosomal paralogue of ribosomal protein S4, X-linked, in mice: potential involvement of testis-specific ribosomal proteins in translation and spermatogenesis. Gene *521*, 91–99.

Sugimoto, M., Kuo, M.-L., Roussel, M.F., and Sherr, C.J. (2003). Nucleolar Arf tumor suppressor inhibits ribosomal RNA processing. Mol. Cell *11*, 415–424.

Sulima, S.O., and De Keersmaecker, K. (2017). Ribosomal proteins: a novel class of oncogenic drivers. Oncotarget *8*, 89427–89428.

Sulima, S.O., Gülay, S.P., Anjos, M., Patchett, S., Meskauskas, A., Johnson, A.W., and Dinman, J.D. (2014). Eukaryotic rpL10 drives ribosomal rotation. Nucleic Acids Res. *42*, 2049–2063.

Sulima, S.O., Hofman, I.J.F., De Keersmaecker, K., and Dinman, J.D. (2017). How Ribosomes Translate Cancer. Cancer Discov. *7*, 1069–1087.

Sultan, A., Nesslany, F., Violet, M., Bégard, S., Loyens, A., Talahari, S., Mansuroglu, Z., Marzin, D., Sergeant, N., Humez, S., et al. (2011). Nuclear tau, a key player in neuronal DNA protection. J. Biol. Chem. *286*, 4566–4575.

Sun, F., Park, K.K., Belin, S., Wang, D., Lu, T., Chen, G., Zhang, K., Yeung, C., Feng, G., Yankner, B.A., et al. (2011). Sustained axon regeneration induced by co-deletion of PTEN and SOCS3. Nature *480*, 372–375.

Sun, X.-X., Wang, Y.-G., Xirodimas, D.P., and Dai, M.-S. (2010). Perturbation of 60 S ribosomal biogenesis results in ribosomal protein L5- and L11-dependent p53 activation. J. Biol. Chem. *285*, 25812–25821.

Sundaramoorthy, E., Leonard, M., Mak, R., Liao, J., Fulzele, A., and Bennett, E.J. (2017). ZNF598 and RACK1 Regulate Mammalian Ribosome-Associated Quality Control Function by Mediating Regulatory 40S Ribosomal Ubiquitylation. Mol. Cell *65*, 751-760.e4.

Sweeney, T.R., Abaeva, I.S., Pestova, T.V., and Hellen, C.U.T. (2014). The mechanism of translation initiation on Type 1 picornavirus IRESs. EMBO J. *33*, 76–92.

Szewczak, A.A., Moore, P.B., Chang, Y.L., and Wool, I.G. (1993). The conformation of the sarcin/ricin loop from 28S ribosomal RNA. Proc. Natl. Acad. Sci. *90*, 9581–9585.

Tahmasebi, S., Khoutorsky, A., Mathews, M.B., and Sonenberg, N. (2018). Translation deregulation in human disease. Nat. Rev. Mol. Cell Biol. *19*, 791–807.

Takahashi, S., Onodera, K., Motohashi, H., Suwabe, N., Hayashi, N., Yanai, N., Nabesima, Y., and Yamamoto, M. (1997). Arrest in primitive erythroid cell development caused by promoter-specific disruption of the GATA-1 gene. J. Biol. Chem. *272*, 12611–12615.

Takamatsu, S., Ohashi, Y., Onoue, N., Tajima, Y., Imamichi, T., Yonezawa, S., Morimoto, K., Onouchi, H., Yamashita, Y., and Naito, S. (2020). Reverse genetics-based biochemical studies of the ribosomal exit tunnel constriction region in eukaryotic ribosome stalling: spatial allocation of the regulatory nascent peptide at the constriction. Nucleic Acids Res. *48*, 1985–1999.

Takehara, Y., Yashiroda, H., Matsuo, Y., Zhao, X., Kamigaki, A., Matsuzaki, T., Kosako, H., Inada, T., and Murata, S. (2021). The ubiquitination-deubiquitination cycle on the ribosomal protein eS7A is crucial for efficient translation. IScience *24*, 102145.

Tamm, T., Kisly, I., and Remme, J. (2019). Functional Interactions of Ribosomal Intersubunit Bridges in Saccharomyces cerevisiae. Genetics *213*, 1329–1339.

Taoka, M., Nobe, Y., Yamaki, Y., Yamauchi, Y., Ishikawa, H., Takahashi, N., Nakayama, H., and Isobe, T. (2016). The complete chemical structure of Saccharomyces cerevisiae rRNA: partial pseudouridylation of U2345 in 25S rRNA by snoRNA snR9. Nucleic Acids Res. *44*, 8951–8961.

Taylor, A.M., Berchtold, N.C., Perreau, V.M., Tu, C.H., Li Jeon, N., and Cotman, C.W. (2009). Axonal mRNA in uninjured and regenerating cortical mammalian axons. J. Neurosci. Off. J. Soc. Neurosci. *29*, 4697–4707.

Terenzio, M., Koley, S., Samra, N., Rishal, I., Zhao, Q., Sahoo, P.K., Urisman, A., Marvaldi, L., Oses-Prieto, J.A., Forester, C., et al. (2018). Locally translated mTOR controls axonal local translation in nerve injury. Science *359*, 1416–1421.

Thakor, N., and Holcik, M. (2012). IRES-mediated translation of cellular messenger RNA operates in eIF2α- independent manner during stress. Nucleic Acids Res. *40*, 541–552.

Thoms, M., Buschauer, R., Ameismeier, M., Koepke, L., Denk, T., Hirschenberger, M., Kratzat, H., Hayn, M., Mackens-Kiani, T., Cheng, J., et al. (2020). Structural basis for translational shutdown and immune evasion by the Nsp1 protein of SARS-CoV-2. Science *369*, 1249–1255.

Thorrez, L., Van Deun, K., Tranchevent, L.-C., Van Lommel, L., Engelen, K., Marchal, K., Moreau, Y., Van Mechelen, I., and Schuit, F. (2008). Using ribosomal protein genes as reference: a tale of caution. PloS One *3*, e1854.

Tikole, S., and Sankararamakrishnan, R. (2006). A survey of mRNA sequences with a non-AUG start codon in RefSeq database. J. Biomol. Struct. Dyn. *24*, 33–42.

Timsit, Y., and Bennequin, D. (2019). Nervous-Like Circuits in the Ribosome Facts, Hypotheses and Perspectives. Int. J. Mol. Sci. *20*, 2911.

Timsit, Y., Sergeant-Perthuis, G., and Bennequin, D. (2021). Evolution of ribosomal protein network architectures. Sci. Rep. *11*, 625.

Tiu, G.C., Kerr, C.H., Forester, C.M., Krishnarao, P.S., Rosenblatt, H.D., Raj, N., Lantz, T.C., Zhulyn, O., Bowen, M.E., Shokat, L., et al. (2021). A p53-dependent translational program directs tissue-selective phenotypes in a model of ribosomopathies. Dev. Cell S1534-5807(21)00520-7.

Tiwari, N.K., Sathyanesan, M., Kumar, V., and Newton, S.S. (2021). A Comparative Analysis of Erythropoietin and Carbamoylated Erythropoietin Proteome Profiles. Life Basel Switz. *11*, 359.

Todd, P.K., Oh, S.Y., Krans, A., He, F., Sellier, C., Frazer, M., Renoux, A.J., Chen, K., Scaglione, K.M., Basrur, V., et al. (2013). CGG repeat-associated translation mediates neurodegeneration in fragile X tremor ataxia syndrome. Neuron *78*, 440–455.

Trabuco, L.G., Schreiner, E., Eargle, J., Cornish, P., Ha, T., Luthey-Schulten, Z., and Schulten, K. (2010). The role of L1 stalk-tRNA interaction in the ribosome elongation cycle. J. Mol. Biol. *402*, 741–760.

Treangen, T.J., and Salzberg, S.L. (2011). Repetitive DNA and next-generation sequencing: computational challenges and solutions. Nat. Rev. Genet. *13*, 36–46.

Tseng, H., Chou, W., Wang, J., Zhang, X., Zhang, S., and Schultz, R.M. (2008). Mouse ribosomal RNA genes contain multiple differentially regulated variants. PloS One *3*, e1843.

Tsofack, S.P., Meunier, L., Sanchez, L., Madore, J., Provencher, D., Mes-Masson, A.-M., and Lebel, M. (2013). Low expression of the X-linked ribosomal protein S4 in human serous epithelial ovarian cancer is associated with a poor prognosis. BMC Cancer *13*, 303.

Tsukiyama-Kohara, K., Iizuka, N., Kohara, M., and Nomoto, A. (1992). Internal ribosome entry site within hepatitis C virus RNA. J. Virol. *66*, 1476–1483.

Turi, Z., Lacey, M., Mistrik, M., and Moudry, P. (2019). Impaired ribosome biogenesis: mechanisms and relevance to cancer and aging. Aging *11*, 2512–2540.

Uchiumi, T., Honma, S., Endo, Y., and Hachimori, A. (2002a). Ribosomal Proteins at the Stalk Region Modulate Functional rRNA Structures in the GTPase Center *. J. Biol. Chem. *277*, 41401–41409.

Uchiumi, T., Honma, S., Nomura, T., Dabbs, E.R., and Hachimori, A. (2002b). Translation elongation by a hybrid ribosome in which proteins at the GTPase center of the Escherichia coli ribosome are replaced with rat counterparts. J. Biol. Chem. *277*, 3857–3862.

Uechi, T., Tanaka, T., and Kenmochi, N. (2001). A Complete Map of the Human Ribosomal Protein Genes: Assignment of 80 Genes to the Cytogenetic Map and Implications for Human Disorders. Genomics *72*, 223–230.

Uechi, T., Maeda, N., Tanaka, T., and Kenmochi, N. (2002). Functional second genes generated by retrotransposition of the X-linked ribosomal protein genes. Nucleic Acids Res. *30*, 5369–5375.

Uechi, T., Nakajima, Y., Nakao, A., Torihara, H., Chakraborty, A., Inoue, K., and Kenmochi, N. (2006). Ribosomal protein gene knockdown causes developmental defects in zebrafish. PloS One *1*, e37.

Uechi, T., Nakajima, Y., Chakraborty, A., Torihara, H., Higa, S., and Kenmochi, N. (2008). Deficiency of ribosomal protein S19 during early embryogenesis leads to reduction of erythrocytes in a zebrafish model of Diamond-Blackfan anemia. Hum. Mol. Genet. *17*, 3204–3211.

Ulirsch, J.C., Verboon, J.M., Kazerounian, S., Guo, M.H., Yuan, D., Ludwig, L.S., Handsaker, R.E., Abdulhay, N.J., Fiorini, C., Genovese, G., et al. (2018). The Genetic Landscape of Diamond-Blackfan Anemia. Am. J. Hum. Genet. *103*, 930–947.

Unbehaun, A., Borukhov, S.I., Hellen, C.U.T., and Pestova, T.V. (2004). Release of initiation factors from 48S complexes during ribosomal subunit joining and the link between establishment of codon-anticodon base-pairing and hydrolysis of eIF2-bound GTP. Genes Dev. *18*, 3078–3093.

Van Raay, T.J., Connors, T.D., Klinger, K.W., Landes, G.M., and Burn, T.C. (1996). A novel ribosomal protein L3-like gene (RPL3L) maps to the autosomal dominant polycystic kidney disease gene region. Genomics *37*, 172–176.

Vard, C., Guillot, D., Bargis, P., Lavergne, J.P., and Reboud, J.P. (1997). A specific role for the phosphorylation of mammalian acidic ribosomal protein P2. J. Biol. Chem. *272*, 20259–20262.

Venturi, G., and Montanaro, L. (2020). How Altered Ribosome Production Can Cause or Contribute to Human Disease: The Spectrum of Ribosomopathies. Cells *9*, 2300.

Vialaret, J., Schmit, P.-O., Lehmann, S., Gabelle, A., Wood, J., Bern, M., Paape, R., Suckau, D., Kruppa, G., and Hirtz, C. (2018). Identification of multiple proteoforms biomarkers on clinical samples by routine Top-Down approaches. Data Brief *18*, 1013–1021.

Vidova, V., and Spacil, Z. (2017). A review on mass spectrometry-based quantitative proteomics: Targeted and data independent acquisition. Anal. Chim. Acta *964*, 7–23.

Voit, R., and Grummt, I. (2001). Phosphorylation of UBF at serine 388 is required for interaction with RNA polymerase I and activation of rDNA transcription. Proc. Natl. Acad. Sci. U. S. A. *98*, 13631–13636.

Volarevic, S., Stewart, M.J., Ledermann, B., Zilberman, F., Terracciano, L., Montini, E., Grompe, M., Kozma, S.C., and Thomas, G. (2000). Proliferation, but not growth, blocked by conditional deletion of 40S ribosomal protein S6. Science *288*, 2045–2047.

Voorhees, R.M., Fernández, I.S., Scheres, S.H.W., and Hegde, R.S. (2014). Structure of the mammalian ribosome-Sec61 complex to 3.4 Å resolution. Cell *157*, 1632–1643.

Wada, A. (1986). Analysis of Escherichia coli ribosomal proteins by an improved two dimensional gel electrophoresis. I. Detection of four new proteins. J. Biochem. (Tokyo) *100*, 1583–1594.

Wade, M., Li, Y.-C., and Wahl, G.M. (2013). MDM2, MDMX and p53 in oncogenesis and cancer therapy. Nat. Rev. Cancer *13*, 83–96.

Wang, M., and Pestov, D.G. (2011). 5'-end surveillance by Xrn2 acts as a shared mechanism for mammalian pre-rRNA maturation and decay. Nucleic Acids Res. *39*, 1811–1822.

Wang, H., Sun, L., Gaba, A., and Qu, X. (2020a). An in vitro single-molecule assay for eukaryotic cap-dependent translation initiation kinetics. Nucleic Acids Res. *48*, e6.

Wang, L., Xu, Y., Rogers, H., Saidi, L., Noguchi, C.T., Li, H., Yewdell, J.W., Guydosh, N.R., and Ye, Y. (2020b). UFMylation of RPL26 links translocation-associated quality control to endoplasmic reticulum protein homeostasis. Cell Res. *30*, 5–20.

Wang, X., Li, W., Williams, M., Terada, N., Alessi, D.R., and Proud, C.G. (2001). Regulation of elongation factor 2 kinase by p90(RSK1) and p70 S6 kinase. EMBO J. *20*, 4370–4379.

Wang, X., Rusin, A., Walkey, C.J., Lin, J.J., and Johnson, D.L. (2019). The RNA polymerase III repressor MAF1 is regulated by ubiquitin-dependent proteasome degradation and modulates cancer drug resistance and apoptosis. J. Biol. Chem. *294*, 19255–19268.

Warner, J.R. (1999). The economics of ribosome biosynthesis in yeast. Trends Biochem. Sci. *24*, 437–440.

Warner, J.R., and McIntosh, K.B. (2009). How common are extraribosomal functions of ribosomal proteins? Mol. Cell *34*, 3–11.

Washburn, M.P., Wolters, D., and Yates, J.R. (2001). Large-scale analysis of the yeast proteome by multidimensional protein identification technology. Nat. Biotechnol. *19*, 242–247.

Watkins, N.J., and Bohnsack, M.T. (2012). The box C/D and H/ACA snoRNPs: key players in the modification, processing and the dynamic folding of ribosomal RNA. WIREs RNA *3*, 397–414.

Weber, H.J. (1972). Stoichiometric measurements of 30S and 50S ribosomal proteins from Escherichia coli. Mol. Gen. Genet. MGG *119*, 233–248.

Wek, R.C. (2018). Role of eIF2α Kinases in Translational Control and Adaptation to Cellular Stress. Cold Spring Harb. Perspect. Biol. *10*, a032870.

Wekselman, I., Zimmerman, E., Davidovich, C., Belousoff, M., Matzov, D., Krupkin, M., Rozenberg, H., Bashan, A., Friedlander, G., Kjeldgaard, J., et al. (2017). The Ribosomal Protein uL22 Modulates the Shape of the Protein Exit Tunnel. Struct. Lond. Engl. 1993 *25*, 1233-1241.e3.

Wells, G.R., Weichmann, F., Colvin, D., Sloan, K.E., Kudla, G., Tollervey, D., Watkins, N.J., and Schneider, C. (2016). The PIN domain endonuclease Utp24 cleaves pre-ribosomal RNA at two coupled sites in yeast and humans. Nucleic Acids Res. *44*, 5399–5409.

Westermann, P., Heumann, W., and Bielka, H. (1976). On the stoichiometry of proteins in the small ribosomal subunit of hepatoma ascites cells. FEBS Lett. *62*, 132–135.

Wilson, D.M., Li, Y., LaPeruta, A., Gamalinda, M., Gao, N., and Woolford, J.L. (2020). Structural insights into assembly of the ribosomal nascent polypeptide exit tunnel. Nat. Commun. *11*, 5111.

Wilson, D.N., Arenz, S., and Beckmann, R. (2016). Translation regulation via nascent polypeptide-mediated ribosome stalling. Curr. Opin. Struct. Biol. *37*, 123–133.

Wilson-Edell, K.A., Kehasse, A., Scott, G.K., Yau, C., Rothschild, D.E., Schilling, B., Gabriel, B.S., Yevtushenko, M.A., Hanson, I.M., Held, J.M., et al. (2014). RPL24: a potential therapeutic target whose depletion or acetylation inhibits polysome assembly and cancer cell growth. Oncotarget *5*, 5165–5176.

Witcher, K.G., Bray, C.E., Chunchai, T., Zhao, F., O'Neil, S.M., Gordillo, A.J., Campbell, W.A., McKim, D.B., Liu, X., Dziabis, J.E., et al. (2021). Traumatic Brain Injury Causes Chronic Cortical Inflammation and Neuronal Dysfunction Mediated by Microglia. J. Neurosci. Off. J. Soc. Neurosci. *41*, 1597–1616.

Wittenberg, A.D., Azar, S., Klochendler, A., Stolovich-Rain, M., Avraham, S., Birnbaum, L., Binder Gallimidi, A., Katz, M., Dor, Y., and Meyuhas, O. (2016). Phosphorylated Ribosomal Protein S6 Is Required for Akt-Driven Hyperplasia and Malignant Transformation, but Not for Hypertrophy, Aneuploidy and Hyperfunction of Pancreatic β-Cells. PloS One *11*, e0149995.

Woese, C.R., Fox, G.E., Zablen, L., Uchida, T., Bonen, L., Pechman, K., Lewis, B.J., and Stahl, D. (1975). Conservation of primary structure in 16S ribosomal RNA. Nature *254*, 83–86.

Wong, Q.W.-L., Li, J., Ng, S.R., Lim, S.G., Yang, H., and Vardy, L.A. (2014). RPL39L is an example of a recently evolved ribosomal protein paralog that shows highly specific tissue expression patterns and is upregulated in ESCs and HCC tumors. RNA Biol. *11*, 33–41.

Wruck, F., Tian, P., Kudva, R., Best, R.B., von Heijne, G., Tans, S.J., and Katranidis, A. (2021). The ribosome modulates folding inside the ribosomal exit tunnel. Commun. Biol. *4*, 523.

Wu, S., Tutuncuoglu, B., Yan, K., Brown, H., Zhang, Y., Tan, D., Gamalinda, M., Yuan, Y., Li, Z., Jakovljevic, J., et al. (2016). Diverse roles of assembly factors revealed by structures of late nuclear pre-60S ribosomes. Nature *534*, 133–137.

Wu, X., Bayle, J.H., Olson, D., and Levine, A.J. (1993). The p53-mdm-2 autoregulatory feedback loop. Genes Dev. *7*, 1126–1132.

Wu, X., Liu, S., Lyu, J., Zhou, S., Yang, Y., Wang, C., Gu, W., Zuo, Q., Li, B., and Fan, C. (2017). Endogenous controls of gene expression in N-methyl-N-nitrosourea-induced T-cell lymphoma in p53-deficient mice. BMC Cancer *17*, 545.

Xiang, Y., Zhou, S., Hao, J., Zhong, C., Ma, Q., Sun, Z., and Wei, C. (2020). Development and validation of a prognostic model for kidney renal clear cell carcinoma based on RNA binding protein expression. Aging *12*, 25356–25372.

Xiao, Z.X., Chen, J., Levine, A.J., Modjtahedi, N., Xing, J., Sellers, W.R., and Livingston, D.M. (1995). Interaction between the retinoblastoma protein and the oncoprotein MDM2. Nature *375*, 694–698.

Ximerakis, M., Lipnick, S.L., Innes, B.T., Simmons, S.K., Adiconis, X., Dionne, D., Mayweather, B.A., Nguyen, L., Niziolek, Z., Ozek, C., et al. (2019). Single-cell transcriptomic profiling of the aging mouse brain. Nat. Neurosci. *22*, 1696–1708.

Xue, S., Tian, S., Fujii, K., Kladwang, W., Das, R., and Barna, M. (2015). RNA regulons in Hox 5' UTRs confer ribosome specificity to gene regulation. Nature *517*, 33–38.

Yamashita, R., Suzuki, Y., Takeuchi, N., Wakaguri, H., Ueda, T., Sugano, S., and Nakai, K. (2008). Comprehensive detection of human terminal oligo-pyrimidine (TOP) genes and analysis of their characteristics. Nucleic Acids Res. *36*, 3707–3715.

Yang, D.-Q., Halaby, M.-J., and Zhang, Y. (2006). The identification of an internal ribosomal entry site in the 5'-untranslated region of p53 mRNA provides a novel mechanism for the regulation of its translation following DNA damage. Oncogene *25*, 4613–4619.

Yang, J., Sharma, S., Kötter, P., and Entian, K.-D. (2015). Identification of a new ribose methylation in the 18S rRNA of S. cerevisiae. Nucleic Acids Res. *43*, 2342–2352.

Yang, T.-H., Wang, C.-Y., Tsai, H.-C., and Liu, C.-T. (2021). Human IRES Atlas: an integrative platform for studying IRES-driven translational regulation in humans. Database J. Biol. Databases Curation *2021*, baab025.

Yi, Y., Li, Y., Meng, Q., Li, Q., Li, F., Lu, B., Shen, J., Fazli, L., Zhao, D., Li, C., et al. (2021). A PRC2-independent function for EZH2 in regulating rRNA 2'-O methylation and IRES-dependent translation. Nat. Cell Biol. *23*, 341–354.

Yoon, B.C., Jung, H., Dwivedy, A., O'Hare, C.M., Zivraj, K.H., and Holt, C.E. (2012). Local translation of extranuclear lamin B promotes axon maintenance. Cell *148*, 752–764.

Yoshikawa, H., Ishikawa, H., Izumikawa, K., Miura, Y., Hayano, T., Isobe, T., Simpson, R.J., and Takahashi, N. (2015). Human nucleolar protein Nop52 (RRP1/NNP-1) is involved in site 2 cleavage in internal transcribed spacer 1 of pre-rRNAs at early stages of ribosome biogenesis. Nucleic Acids Res. *43*, 5524–5536.

Youngman, E.M., Cochella, L., Brunelle, J.L., He, S., and Green, R. (2006). Two Distinct Conformations of the Conserved RNA-rich Decoding Center of the Small Ribosomal Subunit Are Recognized by tRNAs and Release Factors. Cold Spring Harb. Symp. Quant. Biol. *71*, 545–549.

Youngman, E.M., He, S.L., Nikstad, L.J., and Green, R. (2007). Stop Codon Recognition by Release Factors Induces Structural Rearrangement of the Ribosomal Decoding Center that Is Productive for Peptide Release. Mol. Cell *28*, 533–543.

Yu, Y., Maggi, L.B., Brady, S.N., Apicelli, A.J., Dai, M.-S., Lu, H., and Weber, J.D. (2006). Nucleophosmin is essential for ribosomal protein L5 nuclear export. Mol. Cell. Biol. *26*, 3798–3809.

Yusupov, M.M., Yusupova, G.Z., Baucom, A., Lieberman, K., Earnest, T.N., Cate, J.H., and Noller, H.F. (2001). Crystal structure of the ribosome at 5.5 A resolution. Science *292*, 883–896.

Zentner, G.E., Saiakhova, A., Manaenkov, P., Adams, M.D., and Scacheri, P.C. (2011). Integrative genomic analysis of human ribosomal DNA. Nucleic Acids Res. *39*, 4949–4960.

Zhang, J., Harnpicharnchai, P., Jakovljevic, J., Tang, L., Guo, Y., Oeffinger, M., Rout, M.P., Hiley, S.L., Hughes, T., and Woolford, J.L. (2007). Assembly factors Rpf2 and Rrs1 recruit 5S rRNA and ribosomal proteins rpL5 and rpL11 into nascent ribosomes. Genes Dev. *21*, 2580–2592.

Zhang, X., Shu, L., Hosoi, H., Murti, K.G., and Houghton, P.J. (2002). Predominant nuclear localization of mammalian target of rapamycin in normal and malignant cells in culture. J. Biol. Chem. *277*, 28127–28134.

Zhang, X., Wang, W., Wang, H., Wang, M.-H., Xu, W., and Zhang, R. (2013a). Identification of ribosomal protein S25 (RPS25)-MDM2-p53 regulatory feedback loop. Oncogene *32*, 2782–2791.

Zhang, Y., Wolf, G.W., Bhat, K., Jin, A., Allio, T., Burkhart, W.A., and Xiong, Y. (2003). Ribosomal protein L11 negatively regulates oncoprotein MDM2 and mediates a p53-dependent ribosomal-stress checkpoint pathway. Mol. Cell. Biol. *23*, 8902–8912.

Zhang, Y., Wölfle, T., and Rospert, S. (2013b). Interaction of nascent chains with the ribosomal tunnel proteins Rpl4, Rpl17, and Rpl39 of Saccharomyces cerevisiae. J. Biol. Chem. *288*, 33697–33707.

Zhang, Y., Duc, A.-C.E., Rao, S., Sun, X.-L., Bilbee, A.N., Rhodes, M., Li, Q., Kappes, D.J., Rhodes, J., and Wiest, D.L. (2013c). Control of hematopoietic stem cell emergence by antagonistic functions of ribosomal protein paralogs. Dev. Cell *24*, 411–425.

Zhang, Y., O'Leary, M.N., Peri, S., Wang, M., Zha, J., Melov, S., Kappes, D.J., Feng, Q., Rhodes, J., Amieux, P.S., et al. (2017). Ribosomal Proteins Rpl22 and Rpl22l1 Control Morphogenesis by Regulating Pre-mRNA Splicing. Cell Rep. *18*, 545–556.

Zhao, J., Li, Y., Wang, C., Zhang, H., Zhang, H., Jiang, B., Guo, X., and Song, X. (2020). IRESbase: A Comprehensive Database of Experimentally Validated Internal Ribosome Entry Sites. Genomics Proteomics Bioinformatics *18*, 129–139.

Zhong, J., Zhang, T., and Bloch, L.M. (2006). Dendritic mRNAs encode diversified functionalities in hippocampal pyramidal neurons. BMC Neurosci. *7*, 17.

Zhou, X., Hao, Q., Liao, J., Zhang, Q., and Lu, H. (2013). Ribosomal protein S14 unties the MDM2-p53 loop upon ribosomal stress. Oncogene *32*, 388–396.

Zhu, J.W., DeRyckere, D., Li, F.X., Wan, Y.Y., and DeGregori, J. (1999). A role for E2F1 in the induction of ARF, p53, and apoptosis during thymic negative selection. Cell Growth Differ. Mol. Biol. J. Am. Assoc. Cancer Res. *10*, 829–838.

Zinn, A.R., Bressler, S.L., Beer-Romero, P., Adler, D.A., Chapman, V.M., Page, D.C., and Disteche, C.M. (1991). Inactivation of the Rps4 gene on the mouse X chromosome. Genomics *11*, 1097–1101.

Zinn, A.R., Alagappan, R.K., Brown, L.G., Wool, I., and Page, D.C. (1994). Structure and function of ribosomal protein S4 genes on the human and mouse sex chromosomes. Mol. Cell. Biol. *14*, 2485–2492.

Zirin, J., Ni, X., Sack, L.M., Yang-Zhou, D., Hu, Y., Brathwaite, R., Bulyk, M.L., Elledge, S.J., and Perrimon, N. (2019). Interspecies analysis of MYC targets identifies tRNA synthetases as mediators of growth and survival in MYC-overexpressing cells. Proc. Natl. Acad. Sci. *116*, 14614–14619.

Zu, T., Gibbens, B., Doty, N.S., Gomes-Pereira, M., Huguet, A., Stone, M.D., Margolis, J., Peterson, M., Markowski, T.W., Ingram, M.A.C., et al. (2011). Non-ATG-initiated translation directed by microsatellite expansions. Proc. Natl. Acad. Sci. U. S. A. *108*, 260–265.

Résumé en français

Introduction

Au sein des cellules, les protéines sont formées suite à la traduction de molécule d'ARN messager ou ARNm par le complexe de traduction. Ce complexe de traduction comporte quatre composantes : les ribosomes, les facteurs de traductions, les facteurs associés au ribosomes et les ARN de transfert (ARNt). Chaque composante a un rôle spécifique au cours de la traduction.

- Les ribosomes. Ils sont composés de quatre molécules d'ARN ribosomiques (ARNr) appelés 5S, 5.8S, 28S et 18S ainsi et d'environ 80 protéines ribosomales (PR). Ils possèdent une activité ribozyme où l'ARNr catalyse la formation de la liaison peptidique entre les acides aminées composant la protéine.
- Les facteurs de traduction. Il en existe 3 types : facteur d'initiation, d'élongation et de terminaison. Ses facteurs sont nécessaires pour une traduction efficace.
- Les facteurs associés au ribosomes. Ce groupe rassemble toutes les molécules interagissant de façon transitoire au cours de la traduction, à l'exception des facteurs de traduction.
- Les ARN de transfert. Ces ARNs sont des adaptateurs entre l'ARNm et la protéine.

Au cours de mes travaux, je me suis majoritairement focalisée sur un composant de ce complexe de traduction : le ribosome.

1. Synthèse et structure du ribosome

La synthèse du ribosome a lieu au sein du nucléole où sont regroupés des gènes ribosomaux activement transcrits. Les protéines ribosomales sont transcrites dans le noyau, exportées pour être traduites dans le cytoplasme plus relocalisé au noyau pour être intégrées aux ribosomes en cours de synthèse. Le pré-ARN ribosomal est transcrit et modifié en cours de synthèse par l'ajout de 2-O méthylations ou de pseudouridylations. Cet ARN successivement clivé par les endo- et des exonucléases. Les protéines ribosomales sont rajoutées au fur et à mesure pour former les sous-unités ribosomales. L'étape de maturation des sous-unités se termine dans le cytoplasme. La synthèse ribosomale est un processus finement régulé. Tout dérèglement mène à l'arrêt du cycle cellulaire pour mener à une mort cellulaire par apoptose.

Comme mentionné précédemment, le ribosome est composé d'environ 80 protéines ribosomales et de quatre molécules d'ARN ribosomales réparties en deux sous-unités, la petite et la grande sous unités. Ces sous unités sont maintenues par des ponts inter-sous-unité contiennent elles-mêmes des domaines fonctionnelles (figure xx

La grande sous-unité 60S est composée d'environ 47 RP et de trois molécules d'ARN ribosomales : la 5S, 5.8S et la 28S. Cette sous-unité comporte :

- La protubérance centrale qui participe à la formation de pont entre les deux sous-unités permettant ainsi la coordination du processus de traduction.
- La tige L1 qui est nécessaire pour l'export du ribosome du noyau. Elle se situe à la sortie de l'ARNt du site P
- La région associé à la GTPase qui est une région composé de
    - La tige P qui permet de recrutement de facteurs d'élongation et est nécessaire à l'activité ribosomale
    - La boucle sarcin-ricin qui est exclusivement composée d'ARNr et qui est impliquée dans le recrutement de facteurs de traduction.
- Le tunnel de sortie du polypeptide où pourraient avoir lieu les premiers replis de la protéine naissante.
- Le centre de transfert peptidyl qui est composé uniquement par l'ARN 28S. Son rôle est de catalyser la formation de la liaison peptidique entre les acide aminés

La petite sous-unité 40S contient quant à elle le centre de décodage de l'ARNm. C'est l'endroit où sera évaluée la force de liaison entre l'ARNt et l'ARNm au cours de l'initiation.

Les deux sous unités comportent 3 sites à l'interface :

- le site aminoacyl ou site A, qui est le lieu de décodage de l'ARNm
- le site peptidyl ou site P qui contient l'ARNt estérifié à la chaîne peptidique en cours de synthèse.
- le site de sortie appelé site E qui est le lieu de sortie de l'ARNm et de l'ARNt.

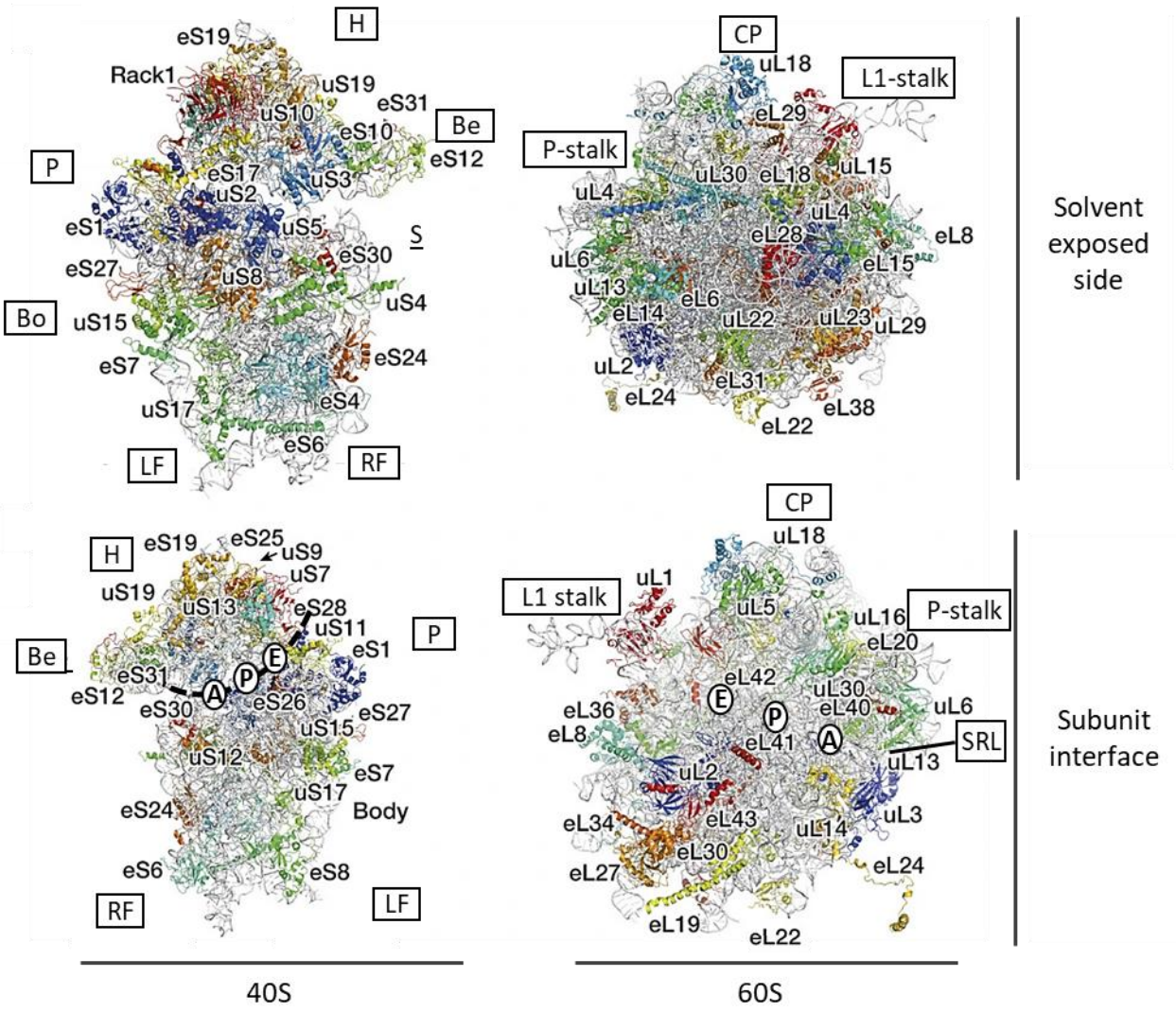

Figure 2 structure du ribosome

2. Rôle des ribosomes au cours de la traduction

La traduction se déroule en trois étapes. Au cours de l'initiation, les facteurs d'initiation eIF4A, eIF4E et eIF4G s'assemblent pour former le complexe eIF4F qui se liera à la coiffe en 5' présent sur les ARNm. eIF2-GTP se lie à un ARNt initiateur pour former le complexe ternaire, qui recrutera à son tour une sous-unité 40S lié à eIF1, eIF1A, eIF3 et eIF5 formant ainsi le complexe de préinitiation. Ce complexe de préinitiation se rassemblera au complexe eIF4F formant ainsi le complexe d'initiation. Ce complexe scanne l'ARNm jusqu'au reconnaître le site d'initiation de la traduction qui marque le début du cadre ouvert de lecture de l'ARNm. Il existe également une initiation coiffe indépendante ou IRES dépendante où la sous unité 40S est directement recrutée à site d'initiation via la reconnaissance de structure

secondaire formée par le repliement de l'ARNm. La sous-unité 60S est ensuite recrutée formant ainsi un ribosome compétent, avec l'ARNt initiateur dans le site P.

L'élongation est l'étape où l'ARNm est décodé par les ribosomes. Les ARNt, chargés d'un acide aminé (aa) sont recrutés sur le site A. L'aa incorporée dans la chaîne polypeptidique est déterminée par l'interaction entre l'ARNt entrant et le codon présent à l'intérieur du site A du ribosome. Le facteur d'élongation eucaryote 1A (eEF1A) lié au GTP est également requis. L'ARNt entrera dans le site A avec eEF1A-GTP et interagit avec le codon présent à l'intérieur du site A. Les interactions sont stabilisées par appariement de bases Watson & Crick sur la position des codons +1 et +2. Plus de tolérance est fournie sur la 3ème base appelée base oscillante. Lors de l'appariement, l'interaction codon-anticodon entre l'ARNm et l'ARNt induit l'hydrolyse du GTP en GDP et la dissociation de eEF1A du ribosome (Crepin et al., 2014).

La proximité des deux ARNt avec les sites A et P conduit à la formation de la liaison peptidique entre l'aa entrant et le polypeptide naissant. La formation de liaison peptidique est concomitante au transfert de la chaîne polypeptidique vers l'ARNt présent dans le site A. L'ensemble du processus est catalysé par l'ARNr 28S dans le ribosome. Le ribosome va alors subir un réarrangement conformationnel qui conduit à la translocation de l'ARNt du site P vers le site de sortie (E) et du site A vers le site P. L'achèvement de la translocation nécessite eEF2 dans le site A. L'ARNt désacétylé présent dans le site E sortira du ribosome tandis que le site A est prêt pour le prochain ARNt chargé. Ce cycle se poursuivra jusqu'à ce que le ribosome atteigne un codon d'arrêt.

La terminaison de la traduction est caractérisée par la présence d'un codon stop (UAA, UAG, UGA) dans le site A. Les facteurs de relargage eucaryotes eRF1 et eRF3 se lient au site A et induisent, par un changement de conformation, l'hydrolyse de la liaison peptidyl-ARNt libérant ainsi le polypeptide nouvellement synthétisé. Le complexe ribosomique post-terminaison, composé du ribosome 80S encore lié à l'ARNm, de l'ARNt désacylé au site P et des facteurs de libération, est ensuite recyclé. Les facteurs de libération se détachent du ribosome et les sous-unités ribosomiques se dissocient. Cette étape nécessite des facteurs d'initiation. Dans un environnement à faible Mg2+, eIF3, eIF1 et eIF1A interagissent avec le ribosome 80S lié à l'ARNm, avec l'ARNt dans le site P. eIF3 induit la dissociation de la grande et de la petite sous-unité tandis que eIF1 induit la dissociation et la libération de l'ARNm et de l'ARNt (Unbehaun et al., 2004). eIF3, eIF1 et eIF1A restent fixés à la sous-unité 40S pour empêcher sa réassociation avec la sous-unité 60S. Dans des conditions de concentration élevée

en Mg2+, la séparation de la sous-unité nécessitera la présence supplémentaire du transporteur de cassette de liaison à l'ATP ABCE1.

3. Hétérogénéité des ribosomes et traduction

Le concept de l'hétérogénéité des ribosomes a commencé à apparaître à la fin des années 80s suite à une étude qui révélait que toutes les PR n'étaient pas essentielles à la survie et la croissance de cultures d'*E.coli*. (Dabbs, 1986). Des études ont également été faites chez la drosophile, sur le mutant *minute* qui présente des mutations sur les gènes codant pour les PR mutants (Kongsuwan et al., 1985; Marygold et al., 2007). Des études effectuées chez la levure, le zebraFish, la souris et l'homme démontrent des dysfonctionnements similaires. Il existe différents degrés de pénétrance des mutations perte de fonction affectant les RP dans chaque organisme (Polymenis, 2020).

Il existe deux théories opposées qui ont été proposées pour expliquer la spécificité tissulaire de la traduction de l'ARNm et des ribosomopathies, c'est-à-dire des maladies causées par la dérégulation des ribosomes. La première théorie pour expliquer la spécificité observée de l'activité ribosomique a été la théorie dominante pendant des décennies. La théorie est appelée modèle d'abondance ou de concentration qui repose sur la disponibilité limitée des ribosomes en raison d'un défaut d'assemblage des ribosomes (Lodish, 1974). Selon cette théorie, la spécificité tissulaire observée dans la traduction des ARNm s'explique par un nombre limité de ribosomes disponibles (Ludwig et al., 2014 ; Kirby et al., 2015). La deuxième théorie est celle dans laquelle le ribosome joue un rôle central dans la régulation de la traduction. Selon cette théorie, une hétérogénéité dans le complexe de traduction pourrait expliquer les aspects spécifiques des tissus. Il pourrait s'adapter au contexte cellulaire pour influencer la traduction des ARNm.

L' hétérogénéité des RP est due à la présence de paralogues spécifiques comme RPL3 ou RPL10L. Des études ultérieures ont révélé que ces paralogues sont toujours associés à une localisation et/ou à des fonctions spécifiques (Gupta et Warner, 2014 ; Guimaraes et Zavolan, 2016). Il y a également une hétérogénéité au niveau de la composition en termes de PR. Toutes mes PR ne sont pas nécessaires au fonctionnement du ribosome. La comparaison des monosomes et des polysomes de cellules embryonnaires de souris par analyse spectrale révèle une expression différentielle de RPS4X, RPS3, RPL30 et RPL27A. La composition des ribosomes influencerait l'efficacité de traduction du ribosomes. Des modifications post-

traductionnelles (PTM) telles que la phosphorylation, l'hydroxylation et l'ubiquitination peuvent être ajoutées sur les PR. Des modifications peuvent également être supprimées pour moduler la structure des PR et éventuellement la structure du ribosome. L'hétérogénéité est aussi observée au niveau de la modification d'ARN ribosomales et des facteurs associés au ribosomes

Nous étions intéressés à connaître la composition du ribosome en condition physiologique *in vivo* ainsi que les facteurs associés au ribosome. Nous avons aussi investigué l'effets des protéines ribosomales et des 2'O méthylation sur la régénération axonal au sein du système nerveux centrale

Résultats

Etude 1 : Hétérogénéité des ribosomes chez le modèle murin

Afin de déterminer la composition des ribosomes in vivo, nous avons purifier les ribosomes à partir de 10 organes (poumon, rein, glandes surrénales, foie, intestin grêle, rate, testicule, cœur et le muscle quadriceps femoris muscle). Nous avons également purifié des ribosomes à partir de différentes régions du système nerveux central (CNS) (cervelet, bulbe olfactif, cortex, hippocampes et rétines). Chaque échantillon a été généré en triplicata biologique. Les ribosomes ont été purifiés en utilisant un coussin de sucrose (Belin et al., 2010b). Les ribosomes ainsi que leurs intéractants (facteurs de traduction et facteurs associés au ribosome) sont purifiés. La pureté de chaque échantillon a été évaluée par western blot pour l'absence de marqueur nucléaire (histone H3), mitochondriale (HSP60) ou cytoplasmique (GAPDH). Les échantillons ont ensuite été analysés par chromatographie en phase liquide couplée à une spectrométrie de masse en tandem en label-free.

Entre 587 et 2613 molécules ont été identifiées sur l'ensemble des échantillons. L'analyse de composante principale sur l'ensemble des échantillons révèle une bonne clustérisation des réplicats biologiques démontrant ainsi la reproductibilité des résultats. Elle démontre aussi une hétérogénéité entre régions du même organe (cervelet, bulbe olfactif, cortex, hippocampes et rétines).

L'analyse du profil d'expression des PR sur l'ensemble des échantillons révèle l'existence de deux types de PR : 75% des PR sont invariables et ont une expression stable sur

l'ensemble des organes analysés. Ces protéines contribuent à former la base structurale du ribosome et sont probablement nécessaires à la fonction basale de traduction du ribosome. Le deuxième groupe est composé de protéines dites variables et sont divisées en sous-groupe selon la spécificité de leur expression :

- Expression tissu-spécifique. Les paralogues (ex. RPL3L/uL3l, RPL39L/eL39L, RPL10L/uL16L) et autres PR (RPL10/uL16, RPS29/uS14, RPLP2/P2)
- Expression variable sur l'ensemble des organes (ex. RPS15/uS19, RPLP1/P1, RPL39/eL39)

De façon très surprenante, ces protéines variables sont situées à proximité ou à l'intérieur de domaines fonctionnels. Par exemple, RPL10/uL16 se situe dans le site P du ribosome et RPL3/uL3 se situe à l'entrée du tunnel l'ARNm. Il est à noter également que la majorité des PR variables ne sont présentes que chez les eucaryotes. Afin de valider profils de PR, nous avons sélectionné 12 PR (RPS2, RPS26, RPS30, RPL3, RPL3L, RPL10, RPL10L, RPL39, RPL39L, RPL36 et RPLP2) et fait une analyse par quantification absolue en utilisant des peptides marqués. 10 profils ont été confirmés.

Nous avons finalement évalué la corrélation entre le taux de d'ARNm et le taux de protéines. Nous avons utilisé trois bases de données de transcriptomique. Pour la majeure partie des PR, il y avait un bon taux de corrélation à trouver pour les PR stable. Le groupe des PR variables était plus hétérogène avec une corrélation faible observée avec quelques PR.

Figure 3

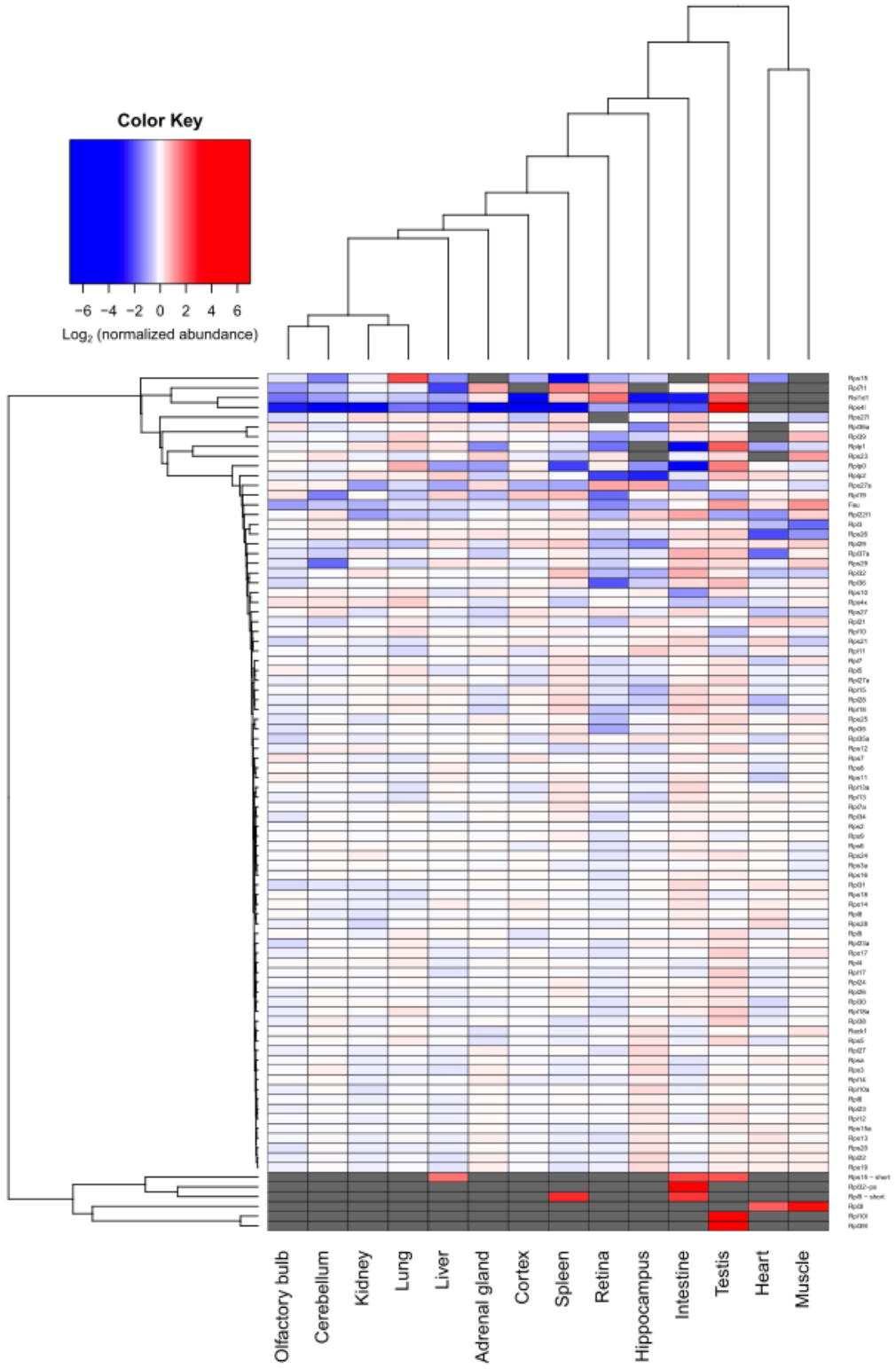

Figure 1 – Hétérogénéité du profil expression des protéines ribosomales.

Étude 2 : Analyse in silico des facteurs associés au ribosome

Nous nous sommes également intéressés aux facteurs qui ont été co-précipités avec les ribosomes au cours de la purification. Une analyse d'enrichissement sur STRING (von Mering et al., 2003) a rapidement mis en évidence la présence de molécules nucléaires et mitochondriales. Afin d'avoir une meilleure vue d'ensemble sur les intéractants cytoplasmiques, les listes ont été manuellement triés afin d'éliminer les facteurs nucléaires et mitochondriaux et ont ensuite été analysées sur DAVID et STRING. Nous nous sommes concentrés sur les différentes parties du système nerveux central et sur les 2 types musculaires. Une comparaison des facteurs issus du CNS révèle que le cervelet, bulbe olfactif, cortex, hippocampes et rétine partagent 612 protéines communes mais ont entre 88 et 602 protéines qui les distinguent. Les analyses d'enrichissement montrent que les protéines spécifiques sont impliquées dans des fonctions spécifiques A titre d'exemple, les facteurs identifiés dans la rétine sont impliqués dans les perceptions visuelles et la maintenance des photorécepteurs. De façon similaire, les muscles et le cœur partagent 153 protéines en commun. Elles sont impliquées dans la contraction et le développement musculaire. Les facteurs spécifiques au cœur participent à la contraction de la cellule musculaire cardiaque alors que ceux des muscles sont enrichis en facteurs régulant la contraction musculaire. Les facteurs associés au ribosome semblent donc être très liés à la fonction tissulaire.

CNS subpart	GO biological process category	Fold enrichment	P value
Cerebellum	positive regulation of synapse maturation	37.64	0.003
	long-term synaptic potentiation	11.27	0.005
	ion transport	2.60	0.010
	regulation of translation	5.70	0.011
	cell migration	4.34	0.012
Cortex	calcium ion transport	8.02	0.003
	transport	2.11	0.005
	calcium ion transmembrane transport	10.27	0.007
	protein oligomerization	10.12	0.035
	positive regulation of peptidyl-serine phosphorylation	9.16	0.042
Hippocampus	RNA splicing	6.54	7.65E-10
	protein phosphorylation	4.03	1.52E-09
	phosphorylation	3.79	5.57E-09
	mRNA processing	4.89	7.09E-08
	nervous system development	3.52	5.31E-05
Olfactory Bulb	neuron projection development	8.91	0.002
	nervous system development	4.60	0.004
	positive regulation of neuron projection development	7.18	0.018
	negative regulation of cytoplasmic translation	82.57	0.024
	response to herbicide	61.92	0.031
Retina	visual perception	11.91	5.86E-36
	response to stimulus	5.22	9.39E-14
	covalent chromatin modification	4.14	4.62E-11
	photoreceptor cell maintenance	12.05	5.16E-11
	transcription, DNA-templated	1.92	5.95E-11

Tissue	GO biological process category	Fold enrichment	P value
Heart	cardiac muscle contraction	17.41	5.233E-10
	sarcomere organization	19.61	1.223E-07
	transport	2.04	1.889E-06
	regulation of anion transport	42.21	3.443E-06
	positive regulation of organelle organization	75.97	8.808E-06
Muscle	muscle contraction	35.08	1.419E-15
	positive regulation of protein localization to Cajal body	101.21	1.098E-09
	regulation of muscle contraction	41.07	1.288E-08
	positive regulation of telomerase RNA localization to Cajal body	53.98	5.651E-08
	Positive regulation of establishment of protein localization to telomere	74.97	3.426E-07
Common	muscle contraction	24.47	2.702E-09
	glycolytic process	22.66	6.04E-06
	muscle organ development	12.95	9.618E-05
	mitochondrial electron transport, ubiquinol to cytochrome c	41.83	0.0001
	regulation of the force of heart contraction	23.64	0.0006

Figure 2 : Analyse d'enrichissement des facteurs associés aux ribosomes dans le CNS et les muscles.

Etude 3 : Implication du ribosome dans la régénération axonal du CNS

Nous avons étudié l'implication des PR et des 2'O méthylations sur la régénération. A partir de la littérature et de données internes, nous avons sélectionné 3 PR : RPS4X, RPS14 et RPL22. Après validation in vitro et in vivo de l'expression de la protéine et de son intégration dans les ribosomes, les PR ont été injectés individuellement dans la cavité intravitréen de l'œil de souris WT pour infecter les cellules ganglionnaires de la rétine. Au bout de 2 semaines, une lésion a été induite via le pincement du nerf optique qui contient uniquement les projections des cellules ganglionnaires. La suivie et la régénération axonale ont été mesurées deux semaines post-lésion. Pour analyser les effets des 2'O méthylations, la 2'O méthyltransférase fibrillarin a été surexprimée.

En analysant la survie des cellules ganglionnaires de la rétine, seul RPL22 semble avoir un effet négatif sur la régénération. En effet, nous observons moins de survie que dans la condition contrôle. Aucun effet n'a été détecté avec les autres PRs, ni la fibrillarine. Concernant la régénération, RPS4X semble induire une régénération à courte distance mais cette différence, par rapport au contrôle n'est pas significative. La surexpression de RPS14 ou RPL22 ne semble pas induire d'effet. En revanche, l'effet de la fibrilline est plus incertain. Une régénération axonale a bien été observée en surexprimant la fibrillarin, Cette régénération est perdue quand le site actif de l'enzyme est muté. Cependant, l'effet régénérateur semble être perdu quand la fibrilline est exprimée à très forte dose.

Ces résultats restent cependant préliminaires et nécessitent d' expériences supplémentaires pour en confirmer les effets.

Conclusions

Le ribosome est un complexe de 4,3 MDa composé d'environ 80 RP. La plupart des PR sont situés du côté du solvant alors que très peu sont situés à l'interface de la sous-unité. Même de nos jours, des études se demandent encore si les ribosomes, et plus précisément les PR, sont exprimés de manière différentielle (Amirbeigiarab et al., 2019 ; Kyritsis et al., 2020). Des doutes subsistaient car la plupart des études utilisaient une analyse transcriptomique ou étaient réalisées in vitro (Slavov et al., 2015 ; Shi et al., 2017). Il était nécessaire d'avoir une image plus claire de la composition des ribosomes in vivo.

En comparant les ribosomes de 14 tissus et organes différents, nous avons identifié une RP stable et variable. Nous avons vérifié 2 PR stables et 10 variables par quantification absolue. Nous avons confirmé l'enrichissement de RPL3L, RPL10L, RPL39L, l'épuisement de RPL3, RPL10, les variations de RPLP2, RPS30. Cependant, aucune variation n'a été détectée avec RPS26, RPS2. Nous avons également vérifié la corrélation en comparant nos données protéomiques avec les données transcriptomiques disponibles. Alors que certains RP ont montré un bon niveau de corrélation entre la protéine et le niveau de transcription (par exemple RPS3, RPL7A, RPL34), d'autres ont montré moins de corrélation (par exemple RPLP0, RPS26)

Nous avons montré que près de 75 % des RP ne présentent aucune variation. Ils sont localisés principalement du côté solvant, constituant probablement la structure de base des ribosomes et ont un rôle dans la stabilisation de l'architecture ribosomique. Ces RP contribuent probablement aux fonctions de traduction de base des ribosomes telles que la reconnaissance de l'ARNm, le balayage et le contrôle de la qualité des protéines. Des exemples de RP stables sont RACK1, RPL10A et RPS14. RACK1 régule la traduction en recrutant la protéine kinase C qui est connue pour empêcher le facteur d'initiation eIF6 de se lier au ribosome (Grosso et al., 2008). Cependant, nos résultats ne peuvent pas éliminer la probabilité d'une distribution préférentielle de ces protéines parmi les monosomes ou les polysomes car tous les ribosomes ont été analysés collectivement (Slavov et al., 2015).

Les 25 % restants des PR présentaient des variations soutenant l'idée qu'il existe une distribution sous-stœchiométrique du PR au sein des ribosomes (Slavov et al., 2015 ; Shi et al., 2017). Un seul RP de notre étude, RPL10, partageait le même appauvrissement avec l'étude de Shi et ses collègues sur les cellules souches embryonnaires de souris. Aucune variation significative n'a été détectée avec RPL10A, RPL11, RPL38, RPL40, RPS7 et RPS25 soulignant la différence entre les cellules souches et les organes matures (Shi et al., 2017). Cependant, dans leur étude de 2017, Shi et ses collègues n'ont utilisé qu'un seul peptide pour RPL38, RPL40 et RPS7, 3 des 6 RP présentant des variations. Sur la base de nos observations, une difficulté majeure dans la quantification absolue est que les peptides de la même protéine n'ont pas nécessairement donné les mêmes résultats quantitatifs en raison de difficultés à solubiliser les peptides dans les solvants ou de problèmes de stabilité des peptides. Par conséquent, il serait prudent de prendre des critiques avec des résultats basés sur un seul peptide. Une solution meilleure mais coûteuse consiste à utiliser des protéines marquées au lieu de peptides marqués.

De plus, il est à noter que la majeur partie des PR signant des tissus n'ont aucune fonction connue dans ces tissus. Plus d'études seront nécessaires afin d'étudier les implications de cette distribution particulière. Ceci est aussi applicable aux facteurs associés aux ribosomes.